Deltares

Analysis Report Coarse Sand Barrier Verification Tests

Analysis of medium-scale configuration with protuberance (phase 3)

Analysis Report Coarse Sand Barrier Verification Tests
Analysis of medium-scale configuration with protuberance (phase 3)

Author(s)
Ulrich Förster
Vera van Beek (contribution to Section 4.2.4)
Esther Rosenbrand (Appendix A)

Analysis Report Coarse Sand Barrier Verification Tests
Analysis of medium-scale configuration with protuberance (phase 3)

Client	Waterschap Rivierenland
Contact	B. Heutinks, B.Heutink@wsrl.nl
Reference	-
Keywords	Piping, preventive measure, coarse sand barrier, innovation, medium-scale, scale effects, protuberance, physical modelling, GZB, CSB

Document control	
Version	1.0
Date	17-03-2021
Project nr.	11200952-063
Document ID	11200952-063-GEO-0001
Pages	145
Status	final

Author(s)		
	Ulrich Förster	

Doc. version	**Author**	**Reviewer**	**Approver**	**Publish**
1.0	ir. Ulrich Förster 	prof.dr.ir. Adam Bezuijen 	ing.Goaitskede Vries b/a Remon Pot 	
		Ir. Leo Voogt		

Summary

Piping is one of the most important threats for the safety of Dutch levees, especially for the sections that are located along the main rivers. Based on research conducted in the past years several piping mitigating measures have been developed that prevent the pipe from progressing towards the river. One of these measures is the coarse sand barrier. The coarse sand barrier (CSB) is a trench of coarse sand that prevents fine sand from upstream of the barrier from being eroded, and thereby hinders the pipe from progressing upstream below the dike. The CSB was already tested in small-scale, medium-scale and large-scale experiments (phase 2a, 2b, 2c) within the feasibility study for the CSB.

The report at hand describes the analysis of two additional medium-scale tests of identical type which were performed to test the influence of a protuberance (or “inkassing”, in Dutch) at the CSB (phase 3 of the feasibility study). For a barrier that protrudes into the cover layer, different mechanisms govern an increase of the strength as compared to the strength of a flat barrier, because a slope is forming in the barrier. The aim of these tests with a protuberance was to validate the presumed failure mechanism which was devised based on an earlier test with a shallow protuberance and to check if the critical gradient according to that failure mechanism can be found in these tests.

The outcome of this test series is that the strength of the CSB is indeed increased by the presence of a protuberance. The results are also in agreement with the numerical calculation models whereby reproducible results were obtained about the occurrent discharge and gradients at the critical stage before failure, which means that the assumed strength criteria are suitable for design purposes.

The erosion process appears to be governed by the formation of a slope in the barrier and finally failure of the lower part of the slope and subsequently piping due to heave at the upstream end of the barrier.

A CSB which protrudes into the cover layer retains a considerable higher head drop than a barrier top level with the aquifer top. This increase in strength is a consequence of the larger outflow area which is created by the slope of the protruding barrier. Since the discharge is limited by the upstream fine sand, the gradient in the CSB is lower and thus the barrier more stable.

It should be realized that maximum stability is only present when the slope in the protuberance is fully developed. This means that considerable sand transport and thus sand producing wells and consequently some (water-filled) hollow space above the barrier will exist before the maximum strength will be achieved.

Besides, the results can be highly influenced by a decrease in permeability of the (upstream) background sand as was observed during a failed test in which clogging occurred at an interface further upstream of the CSB under the influence of mould formation in the reservoir water, leading to a head drop in the aquifer upstream of the CSB which led to very low gradients inside the CSB and made failure impossible under the head differences available in the lab. Assuming a comparatively high inflow of clogging material or organic / biological particles into a piping sensitive sand layer with a CSB, we can assume that fine background sand will be clogged before the CSB will be reached. The permeability of the whole aquifer will decrease intensively, resulting in a structure with a high resistance against piping. Therefore, it is worthwhile to perform in-situ permeability tests to enable an accurate estimate of the possible hydraulic load on the CSB.

In the experiments, it was found that a protruding barrier is stable up to an outward directed gradient of 0.7 in the centre of the barrier (based on velocity/hydraulic conductivity). The underlying model of van Rhee & Bezuijen is still valid and there will be no loss of geotechnical stability up to this gradient. This value can be used as criterium when the gradient is calculated numerically for a field situation. However, safety and model factors will apply.

Contents

	Summary	**4**
1	**Introduction**	**9**
1.1	General framework	9
1.2	Aim of the study	11
1.3	Structure of the report	12
2	**Set-up of the experiments**	**13**
2.1	Set-up	13
2.2	Experimental procedure	17
2.3	Soil properties	18
2.4	Adapted conceptual model	20
2.4.1	Pipe initiation and progression	20
2.4.2	Lateral pipe development	20
2.4.3	Slope development in upstream direction	20
2.4.4	Subsiding of the slope	20
2.4.5	Failure	21
3	**Analysis of experimental results**	**22**
3.1	Observations	22
3.1.1	Pipe and slope progression – observations and measurements	22
3.1.1.1	Test MS-GZB3-B25-38	22
3.1.1.2	Test MS-GZB3-B25-40	30
3.1.2	Slope formation	38
3.1.3	Slope failure analysis	39
3.1.4	Test MS39	44
3.2	Head measurements	45
3.3	Head drop versus flow rate and erosion	46
3.4	Check of the measured data	47
3.4.1	Test MS38	48
3.4.1.1	Check of development of the measured heads as a function of time	48
3.4.1.2	Vertical gradients	54
3.4.1.3	Horizontal gradients	56
3.4.2	Test MS 40	59
3.4.2.1	Check of gauges concerning the development of measured heads as a function of time	59
3.4.2.2	Vertical gradients	61
3.4.2.3	Horizontal gradients	64
3.5	Conclusions regarding the check of gauges	66
3.6	Input parameters for comparison with numerical model	66
4	**Numerical simulations of the experiments**	**73**
4.1	2D numerical simulations MSP experiments	73
4.1.1	Stability of a slope subjected to outward seepage	74
4.1.2	Model geometry and mesh	76
4.1.2.1	Geometry and modelling of the pipe and the slope	76
4.1.2.2	Material parameters	77
4.1.2.3	Mesh	79
4.1.2.4	Boundary conditions	81
4.1.3	Procedure	83

4.2	Results	84
4.2.1	Head distributions at the end of stage I	84
4.2.2	Head profiles close to failure	87
4.2.3	Flow rate at critical stage	91
4.2.4	Sensitivity analysis concerning relative density of barrier material	92
4.2.4.1	Variation of the hydraulic conductivity	92
4.2.4.2	Determination of exit gradients at critical stage	94
4.2.5	Discussion and Conclusions	97
5	**How strong is a protruding CSB?**	**100**
6	**Adapted conceptual model regarding the initial model**	**102**
6.1	Pipe formation downstream of the barrier	102
6.2	Damage of the barrier and pipe development along the barrier	102
6.3	Erosion of the barrier	103
6.4	Failure	105
7	**Conclusions and Recommendations**	**107**
7.1	Conclusions	107
7.2	Recommendations	109
8	**References**	**111**
Appendices113		
A	**Prediction models**	**116**
A.1	General Model input	116
A.1.1	Geometry	116
A.1.2	Boundary conditions	117
A.1.3	Mesh	118
A.1.4	Material properties	119
A.1.4.1.	Preliminary sensitivity analysis	119
A.1.4.2.	Predictions	120
A.2	General model analysis	120
A.3	Initial sensitivity analysis results	121
A.3.1	Conclusions	124
A.4	Predictions Basis Contrast	124
A.4.1	Situation without GZB3 upstream of background sand	125
A.4.2	Effect of slope angle on gradients out of slope	126
A.4.3	Effect of slope angle on head distribution	127
A.4.4	Effect of slope angle on ratio vertical gradient/gradient out of slope	129
A.4.5	Situation where heave occurs	129
A.4.6	Flow rate	130
A.5	Prediction lower contrast	130
A.5.1	Effect of contrast on gradients out of slope and vertical gradient	131
A.5.2	Situation where heave occurs	132
A.5.3	Flow rate	133
A.5.4	Conclusions	133
B	**Postdiction details**	**135**
B.1	Variatiations of intrinsic permeabilities for fitting numerical results with measured values	135
B.2	Gradients at critical stage for numerical fits I2 (MS38) and F2 (MS40)	136
B.2.1	Outward hydraulic gradients perpendicular to the slope	136
B.2.2	Vertical gradients	138

C Geotechnical stability against sliding of upstream fine sand 141
C.1 Introduction 141
C.2 Calculation 142

1 Introduction

1.1 General framework

Backward erosion piping (BEP) is an erosion process under low permeable clay layers and a clay dike (referred to here as blanket layer) situated on top of a sand aquifer (referred to here as background sand). An elevated water level on the river side of the dike will cause water to flow through the aquifer. If an opening in the blanket layer exists downstream of the dike, sand will be transported from under the dike, eventually leading to macro instability and breaching. In this report, it is assumed that the reader is familiar with backward erosion piping (BEP), the concept of the CSB and the Deltares medium-scale piping set-up. For details, refer to earlier reports in this study (e.g. Deltares 2020a).

The current safety assessment method for piping, applied in the Netherlands, results in a large amount of dike sections to be reinforced. Traditional reinforcement methods, like berms to increase seepage length, become less and less attractive due to the large required seepage length and the dense population and building development in this area. Several alternative (and innovative) methods are available that require less space. A new alternative method is the coarse sand barrier (CSB). This method entails the replacement of existing sand with coarse sand in a trench on the landside of the levee directly below the blanket layer. The blanket layer is restored after trenching.

The regional Water Authority Rivierenland intends to apply the coarse sand barrier as an innovative measure against backward erosion piping in a pilot. This pilot is financed by the Dutch National Flood Protection Programme HWBP of Rijkswaterstaat with the aim to develop a reliable innovative alternative for piping mitigation measures for a wider application in the Netherlands. Therefore, a suitable pilot location was chosen to build this innovative measure in a dike strengthening stretch without having spatial constraints.

One of the sections that failed the safety assessment criteria is located within dike ring 38-1, nearby the village of Gameren. A dike stretch of 0.3 km failed the safety assessment criteria in the third national levee safety assessment round that was conducted in the period 2006-2011 and will need to be reinforced within short term. An indicative analysis with the current, more stringent safety assessment criteria indicated even that nearly all the 1.0 km dike in front of Gameren could be unsafe. However, this is not the only dike section that will need to be reinforced. Indicative studies show that approximately half of the levees that are operated by Dutch Water Authority Rivierenland will not pass the current safety assessment criteria for piping. The aim of the pilot is to design a piping mitigating measure that is safe for this location but is also giving enough reliance in a wider applicability.

Although experiments in the laboratory and at the IJkdijk (a former full-scale test facility in the North-Eastern part of the Netherlands) indicate the potential of the method, it is required to conduct a feasibility study to investigate whether the method offers sufficient resistance against piping in the field, both for the intended pilot location and for other, comparable locations. Based on the result of this feasibility study and the exploration of alternative measures, a preferential measure will be selected for the pilot location.

The purpose of the study is to assess the feasibility of the application of a coarse sand barrier as a BEP mitigating measure for the location of Gameren in particular, and for other locations along the Dutch main rivers in a more generic sense. The CSB as a mitigation measure for the erosion means placing a section of coarse material under the landside toe of the dike, allowing water to flow

through, but stopping the erosion. To quantify the strength of the CSB, a criterion needs to be identified that predicts pipe formation into the barrier.

The approach to the primary feasibility study is described in (Deltares 2017a) and consists of the following phases:

- Phase 1: Literature study filter requirements (Deltares memo 11200952-003-GEO-0001) and Sand Selection of Coarse Sand Barrier experiments (Deltares memo 11200952-004-GEO-0001-m)
- Phase 2a: Small-scale experiments and numerical simulation (Deltares 2017b, 2017c)
- Phase 2b: Medium-scale experiments and numerical simulation (Deltares 2018a, 2018b and Deltares 2019c, 2020a)
- Phase 2c: Large-scale experiments and numerical simulation (Deltares 2019a, 2019b).

The feasibility study is oriented towards one pilot location, but much of the knowledge developed in this study will be applicable in a more generic sense (at other locations). The study focusses explicitly on the technical feasibility of the measure and will not address the practical aspects of installing the coarse sand barrier in the field.

The first phases illustrated the potential of the concept of a CSB in general. A protuberance (or “inkassing”, in Dutch) seems to offer additional strength in comparison to the configuration with a CSB with its top being level with the bottom of the blanket layer. Preliminary design calculations for the situation at Gameren (Deltares 2020c) showed that it is difficult to design a sufficiently safe strengthening for this location on the base of the criterion which was deduced from the other scale-tests with no protuberance. However, with a protuberance of the CSB a reliable design seemed possible.

The purpose of the two additional experiments is to study the effect of the protuberance (or “inkassing”, in Dutch) of the CSB into the blanket layer. This protuberance is inherent to the construction of the CSB in the field, cutting a trench at the toe of the dike in the blanket layer and sand aquifer. This trench is filled with coarse sand (compared to the original sand layer) until it partially extends into the blanket layer to ensure a full connection. The remaining volume is filled with cohesive, low permeable material to restore the blanket layer. In practice, natural (and artificial) variations in the level of the top of the aquifer vulnerable to piping render a continuously flat connection of the CSB impossible. Then an upward protuberance is in several ways preferable – not only because of the gain in strength, but also because an interface below the top of the aquifer would lead to additionally troublesome concentrations of the groundwater flow in case of a pipe arriving at the CSB from downstream. A disadvantage of the (upward) protuberance is the resulting smaller thickness of the blanket layer.

In an earlier experiment (Deltares 2020a, MS-GZB2-B25-37) the protuberance was simulated by casting two 0.10 m high silicone blocks inside the medium-scale piping set-up, both upstream and downstream of the CSB, resulting in smaller thickness of the aquifer. However, the protuberance was too shallow to observe processes that are expected in the field. The barrier could not completely develop a natural slope inside the protuberance reaching the upstream edge of the protuberance, instead it showed horizontal pipe development underneath the cover of the protuberance before fluidization occurred.

The erosion mechanism where the slope protrudes into the cover layer is most likely to occur in the field, as in practice it is unlikely that it is possible to construct the barrier exactly level with the cover layer. As the height of the barrier above the aquifer will be larger in the field, such tests should also be conducted in a geometry where the upstream end of the slope in the barrier touches the upstream end of the barrier, rather than the cover layer at the top of the barrier, which occurred during the test that was analysed.

For this study a new acrylate cover was designed, which maintained the full 0.40 m high sand aquifer of the medium-scale piping set-up, in addition to a 0.30 m high penetration of the CSB (totalling 0.70 m). The configuration of the two experiments was basically identical, serving as a validation of the results.

The report at hand deals with the analyses of the processes and factual results reported in (Deltares 2020b) and presents a detailed comparison with numerical calculations performed before and after the experiments.

Based on these results the consequences for application of the CSB in Gameren will be described in a final report (Deltares 2021a). A first approach for a design and assessment guideline will be given in (Deltares 2021b).

1.2 Aim of the study

The results of the previous test MS37 (Deltares 2020a) with a fairly shallow protuberance created by small silicone blocks underneath the covering acryl glass plate allowed to create a calculation model that describes the processes for the situation with a protruded barrier. This model (described in Deltares 2020a) is based on separate processes from the literature. It is expected that pipe formation in the background sand causes the transport of barrier material, resulting in the formation of a slope in the barrier. Since water flows through the barrier, the angle and the stability of the slope are controlled by the outward hydraulic gradient. The failure of the barrier is expected to take place as a result of loss of effective stresses at the upstream side of the barrier. Criteria are available from the literature for the two processes of slope formation and loss of strength due to fluidisation.

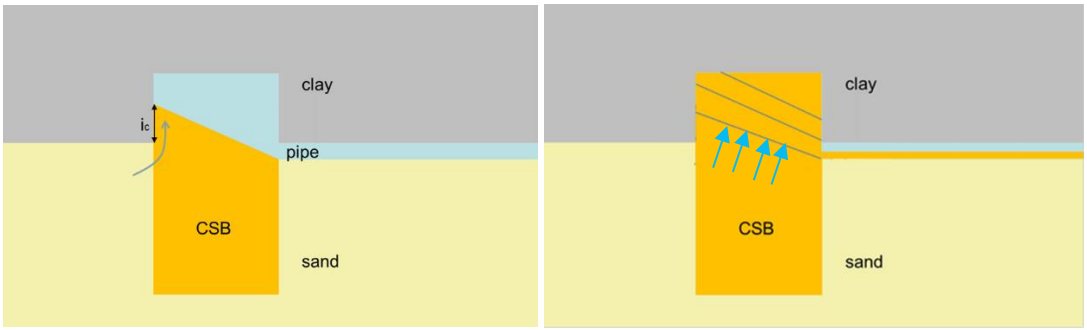

Figure 1.1 Critical situation CSB with protuberance

Figure 1.1 shows the critical situation for a CSB with protuberance. The pipe has developed to barrier and the eroded coarse grains of the barrier material are transported to the pipe and then to the outlet. A slope with a natural slope angle has developed which is in equilibrium with the water outflow from the slope. When the gradient i is high enough for initiating fluidization over the vertical distance h on the upstream side of the protuberance, thus $i > i_c \approx 1$, it is expected that the pipe progression can continue in the fine sand in upstream direction.

The conceptual model of a CSB with a shallow protuberance as described in (Deltares 2020a) assumes that this critical situation can be described by superposing two criteria:

- The fluidization of sand can be predicted by the Terzaghi heave criterion, which means that sand will be fluidized if the gradient over the vertical distance h is higher than approximately 1
- The vertical distance h is determined by the natural slope angle arising under the influence of the water which is streaming out of the barrier. This is described by the criterion of Van Rhee and Bezuijen (1992).

$$i = V/k = -(1-n)\Delta\frac{\sin(\varphi-\beta)}{sin\varphi}$$

with :
β: slope angle
φ: internal friction angle
n: porosity
Δ: relative grain density = $(\rho_s - \rho_w)/\rho_w$
V: seepage velocity
k: permeability
ρ_s: density of grains
ρ_w: density water

The stability of the slope is influenced by the hydraulic gradient at the surface of the slope.

The criterion of Van Rhee & Bezuijen (1992) presupposes a uniform pressure distribution as a result of the experimental set-up used for developing and underpinning this criterion. In the experimental set-up of the CSB test a different non-uniform flow pattern is to be expected.

This conceptual model for the failure mechanism has been set up based on experience concerning BEP and one single medium-scale test with a fairly shallow protrusion of the barrier. In this test the slope could not fully develop up to the upstream side of the protuberance so that horizontal pipe development occurred underneath the cover of the protuberance and finally heave occurred at the upstream side of the barrier.

The aim of the analysis of these two experiments is to validate the expected failure mechanism and to check if both expected processes indeed take place. It appears that the processes (flattening of the slope and fluidisation) described in the conceptual model occurred during the tests. However, also an other failure mode was observed which led to some adaptation of the conceptual model.

1.3 Structure of the report

The medium scale experiments are described in the Factual Report (Deltares 2020b), a short summary of the most important details of the experiments essential for the analysis is given in Chapter 2, added by a brief description of the expected conceptual model. During the execution of the tests and as part of the analysis, the presumed failure mechanism has been slightly adapted by adding certain nuances by the application of the criteria. The analysis of the observations and measurements is given in Chapter 3. In Chapter 4 numerical simulations (postdictions) of the medium-scale tests are presented based on head measurements at the top and the bottom of the container and flow rates, because it is technically not possible to measure the gradients inside the barrier – especially the outward gradients along the developing slope of the barrier. Chapter 5 contains an explanation of the strength of a protuberance by comparing the measured heads with a test in the same set-up with a non-protruding CSB. In Chapter 6 the adapted conceptual model for a barrier with protuberance with the corresponding gradients is described, and in Chapter 7 conclusions and recommendations are presented. Finally, the appendices provide more details on the numerical predictions and simulations of the tests.

2 Set-up of the experiments

The current chapter provides a brief description of the set-up and the execution of the tests MS-GZB3-B25-38, GZB3-B25-39 and GZB3-B25-40. Full detail regarding the experiments with a protuberance of the CSB is described in the Factual Report (Deltares 2020b).

2.1 Set-up

The river, CSB and dike system have been simplified by isolating the sand around the CSB into a single container. The set-up is in principle the same as in the first and second phase of the medium-scale tests, the experiments in which the barrier is level with the cover layer (Deltares 2018a and Deltares 2019c. A schematic overview of the set-up used for the standard tests, where the barrier does not protrude into the cover layer, is shown in Figure 2.1. The inner dimensions of the container used are 1914*881*404 mm.

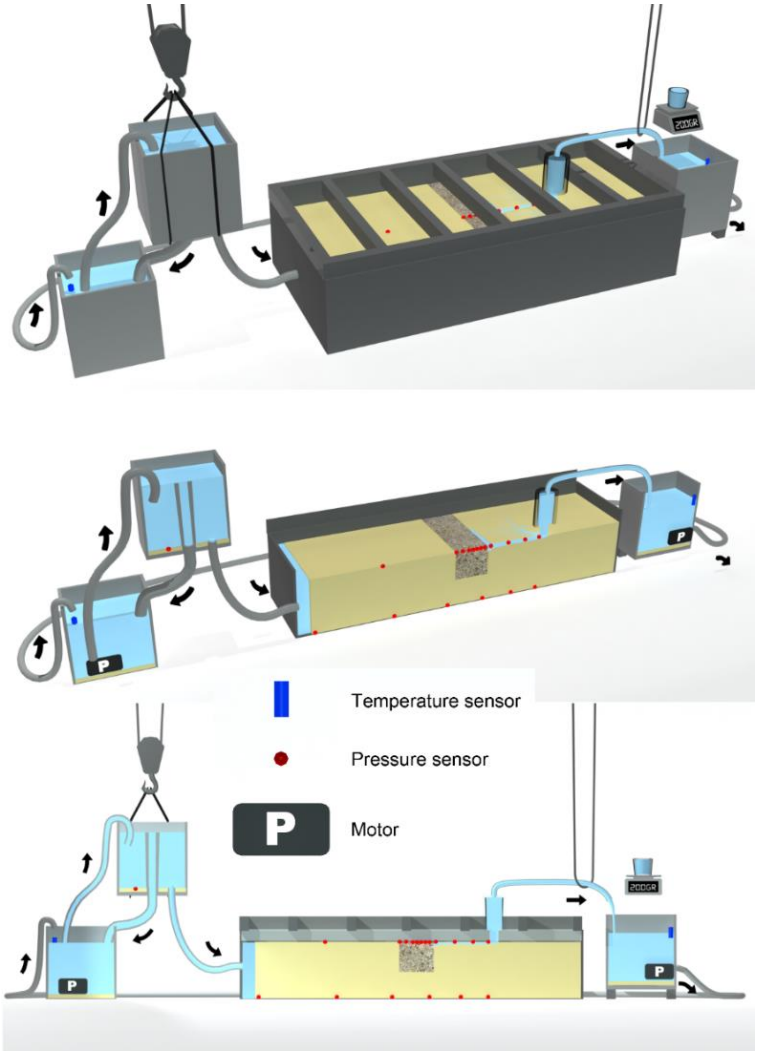

Figure 2.1 Schematic figure showing the set-up of the experiment for the standard tests including locations of the pore pressure transducers and the barrier inside the sample. There is a pump around circuit and flow measurements are made intermittently in 5-minute intervals. In this illustration the barrier is only applied over the upper part of the aquifer. In the present research the barrier is applied over the whole height of the aquifer.

Figure 2.2 shows the adapted set-up for the test with a protuberance of the CSB into the cover layer.

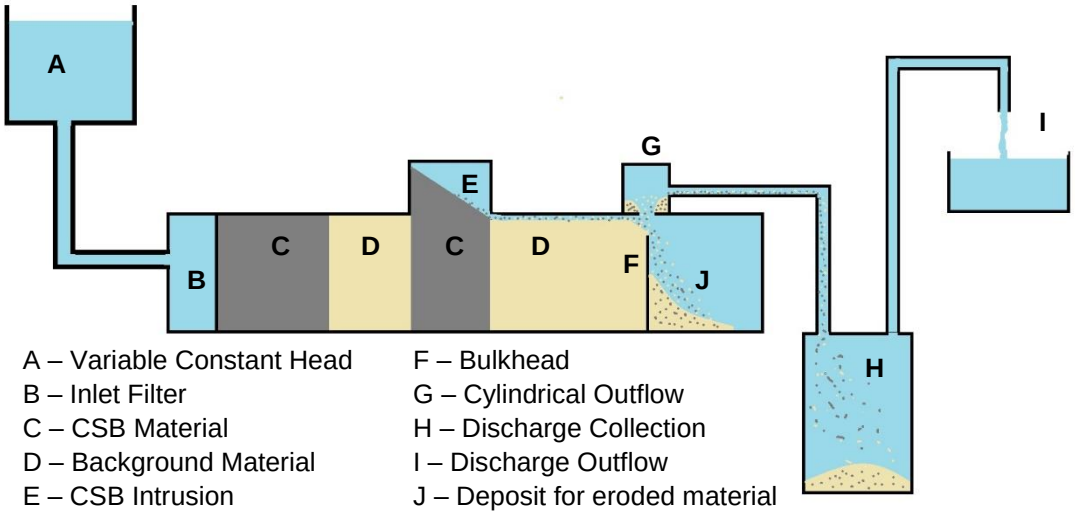

A – Variable Constant Head
B – Inlet Filter
C – CSB Material
D – Background Material
E – CSB Intrusion
F – Bulkhead
G – Cylindrical Outflow
H – Discharge Collection
I – Discharge Outflow
J – Deposit for eroded material

Figure 2.2 Schematized longitudinal section (in the flow direction) of the set-up with the barrier protruding above the aquifer

The adaptation of the set-up includes the following aspects:

- An additional column of CSB material. To effectively shorten the seepage length, a column of CSB material (C) was added directly after the inlet filter (B). This was added to be able to apply higher pressure gradients over the test set-up and make sure failure of the CSB could be achieved
- CSB protrusion. This protrusion (E) was added to simulate the effect of the barrier protruding into the cover layer
- Bulkhead. The CSB will erode with increasing flow rate, causing material to accumulate at the outflow. This accumulation may cause clogging and/or increased resistance at the outflow. In order to create a constant situation, this eroded CSB material must be removed. This has been realized by positioning a bulkhead (F) under the outflow cylinder; water will be discharged via the cylindrical outflow (G) - the acrylate lid has an outlet hole of 82 mm diameter - while the CSB material will be deposited at the other side of the bulkhead (J). The top of the bulkhead is in contact with the top acrylate plate, save for the diameter cylindrical outflow. Here an opening exists with a height of 20 mm which allows the CSB to spill over
- Discharge Collection. Fine material may be transported with the discharged water. This discharged water is being recirculated to maintain the constant head (A) and may possibly clog the inlet filter (B). Therefore, a container (H) was added to allow the fine material to settle and avoid contamination at the discharge point (I).

In principle, the experiments were prepared as identical tests with the aim to conduct two tests in order to prove that the appearing process are reproducible. Therefore, two tests had to be performed. By mischance, in the second test it was not possible to achieve failure of the barrier at the maximum attainable head drop in the laboratory. This test was affected by clogging of the first GZB3 – B25 interface (C-D), as seen from the inlet filter (B). The clogging was assessed to be related to contamination of the used water in the water reservoir (A). A slightly discoloured band of mould (about 5 mm thick) was observed along the entire height of the upstream interface. This mould band resulted in lower heads downstream the interface.
The results were assessed not to be representative for the research aim of these experiments and are therefore only briefly discussed in this report. More details concerning the observed clogging are described in the factual report (Deltares 2020b). The test was conducted once more with a new

prepared set-up after cleaning the whole equipment containers and pumps) with hydrogen peroxide. and replacing the hoses by new ones.
Scale drawings of the box with the locations of transducers in the top and bottom of the model and in the protuberance are shown in Figure 2.3 for test MS 38 and Figure 2.4 for test MS 40. In the tables hereafter (Chapter 3 and 4) a different coordinate system is used.

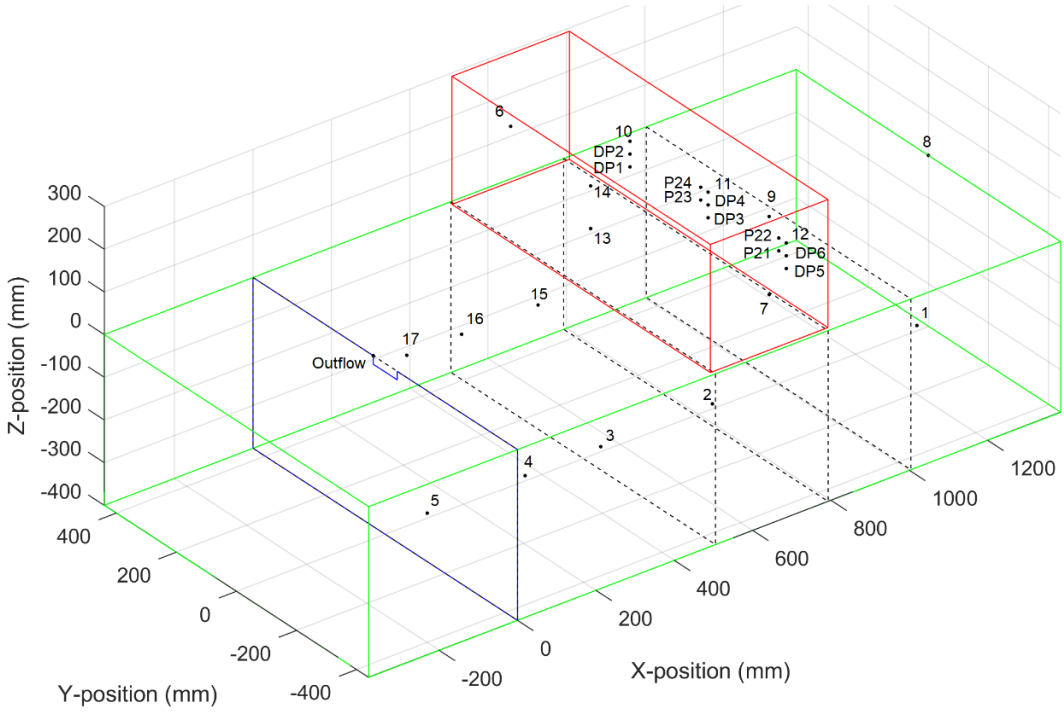

Figure 2.3 Locations of pressure transducers in experiment MS-GZB3-B25-38

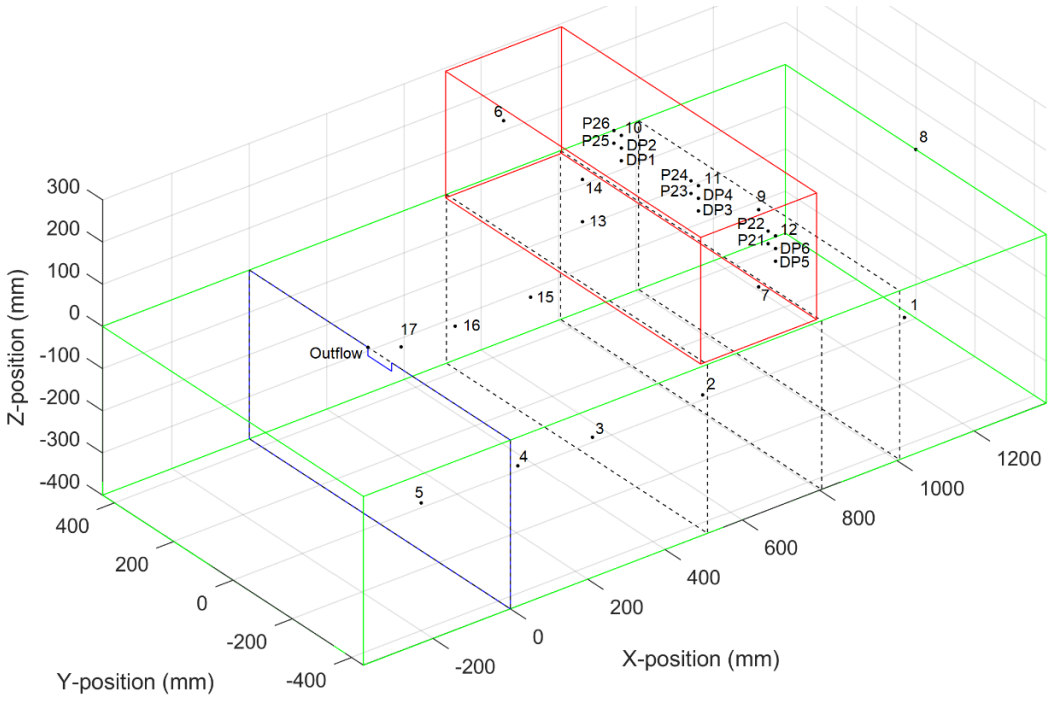

Figure 2.4 Locations of pressure transducers in experiment MS-GZB3-B25-40

The position of the head sensors (distance in relation to the outlet, the top of the sand bed and the centreline respectively) are given in Table 2-1.

Table 2-1 Pressure sensor locations (x-, z-, y-position)

Transducer (-)	Distance from outlet (mm)	Distance from top of sand bed (mm)	Distance from centreline (mm)	Comments
P17	55	0	0	
P16	195	0	0	
P15	390	0	0	
P01	1357	-388	0	
P02	835	-388	0	
P03	550	-388	0	
P04	357	-388	0	
P05	107	-388	0	
P14	505	250	-25	
P13	505	150	-25	
P12	805	130	-285	
DP6	805	100	-285	Differential Pressure, measured between DP6 and P12
DP5	805	70	-285	Differential Pressure, measured between DP5 and DP6
P11	805	130	-25	
DP4	805	100	-25	Differential Pressure, measured between DP4 and P11
DP3	805	70	-25	Differential Pressure, measured between DP3 and DP4
P10	805	130	235	
DP2	805	100	235	Differential Pressure, measured between DP2 and P10
DP1	805	70	235	Differential Pressure, measured between DP1 and DP2
P09	980	0	0	
P08	1386.5	0	0	
P07	650	130	-430	
P06	650	130	430	
P21	805	100	-260	Absolute, but used for differential pressure
P22	805	130	-260	Absolute, but used for differential pressure
P23	805	100	0	Absolute, but used for differential pressure
P24	805	130	0	Absolute, but used for differential pressure
P25	805	100	260	Absolute, but used for differential pressure, only in MS40-GZB3-B25
P26	805	130	260	Absolute, but used for differential pressure, only in MS40-GZB3-B25

The distance from the centre of the outlet to entrance filter at the upstream side is 1385 mm. This means that the distance between p01 and the filter is 28 mm.

2.2 Experimental procedure

During the experiments, the head drop across the sample is incrementally increased. The size of the head increments applied were increased progressively as the head drop over the sample was larger, since the relative effect of a certain change in head drop is different for the different stages within the process. Generally, the head is increased after every 5 minutes, but if erosion at the tip of the pipe is observed, the head is maintained until an equilibrium is reached at the tip of the pipe. Both tests started with increments of 1 cm until the pipe had reached the barrier. After this, the increment size was increased to 5 cm. When the crest of the slope in the barrier had reached the upstream side of the protuberance, the increment size was increased by 10 cm until failure. During these tests, laser measurements of the slope were made at several points in time after the pipe had progressed inside the barrier.

The effect of long-term loading is also assessed by maintaining a constant head drop of 301 cm for ca. 11.5 hours in test MS 38 and respectively 299 cm for ca. two hours in test MS 40. The objective of these steps is to analyse whether loading for longer periods during the experimental executions affects the erosion behaviour of the barrier. The aim of explicitly establishing equilibrium is to assess whether the slope angle will flatten and how long this process requires. Although two hours are not considered long in the context of levees, this is long term in relation to the loading steps that are taken during the rest of the experiment. Furthermore, no significant sand transport was noticed at the end of these long loading steps. Therefore, these steps are expected to provide an indication as to whether progressive erosion can be expected during longer periods of constant head loading.

During the tests, the following data is collected:

- Photographs from the top of the box at four positions. Photographs were taken every 10 seconds, except for experiment MS-GZB3-B25-40, while after 21 hours and 43 minutes, i.e. 2 hours and 24 minutes before the end of the recordings of the test the time interval was decreased to 5 seconds
- Short GoPro footage (59.94 frames /second) from up to three fixed positions just before and during failure of the CSB, i.e. at the front (the upstream side of the CSB protuberance) and at the back in experiment MS-GZB3-B25-40 and sidelong the protuberance experiment MS-GZB3-B25-38
- Hydraulic head at several locations in the box from pressure transducers with a sampling frequency of 10 Hz, a measurement range until 1 bar (= 100 kPa ≈ 10.000 mmH_2O) and an estimated absolute uncertainty of 0.25 kPa (25 mmH_2O) (Deltares 2020b). The differential pressure transducers have a measurement range until 75 mmH_20 and an estimated absolute uncertainty of 5 mmH_2O
- Visual observations of erosion, pipe progression and slope development in the barrier and collection of sand at the outflow, registration each five minutes
- Topography of the CSB material in the protuberance. A laser was used to measure the depth of the surface of the barrier below the surface
- Flow rate at the outflow is recorded manually each five minutes with the estimated uncertainty of ca.15% during the test (uncertainty arising from time taken to collect sample and uncertainty in weight of the sample)
- The weight of the outflow of water with three force transducers underneath the outflow tank in experiment MS-GZB3-B25-40. The outflow tank was regularly emptied by a pump. This must be incorporated to calculate the flow rate from these measurements
- The temperature of the water flowing into the model and coming out of the model is continuously measured.

2.3 Soil properties

Soil properties relating to grain size distribution and porosity of the two sand types which were used in the experiments (Baskarp B25 (denoted B25) as background sand and Fine Filter Sand (denoted GZB3) as CSB) are summarised in Table 2-2.

Table 2-2 Sand properties

Property	B25	GZB3
Mass diameter at 10% passing, d_{10} (mm)	0.103	0.762
Mean mass diameter, d_{50} (mm)	0.151	1.024
Mass diameter at 60% passing, d_{60} (mm)	0.161	1.091
Coefficient of Uniformity, $C_U = d_{10}/d_{50}$ (-)	1.6	1.4
Minimum Porosity, n_{min} (-) *	0.352	0.363
Maximum Porosity, n_{max} (-) *	0.459	0.448
Porosity at Relative Density $D_r(n) = 95\%$ (-)	0.357	0.367
Intrinsic Permeability Factor, x_2[1] (m^2)	$1.58 \cdot 10^{-10}$	$4.04 \cdot 10^{-9}$
Hydraulic Conductivity Factor, x_1[2] (m/s)	$1.53 \cdot 10^{-3}$	$3.88 \cdot 10^{-2}$
Intrinsic Permeability K at Relative Density $D_r(n) = 95\%$ (m^2)	$1.74 \cdot 10^{-11}$	$4.98 \cdot 10^{-10}$
Hydraulic Conductivity k at Relative Density $D_r(n) = 95\%$ (m/s)	$1.68 \cdot 10^{-4}$	$4.79 \cdot 10^{-3}$

[1] Intrinsic permeability, at 20°C (m^2), $K_{20} = x_2 \cdot n^3 / (1-n)^2$, where n is the porosity.

[2] Hydraulic conductivity, at 20°C (m/s), $k_{20} = x_1 \cdot n^3 / (1-n)^2$, where n is the porosity.

***) Relative density is calculated based on the wet minimum and maximum porosity.**

The angle of repose for GZB3 was determined to be 35.6° based on 6 samples (standard deviation 1.83, median 35.5).

The relative densities of the different sand sorts (GZB and B25) at the different locations are given in the following tables. The relative density is determined based on porosity.
The notations “lower” and “upper” barrier result from the process of sample preparation where the upper part of the barrier GZB (protrusion) was prepared at least. First, the sand samples were prepared while the box was in vertical position, with the inlet facing downwards and the lid at the downstream side removed. The top part of the protuberance was temporarily filled with a Styrofoam block. The sand samples are prepared by pluviating dry sand into de-aired water while densifying the sand by tamping. Once all the sand has been placed up to the outlet, the bulkhead plate is put into place. The box is then closed and turned into the horizontal position. Then, the remaining part of the CSB was prepared by pluviation and tamping and finally, the top of the protuberance is closed again.

So, the lower barrier is prepared first and has therefore a different RD end porosity than the barrier material and the upstream side of the box and the barrier material inside the protrusion.

Table 2-3 Layer thicknesses, relative densities and porosities at test MS-GZB3-B25-38

Parameter	
Thickness upstream GZB3 (m) *	0.38
Thickness upstream B25 (m) *	0.21
Thickness lower barrier GZB3 (m) *	0.29
Thickness upper barrier GZB3 (protrusion) (m) *	0.30
Thickness downstream B25 (m) *	0.51
Relative Density upstream GZB3 (%)	103
Relative Density upstream B25 (%)	91
Relative Density lower barrier GZB3 (%)	101
Relative Density upper barrier GZB3 (inside protrusion) (%)	99
Relative Density downstream B25 (%)	95
Porosity upstream GZB3 (-)	0.360
Porosity upstream B25 (-)	0.361
Porosity lower barrier GZB3 (-)	0.362
Porosity upper barrier GZB3 (inside protrusion) (-)	0.364
Porosity downstream B25 (-)	0.358

*) thickness measured in x-direction

Table 2-4 Layer thicknesses, relative densities and porosities at test MS-GZB3-B25-40

Parameter	
Thickness upstream GZB3 (m) *	0.38
Thickness upstream B25 (m) *	0.20
Thickness lower protrusion GZB (m) *	0.30
Thickness upper protrusion GZB (m) *	0.30
Thickness downstream B25 (m) *	0.51
Relative Density upstream GZB3 (%)	104
Relative Density upstream B25 (%)	90
Relative Density lower barrier GZB3 (%)	107
Relative Density upper barrier GZB3 (inside protrusion) (%)	95
Relative Density downstream B25 (%)	89
Porosity upstream GZB3 (-)	0.359
Porosity upstream B25 (-)	0.363
Porosity lower barrier GZB3 (-)	0.357
Porosity upper barrier GZB3 (inside protrusion) (-)	0.367
Porosity downstream B25 (-)	0.364

*) thickness measured in x-direction

The relative density of GZB3 at test MS-GZB3-B25-40 is higher than 100%. This may be attributed to measurement uncertainty in both the minimum and maximum density, and the thickness of the layer. The relative density was determined under wet condition.

After the preparation of the sand-bed and the barrier the relative density RD and the porosity n respectively are estimated.

The expected critical vertical heave gradient can be determined by:

$$i_{c,vertical} = \frac{(1-n)(\gamma_p - \gamma_w)}{\gamma_w}$$

GZB MS 38: i_c = (1 – 0.364) 1.65 = 1.049 (upper barrier inside protrusion)
i_c = (1 – 0.362) 1.65 = 1.053 (lower barrier below protrusion)

GZB MS 40: i_c = (1 – 0.367) 1.65 = 1.044 (upper barrier inside protrusion)
i_c = (1 – 0.357) 1.65 = 1.061 (lower barrier below protrusion)

2.4 Adapted conceptual model

For the situation where the barrier penetrates the cover layer due to an upward-facing protuberance, the conceptual model (Deltares, 2020a) is slightly adapted by the results of this analysis of the two additional tests. The model is already described in this chapter to give the reader more guidance in respect to the measurements in Chapter 3. In Chapter 6 of this report the adapted model is compared in more detail to the initial conceptual model.

2.4.1 Pipe initiation and progression

Pipe initiation downstream and progression to the barrier is similar to the situation where the barrier does not protrude into the cover layer. The pipe progresses upstream and is growing immediately further alongside the barrier when having reached it.

2.4.2 Lateral pipe development

When the pipe has reached the barrier, flow inside the barrier is converging to the pipe tip. There appears to be progression of the pipe parallel to the barrier prior to erosion of the barrier. When the pipe along the CSB is deep enough, the support to the vertical side of the barrier is removed and grains from the barrier roll into the pipe, see also the right picture of Figure 1.1. The barrier material at the downstream side of the protuberance is subsiding with the development of the lateral pipe along the barrier.

At the downstream top of the barrier, a flat ellipse is forming along the wall and a slope is forming in the upstream direction. The slope is also widening with the lateral pipe development. At the point where the pipe has reached the barrier, the flow rate is sufficient to transport the eroded barrier grains through the pipe. The pipe progresses further parallel to the barrier, creating a more 2D flow field and a wide slope in the barrier. The erosion ellipse inside the top of the barrier is then widening parallel to the barrier interface due to lateral progression of the pipe downstream of the barrier simultaneously with erosion of the barrier in upstream direction until the lateral erosion is completed.

2.4.3 Slope development in upstream direction

When the lateral pipe development has been completed, erosion is increasing, and the toe of the ellipse is widening along the whole width with only slightly inclined side walls. At a constant head drop, the erosion and upstream progression of the slope is continuing inside the barrier until the crest of the slope reaches the upstream side of the protuberance, forming a nearly symmetric ellipse.

2.4.4 Subsiding of the slope

At a higher head drop, the top of the slope is beginning to lower and flatten along the upstream side of the protuberance. During this period sand is eroding along the whole surface of the slope and

transported over the sand bed to the outlet. The average angle of the slope seems not to change much because the toe of the slope also lowering and widening with a comparable intensity and velocity. Finally, the toe of the slope subsides underneath the downstream bottom edge of the protuberance, making an open connection between the void inside the protuberance and the pipe of the downstream sand bed. From that moment, the opening begins to widen slowly, and the intensity of sand erosion and transport decreases rapidly. The slope is flattening further with additional load increments.

2.4.5 Failure

After applying the last load step, erosion is occurring mainly along the toe of the slope and suddenly failure occurs. The lower part of the slope moves horizontally downstream while the crest of the slope is moving downward. It appears that the heave process in the lower part of the slope, where the vertical sand volume is less heavy than at the upstream side of the slope and the gradients perpendicular to the slope are higher, is the critical process that determines the stability of the slope and hereby the stability of the barrier by reducing effective stress between the grains. The average outward gradient at the slope surface in the centre of the barrier is around 0.7

The lower part of the slope is fluidizing and sliding downstream. Because of the limited open space below the bottom edge of the protuberance, not all material of the sliding slope can move to the downstream sand bed, but accumulation occurs in front of the downstream part of the protuberance and the crest of the slope is lowering along the upstream side of the protuberance. Subsequently, the upstream background sand is also fluidizing around the centre line of the set-up and moving downstream beneath the protuberance whereby a blowout occurs in the upstream part of the protuberance.

3 Analysis of experimental results

This chapter analyses the experimental results of the two medium-scale experiments with a protuberance of the CSB (Deltares 2020b). In Chapter 3.1.4 some brief considerations regarding the failed test MS39 are also given.

First, an overview of the observations is provided. Subsequently the measurements are addressed. A large amount of data was collected, therefore only the most significant topics are presented here.

3.1 Observations

3.1.1 Pipe and slope progression – observations and measurements

During the experiment visual inspections were carried out during regular intervals. Hereby, five key stages were identified, indicating the observation at the end of that stage:

I – Pipe reaches barrier
II – Lateral development along the barrier complete
III – Slope reaches upstream edge
IV – Slope upstream edge fully developed, and toe of slope connected with pipe
V – Failure

Between stage III and IV there is a moment when the toe of the slope reaches the bottom edge of the protuberance and an open connection between the pipe and the void of the protuberance occurs, which can be seen in the head development measured by the transducers.

In this section, the piping process is described, combining visual observations with head measurements and laser measurements in order to facilitate the overall understanding.

3.1.1.1 Test MS-GZB3-B25-38

The following sequence of events was observed:

There are inevitable minor height differences in the bulkhead – B25 interface. These provided some space for the B25 to loosen upon horizontal positioning of the test box, particularly in the corners, which provided a preferential flow path for the pipe at the sides of the test box. During progression of the test, as the flow increased, the pipe development occurred at the centre line of the set-up.

Stage I:
After 01:05 hours from start the pipe which has developed along the side of the box reaches the barrier at a head difference of 0.16 m (Figure 3.1 MS 38. End of stage I: the pipe has developed along the margin of the sand bed and reached the barrier after 1:05 hours at H_up = 0.16 m [joined-23021000423_20200715 164401_IMG_1061]Figure 3.1).
The head is kept constant for another 30 minutes. Coarse sand particles are being deposited, but also transported to the outlet. The lateral pipe development seems to stop after a length of 10 cm and the amount of transported coarse sand particles is decreasing (Figure 3.2). The measured flow is 0.7 l/min.

Figure 3.1 shows the result of pictures taken by 4 cameras. The image combines the results of four camera perspectives. Four digital single lens reflex (DSLR) cameras have been used to log the progress of the experiments. Two cameras were mounted above the set-up for a view from above (camera 1 above the upstream sand bed and camera 2 above the downstream sand bed), one

camera was facing the upstream side of the CSB protuberance (camera 3). The fourth camera was mounted on top of the cylindrical outflow, facing the downstream side of the CSB protuberance. Note that the fourth camera is facing the protuberance under an angle. For interpretation purposes the photos of this camera have been transformed in order to correct for perspective.

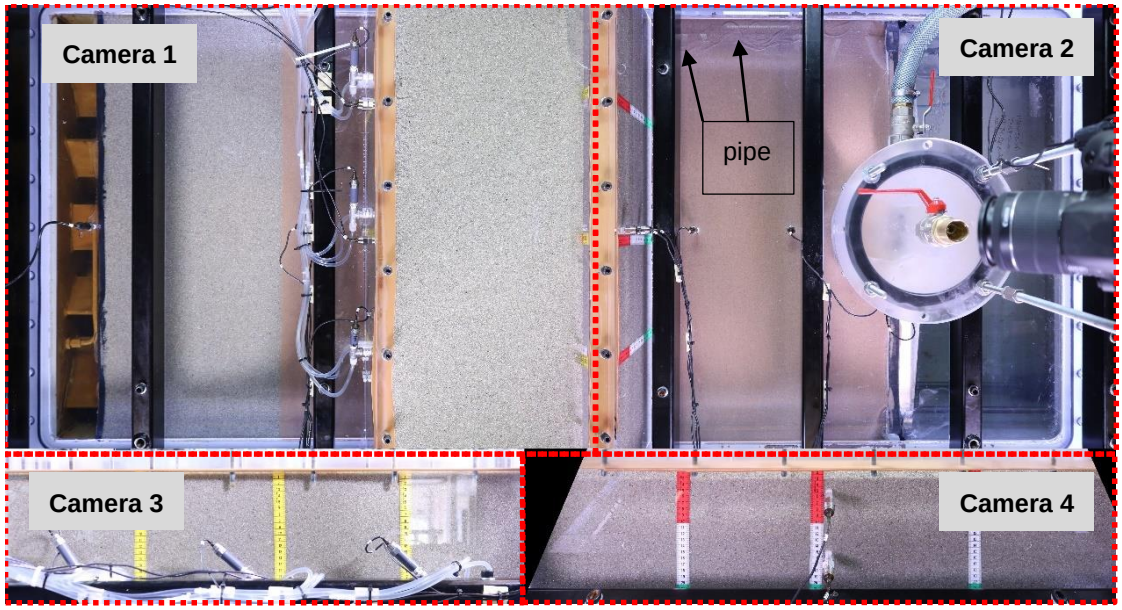

Figure 3.1 MS 38. End of stage I: the pipe has developed along the margin of the sand bed and reached the barrier after 1:05 hours at H_up = 0.16 m [joined-23021000423_20200715 164401_IMG_1061]

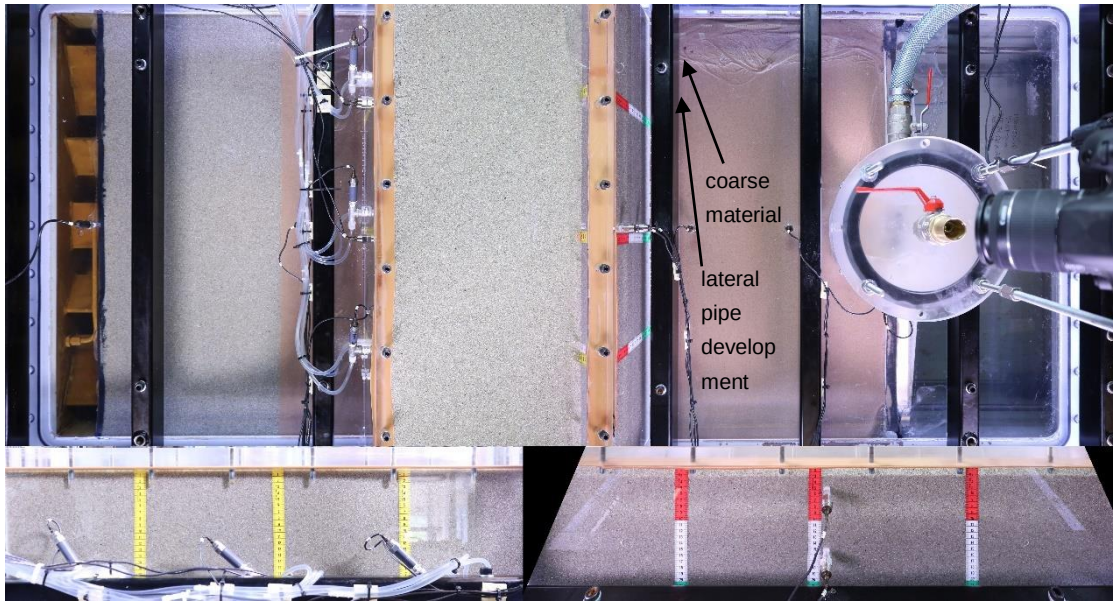

Figure 3.2 MS 38 after 1:35 hours from start at H_up = 0.16 m; lateral pipe development along barrier and coarse particle transport via the meandering pipe [joined-23021000423_20200715 171401_IMG_1241]

Stage II:

The head difference is increased with increments of 5 cm per 5 minutes up to 0.66 m. The lateral pipe is growing further along the barrier. The amount of eroded coarse particles is increasing. The coarse particles that paved the sand-bed cause changes in the pipe position. The particles are transported to the outlet. The main pipe is moving to the centre line of the set-up. The downstream edge of coarse sand barrier is subsiding.

After 2:25 hours from start the lateral development of the pipe along the barrier is completed (Figure 3.3). The maximum subsidence of the toe of the slope is 6 cm and the angle of the slope is 11°. The flow is 8.5 l/min.

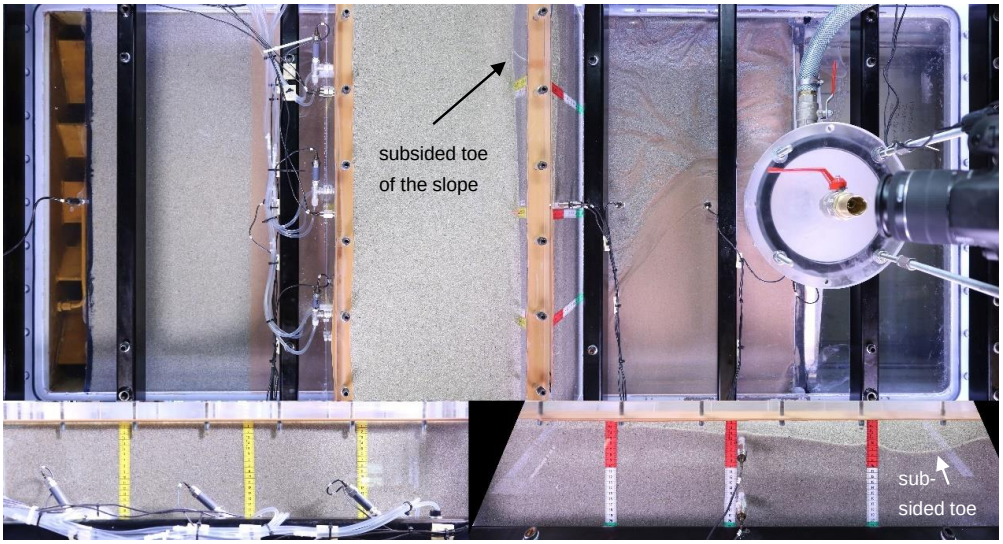

Figure 3.3 MS 38 after 2:25 hours from the start at H_up = 0.66 m. the lateral pipe development along the barrier is completed. Much of the coarse material is eroded and transported over the sand bed to the outlet. The barrier material at the downstream side of the protuberance has subsided 6 cm. [joined-23021000423_20200715 180401_IMG_1541]

Stage III:

The head difference was increased with increments of 5 cm per 5 minutes up to 1.01 m. After 3:10 hours from start the top of the slope has reached the upstream edge of the protuberance (Figure 3.4). (In test MS40 the next applied head - after the lateral pipe development was finished - has been kept constant, so that the top of the slope developed to the upstream side without increasing the head). The toe of the slope has also subsided. The whole downstream sand bed is covered by coarse sand. The pipes are evenly distributed and not clogged by coarse particles. The maximum subsidence of the toe of the slope is 21 cm, flow is 12 l/min and the maximum angle is 35°.

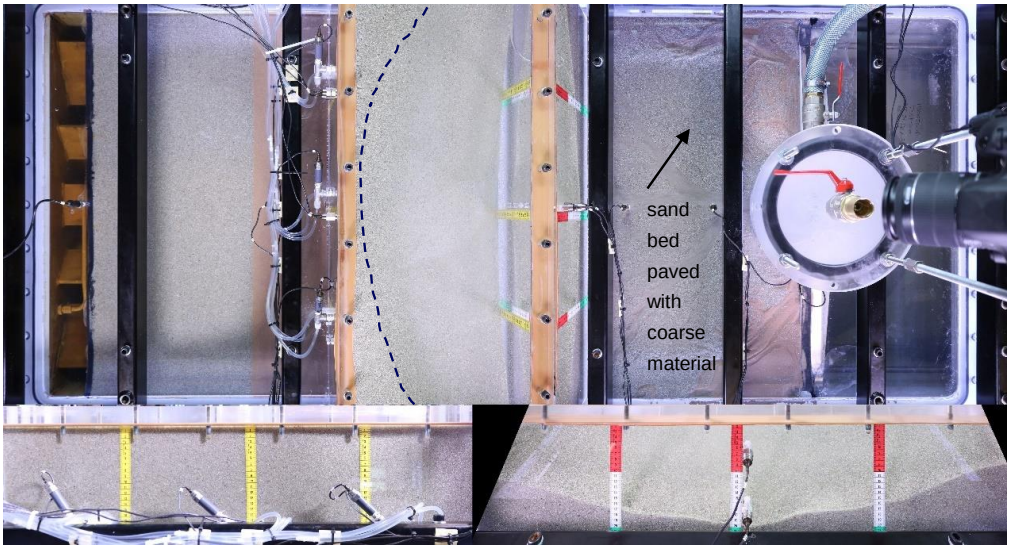

Figure 3.4 Test MS 38 after 3:10 hours from the start. The top of the slope reached the centre of the upstream edge of the protuberance at H_up = 1.01 m. [joined-23021000423_20200715 184901_IMG_1811]

Stage IV:
The head difference has been kept constant at 1.01 m. The erosion process is continuing very actively. Coarse sand is eroding along the whole surface of the slope. After 3:34 hours the toe of the slope has reached the bottom edge of the downstream protuberance, thus the bottom of the cover layer. An open connection between the protuberance and the pipe hole is emerged. See Figure 3.5. The flow rate is still 12 l/min.

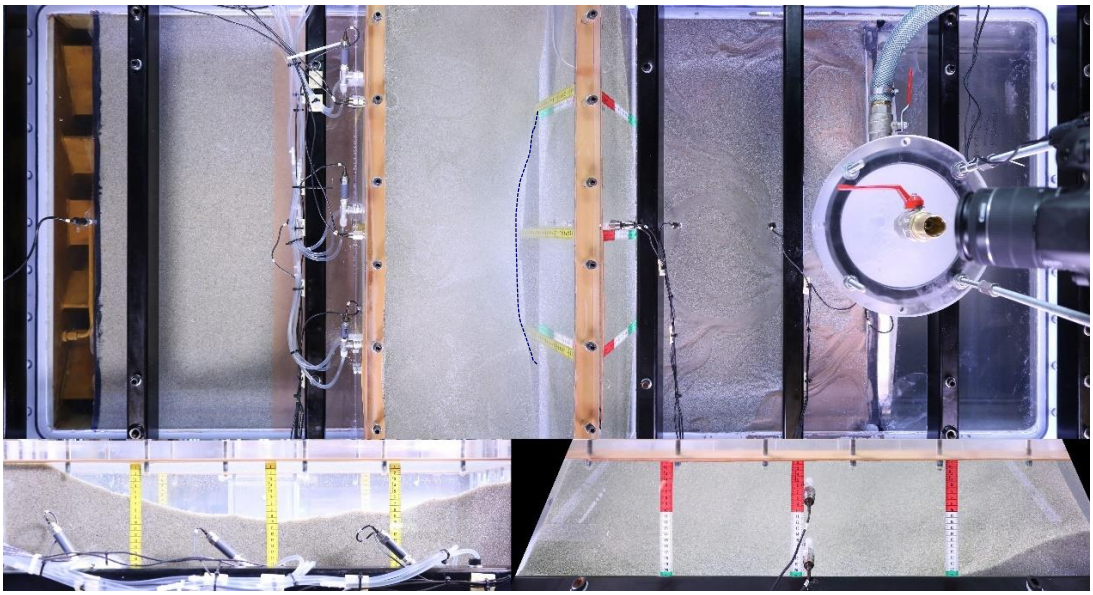

Figure 3.5 Test MS 38. After 3:34 hours m from the start at H_up = 1.01 an open connection emerged at the toe of the slope [joined-23021000423_20200715 191301_IMG_1955]

Within 30 seconds the toe of the slope has reached its lowest position, approximately 2 cm below cover layer, see Figure 3.6Figure 3.6 Test MS 38. The flow rate increases to 13.8 l/min. On the upstream edge of the protuberance the slope has also taken shape of a nearly symmetric curvature with its lowest point in the centre line of the set-up 20 cm high, resulting in an average angle of approximately 36°. The slope has taken shape of an amphitheatre.

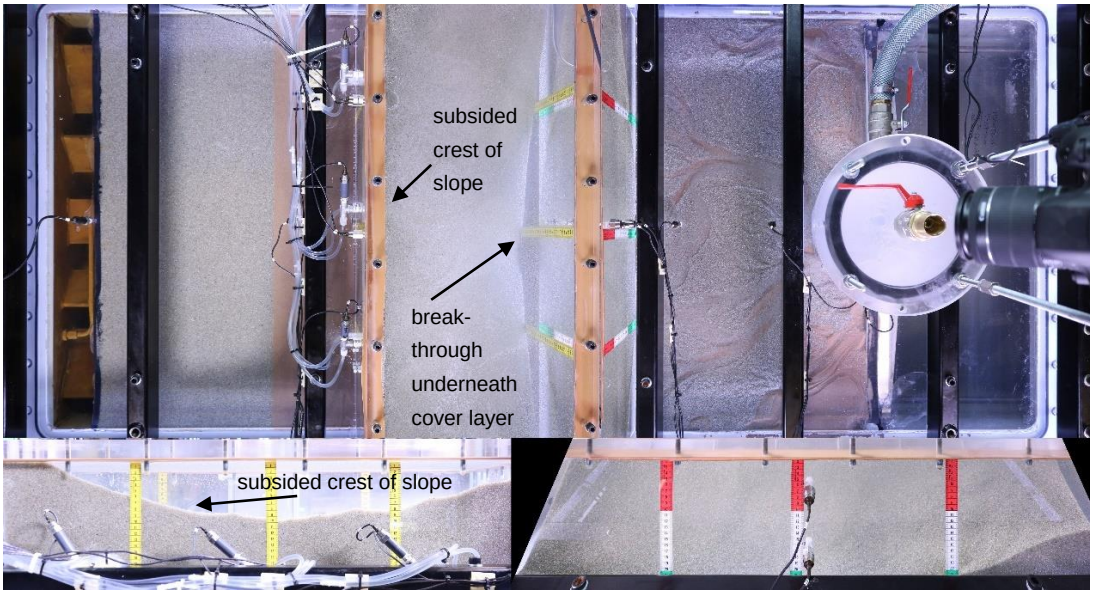

Figure 3.6 Test MS 38. After 3:34:31 the toe of the slope has reached its lowest position. [joined-23021000423_20200715 191331_IMG_1958]

After 5:50 hours from the start the head difference is increased in increments of 10 cm per 30 minutes until a head difference of 1.31 m. The flow rate increases little with every load step. Directly after the first head increase there is evident slumping of the slope surface, particularly in the centreline of the amphitheatre, but this comes to a standstill very fast. Then increments of head difference of 5 cm per approximately 30 minutes up to a head difference of 1.71 m were applied. This load was kept constant for 3:25 hours without showing any appreciable erosion. Then the load is increased in increments of 10 cm and 15 cm, starting with small slumpings which eventually come to a standstill again.

The last head difference before failure is at 3.96 m after 22:45 hours (Figure 3.7). The flow rate at this stage is 52 l/min. The lowest part of the upstream slope shows a subsidence of 16.5 cm (the western side of 13.6 cm and the eastern side a subsidence op 15.5 cm). This means that the upstream part of the slope has a stable minimum height of 13.6 cm before the last load step to failure. Assuming a depth of the pipe at the edge of the protuberance of -2.0 cm, the slope has a minimum angle of 27° (centre line) (respectively left-hand 31.5° and right-hand 28.8°)

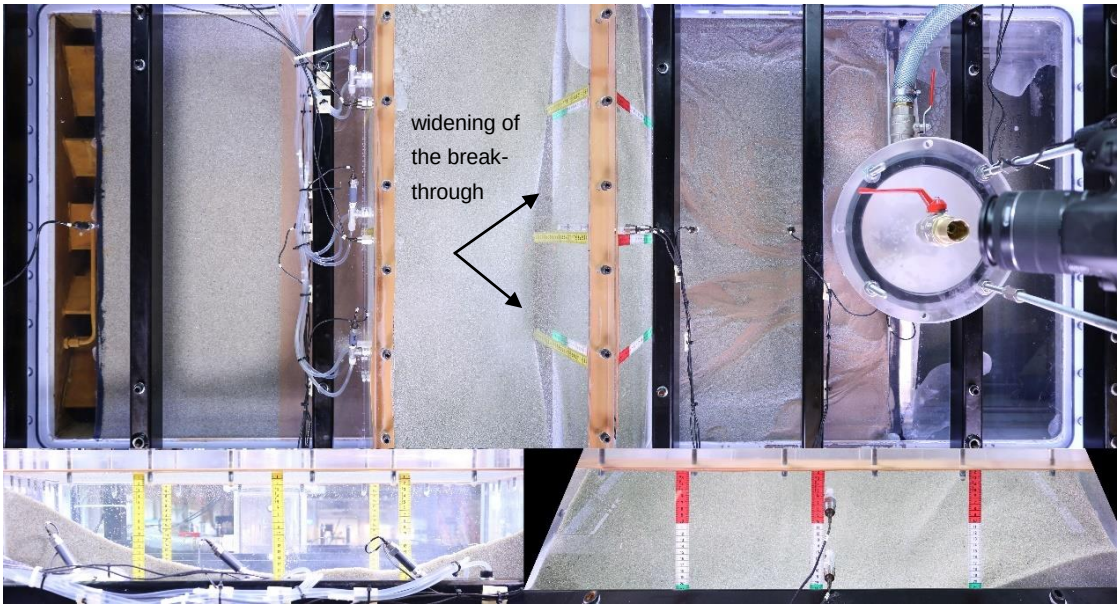

Figure 3.7 Test MS 38. Situation after 23:05 hours at H_up = 3.96 m [joined-23021000423_20200716 144441_IMG_8985]

Stage V:
The last increment of 10 cm is applied after 23:05 hours after the start (Figure 3.8 and Figure 3.9). At this load step erosion of the slope surface starts, the crest of the slope is subsiding, then the slope starts to turn, and a slip surface seems to occur (Figure 3.11 and Figure 3.12). The flow rate before failure is 53.4 l/min. The flow rate during failure was not measured.

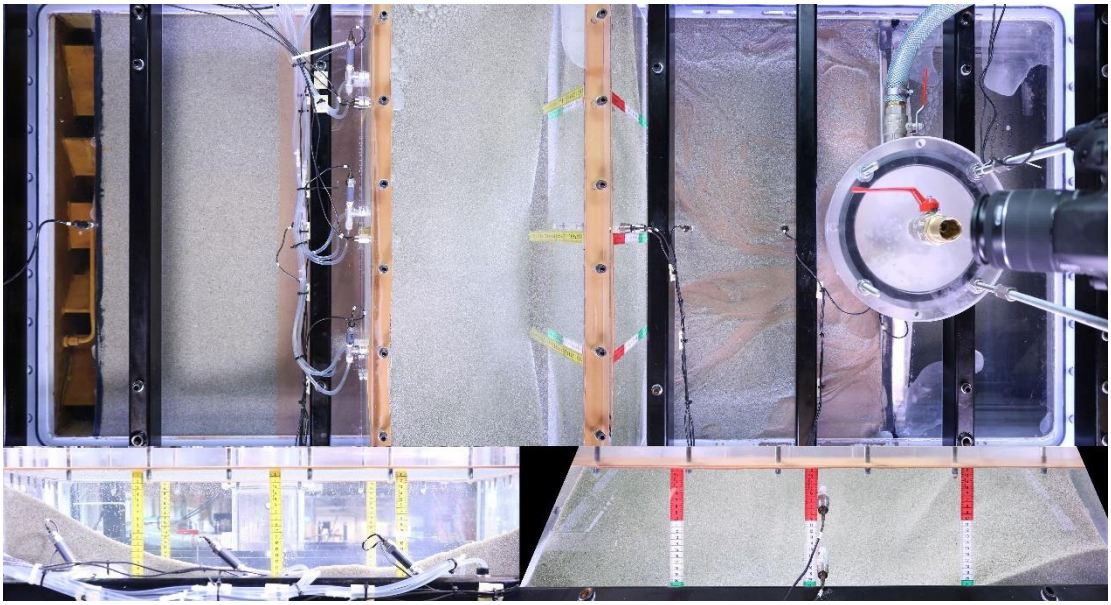

Figure 3.8 Test MS 38 at H_up = 4.06 m: start of subsidence of the slope crest [joined-23021000423_20200716 144501_IMG_8987]

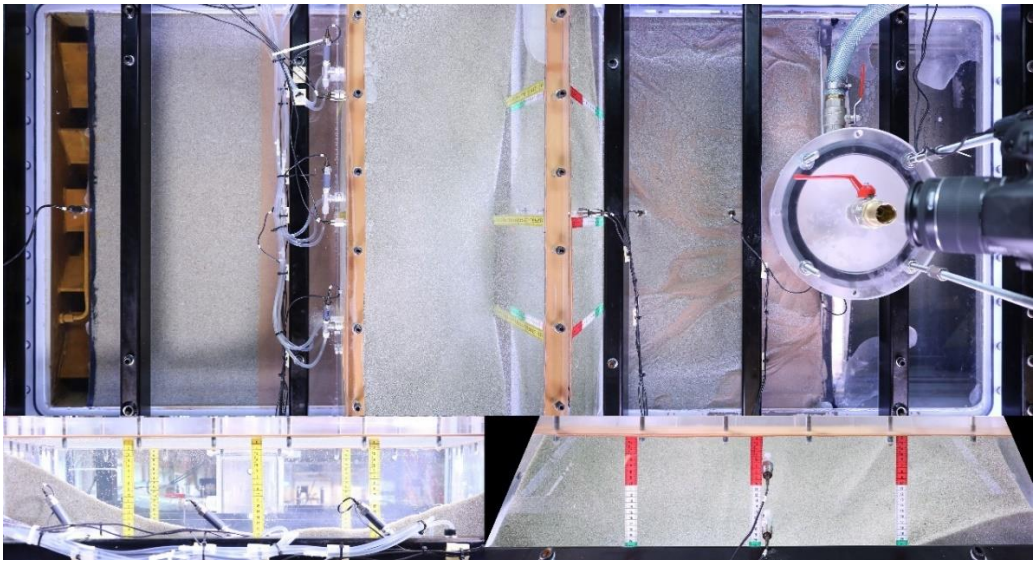

Figure 3.9 Test MS 38 at H_up 4.06 m; subsidence of slope crest during failure [joined-23021000423_20200716 144531_IMG_8990]

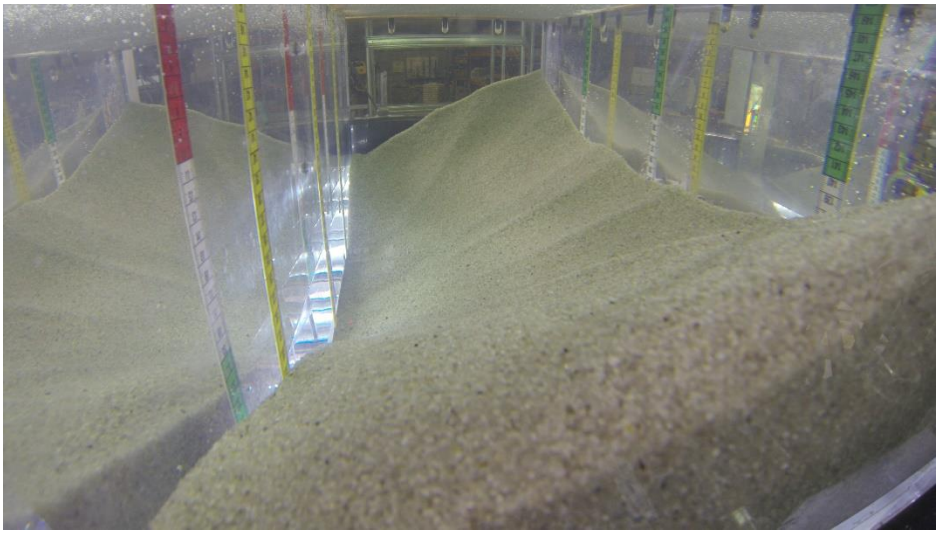

Figure 3.10 Test MS 38, end of stage IV. Situation before applying the last load step.

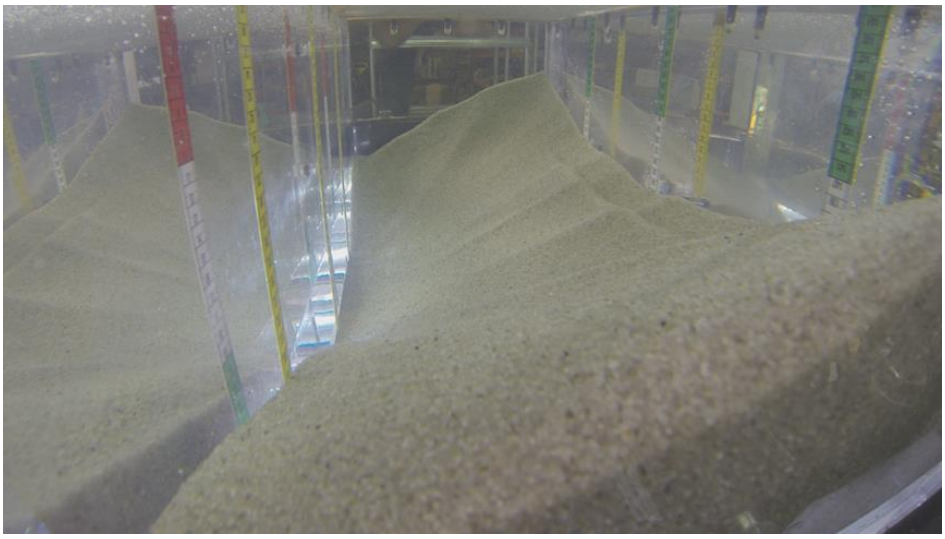

Figure 3.11 Test MS 38, beginning of slope failure. The toe of the slope is subsiding.

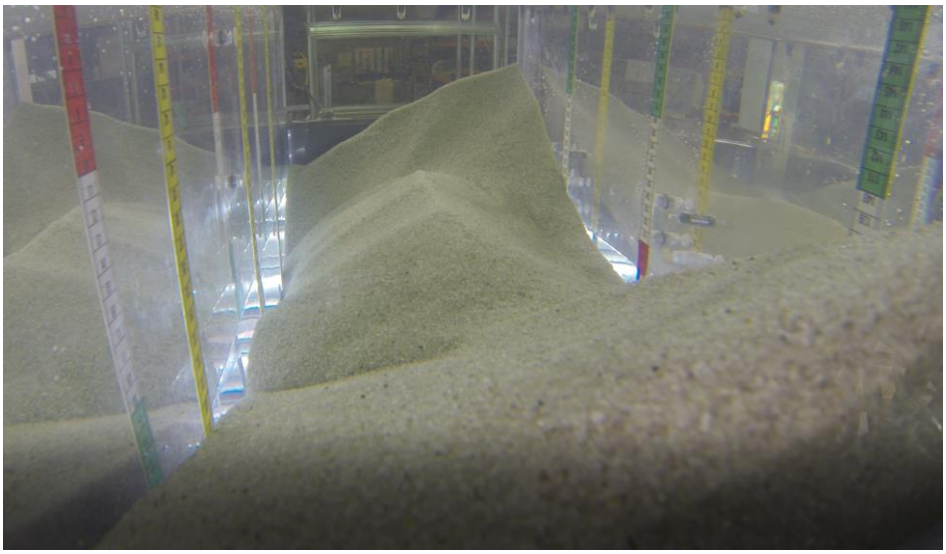

Figure 3.12 Test MS 38, sliding slope at slope failure, MS 38, see also text 3.1.2

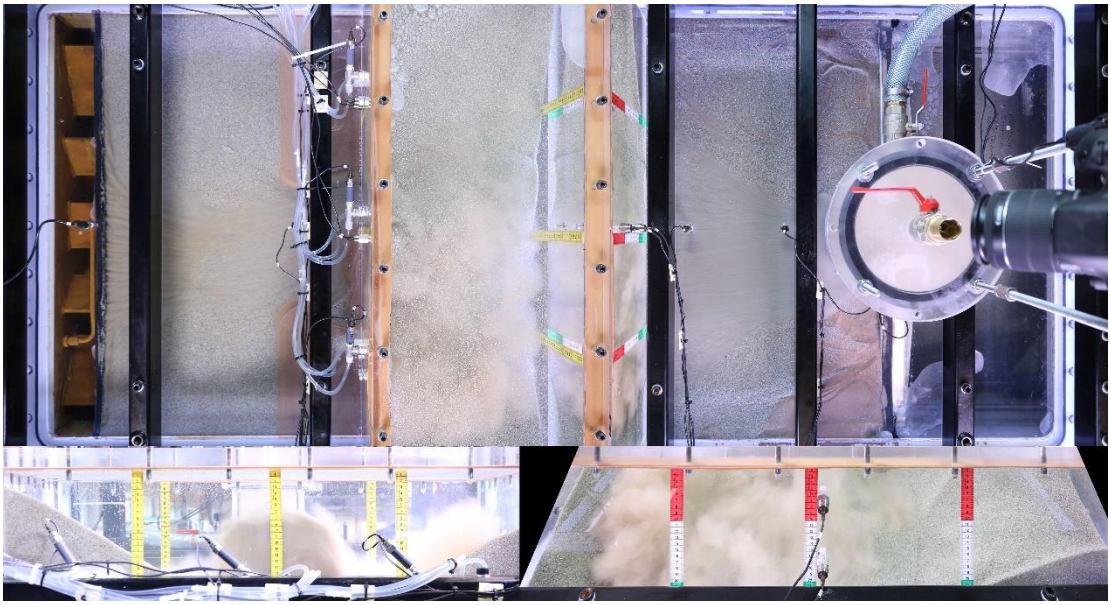

Figure 3.13 Test MS 38. Liquefaction of upstream sand bed and blow-out at upstream side of protuberance after slope failure [joined-23021000423_20200716 144541_IMG_8991]

Figure 3.13 shows the moment of blow-out at the upstream side of the protuberance and fluidisation of the upstream sand bed. From the GoPro footage we can conclude that the process of sliding before the blowout took approximately 15-30 seconds.

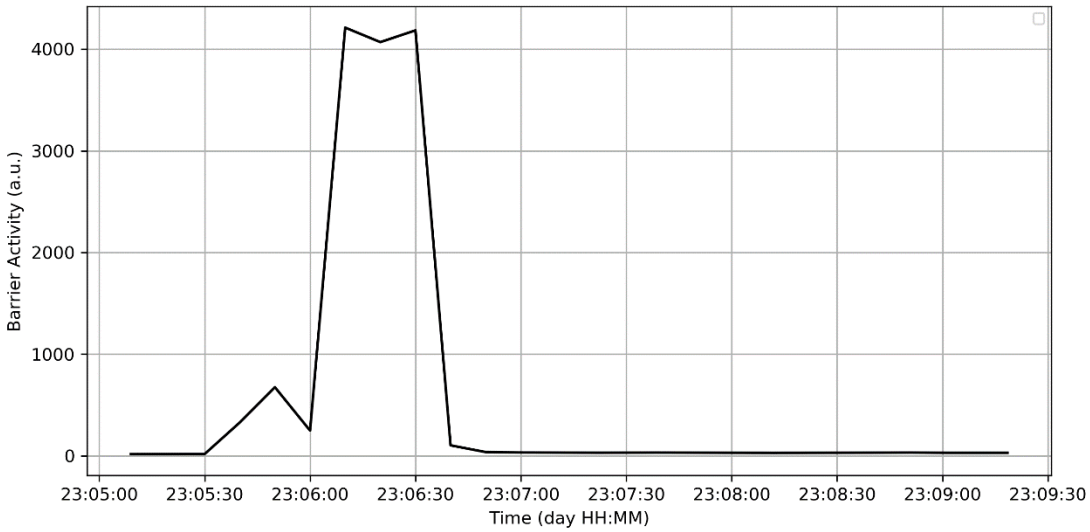

Figure 3.14 Barrier activity in test MS-GZB3-B25-38 around failure.

Figure 3.14 gives an impression of the activity of particle movement in the barrier (making use of Particle Image Velocimetry). The data of camera four (downstream side of the CSB) has also been used to identify moments of movement in the CSB material. Because the image of camera 4 also shows movement inside the barrier (i.e. the data from camera 4 is not a flat plane), the magnitude and direction of movement are rather arbitrary. Therefore, the sum has been taken of all the measured vertical and horizontal displacements for each photo pair and this has been plotted over time. The units of activity are thus for qualitative purposes only but provide a good basis for identifying movement inside the barrier. The first (lower) peak is a result of the slope sliding, the second (higher) peak is a result of the blowout. The turbidity of the water dissipates after a minute by sedimentation of the particles.

3.1.1.2 Test MS-GZB3-B25-40

The size and duration of the loading steps were chosen based on expert judgement, using the experience of Test MS-GZB3-B25-38. The slope reached the upstream side at a head of 1 m. The load has been kept constant for some time at a level of 59 cm, 64 cm, 69 cm and 299 cm to evaluate the effect of longer duration on the erosion process.
The following sequence of events was observed:

Stage I:
After 01:35 hours the third pipe developing in the centreline of the box (i.e. the then only still active pipe after some small pipes that stopped in the background sand) reaches the barrier at a head difference of 0.17 m (Figure 3.15). The flow is 1.0 l/min.

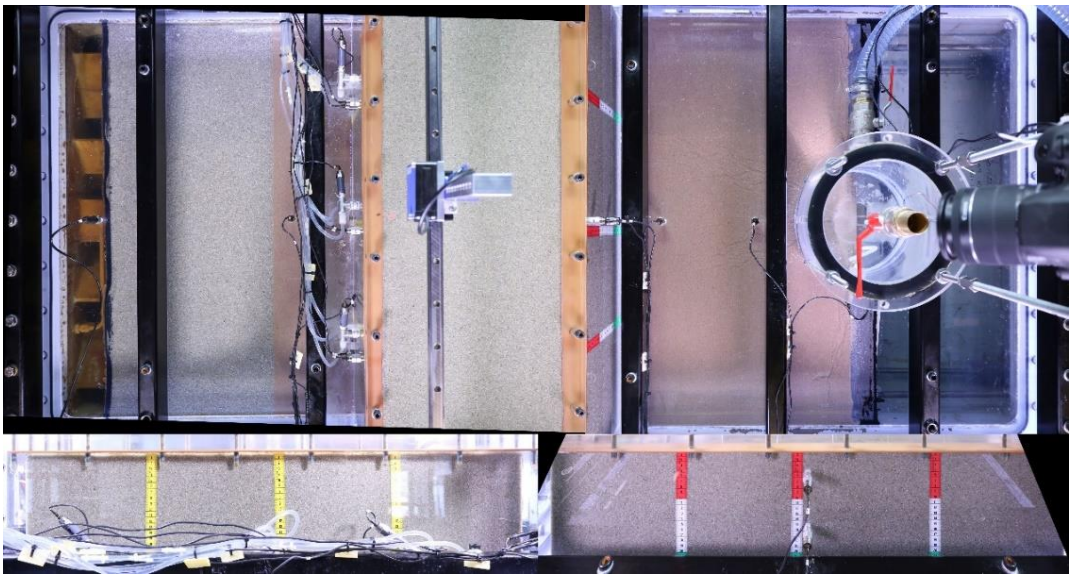

Figure 3.15 Test MS 40 after 1:35 hours. The main pipe reaches the barrier at H_up = 0.17 m. [joined-03072022625_20200805 103500_IMG_3857]

The head is kept constant for another 10 minutes. Coarse sand particles are being eroded and transported to the outlet through the pipes. The top of the downstream CSB subsides 5 mm in the vicinity of the pipe (Figure 3.16).

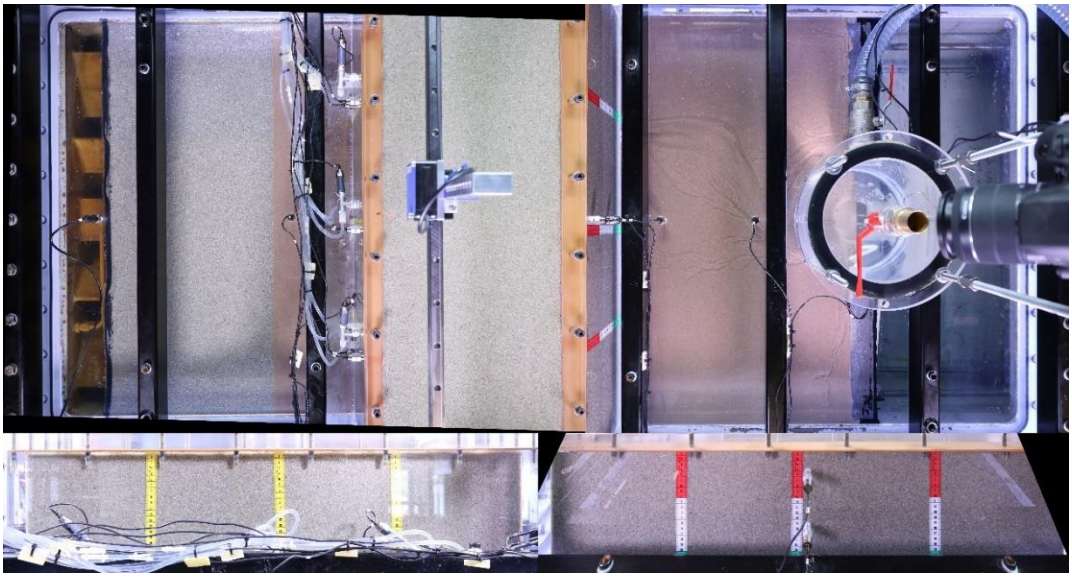

Figure 3.16 Test MS 40 at 1:45 hours, still at H_up = 0.17 m coarse sand is eroded, and a wide fan of pipes has developed. [joined-03072022625_20200805 104500_IMG_3917]

Stage II:

After 3:30 hours the lateral pipe development along the barrier is completed (Figure 3.17). The head difference is at that moment 0.54 m and the flow rate is 7.5 l/min. The coarse sand at the upstream edge of the protuberance is subsided 20 mm over a length of 20 cm. The coarse particles are transported to the basin behind the bulkhead. There is only little pavement of the downstream sand-bed.

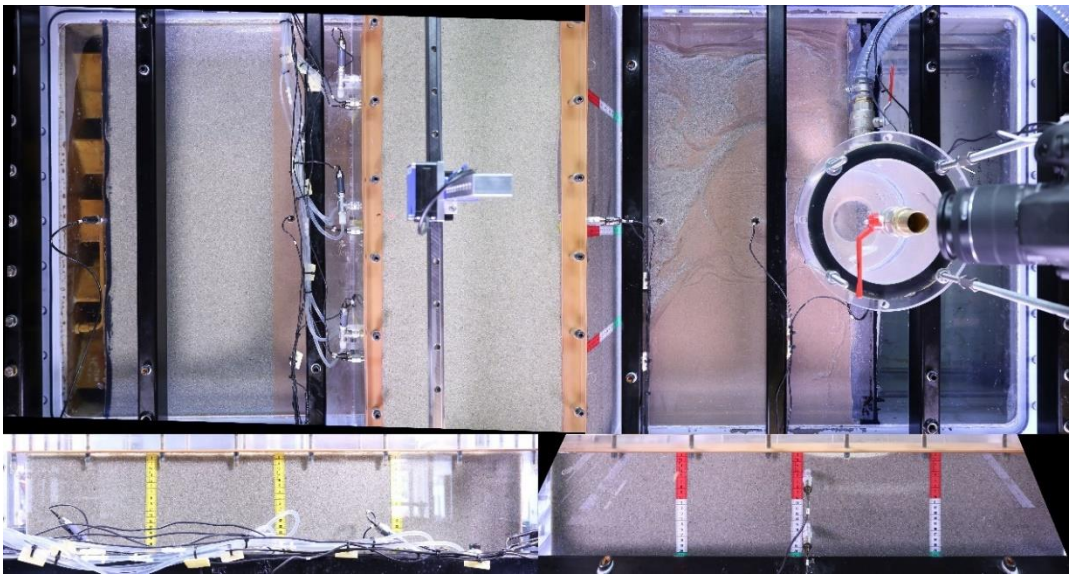

Figure 3.17 Test MS 40. After 3:30 hours the lateral pipe development is completed. H_up 0.54 m [joined-03072022625_20200805 123500_IMG_4577]

Stage III:

Then the head difference is increased two times with an increment of 5 cm to 59 cm and then to 64 cm. The first load step is held for 105 minutes, the second load step for 3:20 hours.

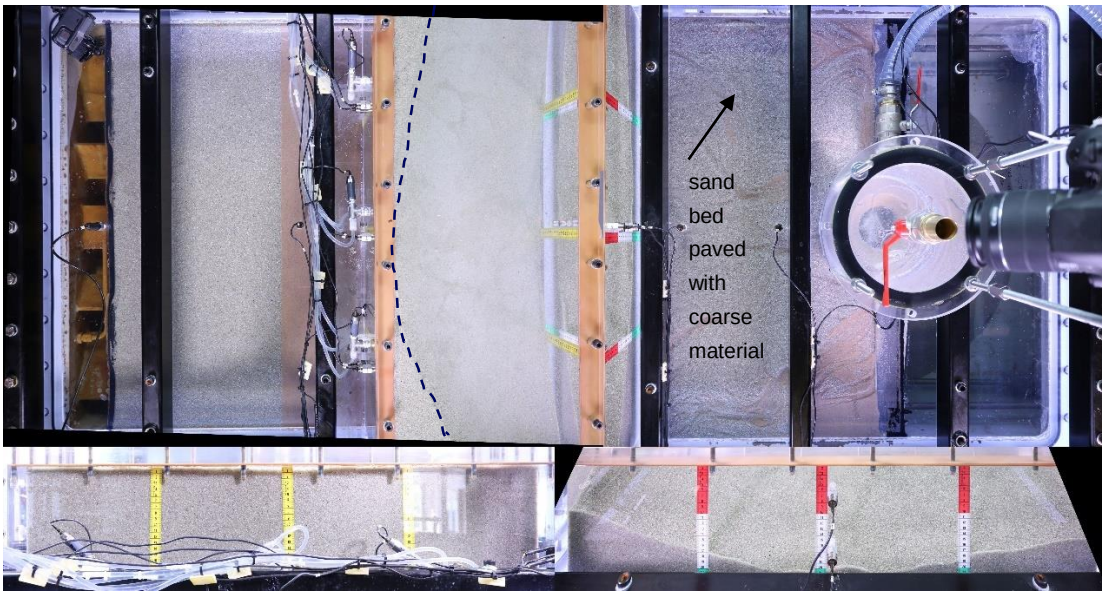

Figure 3.18 Test MS 40. After 8:45 hours the top of the slope has reached the upstream edge of the protuberance [joined-03072022625_20200805 175000_IMG_6467]

The top of the slope has reached the upstream edge of the protuberance after 8:45 hours after the start (Figure 3.18). The flow rate at this stage is 8.8 l/min. The toe of the slope in the centreline of the set-up has 20.5 cm subsided at that moment. The curvature of the downstream part of the barrier in the protuberance is relatively symmetric. The slope has an angle of approximately 35°.

Stage IV:
Then an additional load increment of 5 cm is applied for 2:10 hours. The flow is 9.9 l/min. The top of the slope shows a nearly symmetrical curvature. 10:45 hours after the start the toe of the slope reaches the bottom edge of the protuberance and a connection to the pipe occurs (Figure 3.19).

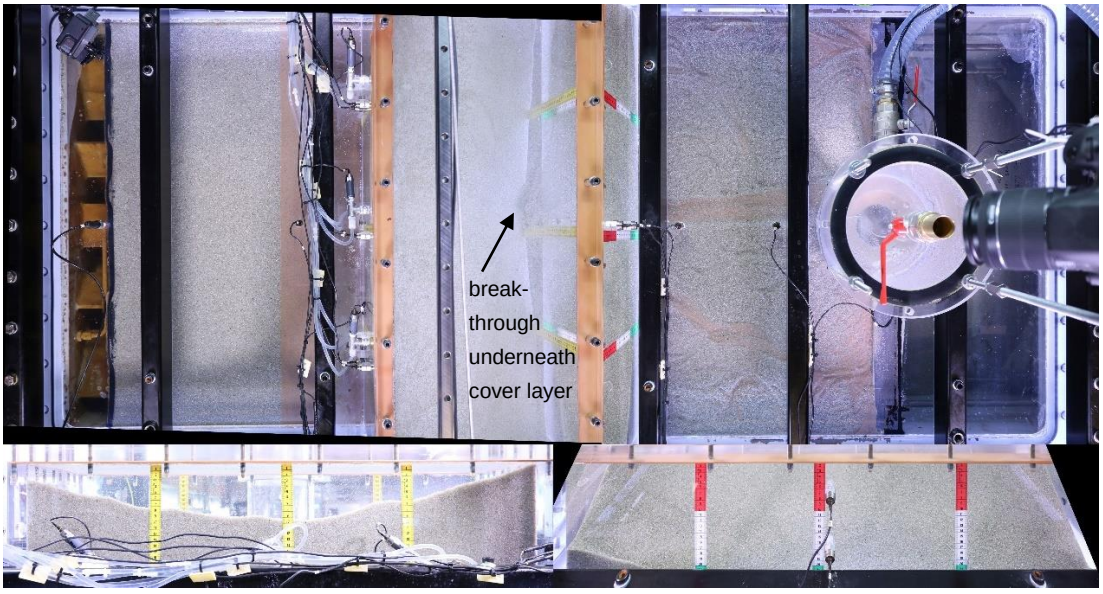

Figure 3.19 Test MS 40: The toe of the slope has subsided below the upstream edge of the protuberance after 10:45 hours at an applied head difference of 0,69 m [joined-03072022625_20200805 195051_IMG_7192]

At that moment the crest of the slope was subsided with 9 cm and the centre line, 7.5 cm on the left and 6 cm on the right reference tape. After the breakthrough when the slope toe has subsided below the cover layer making a connection between the void inside the protuberance and the pipe, the head was increased with increments of 10 cm. The whole surface of the slope began to move (erode) jerkily at the end of the head elevation, causing a little subsidence of the crest, but in the remaining time of each load step there was no further erosion observed.
After 16:30 hours from start, the applied head H_up (299 cm) has been kept constant for two hours. In that period the crest of the slope kept a constant level at the central, left and right reference tape of 14.5 cm, 11 cm and 13 cm respectively. No particle movement has been observed in this period, which also justifies that the head had not been kept constant for a much longer period.

After that long-term load the head was increased with several 10 cm increments. The surface of the slope eroded in the same way as before with little jerky movements across the whole surface just after the increase in head.

After 23:55 hours from start (before applying the final load step) the head difference was 4.69 m. The flow rate at this step is 62.8 l/min. The lowest part of the slope crest has subsided 19.5 cm at the left measuring tape, 14.5 cm in de centre line and 18 cm at the right measuring tape (Figure 3.20). The pipe depth is approximately 2 cm. This means the lowest slope angle is approximately 22° (centre-line) (and left-hand 25° and right-hand 30° respectively).

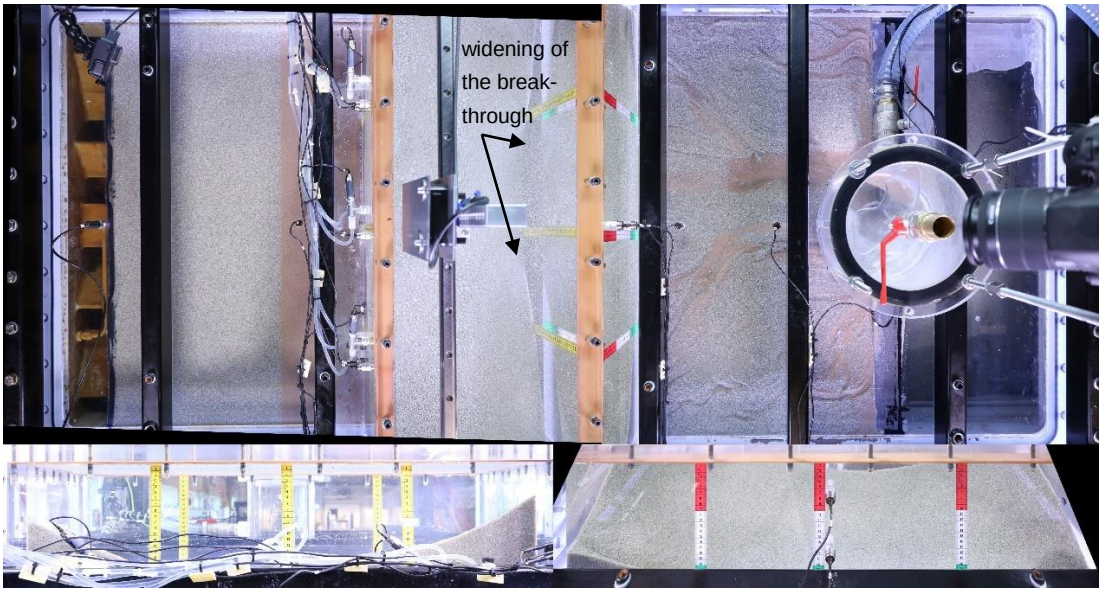

Figure 3.20 Test MS 40 at H_up = 4.69 m after 23:55 hours. The connection with the pipe is widening. The crest of the slope has subsided. [joined-03072022625_20200806 091009_IMG_2841]

Stage V:
After 24:05 hours the last load increment of 10 cm additional head difference is applied. The load at failure is 4.79 m. This is the applied load read at the water reservoir A. Figure 3.21 shows the situation at the moment of applying that load, followed by erosion of the coarse sand along the whole surface of the slope (Figure 3.22 and Figure 3.23).

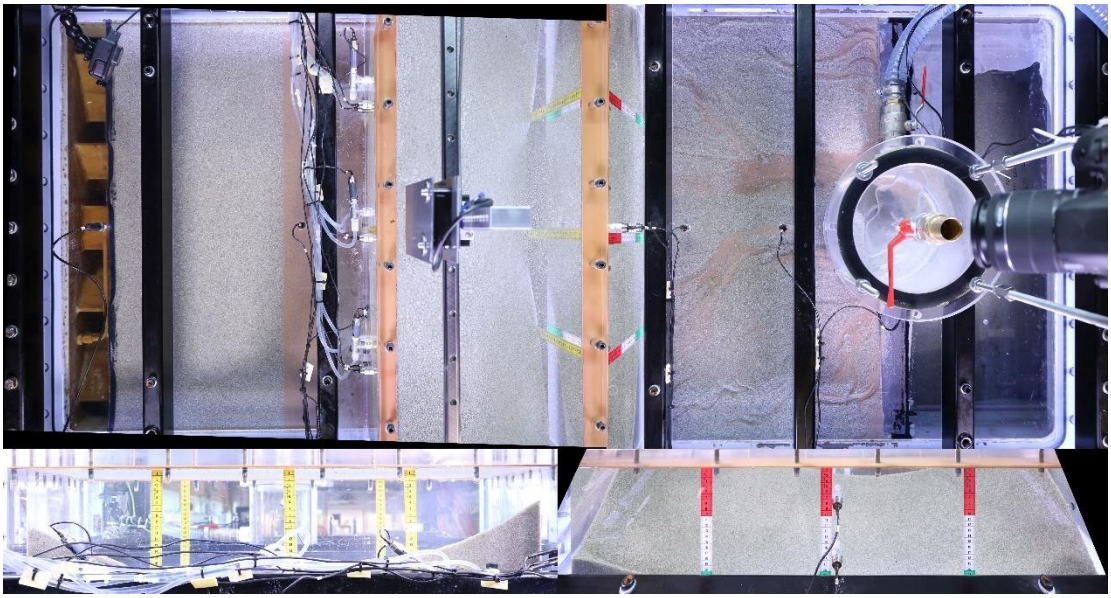

Figure 3.21 Test MS 40. Coarse sand is eroding along the whole surface of the slope. Much coarse sand is transported to the downstream sand bed. [joined-03072022625_20200806 091020_IMG_2843]

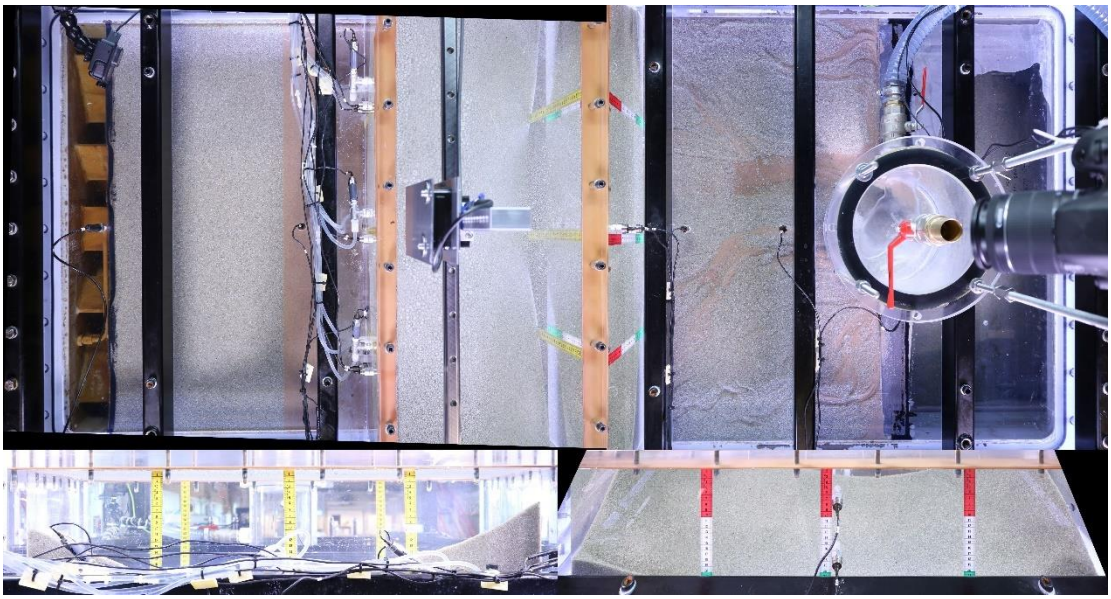

Figure 3.22 Test MS40. [joined-03072022625_20200806 091024_IMG_2844]

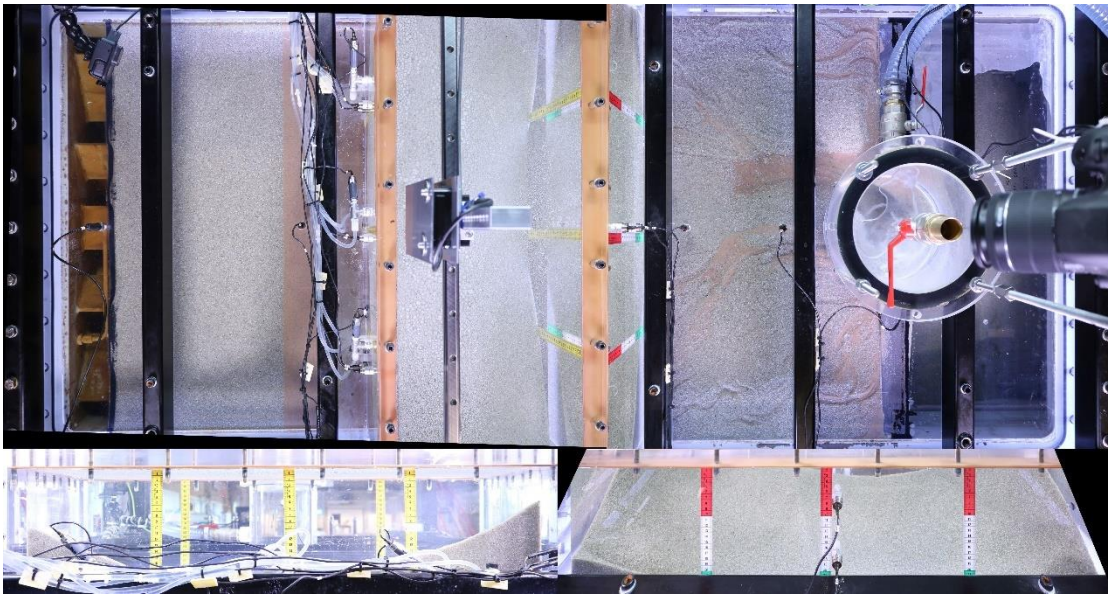

Figure 3.23 Test MS 40 [joined-03072022625_20200806 091029_IMG_2845]

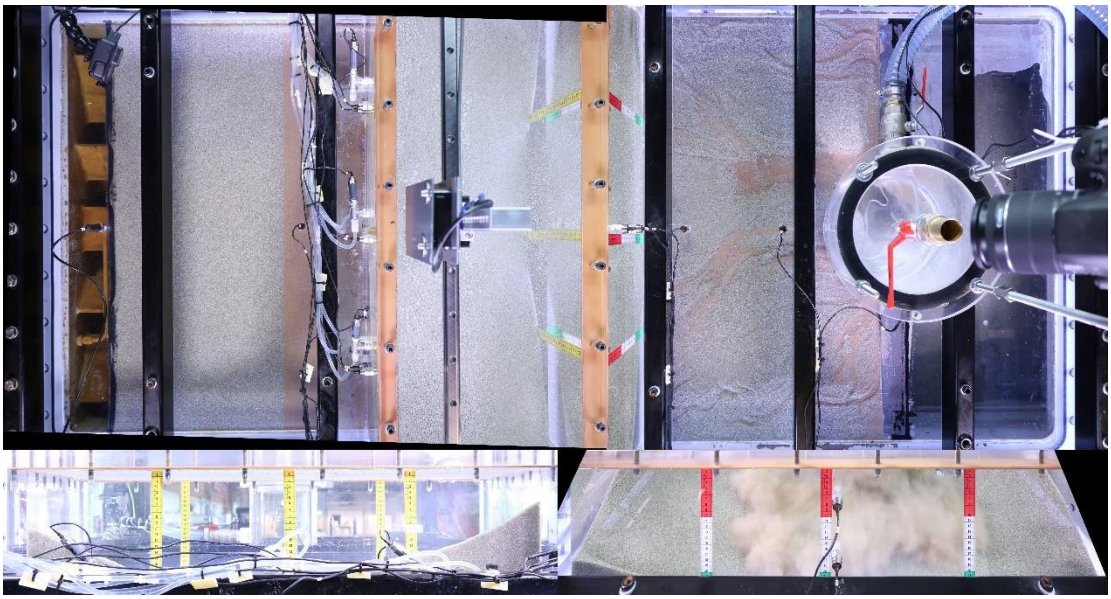

Figure 3.24 Test MS 40. This figure shows the situation during slope failure. There is a little asynchronism at camera 4 which runs faster than the other cameras. Camera 4 shows already the start of the blow-out [joined-03072022625_20200806 091035_IMG_2846].

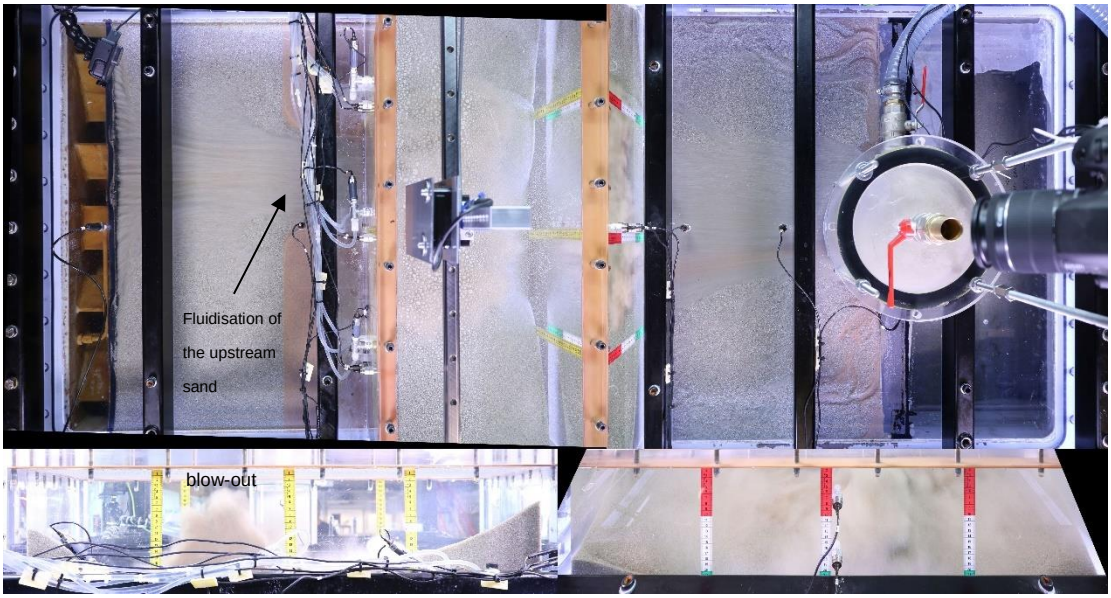

Figure 3.25 Test MS 40. Fluidisation of the upstream sand and blow-out at the upstream edge of the protuberance [joined-03072022625_20200806 091040_IMG_2847]

Figure 3.26 MS 40. Sliding of the slope resulting in an increase of coarse sand moving above the downstream sand bed. (seen from the downstream side).

Figure 3.24, Figure 3.25 and Figure 3.26 show the moment of sliding of the slope from different directions. From a comparison of GoPro footage from the moment of failure, seen from the upstream and downstream side of the protuberance (Figure 3.27), it can be concluded that after the last load increment has been applied a strong erosion process was starting. Sand particles were moving over the whole slope surface and transported to the downstream sand bed. This is also visible on the photos taken from above the set-up. The upstream sand bed was still intact, when the crest of the slope was already sliding. The crest of the slope was subsiding first, followed by an upward movement of the lower part of the slope, pushing this part against the downstream wall of the protuberance. Subsequently, the upstream sand bed begins to fluidize and move downstream. Finally, there is a blowout at the upstream edge of the protuberance. From this we can conclude that the barrier slope is sliding along a slide surface below the lower edge of the protuberance (i.e. at a level below the cover layer).

Figure 3.27 Sequences of the failure mode at MS40, seen from the downstream (left) and upstream side (right) at the same point of time.

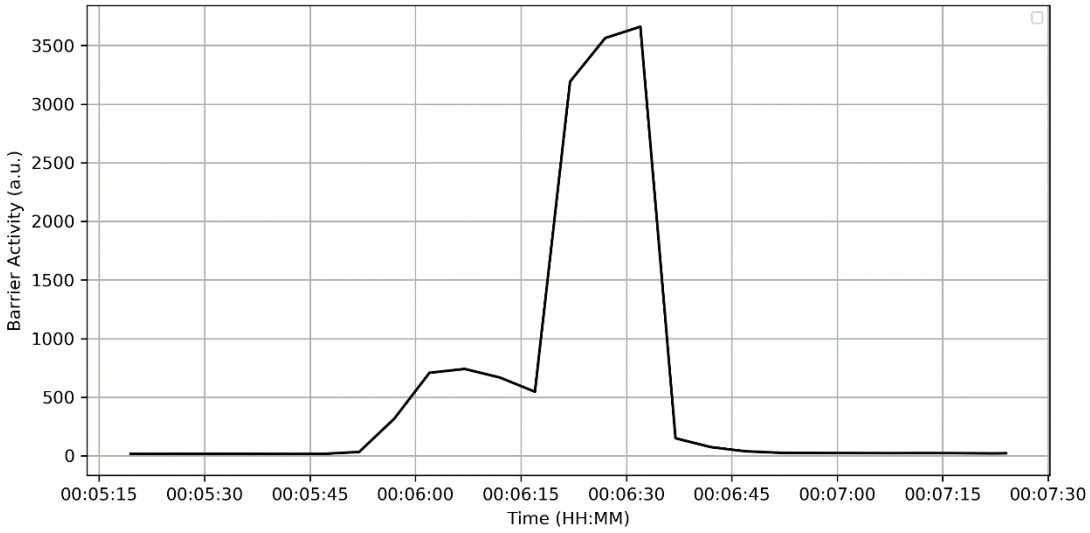

Figure 3.28 Barrier activity in test MS-GZB3-B25-40 around failure.

Figure 3.28 gives an impression of the activity of particle movement in the barrier (making use of Particle Image Velocimetry). The first (lower) peak is a result of the slope sliding, the second (higher) peak is a result of the blowout. The turbidity of the water dissipates after a minute by sedimentation of the particles.

3.1.2 Slope formation

As the pipe reaches the CSB and the depth of the pipe is large enough, the situation as sketched in Figure 3.29 occurs.

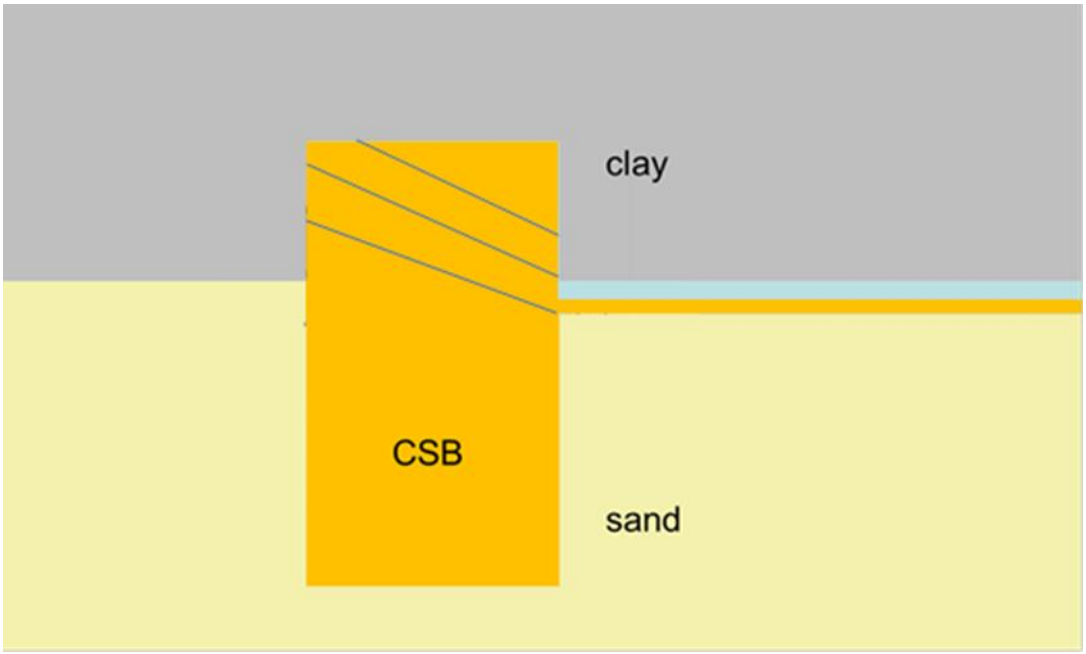

Figure 3.29. Sketch when pipe reaches the barrier.

Since this sandy CSB material has no cohesion, this is not a stable situation. Sand from the CSB will migrate into the pipe and in the protuberance a slope will be formed. The CSB sand will spread over the downstream background sand. In the beginning there will be a slope as shown with the highest diagonal dark line in the CSB, later this will be lowered to the lower line and at the end of this process, it will be the lowest line. It should be realized that until the lowest line is reached, the slope is not stable, thus as soon as the pipe from downstream reaches the barrier and the CSB

starts to erode, there is no equilibrium until the slope reaches the lowest line. This explains the high barrier activity between 06:15 and 06:40 in test MS40 (Figure 3.28). Afterwards, erosion is much less, because there is now a more or less stable situation. The slope flattened a bit and there is limited erosion until there is failure. The ratio between the head difference at which the instability of the CSB sand in the protuberance occurs because pipe from downstream reaches the barrier and the complete failure of the barrier was 1 to 4 in this case. This means that when there is quite some erosion and a sand boil will occur in the field, there is still a considerable safety against failure.

3.1.3 Slope failure analysis

The mechanism that initiates failure in these tests is important for the applicability of the CSB in the field. Since the situation in the field can only partly be simulated during the tests, the field situation can only be predicted if the mechanism is known. Both tests MS38 and MS40 failed the same way, see section 3.1.1, therefore it is concentrated on test MS40 in this section.
The theory, before the execution of these tests, was that the higher hydraulic head over the set-up causes an outward directed gradient over the slope and a vertical gradient on the very upstream side of the CSB. This was based on numerical calculations as shown in Figure 3.30.

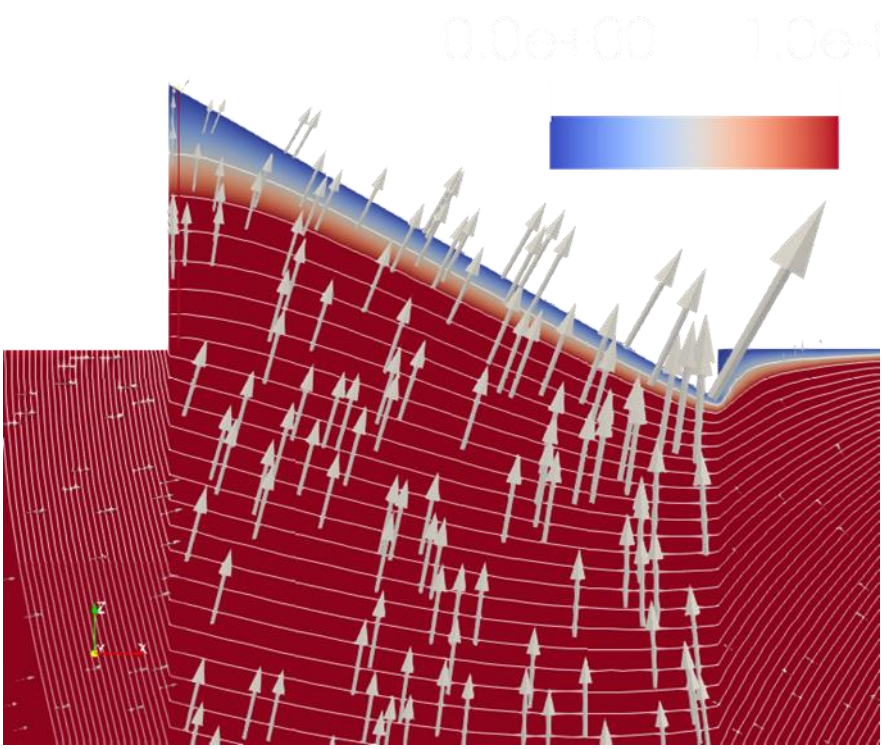

Figure 3.30 Result of numerical prediction. The length of the grey arrows indicates the flow velocity (taken from 11200952-057-GEO-0006, see there for more details on the calculations).

Looking more in detail to the arrows the largest arrows are calculated at the lower part of the slope. At a certain moment this leads to an instable slope at the lower end, see Figure 3.11. Because the upper part has lower gradients, this does not fail in the same direction but sinks vertically downwards into the space created by the failing lower part of the slope, Figure 3.12.

Just before failure, the background sand upstream is loaded with a hydraulic gradient of around 17 (approximately 3.4 m of head difference over 0.2 m of fine background sand). Such a head cannot exist in the background sand unless it is ‘locked’. If there is no horizontal stress acting on the upstream background sand from the CSB, it will fail due to the high hydraulic loading (without locking in, the maximum horizontal gradient the sand can withstand is around 0.7, the tangent of the friction angle).

The upstream background sand was ‘locked’ downstream by the CSB, until this fails due to the high gradient as described above. Regarding the loss of geotechnical stability as a result of loss of effective stress due to a high horizontal gradient upstream the barrier, see Appendix C.

Shortly (0.5 s) after that slope failure in the CSB occurs, the upstream background sand starts to move and pushes the CSB sand downstream, creating a temporarily steep slope until fluidisation of the fine sand occurs inside the protuberance leading to total failure. The sequence is shown in the pictures below (Figure 3.31 until Figure 3.34). These show the set-up just before and during failure of test M40 and the pressure distribution. A vertical blue line shows the time that corresponds with the pictures. Pictures are synchronised by hand, so a small time shift between the 2 pictures and the plot in the figures is possible. After the test it was also found that fine B25 sand had moved into the CSB (Deltares 2020b). A maximum thickness of 0.05 m of B25 sand was found in the CSB.

The pictures showed that very soon (0.5 s) after initial slope failure in the upstream part fine sand starts to penetrate the CSB sand. This leads to a decrease in pore pressure at location P9 (upstream the barrier where the fine sand starts to move). Fluidisation in the upstream part of the CSB occurs after the fine sand has moved into the barrier. The low pressure temporarily measured at P9 is likely caused by dilatation of the fine upstream background sand. This has a high relative density and can therefore only move after some dilation.

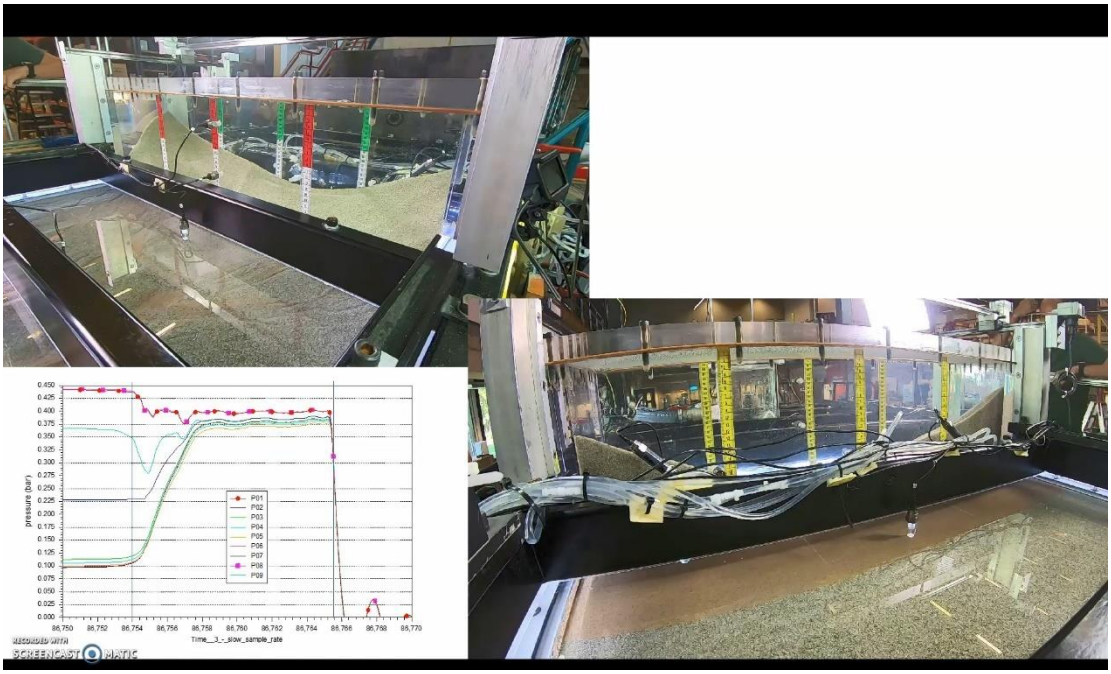

Figure 3.31 Test MS40 at the start of slope failure, see failure surface at top of slope in the upper left figure.

Figure 3.32 Test MS40. This is the moment that the slope is already sliding (left image). On the right image there is still no movement of the upstream sand bed noticeable.

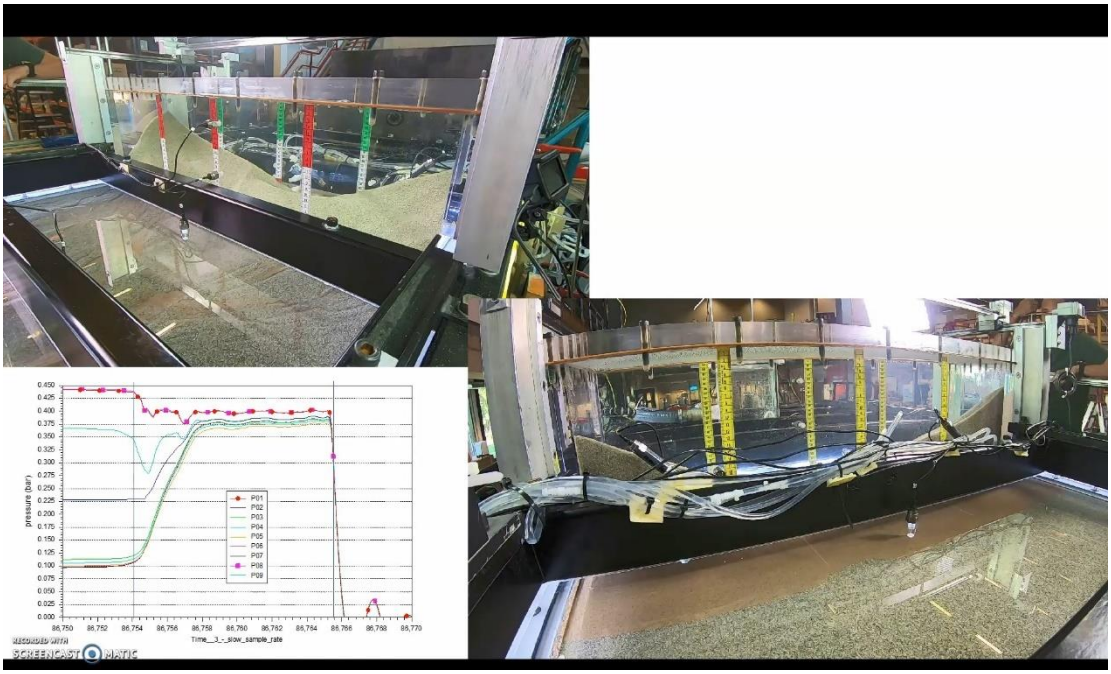

Figure 3.33 Test MS40, half a second later than previous plot (Figure 3.31). Upstream sand starts to move.

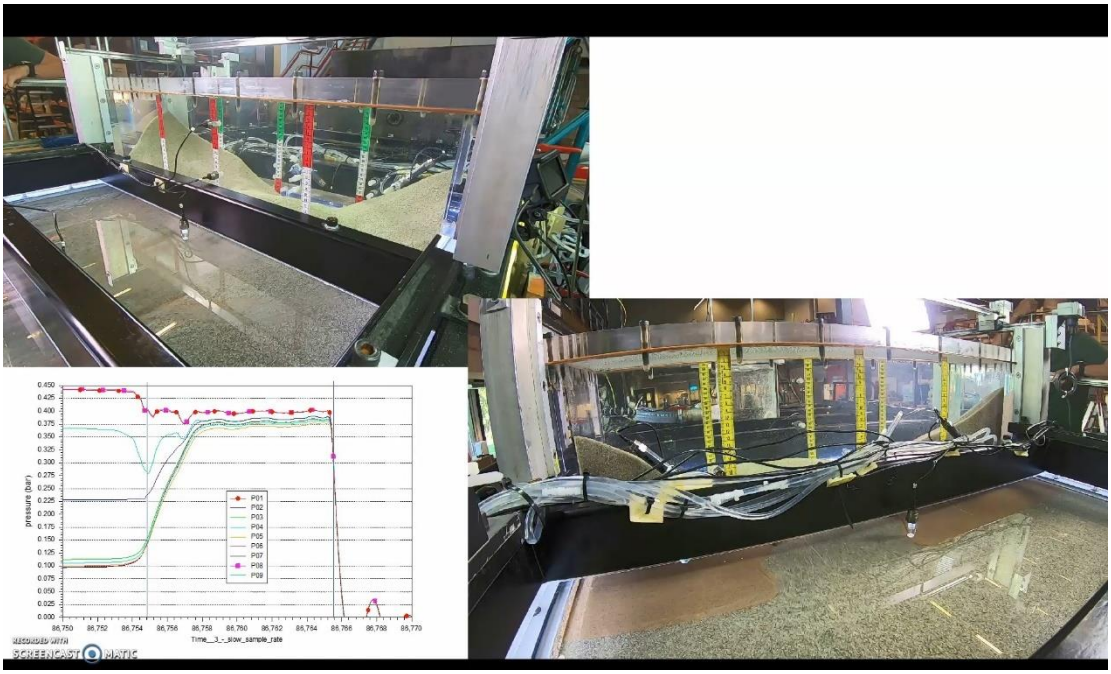

Figure 3.34 Test MS40, minimum in pore pressure for P9 (upstream fine sand). 1.2 s after previous figure.

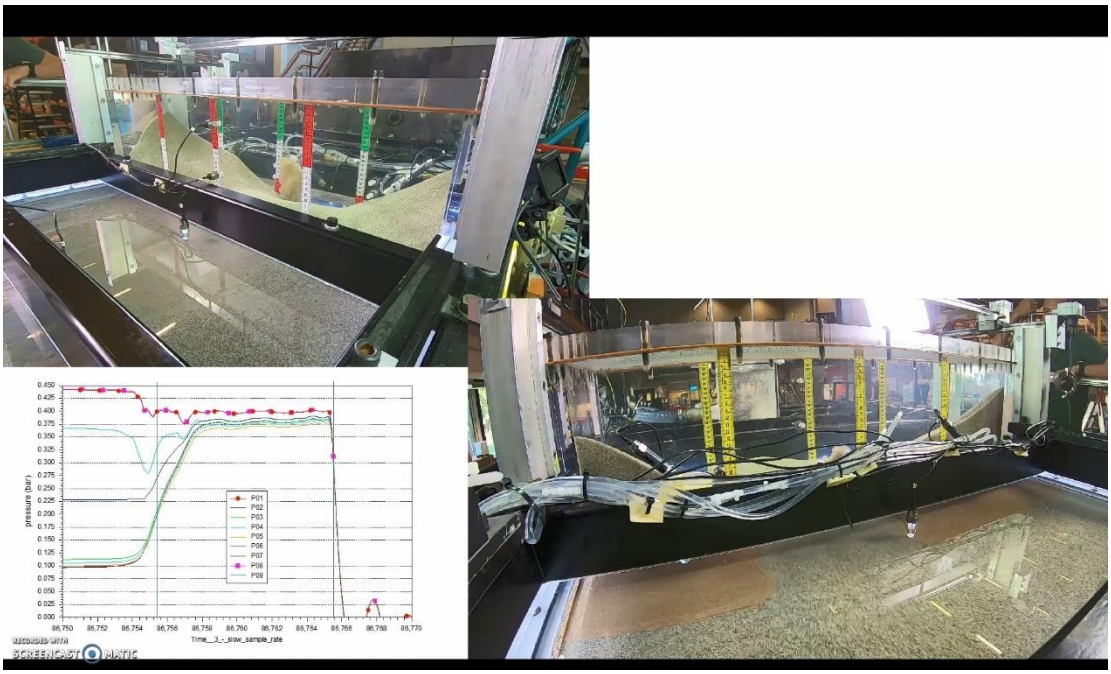

Figure 3.35 Test MS40, start fluidisation upstream of CSB, 0.5 s after previous

Looking at the results of the pore pressure gauges, it is remarkable that the ones on the upstream side of the model show a limited decrease in pore pressure, all others show an increase during failure. The reason for that can be seen in Figure 3.36. This figure shows the same pore pressure measurement as the graph in the pictures Figure 3.31 until Figure 3.34), but now also shows the measured discharge. The discharge was measured continuously only in this test by weighing the amount of water discharged continuously. The plot shows that during failure the discharge through the model nearly doubles. The reason for the larger discharge is that the flow resistance in the whole model significantly decreases, leaving the largest flow resistance at the outflow location. Consequently, the pressure is high in the whole model.

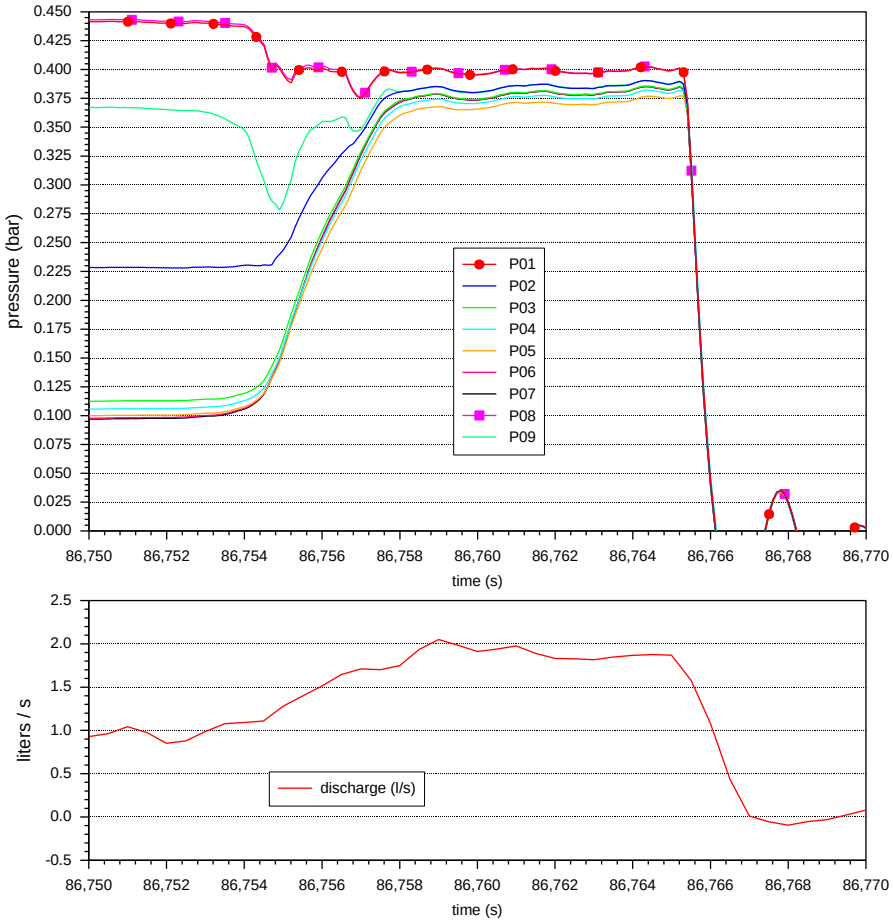

Figure 3.36 Test MS40, pressure distribution during failure and discharge.

The measured vertical gradients at the upstream side of the CSB have reached values close to one during failure. Therefore, it is concluded both possible failure modes, slope instability and fluidisation of the upstream side of the CSB occurred in these tests very shortly after each other. Based on the measurement results it cannot evidently be excluded that fluidisation of the upstream sand column occurred after the fluidisation of the barrier material. The criterion for failure is a low effective stress in the CSB, this can lead to fluidisation but also to instability. Both failure mechanisms do not occur when there is still a high effective stress in the GZB as in test MS39 (see next section).

Figure 3.36 shows the development of the heads upstream the barrier (top sand bed: p09; bottom sand bed: p01), directly upstream the barrier at the bottom (p03) and inside the protuberance (p06). The applied head p08 remains constant to some extent. P06 inside the protuberance shows a strong increase of head during failure. Before failure there is a low head in the protuberance because of the connection of the void with the pipe. During failure the pressure is increasing across the whole set-up because of the decrease in flow resistance in the model and the increased pressure drop over the outlet hole due to the increased discharge.

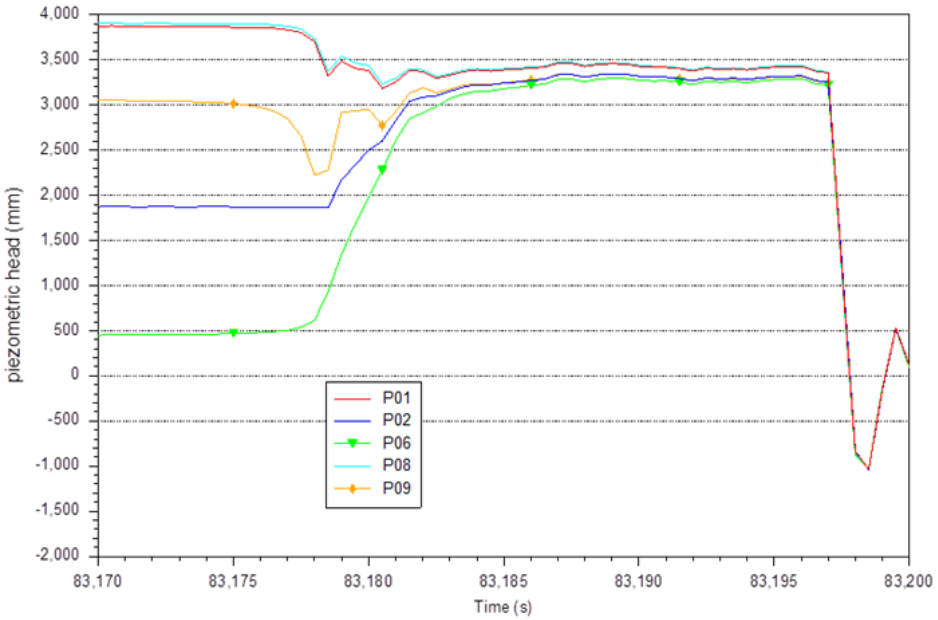

Figure 3.37 Test MS38, pressure distribution during failure for upstream gauge p09 and gauge p06 (inside the protuberance) and p01 (upstream bottom sand bed) and p02 (bottom barrier). P08 is the applied head.

3.1.4 Test MS39

The set-up of Test MS-GZB3-B25-39 was a copy of the Test MS-GZB3-B25-38. During the execution of this test with a comparable loading as the previous one, it appeared that there was clogging at the interface between the upstream coarse sand and the upstream fine sand, see Figure 3.38 at the arrow. This results in a considerable decrease in discharge during the test even when the head difference was increased. In this test the head difference was increased up to 5.5 m (the maximum difference that could be reached over the set-up). Even at this maximum head difference there was no failure of the barrier.

It should be realized that there is a pressure difference of 5 m water column over the 0.21 m of sand upstream of the barrier. However, this appeared not enough to induce failure of this sand layer nor the barrier. This means that the reduction of the effective stress in the barrier due to ground water flow in the barrier is essential for the failure of the barrier.

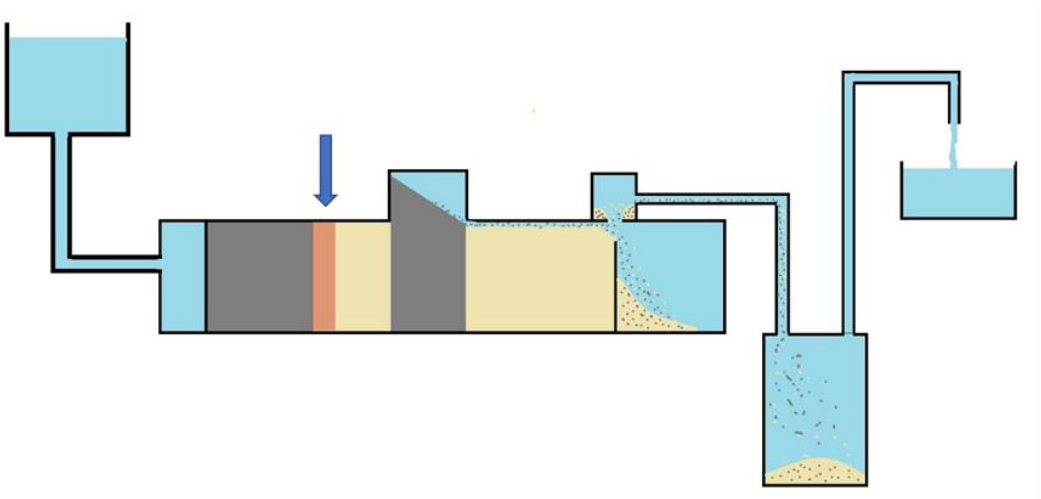

Figure 3.38 Set-up with indication where clogging occurred in Test MS-GZB3-B25-39

3.2 Head measurements

The head applied and registered as the height of the variable constant head of the container A in Figure 2.2 differs a bit from the head upstream of the inlet filter in the set-up box, measured by the transducer P08. The head upstream of the filter (measured by the transducer) increases less with respect to the head in the container H (Figure 3.39 shows the divergency for test MS 40). This is maybe due to resistance (roughness of the inside wall) in the hoses and the three 90° bends of the set-up, and due to some constrictions at the tap couplings.

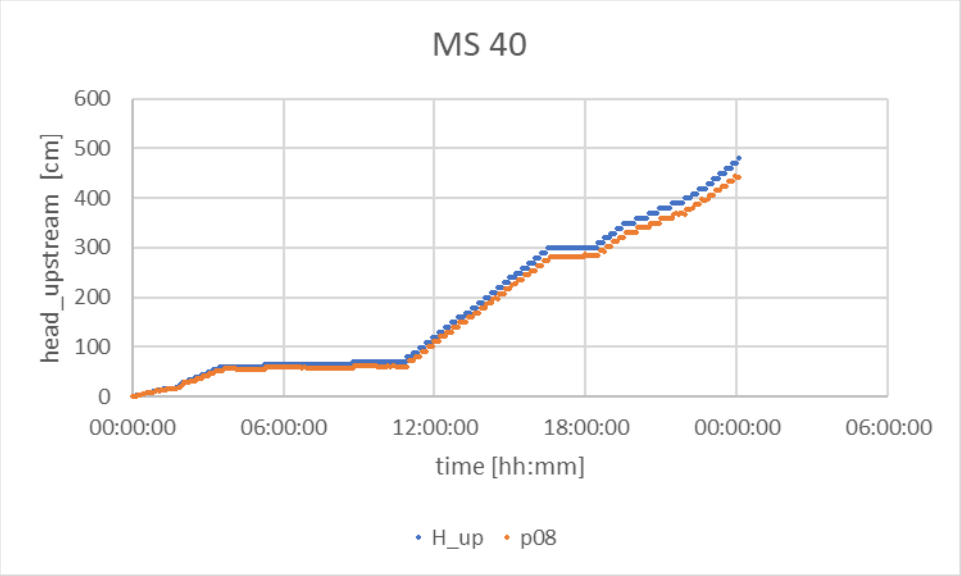

Figure 3.39 Applied head p08 upstream inlet filter compared to applied head in container in test MS 40

It stands out that the applied head measured by gauge p08 and the head downstream the barrier measured by gauge p17 show that there was a lower head drop across the set-up than actually should be expected by only looking at the applied level of the variable water reservoir and the fact that no sand had banked up around the outlet hole.
As there is head loss between H_up (variable constant head) and P08. There is also head loss in the lower part of the set-up between the downstream sand bed near the outlet hole and the discharge outflow, see Figure 2.2; this head loss is measured by P17.

This head loss in the set-up is the result of friction in the hoses, sharp bends and fittings. Furthermore, at the end of the tests a huge area of the downstream sand bed is paved by coarse sand resulting in additional roughness of the surface. This has consequences for the actually applied head difference across the CSB.

The actual head loss over the upstream part and the GZB is therefore the head measured at P08 minus the head loss at p17, see Figure 2.3 and Figure 2.4. At the end of the experiment when the flow through the set-up is more than 50 l/min, the head loss at the downstream end is not negligible. It appeared to be at 0.5 m at maximum in MS38 and even 1 m in MS40. Thus, the maximum head drop over the upstream part and the barrier is lower than the head drop measured with P08 as shown in the figures in the next section. The maximum head drop in the step before failure was 3.4 m in both tests.

3.3 Head drop versus flow rate and erosion

Flow rate measurements were taken three minutes after each head increment in five-minute intervals. In periods where the head increment is kept constant, the five-minute interval was also maintained.

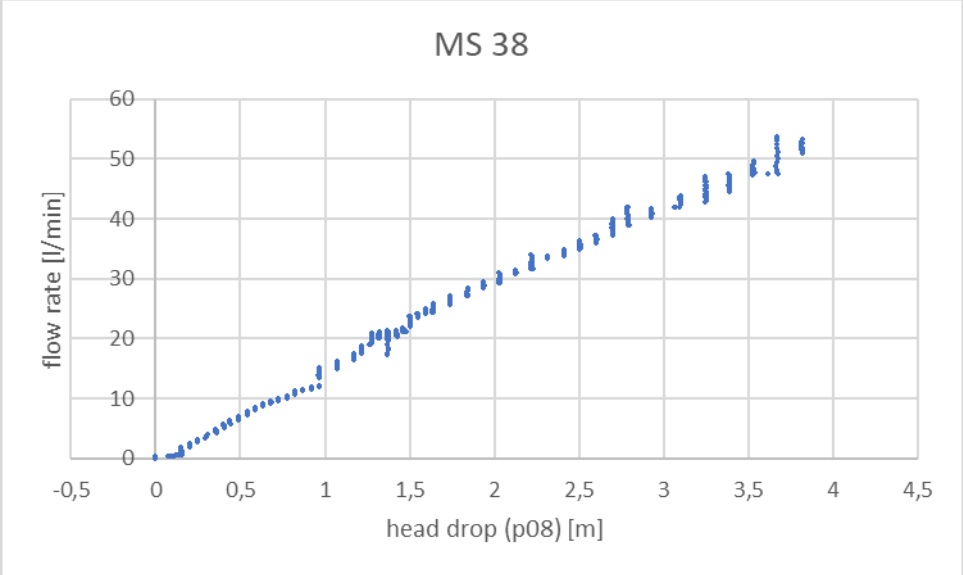

Figure 3.40 Head drop over the set-up and according to p08 as a function of flow rate at MS 38

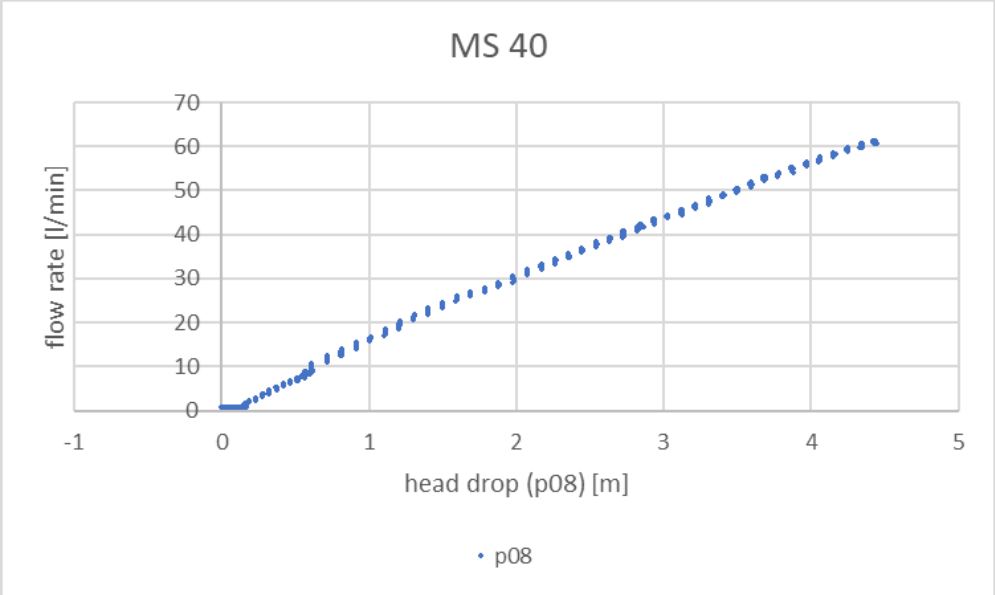

Figure 3.41 Head drop over the set-up according to p08 as a function of flow rate at MS 40

Both tests show a similar development of the flow rate with increasing head drop. Test MS38 shows some slight fluctuation in flow rate at higher head drops which could be because the flow rate was measured manually.

The graphs head drop versus flow rate show details about the erosion process and there are worth studying more in detail. As an example, the curve for MS38 is used, see Figure 3.42

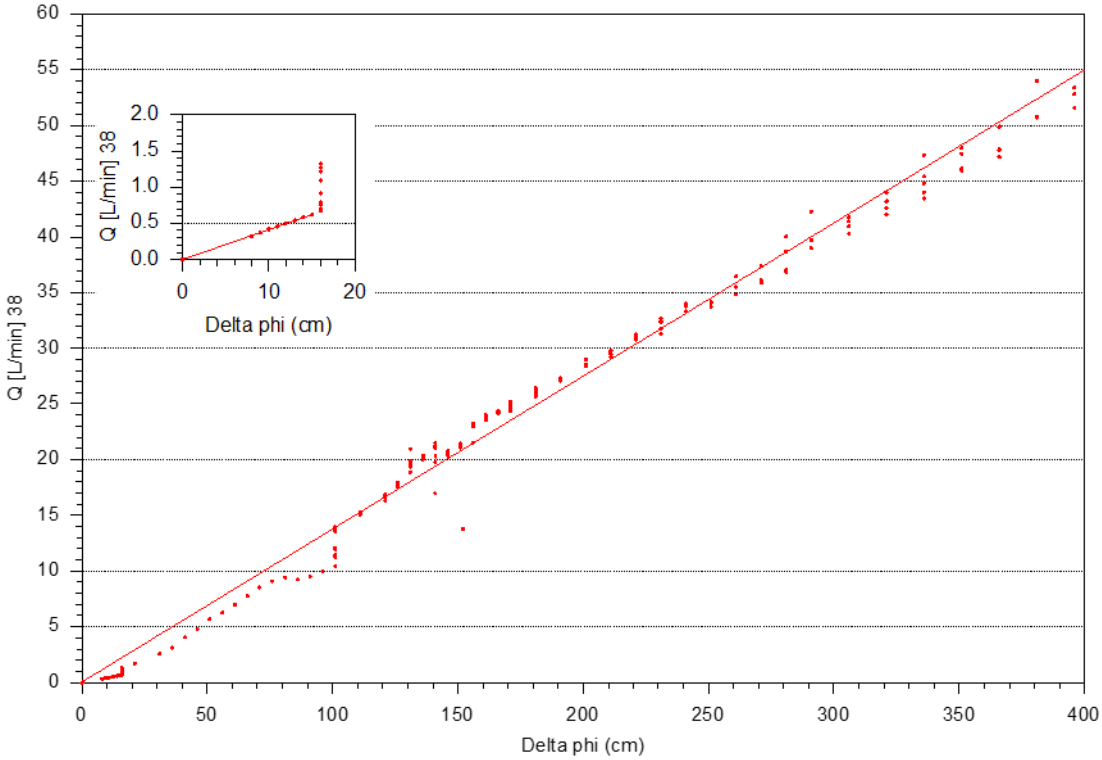

Figure 3.42 Detailed plot flow rate versus applied head drop delta phi (height of water reservoir) MS 38. Inset shows the results at the beginning of the test.

At the very beginning of the test, when the head drop is still less than 20 cm, the flow resistance through the set-up is relatively high. This means that there is only a limited flow for a given head drop. Measurement points are on a straight line indicating that the flow resistance is constant, there is no erosion. At a head difference of 16 cm erosion starts and a pipe is formed in the background sand. At a constant head difference, the resistance decreases, because the increasing pipe creates a larger area where water can flow into the pipe. For higher values of the head difference (between 16 and around 75 cm), the resistance slowly decreases because the pipe reaches a larger part of the barrier. When the barrier starts to erode the resistance increases, probably due to the coarse sand that blocks the pipe. At a head difference 101 cm the slope is formed in the barrier material. The flow resistance decreases again. At higher values of the head difference, the resistance is constant and is for a high percentage composed out of the resistance of the fine upstream background sand. It seems as if the resistance increases at high head drops, probably caused by turbulence somewhere in the set-up.

These results show that for a CSB there is a large range of pressure drops over the model in which there is sand erosion and thus sand producing well, but no failure. In this test, M38, pipe erosion starts at a head difference of only 0.16 m, when the fine background sand starts to erode, and a pipe is formed. At a head difference of 1.1 m the CSB starts to erode and the slope is formed in the protuberance.

3.4 Check of the measured data

First, it is necessary to check the measured heads regarding their reliability (by checking if the measured development of head values matches the observed process, in particular changes during periods of constant head drop and during equilibrium). Then, the gradients during the critical state and failure are assessed. This is necessary to get a good match of the results for the heads, discharges and gradients, which are calculated by the numerical models. Furthermore, it is focussed on obvious divergences between the measured heads of gauges at locations where comparable

measured values should be expected and on drifts in the measured heads in the course of time. This is of special importance in view of the long duration of the tests (around 24 hours) and the relevance of the measured values around failure for the validation of the supposed theoretical model of failure and failure criteria. Therefore, all measured head developments and of the gauges, measuring absolute and differential heads respectively, as a function of time and of the applied head at p08 are plotted and assessed in Appendix D. The main findings and results are described in de following subparagraphs.

3.4.1 Test MS38

In order to check the reliability of the pore pressure gauges the measurements are compared with the registered discharge and the observations during the tests, mainly by focussing on the changes at the end of every stage and the developments of pressure and discharge during (long-term) constant heads.

3.4.1.1 Check of development of the measured heads as a function of time

The head measured in the medium-scale box upstream the inflow filter (p08) is better suited for the analysis than H_up. Due to some head loss in the hoses and couplings H_up is somewhat higher than P08. By using p08 the maximum gradient across the sand bed can be depicted better. The measured head at p08 (Figure 3.43) is therefore used as the applied head in the numerical modelling of the tests for the post diction in Chapter 4 and by the check of the measured heads in Appendix D.

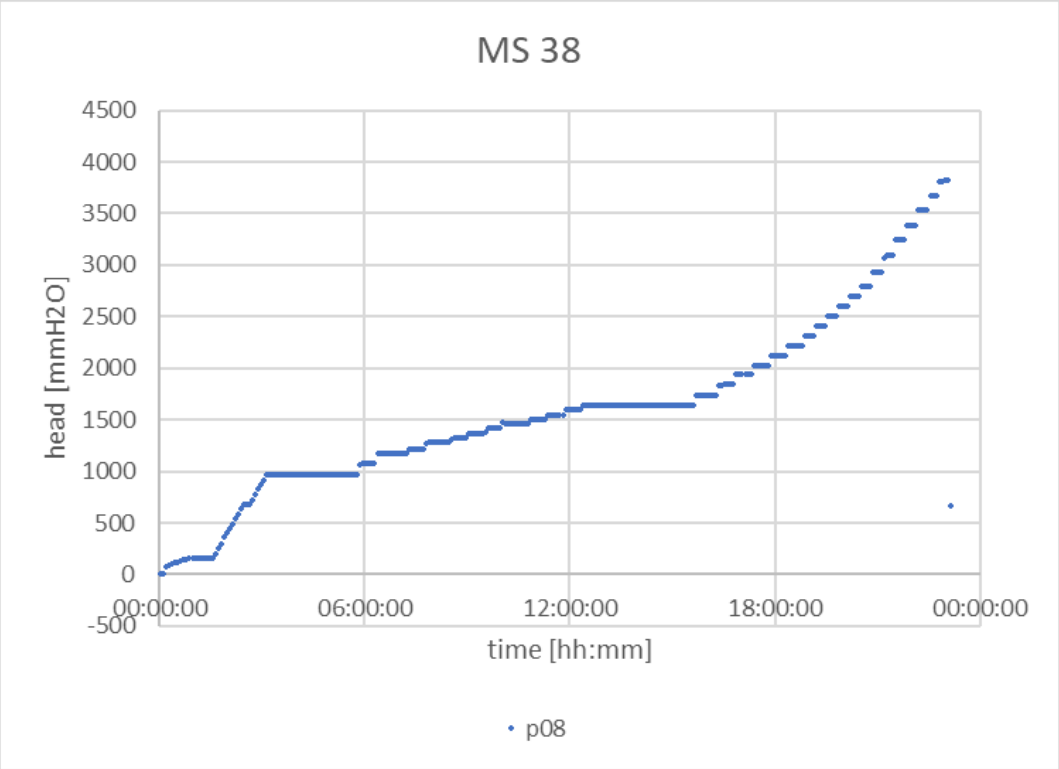

Figure 3.43 Applied head drop (measured by p08) with the passage of time at test MS 38

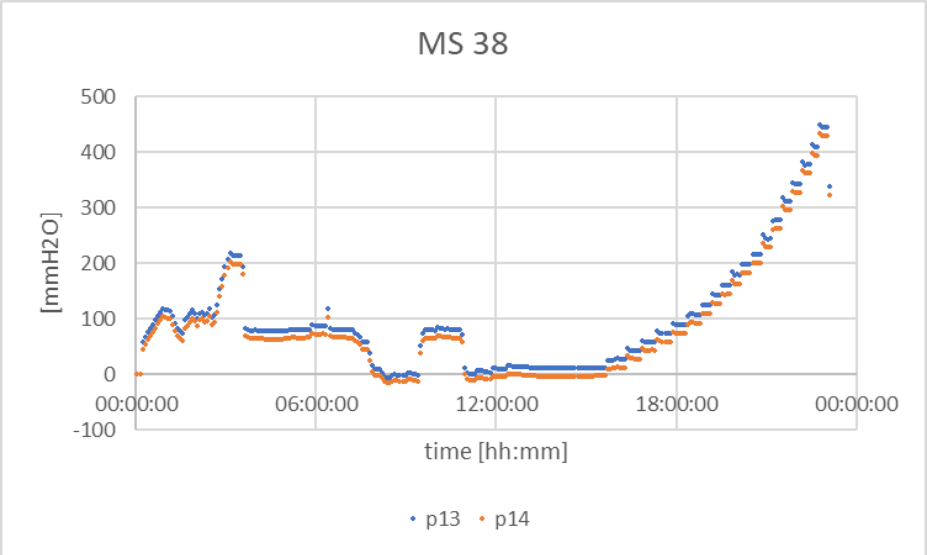

Figure 3.44 Measured heads test MS 38 at the gauges p13 and p14 at the downstream side wall of the protuberance (150 mm and 250 mm respectively above top of aquifer)

Figure 3.44 shows a nearly constant difference between the two gauges at the downstream side of the protuberance during the whole test. The vertical distance between these gauges is 100 mm. Only at the moment when the barrier sand is subsiding in the protuberance, at around 8:00, see Fig. 3.46, these gauges show some variation in head difference. When the barrier sand is subsided below the gauges, they should show the same head. Figure 3.45 shows the heads of these gauges as a function of the head difference between the upstream gauges p1 and p2, which is an indicator for the flow. At the moment of subsidence of the barrier along these gauges this figure shows a little difference in the heads at around 700 mm head difference (p2-p1). The figure also shows that after a load increase the heads p13 and p14 are sometimes increasing while the flow is decreasing and vice versa.

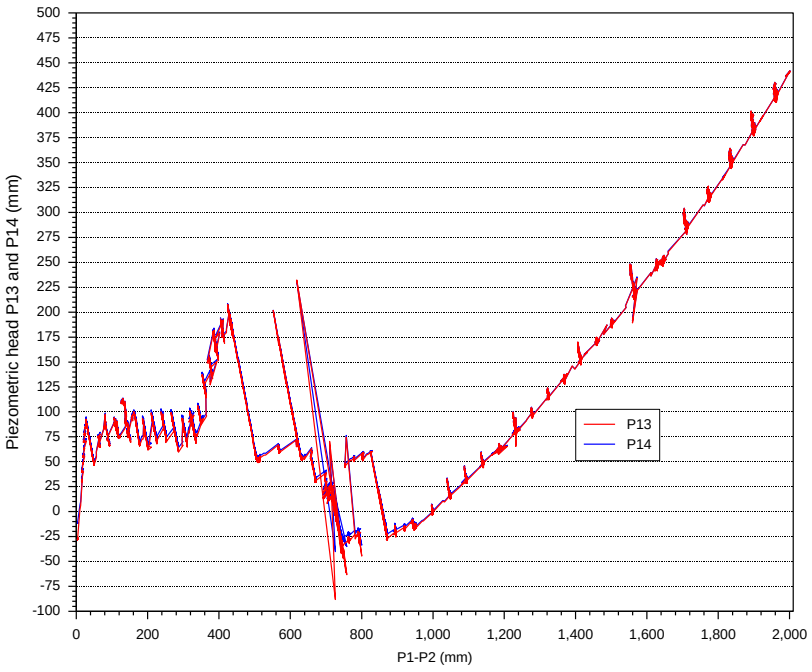

Figure 3.45 MS38. P13 and p14 as a function of flow (indicated by p1-p2)

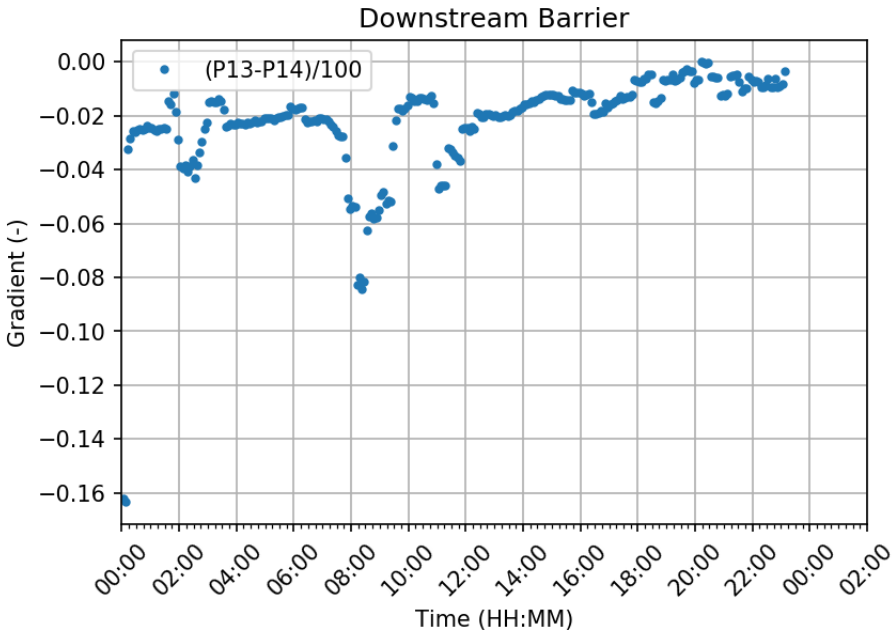

Figure 3.46 MS38. Vertical gradient at the downstream side of the protuberance as a function of time

Figure 3.47 shows that P24 has a different development in measured head than the other gauges after 1:57 hours (at a head p08 of 402 mm): the indicated head is around 50 mm lower than at the other gauges but is decreasing during the last quarter of the test to 20 mm. It is inexplicable why this gauge shows even negative values while all the other gauges show different, but among each other an almost congruent development. The measured heads of p24 are questionable, even when p24 shows almost comparable results as the other gages at critical stage. The resulting gradient between p23 and p24 is therefore questionable.

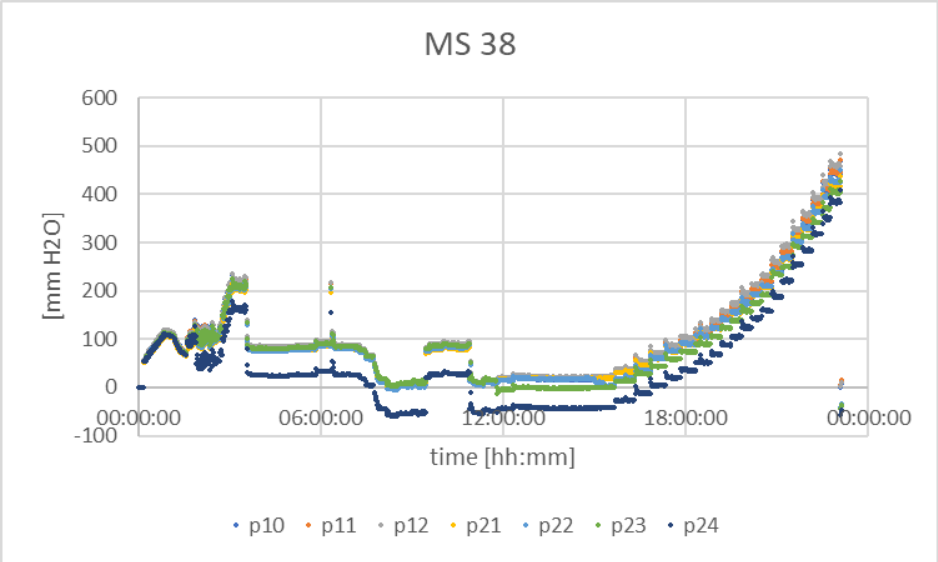

Figure 3.47 MS38. Measured heads at the gauges p10, p11/p24/p23 and p12/p22/p22 at the upstream side wall of the protuberance (p22 and p24 are 130 mm above top aquifer, p21 and p23 are 100 mm above top aquifer). p22 is at the same heights as p12; p11 and p24 are at the same height, but 25 mm away from each other. p23 is 30 mm below p24. p10 is the gauge at the right-hand side of the protuberance in flow direction. In test MS 38 there were no additional absolute head measurements around this gauge.

Figure 3.48 shows the course of the differential gauges at the upstream side wall of the protuberance. These gauges are essential for the validation of the vertical gradient at failure. The

two gauges dp3 and dp4 in the centreline of the set-up seem to be unreliable. It stands out that the course of dp4 is extremely deviant compared with the other gauges, with unreliable fluctuations. dp4 starts immediately with higher values and shows a high range of values. Also, dp3 shows higher values, even positive heads when the other heads are negative. This gauge is not eligible for use.
It also appears that at the end of the test, when all taps are closed and only hydrostatic water pressure should occur, most of the other gauges show heads that differ from the value zero, what could be traced back some drift in the measurements.

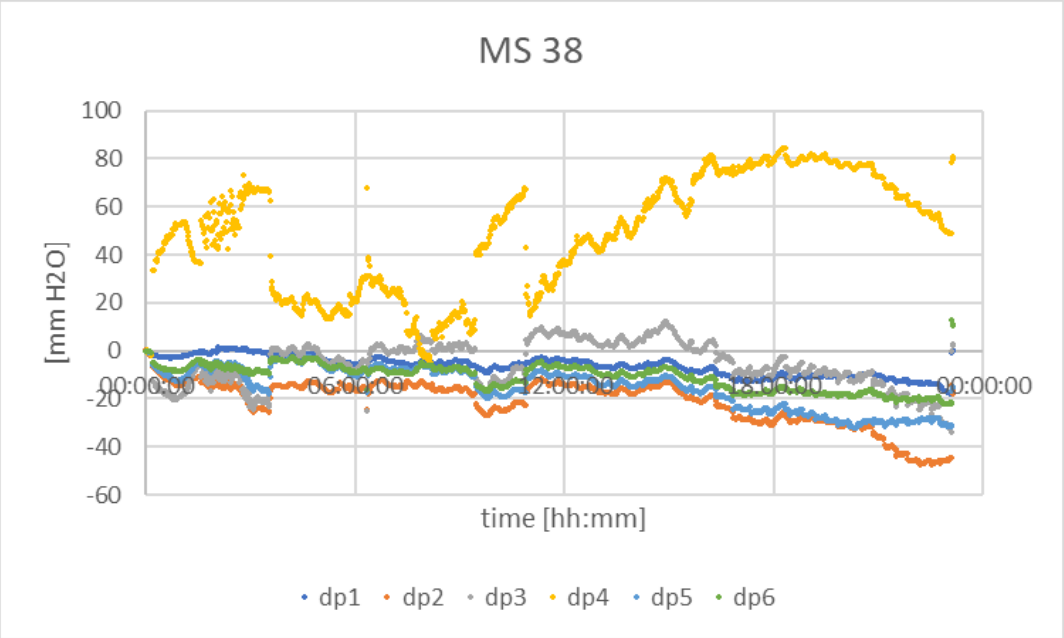

Figure 3.48 Test MS 38. Measured heads at differential gauges dp1/dp2, dp3/dp4 and dp5/dp6.

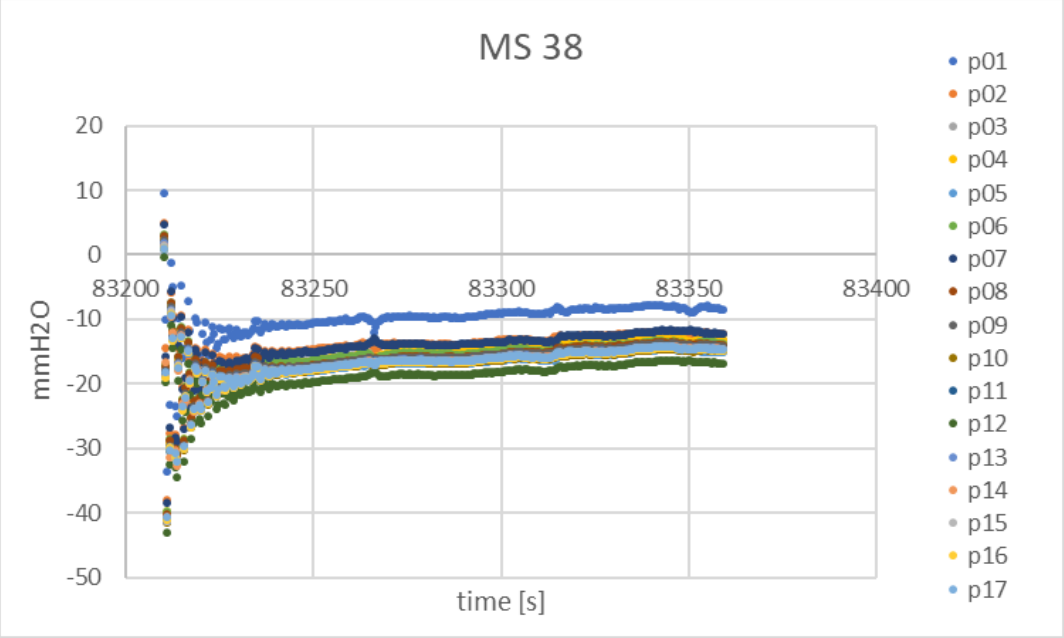

Figure 3.49 MS38. Final values after shutting all taps.

Figure 3.49 shows the final heads of the gauges after shutting all taps, thus at hydrostatic pressure. There is some drift around 15 mm for all gauges.

Figure 3.50 shows the development of the differential pressure gauges during failure. Here we see that only values of dp1 and dp3 are coming close to zero, what should be the case when all water taps are shut off, and only hydrostatic pressure is present. However, the other gauges show higher heads, which is not plausible.

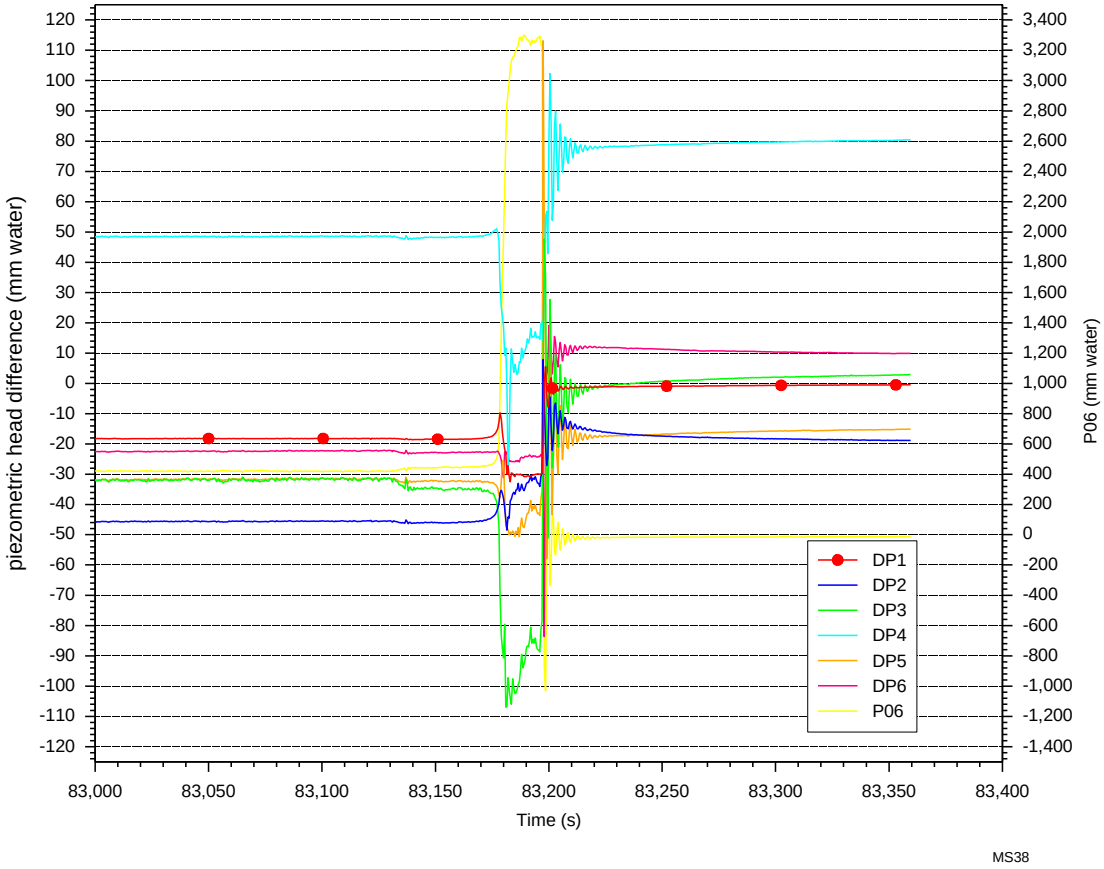

Figure 3.50 MS38. Head development of the differential pressure gauges and of p06 inside the protuberance during failure.

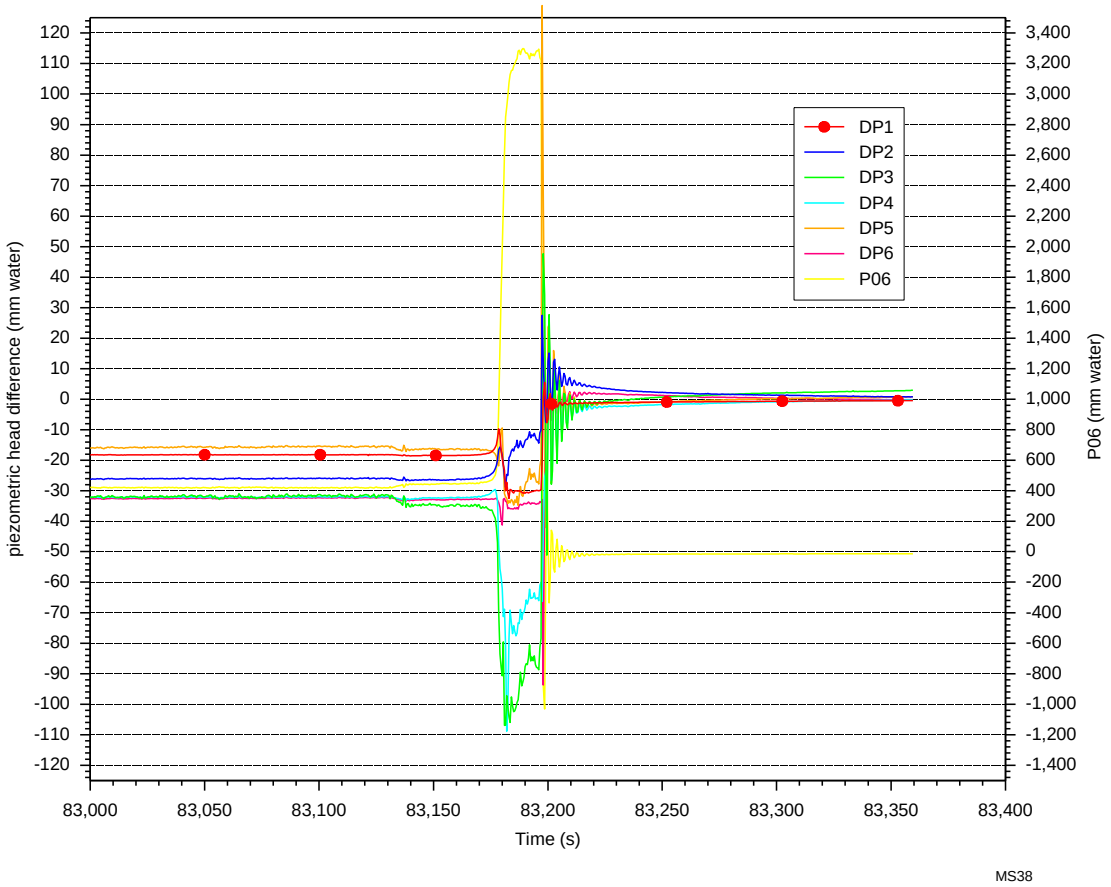

Figure 3.51 MS38. Head development of the differential pressure gauges and of p06 inside the protuberance during failure (all end values of the heads are reset to zero).

Figure 3.51 shows the development of the measured heads during failure by resetting al end values. In the centre of the protuberance dp3 and dp4 show a gradient bigger than 1 (more than 30 mmH_2O pressure drop) before failure, but also dp2 and dp6 show a gradient around 1. During failure, when the pressure inside the protuberance is growing strongly (p06), the maximum gradients dp3/30mm and dp4/30mm are exceeding the Terzaghi criterion 1 in threefold, which supports the presumed theory of the failure mechanism of the CSB.

3.4.1.2 Vertical gradients

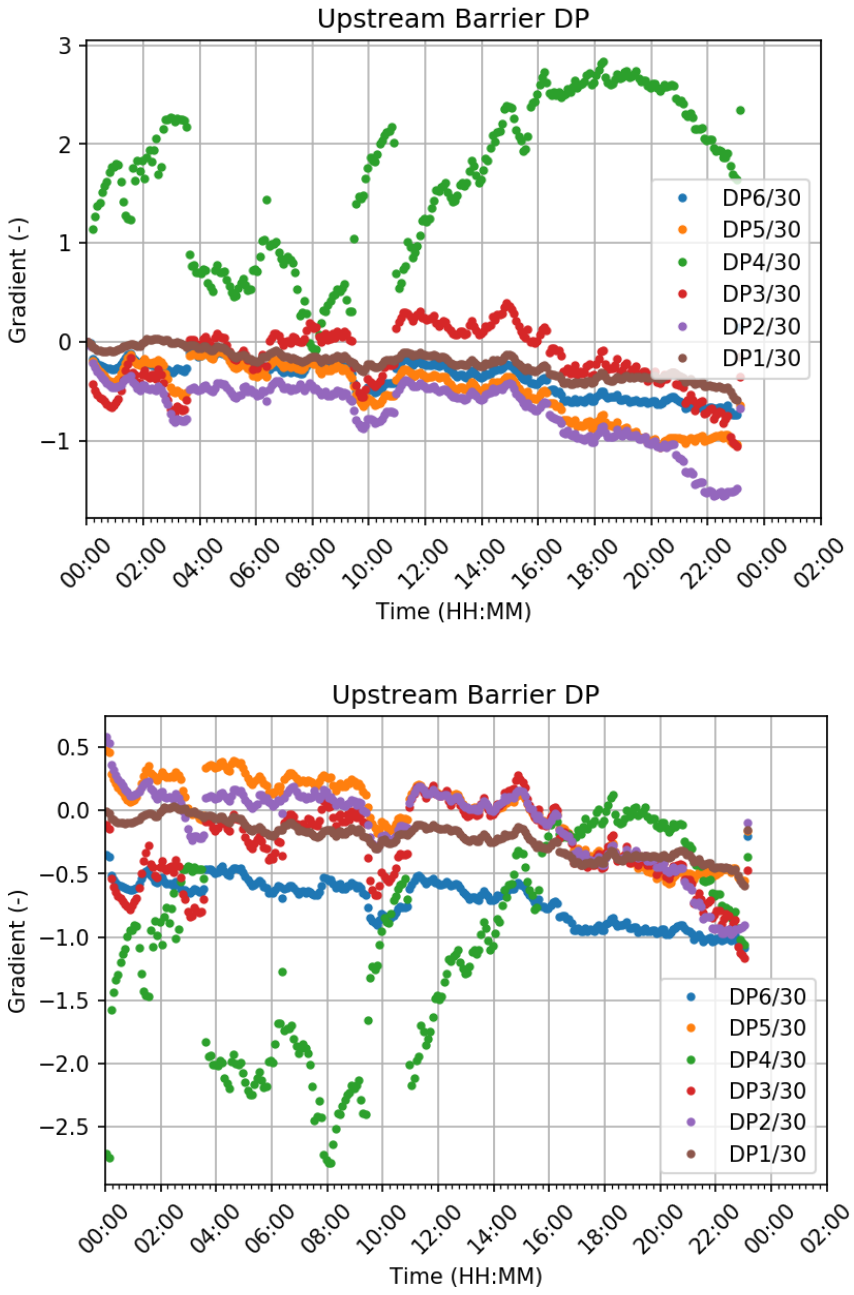

Figure 3.52 Test MS 38. Vertical gradients along the upstream side wall protuberance based on differential pressure gauges as a function of time. Dp1, dp3 and dp5 are the differential heads between 70 mm and 100 mm, dp2, dp4 and dp6 are the differential heads between 100 mm and 130 mm from top of sand bed.

Figure 3.52 shows the developments of the vertical gradients based on differential gauges along the upstream side wall protuberance. Because of some drift in the differential gauges the vertical gradients at the critical state seem te be unrealistic high, especially for dp2. At the end of the test (when only hydrostatic pressure is prevailing, all absolute pressure gauges should record a value of zero.

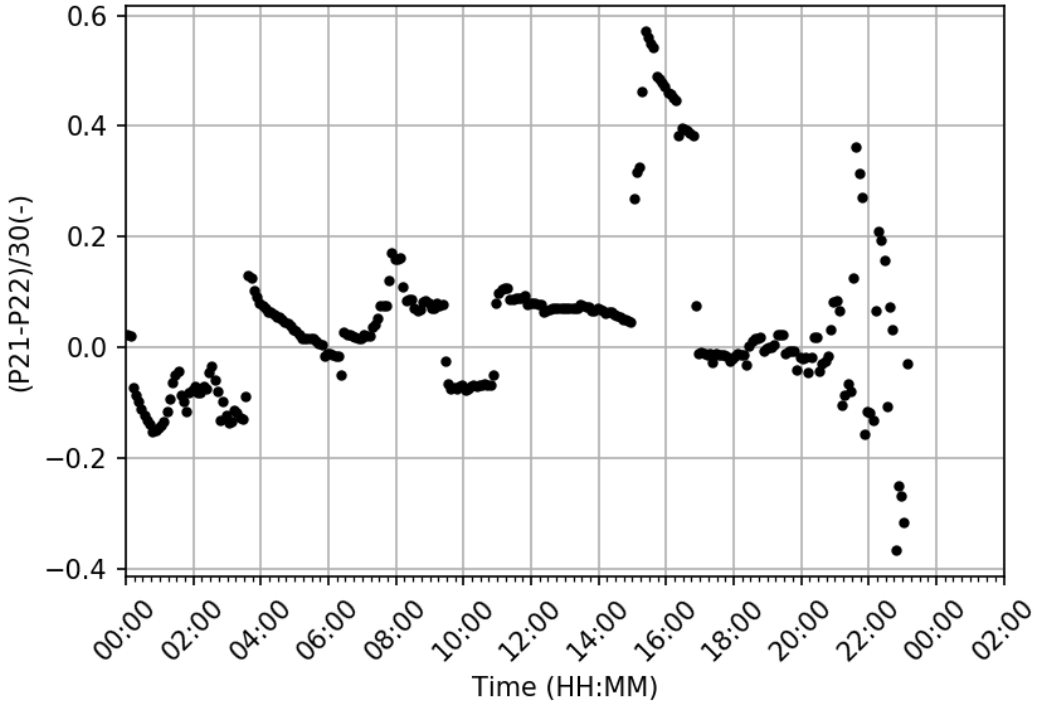

Figure 3.53 Test MS 38. Vertical gradient (p22-p21)/30 at the same elevation as the gradient for differential pressure gauges dp6; as a function of time. The gradient between p21 and p22 is lower that for dp6 and shows much fluctuation at the end of the test.

3.4.1.3 Horizontal gradients

The following figures show the horizontal gradients at the top of the sand bed and at the bottom of the box.

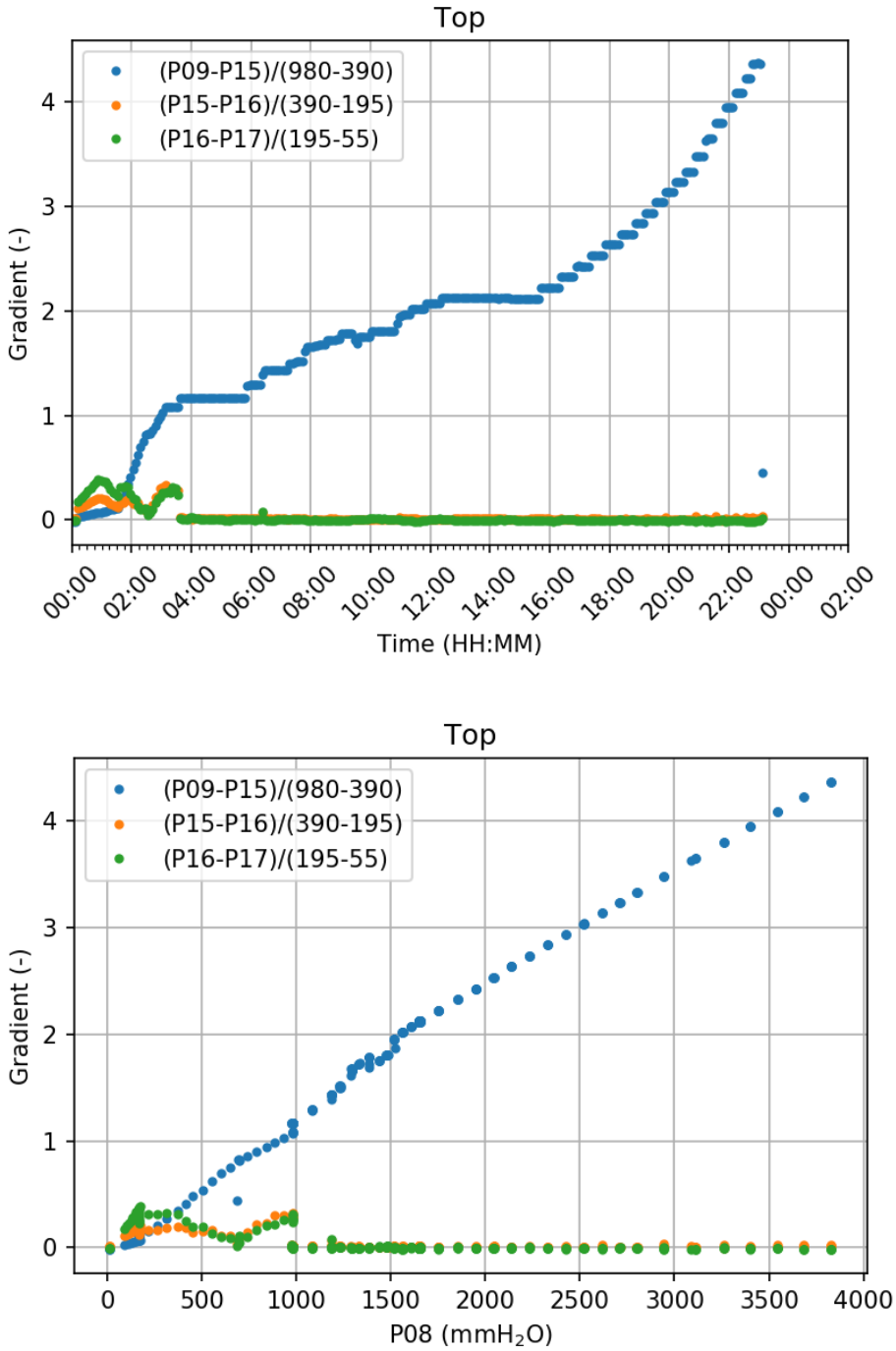

Figure 3.54 Test MS 38. Horizontal gradients over the barrier (p9-p15)/590 and downstream the barrier (p15-p16)/195 and nearby the outlet (p17-p16)/140. Above: as a function of time; below: as a function of applied head p08.

Figure 3.54 shows the horizontal gradient over the barrier. The downstream gradients are around 0.4 – 0.5 after 03:20 h at a head of 965 mmH_2O. This is when the crest of the slope had reached the upstream side wall of the protuberance. At 03:34 h, when the toe of the slope has made contact with the pipe, the gradient downstream the barrier is negligible small.

For the gradient between gauges p9 and p15 the horizontal gradient is much higher, but this is not very meaningful, because gauge p09 is located at the upstream B25 and p15 at the downstream B25, but the gradient is by the relatively broad interjacent area of CSB. The gradient inside the upstream fine sand should be much higher. The horizontal gradient between p02 (at the bottom) and p09 (at the top) over a horizontal distance of 145 mm within the same sand layer is shown in Figure 3.55.

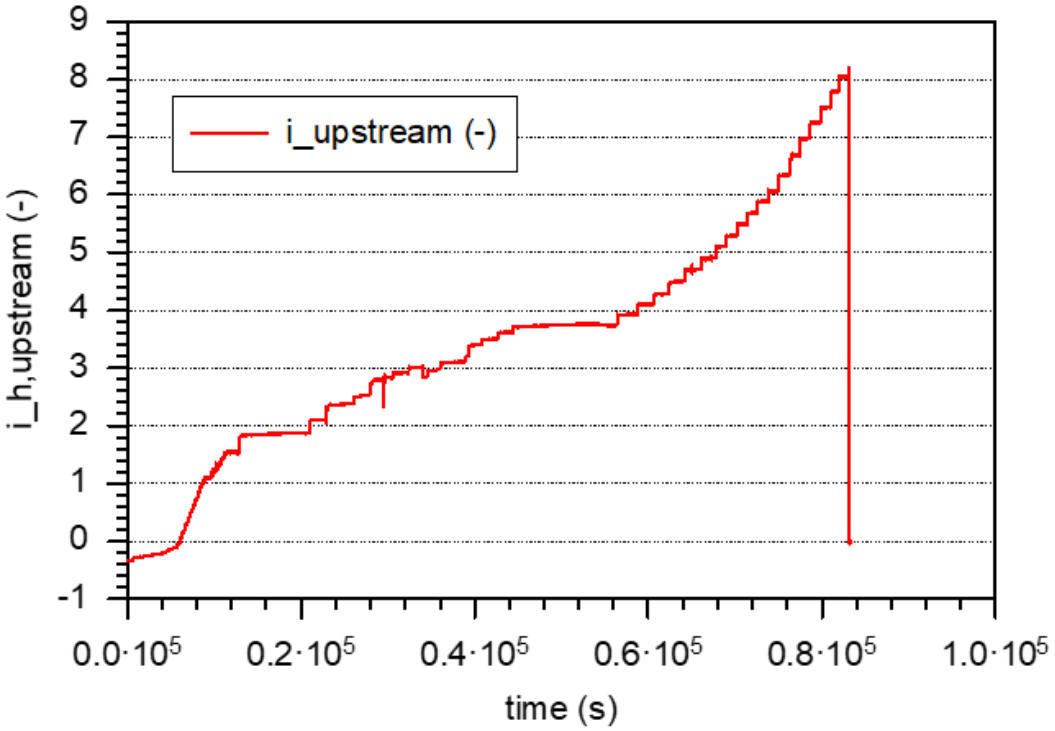

Figure 3.55 MS 38. Horizontal gradient in the upstream, fine sand (B25) between p02 and p09.

The expected average horizontal gradient across the upstream B25 aquifer should be 17 (= 3.4 m / 0.2 m), which is much higher than what was measured between p02 and p09, viz. 8. The upstream flow seems to be more 2D than 1D.

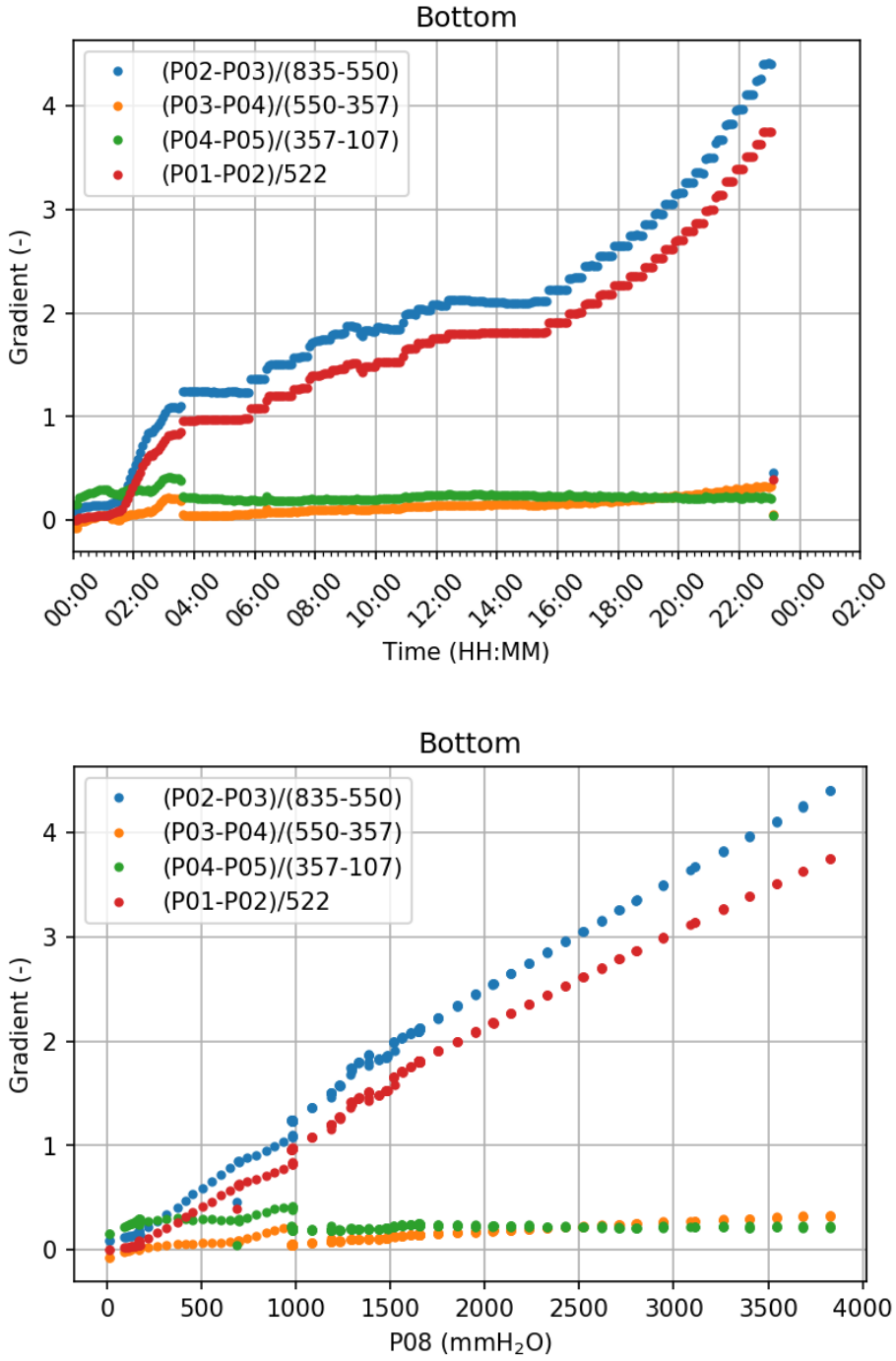

Figure 3.56 Test MS 38. Horizontal gradients at the bottom of sand-bed. Above: as a function of time; below: as a function of applied head p08. (p1-p2)/522 is upstream and (p2-p3)/(835-550) is the gradient across the barrier, (p3-p4)/(550-357) is downstream and (p4-p5)/(357-107) is near the outlet hole.

Figure 3.56 shows a distinct difference in development of the gradients upstream and across the barrier on the one hand and the gradients downstream the barrier at the bottom of the sand-bed. The upstream gradient and the gradient across the barrier develop in a comparable way, but it stands out at test MS 38 that the gradient across the barrier is getting a little bit higher than that in the upstream area. This differs from Figure 3.65 in test MS 40 where the gradient (p01-p02)/522 is little higher than (p02-p03)/(835-550). This means that the two experimental model set-ups differ a bit from each other. The higher gradient (p2-p3)/(835-550) with regard to (p01-p02)/552 in test MS38

is strange, because there is more fine sand in between gauge p01 and p02 than in between p02 and and p03. This raises questions concerning the actual position of gauge p02 regarding its position according to Figure 2.3 and Figure 2.4, i.e. 835 mm distance from the outlet hole. Assuming that the head drop over the fine sand is the dominant head drop in the set-up and a linear pressure drop over the upstream fine sand, the position of P02 should have been 880 mm in test MS38 and 870 mm in MS40. This is in close agreement with the graphical estimation shown in Figure 4.25 where 885 mm and 875 mm was found respectively. The small difference occurs because the small pressure drop in the coarse sand is taken into account in the method of Figure 4.25.

3.4.2 Test MS 40

3.4.2.1 Check of gauges concerning the development of measured heads as a function of time

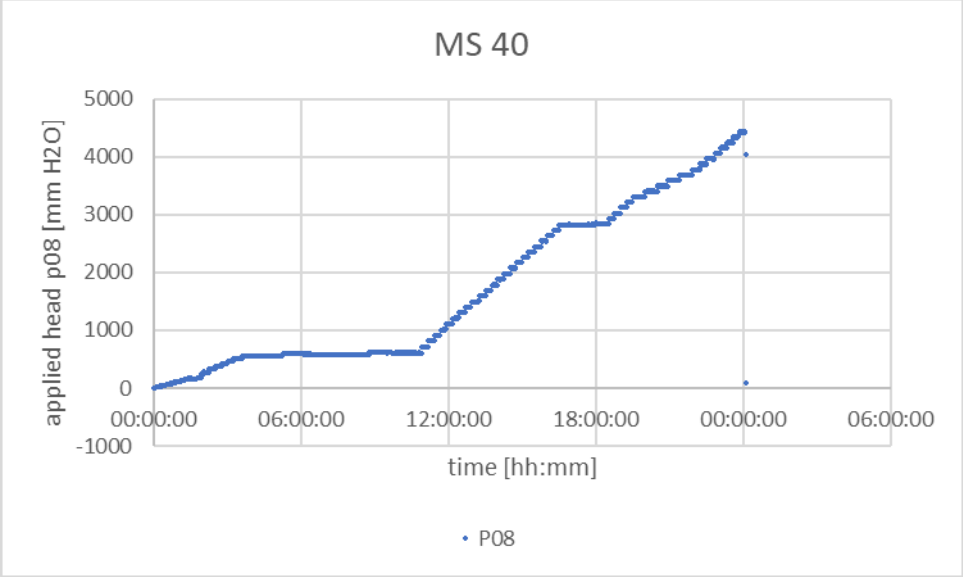

Figure 3.57 MS 40. Applied head p08 as a function of time

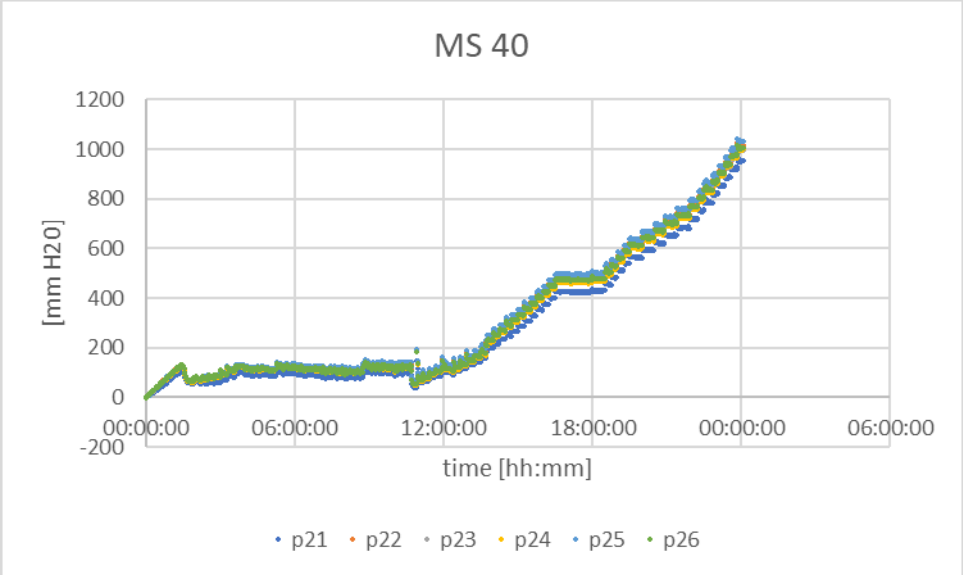

Figure 3.58 MS 40. Development of heads in gauges p21&p22, p23&p24 and p25&p26

Figure 3.58 shows a divergence between the heads measured by gauge p21 and p22. p12 and p22 are at the same elevation and shows an identical development. p22 is located above p21 but shows higher heads, so maybe there is some drift in gauge p22.

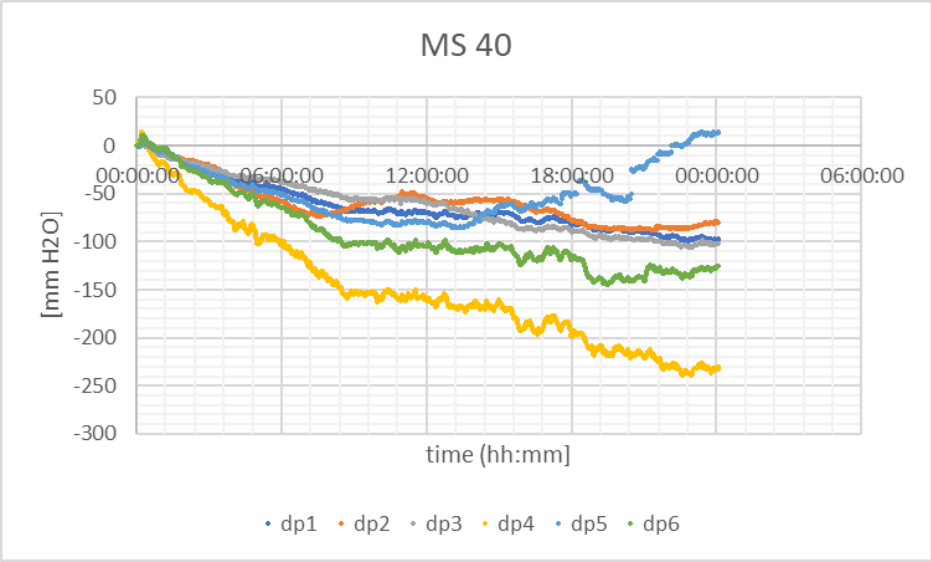

Figure 3.59 M 40. Development of differential heads at the upstream side of the protuberance.

Figure 3.59 shows the development of the measured differential heads at the upstream side of the protuberance. As in test MS38 the differential gauges show a significant drift of the heads at the end of the test, which is not plausible since at the end of the test, after shutting of the taps, only hydraulic pressure should be prevailing. Therefore, the differential heads are plotted, corrected for drift in Figure 3.60. This figure shows the development of the differential heads before and during failure, using the reset end values of the differential gauges. It is not clear why the heads measured by the differential gauges were drifting during the test.

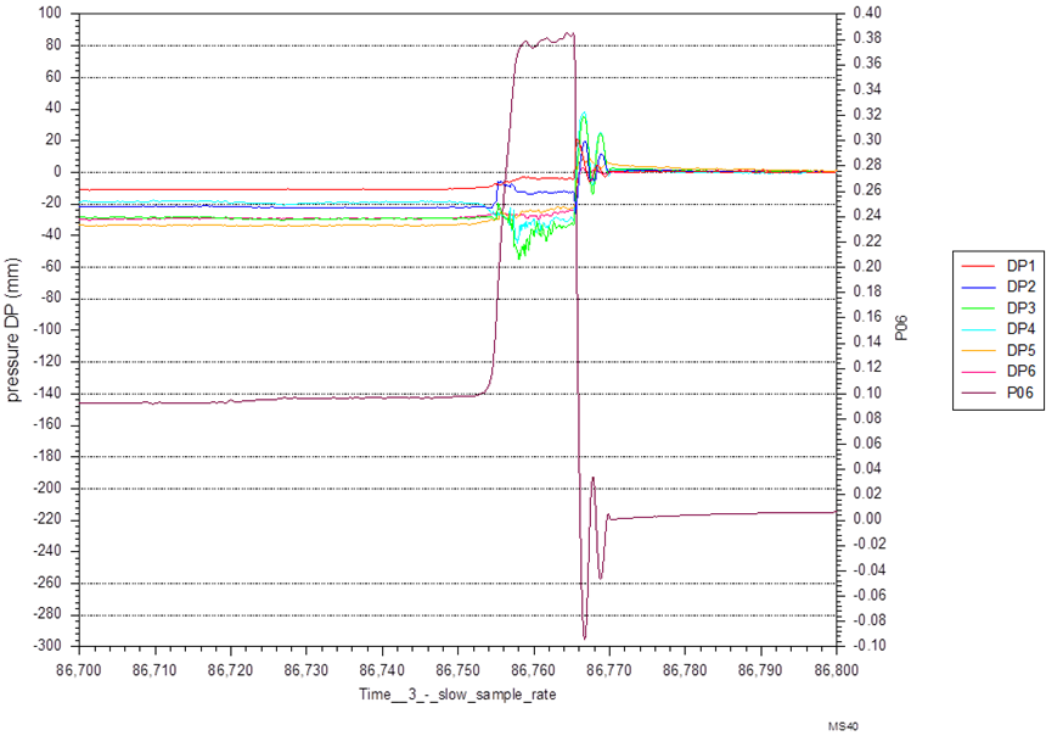

Figure 3.60 Development of differential pressures at the upstream side of the protuberance during failure. The values of the differential pressures are at rest for the end values, when the water tap was closed, and only hydrostatic pressure was prevailing.

3.4.2.2 Vertical gradients

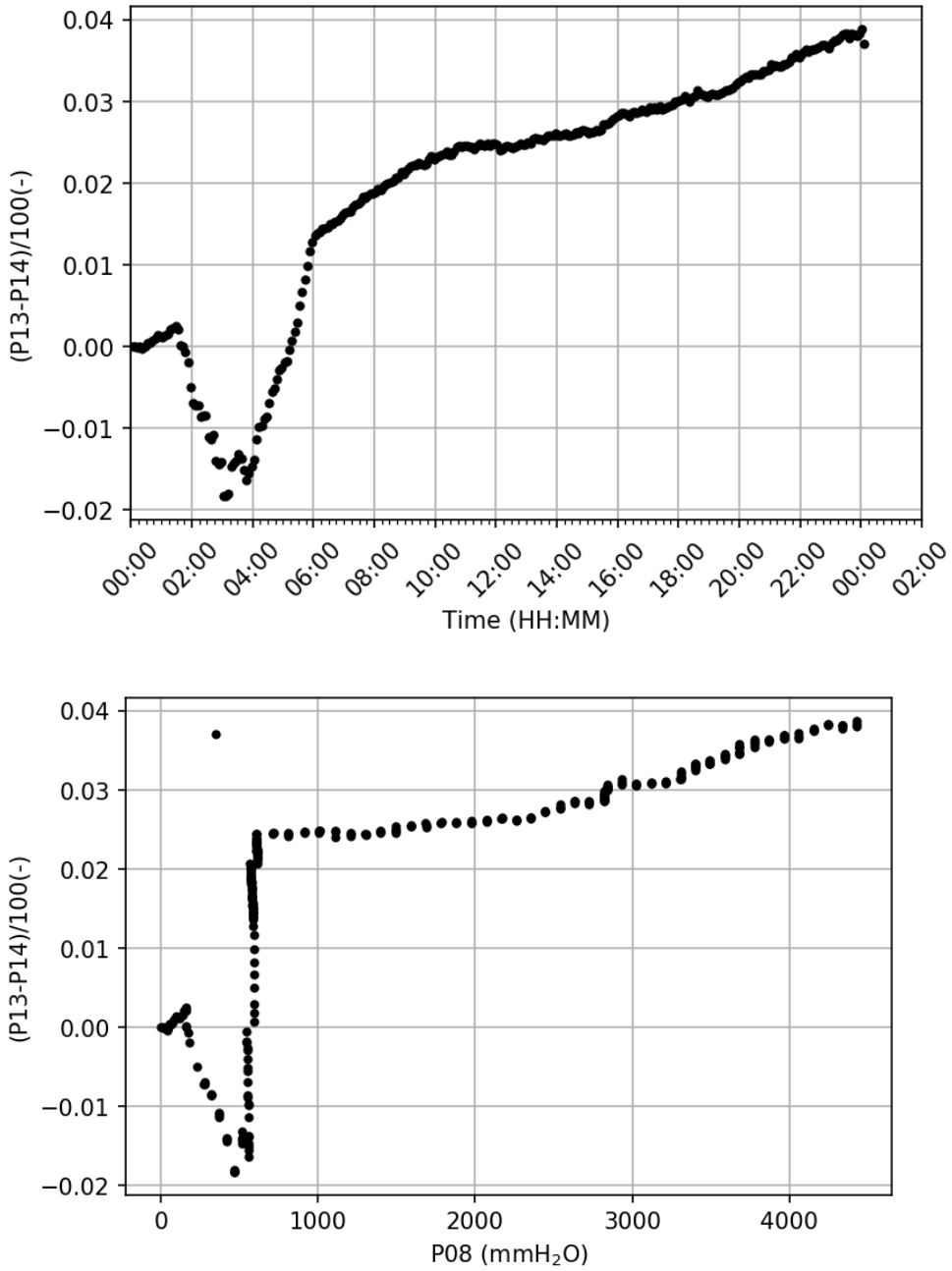

Figure 3.61 MS 40. Vertical gradient at the downstream of the protuberance; above: as a function of time; below: as a function of applied head p08.

Figure 3.61 shows an increase of the vertical gradient at the downstream side of the protuberance at the beginning of the test. At 01:50 (applied head 19 cm/ p08 = 172 mm) a subsidence of the sand (5 mm over a length of 8 cm) at the upstream side of the protuberance occurred. At that moment the gradient decreased an became negative. This development continued until 03:30 h (applied head 54 cm / p08 = 514 mm) when the lateral pipe was fully developed along the barrier. The subsidence was 30 cm over a length of 30 cm at that moment. After that, the applied head was increased with 5 cm (59 cm / p08 = 560 mm) and kept constant for 2:15 h long and then increased with 5 cm (64 cm / p08 = 590 mm) for 3:30 h long. From that moment on the gradient increased again proportional with the applied head. However, it concerns very slight head differences of around 1 to 4 mm. It is questionable if these are really occurring head differences or rather values

within the measurement inaccuracy. Normally the head difference between these two gauges should be zero, in case both are above the top of the sand slope, as shown in Figure 3.46.

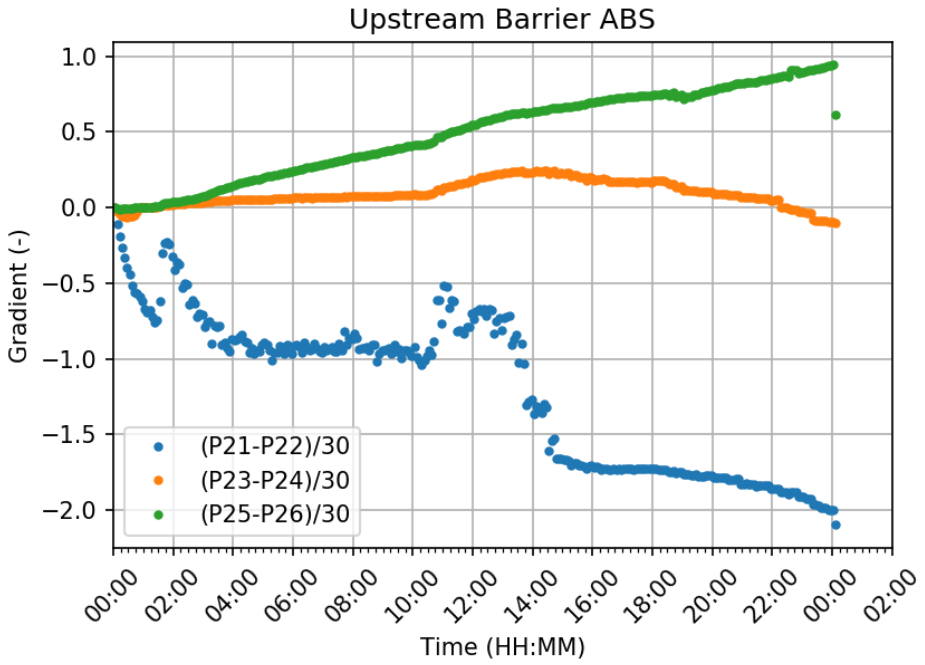

Figure 3.62 MS 40. Vertical gradients at the upstream side of the protuberance, based on absolute pressure gauges;

Figure 3.62 shows the gradients between 3 pairs auf gauges at the upstream side of the protuberance. The pairs are located at the same level (133 and 100 mm respectively above the top of the sand bed). Figure 3.62 shows a divergence in the head development of p21 in relation to the other gauges from the start of the test. The gradient (p21-p22)/30 is unreliable, particularly the gradient of -1 measured at around 04:00 h. The development of the other two gradients is more comprehensible. There is an increase when the pipe has reached the barrier after around 1:35 hours and a second slight bend when a connection between te void and the pipe occurs at around 10:45 hours. The coverage of the gauges with sand was higher at p26 and was still 25 mm before failure. Therefore, the gradient at that side developed further till around 1. In the centre line the gauges were already above the top of the slope at lower decreasing gradients of (p23-p24). However, negative values are unlikely, which suggests that some drift in the gauges has occurred.

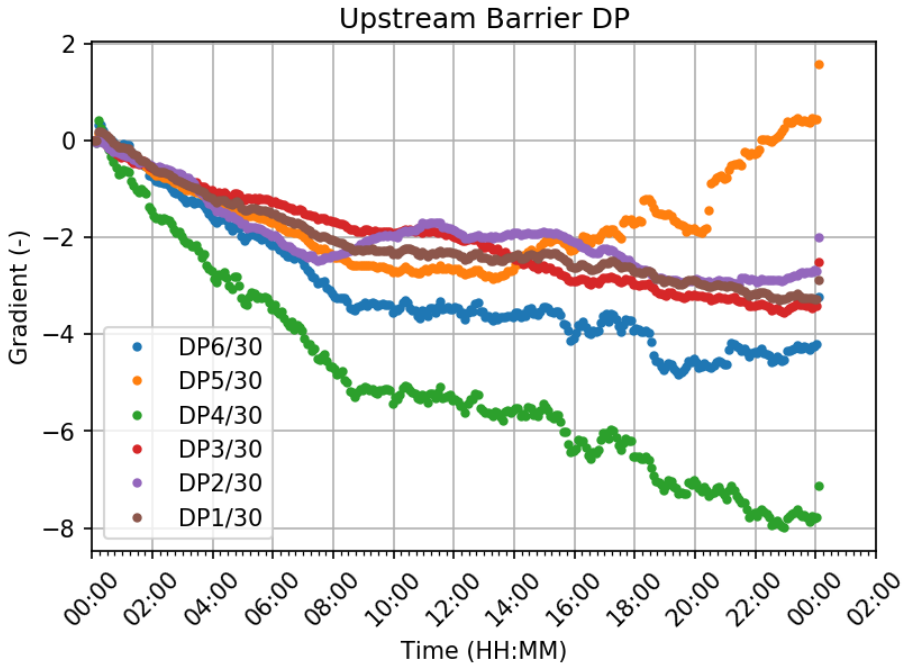

Figure 3.63 MS 40. Vertical gradients at the upstream side of the protuberance, based on differential pressure gauges.

Figure 3.63 shows for all gradients (measured with the differential gauges over a distance of 30 mm) already an increase of the vertical gradient above 1 in an early stage within the first 8 hours from start, which is the period until the top of the slope is going to reach the upstream wall of the protuberance. After that the gradients keep relatively constant, except for dp4 which is the upper gradient in the centre line of the set-up where the crest of the slope is the lowest. At the end of te test before failure, only dp1 and dp2 seems to be in contact with sand.

3.4.2.3 Horizontal gradients

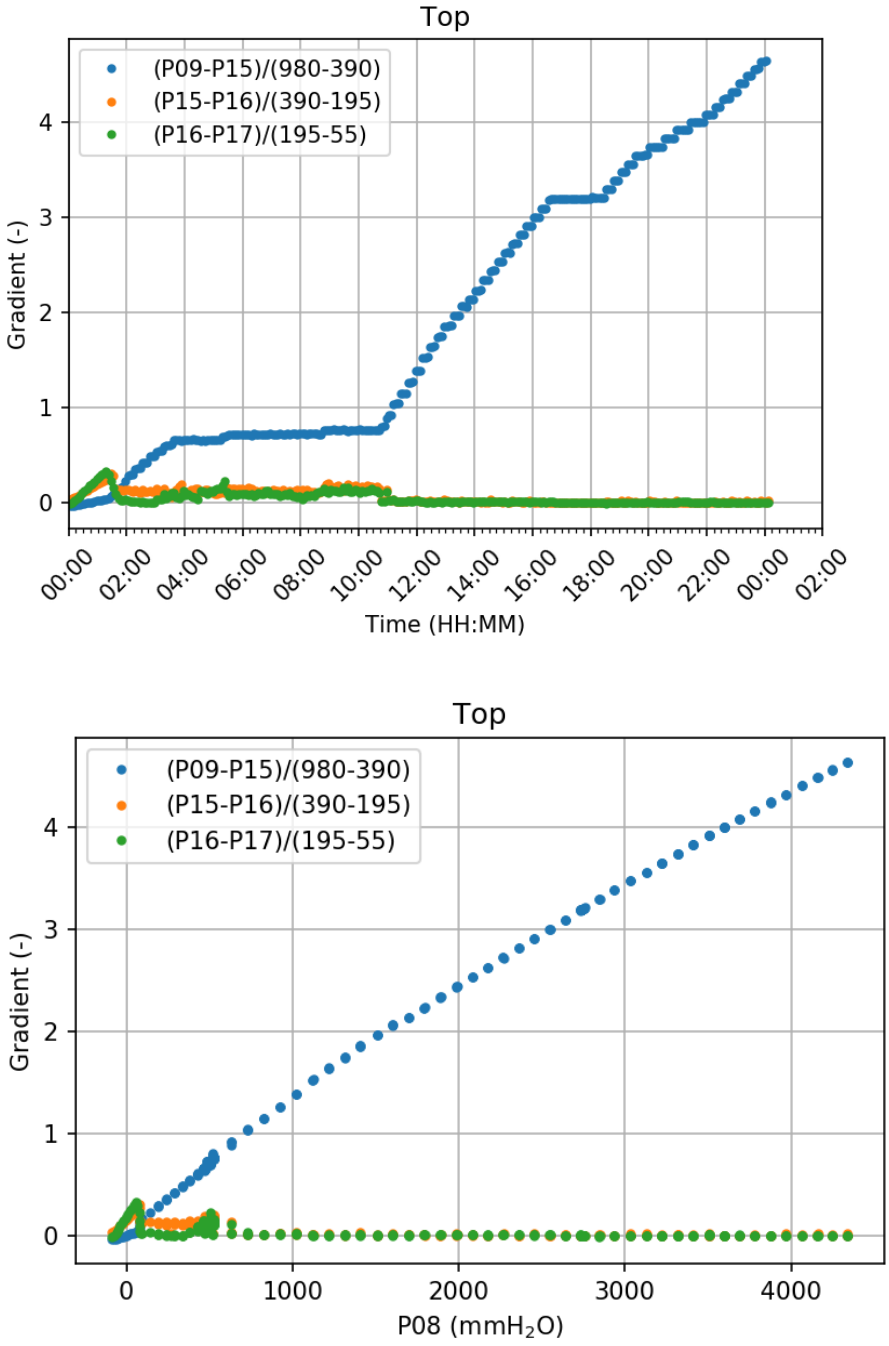

Figure 3.64 MS 40. Horizontal gradients on the top of the sand bed; as a function of time (above) and as a function of applied head p08 (below)

The development of the horizontal gradients is as expected. At the upstream side of the barrier the gradient is increasing with the applied head; downstream of the barrier the gradients decrease to zero when the pipe has reached the barrier and the lateral pipe is fully developed.

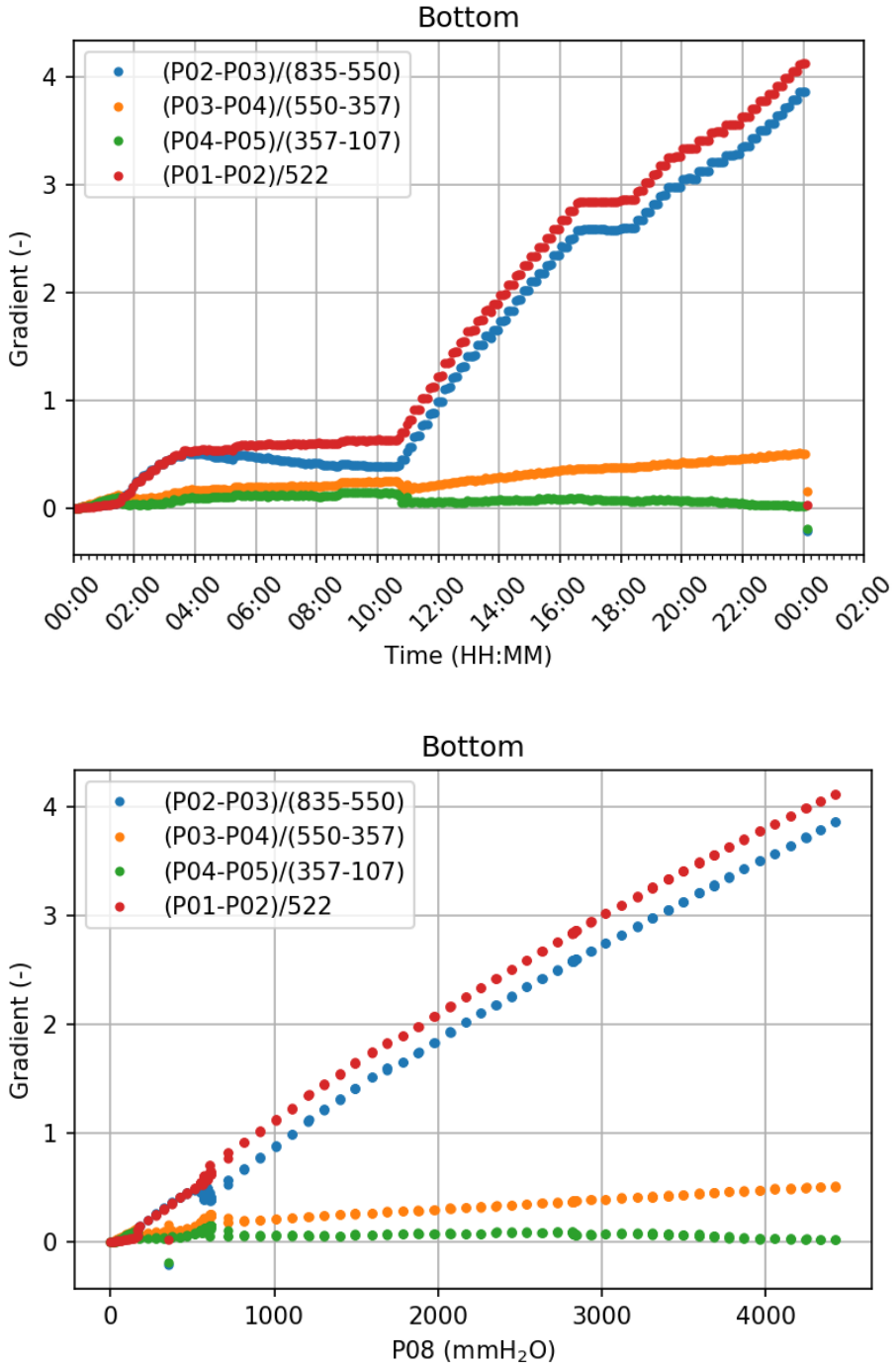

Figure 3.65 MS 40. Horizontal gradients at the bottom of the sand bed; above as a function of time; below: as a function of applied head p08. (p1-p2)/522 and (p2-p3)/285 are the gradients upstream the barrier, (p3-p4)/250 and (p4-p5)250 are the gradients downstream the barrier.

3.5 Conclusions regarding the check of gauges

In general, the gauges for the absolute head measurements seem to be fairly reliable (except for p24 in test MS38), the differential gauges show a drift in the course of time in both tests. For a comparison of the measured values with the results of the numerical modelling it will be focused on the absolute gauges p01, p02, p03, p04 and p05 at the bottom of the box and p09, p15, p16 and p17 at the top of the sand bed. Further, the gauges p21, p23 and p25 are used for a comparison of the calculated heads inside the barrier. These 3 gauges are located 100 mm above the bottom of the protuberance and are below the top the slope at the critical stage in test MS38. For test MS40 these gauges are only partly covered by sand at the outer edges of the slope top at the critical stage. This choice of gauges is a combination of reliable gauges and gauges located at positions which are relevant for the process.

3.6 Input parameters for comparison with numerical model

In the numerical calculations, the head distribution over the model is calculated for several loading steps, which corresponds with different geometries due to the erosion. This section summarizes the input parameters used and the hydraulic head measured at various positions. The hydraulic head upstream (P08) and downstream (P17) are used as a boundary condition. Other measured values are used to compare measurements and calculations. The actual 2D numerical calculations are presented in Chapter 4.

Table 3-1 gives an overview of the moments when the different erosion stages were reached, with the applied head and at p08 measured head and the flow rate at that time.

Table 3-2 and Table 3-3 show the measured heads at the moment that the pipe has reached the barrier (end of stage I), at the moment before applying the last load step (critical situation before failure, and at the moment of failure (stage V). After failure all water taps were shut off, so only hydrostatic pressure was measured. However, the zero-pressure water level can differ. Almost all gauges show higher heads than the starting value at the beginning of the test, which is a consequence of shutting down upstream and downstream taps at different moments. The absolute values of the measured heads are therefore dependent on the order of shutting down the taps; but the differences in heads are hydrostatic. In particular, the differential gauges show implausible values at the critical state at test MS40. The pressure gauges seem to have drifted somewhat during the test. Therefore, all end values have been reset and the values during failure and at the critical stage have been obtained by back calculation.

Table 3-1 Time, flow and applied head/p08 for both tests at the different erosion stages until failure

	MS 38	**MS 40**
STAGE I: pipe reaches the barrier time after start [hh:mm]	1:05 – 1:35	1:35
Flow rate [l/min]	0.75	1.02
Applied head H_up [mm H_2O] / P08 [mm H_2O]	160 / 156	170 / 164
STAGE II: lateral pipe fully developed time after start [hh:mm]	2:25	3:30
Flow [l/min]	8.5	7.5
Applied head H_up [mm H_2O] / P08 [mm H_2O]	660 / 635	540 / 514
STAGE III: slope top reaches upstream edge time after start [hh:mm]	3:10	8:45
Flow rate [l/min]	12.0	8.8
Applied head H_up [mm H_2O] / P08 [mm H_2O]	1010 / 965	640 / 567
STAGE IV: slope toe connected with pipe time after start [hh:mm]	3:34	10:45
Flow rate [l/min]	13.8	9.9
Applied head H_up [mm H_2O] / P08 [mm H_2O]	1010 / 964	690 / 607
STAGE V: critical stage before failure time after start [hh:mm]	22:45 – 23:05	23:50 – 24:05
Flow rate at critical stage before failure [l/min]	52.8	62.3
Applied head H_up [mm H_2O] / P08 [mm H_2O]	3960 / 3819 (back-calculated: 3830)	4690 / 4427 (back-calculated 4342)
Slope angle [°] (linear averaged left-hand, centre, right-hand)	31.5; 27; 28.8	25; 22.6; 30.3
Pipe depth at exit of protuberance [mm] (estimated)	20	20
FAILURE: time after start [hh:mm]	23:05	24:05
Applied head H_up [mm H_2O] / P08 [mm H_2O] to induce failure *	4060 / 3906	4790 / 4436

* This is the head applied at the last load step. At the moment of failure p08 decreased, because the pressure surge moved downstream. These are the values in the following tables.

The above-mentioned slope angles at the end of stage IV are determined on the basis of the three positions of the crest of the slope at the upstream side of the protuberance where tape measure was fixed (some positions have been estimated from the course of the crest, because the position itself was outside the viewing range of camera position (either covered by the bracing bar at the top of the acrylate plate or the level of the crest was in the space of the opening of the cover plate, thus below the acrylate side wall of the protuberance element. The position of the toe of the slope was visually estimated. The angle is calculated based on a linear interpolation between slope crest and toe over the total width of the barrier (i.e. 0.3 m). This is a rough estimate, because the real shape of the surface of the barrier at the end of stage IV is slightly concave (Figure 3.10) and differs also in the longitudinal transects relative to the centre line. The slope angle was also determined based

on topography measurements with a laser and an optical distance sensor (Deltares 2020b). The border areas of the barrier (≈ 1 cm) could not be mapped by this measuring system. Unfortunately, the entrapment of small air bubbles at the top of the protuberance caused measurement noise. In test MS40 a reflection caused a measurement error in about half of the scanned area, so that no determination of the slope angle was possible. In order to estimate the slope angle and toe depth of the CSB, a 2nd order polynomial was fitted for several longitudinal transects. The slope angle was determined by the arctangent of the gradient of the curve.

For MS38 the (extrapolated) toe depth below the edge of the protuberance varied between 2 and 3 cm; the slope angle was 27° in the centre line of the set-up and around 10-22° according to the laser measurements in the other transects.

Table 3-2 MS38: measured heads at the end of stage I, critical situation before stage V and at the very moment of failure (stage V); this means the applied head was higher than measured at this very moment at p08, because the pressure surge went downstream through the set-up

	x	y	z	situation at the end of stage I (5-min mean)	critical situation (5-min mean)	failure (23:06:35)	end value with shut taps	back calculated value at critical situation	back calculated value at failure
	mm	mm	mm	mmH2O	mmH2O	mmH2O	mmH2O	mmH2O	mmH2O
P01	1357	-388	0	155	3764	3411	-7	3771	3418
P02	835	-388	0	131	1806	3312	-13	1819	3325
P03	550	-388	0	115	576	3302	-13	589	3315
P04	357	-388	0	92	498	3254	-13	511	3267
P05	107	-388	0	56	482	3248	-15	497	3263
P06	650	130	430	101	390	3262	-14	404	3276
P07	650	130	-430	110	417	3275	-12	429	3287
P08	1386.5	0	0	156	3816	3439	-14	3830	3453
P09	980	0	0	149	3023	3357	-14	3037	3371
P10	805	130	235	116	444	3319	-15	459	3334
P11	805	130	-25	115	447	3324	-15	462	3339
P12	805	130	-285	116	460	3322	-17	477	3339
P13	505	150	-25	116	445	3322	-15	460	3337
P14	505	250	-25	102	429	3306	-15	444	3321
P15	390	0	0	96	437	3273	-15	452	3288
P16	195	0	0	60	437	3213	-15	452	3228
P17	55	0	0	7	437	3179	-15	452	3194
P21	805	100	-260	105	417	3294	-16	433	3310
P22	805	130	-260	110	427	3296	-15	442	3311
P23	805	100	0	110	405	3295	-15	420	3310
P24	805	130	0	107	385	3295	-15	400	3310
DP1	805	70	235	-2	-18	-29	0	-18	**-30**
DP2	805	100	235	-14	-44	-33	-18	-27	-15
DP3	805	70	-25	-18	-31	-88	3	**-35**	**-92**
DP4	805	100	-25	54	49	15	81	**-31**	**-66**
DP5	805	70	-285	-12	-31	-43	-15	-16	-29
DP6	805	100	-285	-8	-22	-24	10	**-32**	**-34**

Table 3-3 MS40: measured heads at stage I, critical situation before stage V and at failure (stage V)

	x	y	z	situation at the end of stage I (5-min mean)	critical situation (5-min mean)	failure (24:06:04)	end value with shut taps	back calculated value at critical situation	back calculated value at failure
	mm	mm	mm	mmH20	mmH20	mmH2O	mmH2O	mmH2O	mmH2O
P01	1357	-388	0	165	4409	4098	84	4325	4015
P02	835	-388	0	131	2260	3973	80	2180	3893
P03	550	-388	0	111	1160	3990	144	1016	3846
P04	357	-388	0	88	1062	3924	115	947	3809
P05	107	-388	0	66	1057	3924	166	891	3758
P06	650	130	430	112	948	3924	84	864	3841
P07	650	130	-430	102	920	3903	63	857	3840
P08	1386.5	0	0	164	4427	4103	85	4342	4017
P09	980	0	0	160	3757	4064	170	3587	3894
P10	805	130	235	115	1002	3980	142	860	3838
P11	805	130	-25	116	1012	3995	157	855	3838
P12	805	130	-285	114	1001	3971	142	859	3829
P13	505	150	-25	115	1005	3987	150	855	3837
P14	505	250	-25	115	1001	3984	146	855	3838
P15	390	0	0	85	994	3928	148	846	3780
P16	195	0	0	36	999	3878	153	846	3725
P17	55	0	0	13	997	3852	151	846	3701
P21	805	100	-260	97	954	3924	92	863	3833
P22	805	130	-260	116	1014	3929	154	860	3775
P23	805	100	0	113	997	3919	140	857	3779
P24	805	130	0	113	1000	3927	142	858	3785
P25	805	100	260	116	1034	3930	158	876	3772
P26	805	130	260	115	1005	3931	141	864	3790
DP1	805	70	235	-11	-98	-90	-86	-12	-4
DP2	805	100	235	-14	-81	-71	-58	-23	-13
DP3	805	70	-25	-15	-102	-107	-74	-29	**-33**
DP4	805	100	-25	-32	-234	-243	-212	-22	**-31**
DP5	805	70	-285	-12	14	25	46	**-33**	-22
DP6	805	100	-285	-12	-126	-120	-97	**-30**	-23

Table 3-4 MS40: measured heads at stage I, critical situation before stage V and at failure (stage V)

For these data the start values have not been reset to zero.

	X	y	z	situation at the end of stage I (5-min mean)	critical situation (5-min mean)	failure (24:06:04)	end value with shut taps	back calculated value at critical situation	back calculated value at failure
	mm	mm	mm	mmH20	mmH20	mmH2O	mmH2O	mmH2O	mmH2O
P01	1357	-388	0	165	4404	4080	83	4326	4015
P02	835	-388	0	131	2262	3955	84	2176	3889
P03	550	-388	0	111	1098	3906	84	1076	3906
P04	357	-388	0	88	1030	3864	84	978	3840
P05	107	-388	0	66	974	3809	83	974	3841
P06	650	130	430	112	946	3902	84	864	3840
P07	650	130	-430	102	940	3901	83	837	3820
P08	1386.5	0	0	164	4421	4084	84	4344	4019
P09	980	0	0	160	3667	3958	83	3675	3982
P10	805	130	235	115	942	3898	83	919	3897
P11	805	130	-25	116	937	3898	83	929	3911
P12	805	130	-285	114	942	3890	83	919	3888
P13	505	150	-25	115	938	3898	83	921	3904
P14	505	250	-25	115	938	3898	83	917	3900
P15	390	0	0	85	929	3838	83	911	3845
P16	195	0	0	36	929	3768	83	916	3794
P17	55	0	0	13	928	3759	83	914	3768
P21	805	100	-260	97	946	3902	84	870	3841
P22	805	130	-260	116	940	3907	81	933	3848
P23	805	100	0	113	940	3897	83	914	3836
P24	805	130	0	113	940	3904	83	917	3844
P25	805	100	260	116	959	3906	84	949	3846
P26	805	130	260	115	946	3908	83	922	3848
DP1	805	70	235	-11	-98	-90	-86	-12	-4
DP2	805	100	235	-14	-81	-71	-58	-23	-13
DP3	805	70	-25	-15	-102	-107	-74	-29	**-33**
DP4	805	100	-25	-32	-234	-243	-212	-22	**-31**
DP5	805	70	-285	-12	14	25	46	**-33**	-22
DP6	805	100	-285	-12	-126	-120	-97	**-30**	-23

This back-calculated values have not been used for modelling, but were used for plausibility checks of the calculated results

Table 3-5 MS38 vertical gradients

	x	y	z	critical situation (5-min mean)	failure (23:06:35)	back-calculated value at critical situation	back-calculated value at failure
	mm	mm	mm	-	-	-	-
DP1	805	70	235	-0.58	-0.98	-0.59	**-0.98**
DP2	805	100	235	-1.48	-1.10	-0.89	-0.51
DP3	805	70	-25	-1.05	-2.95	**-1.16**	**-3.05**
DP4	805	100	-25	1.65	0.50	**-1.05**	**-2.20**
DP5	805	70	-285	-1.03	-1.44	-0.55	-0.95
DP6	805	100	-285	-0.73	-0.79	**-1.08**	**-1.14**

DP1 Differential pressure, measured between DP1 and DP2
DP2 Differential pressure, measured between DP2 and P10
DP3 Differential pressure, measured between DP3 and DP4
DP4 Differential pressure, measured between DP4 and P11
DP5 Differential pressure, measured between DP5 and DP6
DP6 Differential pressure, measured between DP6 and P12

Table 3-6 MS40 vertical gradients

	x	y	z	critical situation (5-min mean)	failure (24:06:04)	back-calculated value at critical situation	back-calculated value at failure
	mm	mm	mm	-	-	-	-
DP1	805	70	235	-3.27	-3.01	-0.39	-0.13
DP2	805	100	235	-2.70	-2.36	-0.75	-0.42
DP3	805	70	-25	-3.41	-3.56	-0.95	**-1.10**
DP4	805	100	-25	-7.78	-8.08	-0.73	**-1.03**
DP5	805	70	-285	0.45	0.82	**-1.10**	-0.73
DP6	805	100	-285	-4.20	-4.00	**-0.99**	-0.78

Table 3-5 and Table 3-6 show the vertical gradient at the critical state and during failure for test MS38 and MS40 respectively. In both tables, the values, back-calculated from the final value at the moment when all taps were turned off, are assessed to be more reliable than the readings of these gaues because of the drift of the measured heads of the differential gauges in the course of the test.
In test MS38 the vertical gradients dp3 and dp4 in the centre line and dp6 on the left-hand side in the upper part of the slope crest are around 1 at the critical state. During failure the vertical gradients in the centre line of the set-up dp3 and dp4 exceed 1 by far, which is remarkable because a gradient much larger than 1 would not be expected. This could have been caused by a high flow velocity along one of the inlets of the differential pressure gauges.
In test MS40 the vertical gradients dp5 and dp6 reach values around 1 at the critical stage. The gradient between 70 mm and 100 mm above the bottom edge of the protuberance is little higher than the gradient between 100 and 130 mm above the bottom edge, which confirms the observation that the particle pressure at the surface of the slope has almost faded away so that the sand particles are moving downwards.
In the end, there is much uncertainly regarding the reliability of the differential gauges. Therefore, in the numerical simulation of the tests the measurements of the differential gauges are neglected.

4 Numerical simulations of the experiments

This chapter describes the numerical simulation (postdiction) of both medium-scale verification tests for the coarse sand barrier with a protuberance of 0.3 m height and 0.3 m width. For an assessment of the stability and strength of the barrier, simulations of the tests are presented based on head measurements at the top and the bottom of the container and flow rates. The simulations are necessary because it is technically not possible to measure the gradients inside the barrier – especially the outward gradients along the developing slope of the barrier. By modelling the tests, the resulting gradients along the barrier slope give an indication for the occurring gradients along the slope and can be used for the validation of the expected outward gradients based on the criterion by van Rhee & Bezuijen. Therefore, it is aspired to reach a good fit for the calibration of the numerical models with the measured heads and flow rates by varying the contrast in hydraulic conductivity / intrinsic permeability between the different soils of the set-up. The aim is to match all heads and the discharge reasonably well; however, a priority is given to a match of the heads on the upstream side of the barrier and at the toe of the slope. Those are considered most significant for the computation of the local vertical gradients and the gradients perpendicular to the slope surface. The computation of these gradients is the main purpose of the numerical modelling. The computed gradients are compared with the gradients resulting from the stability criterion of van Rhee & Bezuijen for a certain slope angle.

The modelling the 3D reality of the pipe in the experiments in a 2D model requires some simplification, which is discussed first in Section 4.1. In Chapter 5 it will be shown that the head drop over the barrier (correcting for the head drop over the outflow part) at failure is 3.4 m in both tests. Only MS40 has a 20% higher flow rate. This implies that the permeability contrast is more or less the same in both tests, but the permeabilities are higher in test MS40.

4.1 2D numerical simulations MSP experiments

The critical conditions for failure are considered to be the conditions before applying the last head increment that caused failure of the slope in the CSB. For modelling the strength of such a situation, two situations are assumed to be critical: the vertical gradient at the upstream end of the protuberance and the gradient perpendicular to the slope surface. To calculate these gradients the angle of the slope in the barrier is an input parameter. A shallower slope will lead to a thinner vertical covering for fulfilling the heave criterion on the upstream edge of the protuberance, which results in a lower strength. Thus, for a prediction model, it is important to be able to predict what slope is stable at the hydraulic gradients that occur in the field.

The erosion of a slope subjected to an outward directed seepage has been investigated by several researchers. The gradient perpendicular to of the slope surface, is of interest to determine whether the slope is expected to be stable. In the analysis at hand this relation is used to compute the slope angle as a function of the outward directed hydraulic gradient.

The purpose of the numerical models is to characterise the strength of the barrier, by modelling the critical situation before applying the last load step which resulted in failure of the slope of the barrier. In both tests, the slope inside the barrier was measured at several times during the test. The slope that was measured during the last measurement, which was 0.10 m below the critical applied head drop is modelled, using the head at p08 as the actual head as a consequence of head loss in the hose and conduit between water reservoir and medium-scale box.

The 5-minute-average head measured before the application of the last head increment and the flow rate for that interval are used for fitting the numerical simulations. Hydraulic conductivities are fitted to match the measured head profile and flow rate at this critical step.

The modelling approach that is used for the experiments corresponds to a 3D situation where the pipe has the width of the entire set-up in the background sand downstream. The same applies for the slope of the barrier inside the protuberance.

In the 2D models used to model the experiments, the pipe is present from the outflow boundary up to the barrier, and in the barrier, there is a slope with the lowest slope angle that was observed in the centre line of the experiments. In the models the toe of the slope is 2 cm below the downstream cover layer (top level of the primary sand bed). However, before failure there is a clear flow through the centre of the set-up. The steeper slopes on the sides indicate that there is flow from the sides to the centre of the set-up. Nevertheless, a 2D calculation seems to be sufficient as a first approximation for a comparison of the measured and the calculated gradients.

In order to model the strength of the barrier in such a configuration, several aspects are of importance. Firstly, the outward gradient on the slope surface, which is used to analyse the slope stability. Secondly, the vertical gradient at the top of the slope at the upstream end of the barrier, which is used to analyse fluidisation. Laser measurements and meter readings (of the tapes fixed at the upstream and downstream side wall of the protuberance) were made of the depth of the surface of the barrier during the tests. These are used as a basis for schematising the slope in the models. Those models are used to compute the gradients that were acting at the critical stage in the experiments just before failure.

Observations indicate that the deepest point of the toe of the slope before failure was below the bottom edge of the protuberance and thus below the impermeable cover layer, which means that there was contact between the void inside the barrier and the pipe downstream originating from the outlet hole at the critical point before failure. This breakthrough was also observed in the development of the measured heads. Because of this open connection between the void inside the protuberance and the downstream pipe, which was meandering over the whole sand bed a uniform boundary condition from the outlet up to the top of the slope is applied using the measured head p15 at the top of the sand bed nearest to the barrier.

4.1.1 Stability of a slope subjected to outward seepage

For a continuum approach considering the equilibrium of forces on a block of soil on an infinite slope, Kovacs (1981), Van Rhee and Bezuijen (1992) and Philippe and Richard (2008) derive similar expressions. Rewriting these equations gives the stable slope angle as function of the gradient perpendicular to the slope (where the outward directed gradient is positive) as:

$$\beta_{i,cr} = \alpha - arcsin\left(\left[\frac{i}{\frac{(1-n)(\rho_S-\rho_W)}{\rho_W}}\right] sin(\alpha)\right) \qquad \text{(Equation 1)}$$

Symbols
- $\beta_{i,crit}$ = angle of the slope, degrees
- n = porosity
- ρ_w = density of water, kg/m^3
- ρ_w = density of grains, kg/m^3
- α = angle which characterises internal friction in the soil, degrees
- i = gradient perpendicular to the slope (outward direction is positive), -

As described in (Deltares 2020a) the following insights can be obtained directly from this formula:

- When there is no flow, the β is equal to α, and independent of porosity. However, α is still depend on the porosity
- When there is flow, β is higher for denser samples for the same gradient, due to the larger soil weight, counteracting the hydraulic forces, the effect of RD on the friction angle is not directly accounted for in the calculations. Since the friction angle increases with the density this would lead to even more increase of β
- For a given porosity and a flat surface (β = 0) the critical gradient is independent of the friction angle (as the critical gradient is now only determined by the weight of the soil counteracting the seepage force)
- A higher internal friction results in a steeper slope for the same gradient.

4.1.2 Model geometry and mesh

4.1.2.1 Geometry and modelling of the pipe and the slope

First, a model is made for the situation at the end of stage I when the first pipe had just not reached the barrier.

It is chosen to model this moment when there is a measurable head development at the gauges and a certain amount of discharge. These values are used to fit the calculated heads with the measured heads by calibrating the hydraulic conductivities of the modelled materials. The boundary condition in the downstream fine sand will not be very accurate, since the overall permeability will be influenced by the pipe. However, this permeability is not important for the test, since during design conditions with a large pipe, the permeability of that pipe will be dominant.

In the model the barrier is present between x coordinates x = -0.805 m and x = -0.505 m and z coordinates z = +0.300 m to z =-0.404 m. All distances are relative to the centre of the exit hole at the top of the model. Below the impermeable cover layer, background sand is present down to the bottom of the model at z = -0.404 m, from x= = -0.505 m to x = 0.368 m and from x = -1.005 m to x = -0.805 m. At the upstream side there is also coarse sand below the cover layer down to the bottom of the model at z = -0.404 m, from x = -1.385 m to x = -1.005 m. The bulkhead is not modelled, but at the downstream sand bed is reaching further behind the outlet position.

This model Figure 4.1 is adapted for both tests.

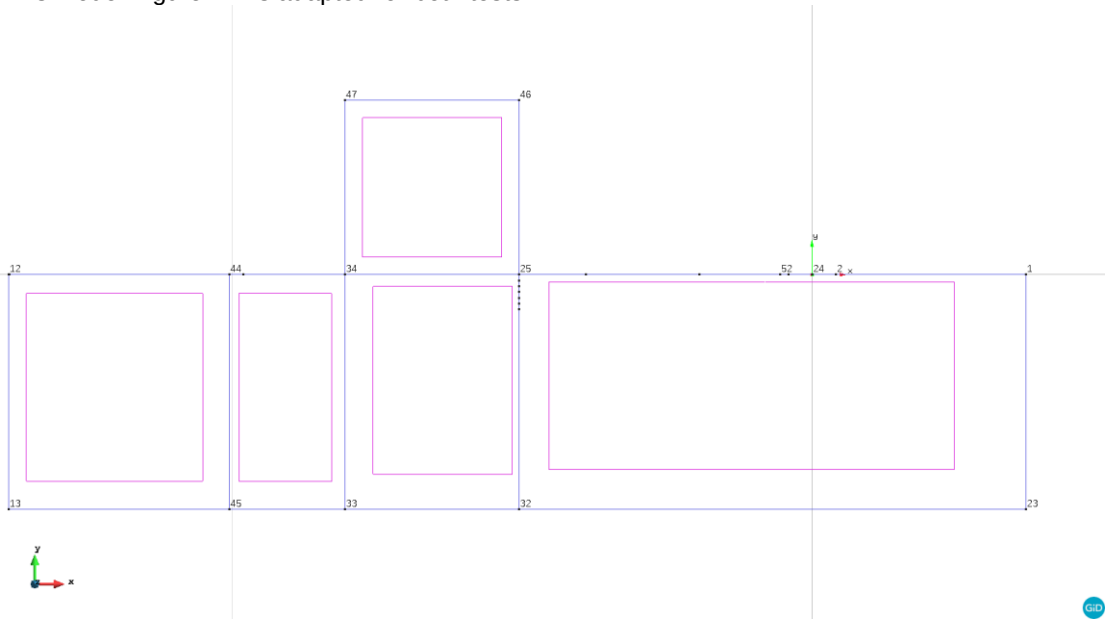

Figure 4.1 Geometry of the initial situation with no pipe, used for MS38 andMS40

Secondly, two models are made for the situation just before failure, thus the critical situation before applying the final load step. The slope of the barrier in the model is a schematisation that is based on the last meter reading of the height of the slope at the upstream side of the protuberance before applying the last load step. In those readings the crest of the slope in the barrier has a height of z = +0.135 m and z = +0.100 m in the centre line of the set-up in test MS 38 and MS 40 respectively. Observations indicate that the deepest point of the toe of the slope was below the impermeable cover layer at the critical point for failure. Laser measurements had a too high uncertainty to be able to reliably determine the bottom of the slope. Observations indicate that the deepest point of the toe of the slope was below the cover layer at the critical point of failure. The toe of the slope is therefore modelled at z = - 0.020 m below the edge of the protuberance; the assumption is that there is no head loss in the pipe. The angle of the slope inside the barrier is the angle between the lowest point that the slope has eroded at the upstream edge of the protuberance at the critical point and the depth of the pipe at the downstream edge of the protuberance, which differs for each of the two experiments.

Therefore, two models are made in which the slope runs from:

- x = - 0.805 m z = + 0.135 m, and the downstream side of the slope is at x = - 0.505 m, z = - 0.20 m (27-degree slope), model MS 38 (Figure 4.4)
- x = - 0.805 m z = + 0.100 m, and the downstream side of the slope is at x = - 0.505 m, z = - 0.20 m (22-degree slope), model MS 40 (Figure 4.5).

The pipe in these two models is modelled as a boundary condition along the top of the sand bed from the outlet until the top of the slope. The impermeable cover layer is not modelled. The void which is present above the slope in the model is not modelled as a material with a hydraulic conductivity that is 10^6 higher than the hydraulic conductivity of the barrier (i.e. it effectively has no resistance to flow) as in earlier modelling, but a boundary condition along the slope is modelled with the head at the top of the sand bed measured by the gauge p15.

4.1.2.2 Material parameters

As there was a different porosity in the coarse sand and background sand upstream of the barrier, in the background sand downstream of the barrier, and in the coarse sand in the lower and the upper barrier, these are distinguished as different soil types. The hydraulic conductivity is based on the relative density during preparation and the correlation between hydraulic conductivity and porosity that was derived, based on column experiments. The porosity that was determined by preparation can be used to calculate the expected hydraulic conductivity.

The intrinsic permeability K is determined according to:

$$K = k \frac{\mu}{\rho g} \qquad \text{(Equation 2)}$$

Where ρ is the water density in kg m³, g the gravitational constant (i.e. 9.81 m s^{-2}) and μ the dynamic viscosity in Pa s. The parameter μ is evaluated with the temperature T in °C following the Vogel-Fulcher-Tammann equation:

$$\mu = e^{-3.7188+\left(\frac{578.919}{(T+273.15)-137.546}\right)} \qquad \text{(Equation 3)}$$

Finally, the temperature is used to apply a correction for change in viscosity and density, relative to 20°C:

$$k_{20} = k \cdot \frac{\mu \cdot \rho}{\mu_{20} \cdot \rho_{20}} \text{ or } K_{20} = K \cdot \frac{\mu \cdot \rho}{\mu_{20} \cdot \rho_{20}}$$ (Equation 4)

The model relating porosity and hydraulic conductivity is adopted from the Kozeny-Carman equation:

$$K = a \cdot \frac{n^3 D_{50}{}^2}{(1-n)^2}$$ (Equation 5)

where a is the proportionality and unit factor an D_{50} is the average particle diameter.

This changes the Kozeny-Carman equation to:

$$k_{20} = x_1 \frac{n^3}{(1-n)^2} \text{ or } K_{20} = x_2 \frac{n^3}{(1-n)^2}$$ (Equation 6)

where the constant x = a D_{50}^2 is a correlation parameter, which describes the relation between the hydraulic conductivity at 20°C k_{20} (m/s) or the intrinsic permeability K_{20} and the porosity n. The regression is based on experimental data obtained from a constant head permeability test set-up. As the mean temperature during the tests varied in the range of 17˚C to 20˚C, the temperature dependence of the viscosity of water was taken into account to compute the hydraulic conductivity that would be expected based on the porosity.

The hydraulic conductivity k_{20} of the different sand columns upstream, downstream and inside the barrier is derived from the porosities of these sections, given in Table 2-3 and Table 2-4 by using the hydraulic conductivity factor x_1 for B25 and GZB3, given in Table 2-2.

In DgFlow, the groundwater model used for this post diction the intrinsic permeability K_{20} (m²) is used as an input value (start value) for the calibration, so the hydraulic conductivity k_{20} has to be determined, using the intrinsic permeability factor x_2.

The porosity *n* of the sample can be determined, assuming full saturation, with the known sample volume *V*, dry mass *m* and particle density ρ_s:

$$n = \frac{V - \frac{m}{\rho_s}}{V}$$ (Equation 7)

The porosity can be used to express results as a function of relative density, $D_r(n)$, according to:

$$D_r(n) = \frac{n_{\max} - n}{n_{\max} - n_{\min}}$$ (Equation 8)

with the minimum and maximum porosities, n_{min} and $n_{max.}$

These hydraulic conductivities and intrinsic permeabilities are used as start values for the calibration of the models in DgFlow (Table 4-1), i.e. the fitting of the calculated heads with the measured heads.

Table 4-1 Start values of hydraulic conductivity k_{20} and intrinsic permeability K_{20} based on porosities which were derived from preparation

sand type	location	MS38: k_{20} [m/s]	MS38: K_{20} [m²]	MS40: k_{20} [m/s]	MS40: K_{20} [m²]
B25	upstream	1.76E-4	1.82E-11	1.80E-4	1.86E-11
B25	downstream	1.70E-4	1.76E-11	1.82E-4	1.88E-11
GZB3	upstream	4.42E-3	4.60E-10	4.37E-3	4.55E-10
GZB3	upper part of barrier in protrusion	4.63E-3	4.82E-10	4.79E-3	4.98E-10
GZB3	lower part barrier below protrusion	4.52E-3	4.71E-10	4.27E-3	4.45E-10

Figure 4.2 shows the position of the different materials in the model.

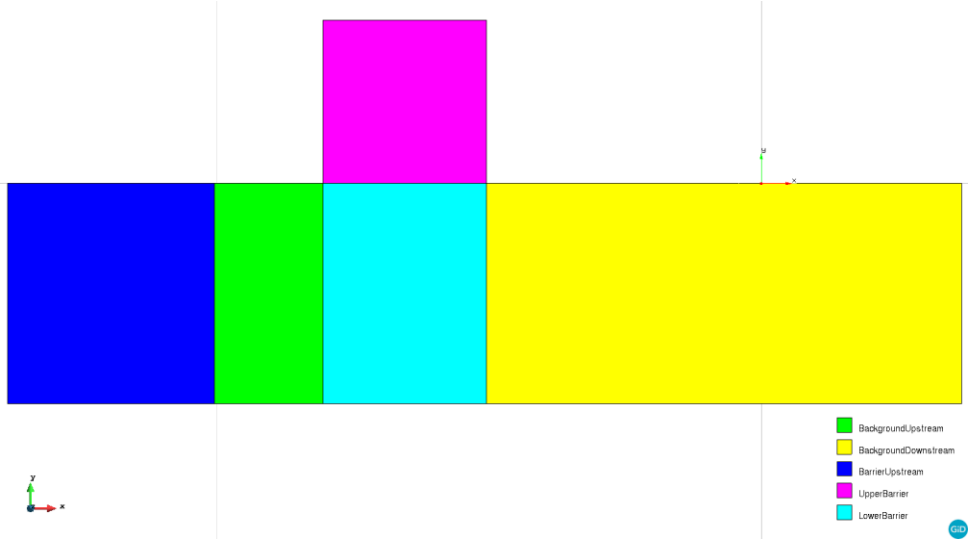

Figure 4.2 Modelled materials

4.1.2.3 Mesh

The model size and the mesh are similar to the mesh that was determined for the prediction of the medium-scale experiment with protuberance. A mesh with triangular elements is used. Element dimensions and mesh refinement are as in the prediction model, with an unstructured mesh and element size of 1 mm in the top of the barrier. The remainder of the model has an element size of 1 cm. Figure 4.3 to Figure 4.5 show the meshes of the tree models. In both models for the critical stage IV the toe of the slope and the top of the downstream sand layer are 2 cm lower than the initial level of the top of the aquifer.

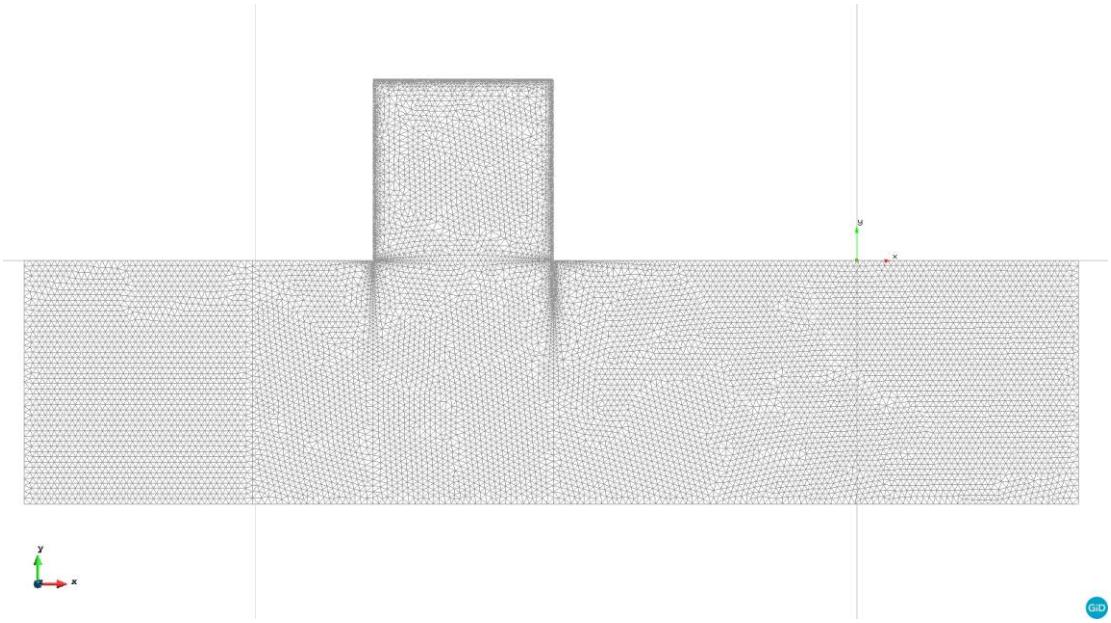

Figure 4.3 Modelled mesh for initial situation (MS38 and MS40)

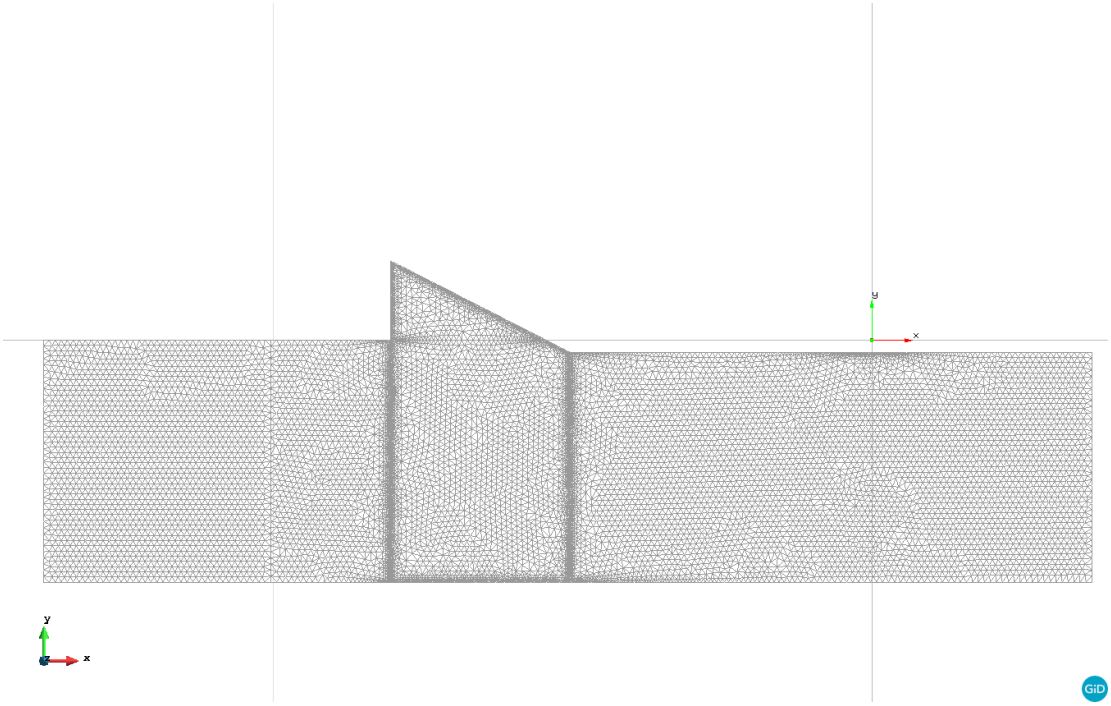

Figure 4.4 Modelled mesh for critical situation (MS38).

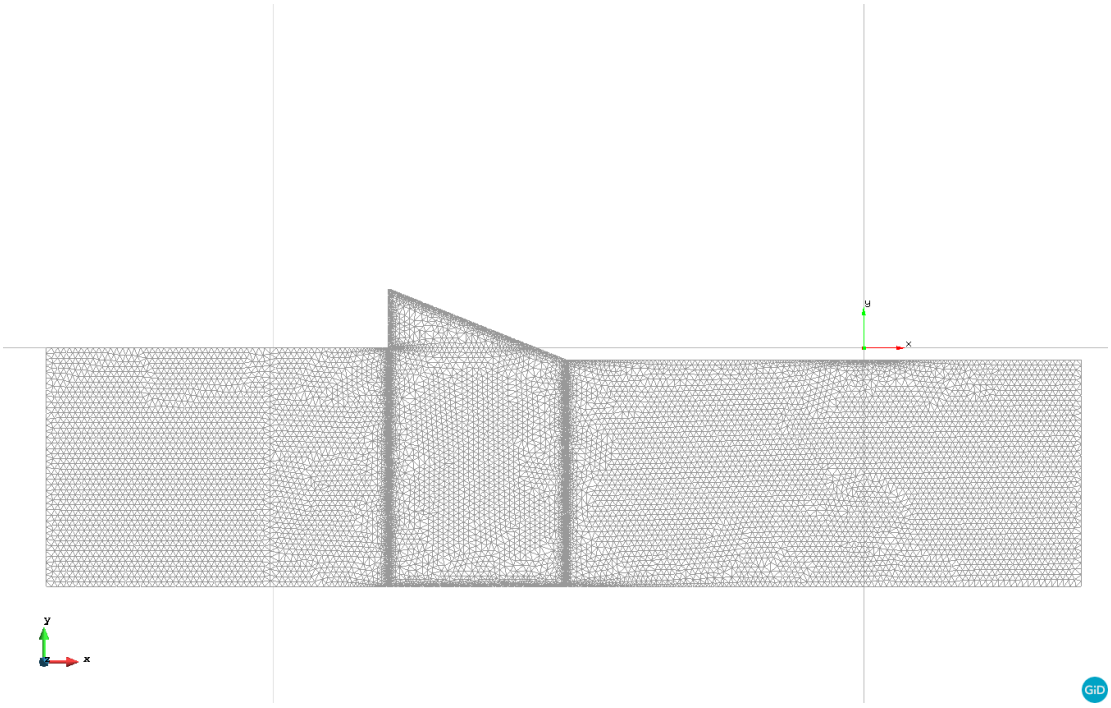

Figure 4.5 Modelled mesh for critical situation (MS40). For MS40 the top of the slope is located 0.035 m lower than for MS38.

4.1.2.4 Boundary conditions

The upstream head measured by transducer p08 is used in the models as an upstream boundary condition. As a downstream boundary condition, the head that was measured in the pipe - which was the same for al pressure gauges at the top (p15, p16 and p17) - is used. This downstream head is also used as a boundary condition along the top of the slope up to the crest of the slope. Heads used as inputs are the heads that are measured in the critical step before failure, i.e. at the next to last load step. The head in the pipe is based on p17 - the head at the gauge nearest to the outlet, see

Table 4-2 and Table 4-3. Figure 4.6, Figure 4.7 and Figure 4.8 show the areas where the boundary conditions are applied.

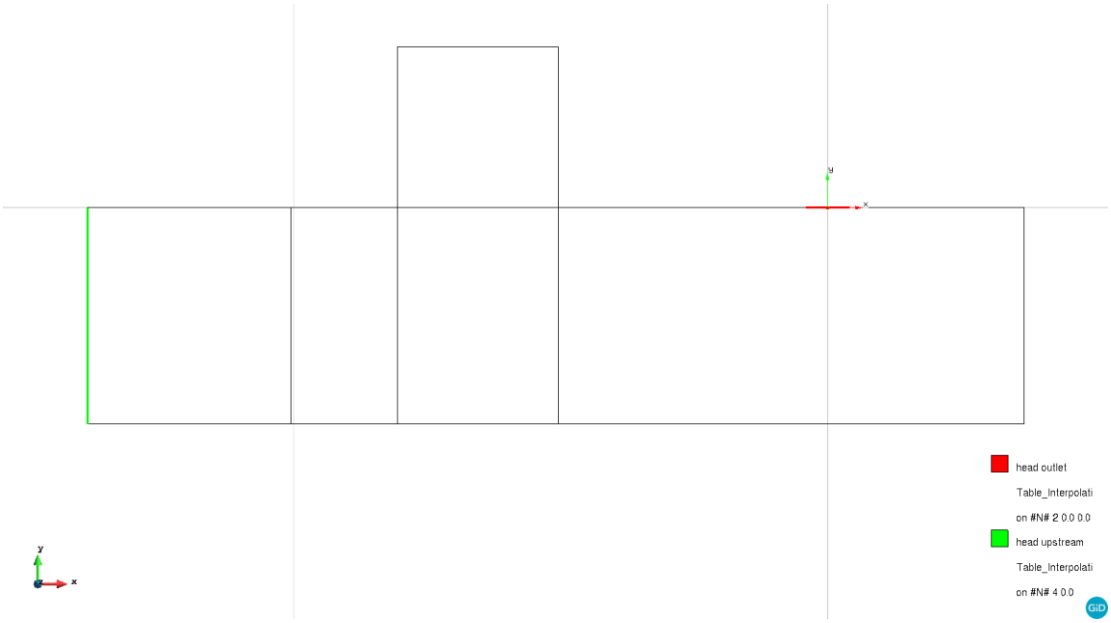

Figure 4.6 Boundary conditions for calibration; downstream head is only applied at outlet

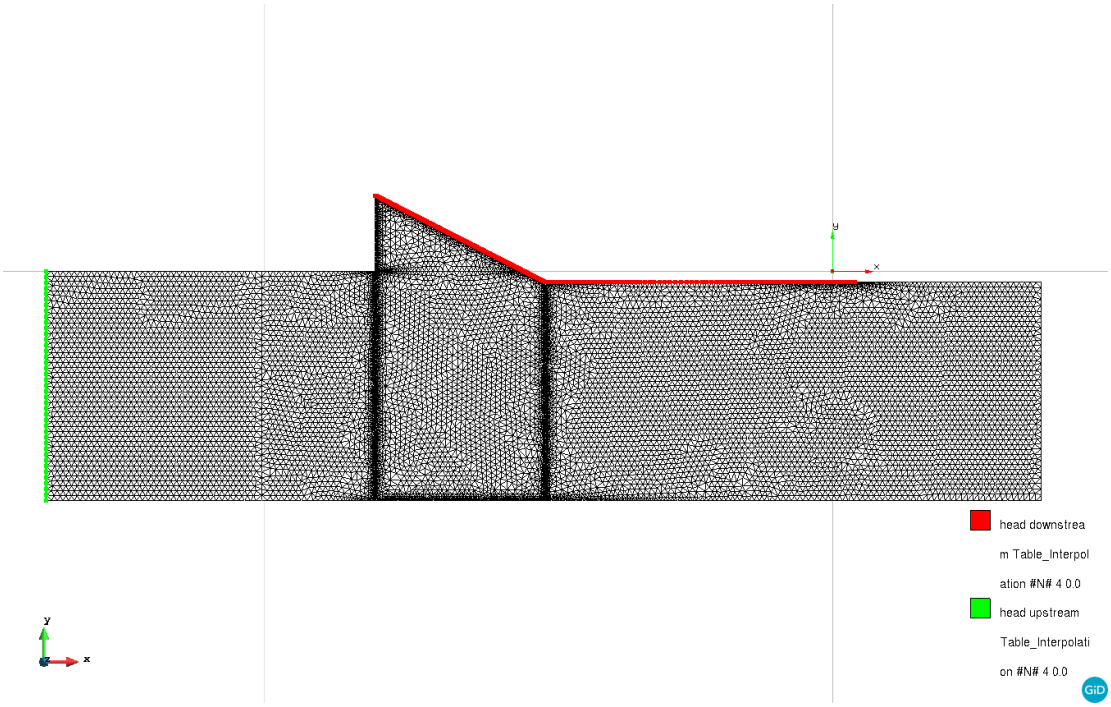

Figure 4.7 Boundary conditions for critical situation before failure for Test MS38

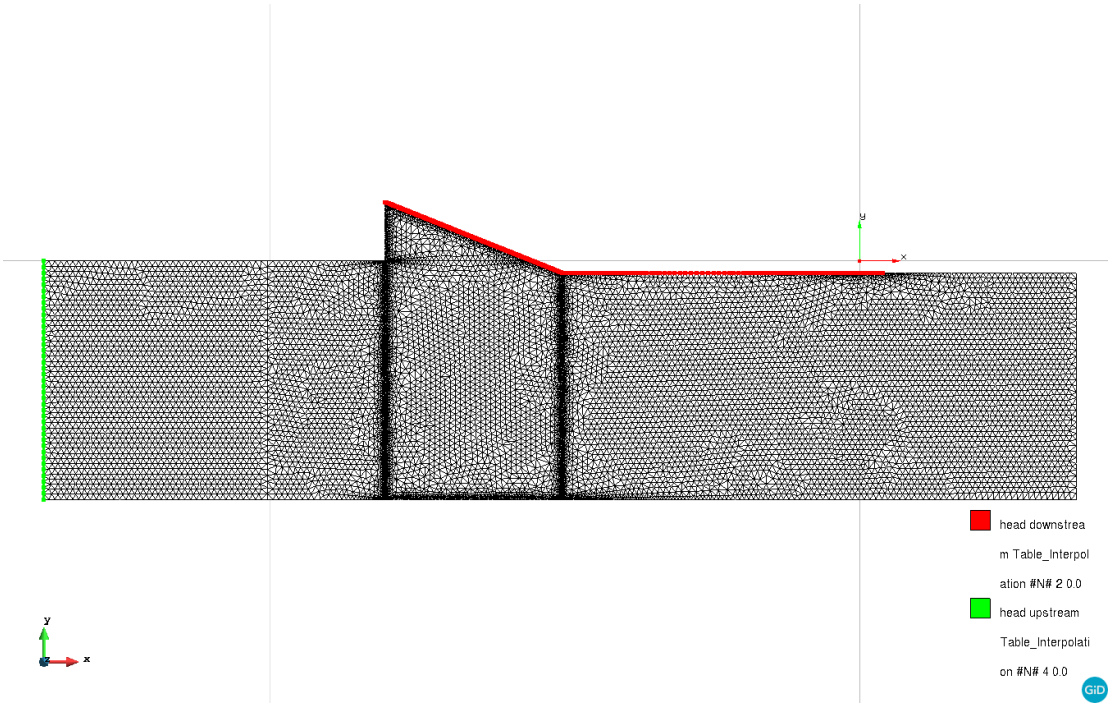

Figure 4.8 Boundary conditions for critical situation before failure for Test MS40

Table 4-2 Upstream and downstream boundary conditions and head drop for the numerical simulation models for the situation when the pipe has just reached the barrier for calibrating the permeabilities

Test	Upstream head, m	Downstream head, m	Head drop, m
MS38_GZB_B25	0.156	0	0.156
MS40_GZB_B25	0.164	0	0.164

Table 4-3 Upstream and downstream boundary conditions and head drop for the numerical simulation models for the critical situation just before applying the last load increment

Test	Upstream head, m	Downstream head, m	Head drop, m
MS38_GZB_B25	3.830	0.452	3.378
MS40_GZB_B25	4.342	0.846	3.496

4.1.3 Procedure

Measured heads and flow rates are used to calibrate the intrinsic permeability of the soils in the numerical simulations. The aim is to match all heads and the discharge reasonably well; however, a priority is given to a match of the heads on the upstream side of the barrier and at the toe of the slope. Those are considered most significant for the computation of the local vertical and perpendicular gradients, the computation these gradients is the main purpose of the numerical models.

The heads on the downstream side of the barrier are considered less important to fit well and are therefore used as a boundary condition. In order to get a fair agreement between the measured heads and discharge and the calculated values, the permeabilities derived from the porosities according to the applied relative densities are used as starting values. First, these permeabilities are varied and then slightly adapted in order to get the best agreement with the measured heads. Secondly, the permeabilities of all materials are scaled by multiplying all permeabilities with a factor that fits the calculated flux at the inlet of the model best with the measured flow rate. By using the same scale factor for all materials, the permeability contrast remains constant. This calibration process is done for stage I where all gauges are covered by soil and an appreciable flow is resulting.

It was expected that this fit can also be applied to model the critical stage, but some fine-tuning was necessary. This could be due to some changes in permeability of the barrier material in the protuberance.

4.2 Results

4.2.1 Head distributions at the end of stage I

The head distribution at the end of stage I for test MS38 is shown in Figure 4.9. For test MS38 the measured flux was 0.7 l/min, the calibrated flux is 0.63 l/min, which is in good agreement, because the calculated heads fit very good. For test MS40 the measured flux was 1.02 l/min, the calibrated flux is 1.00 l/min, but here the calculated heads downstream of the barrier are a little bit higher than the measured ones. The head distribution and the velocities for test MS40 are shown in Figure 4.10. The calibrated permeabilities for stage I are shown in Table 4-4.

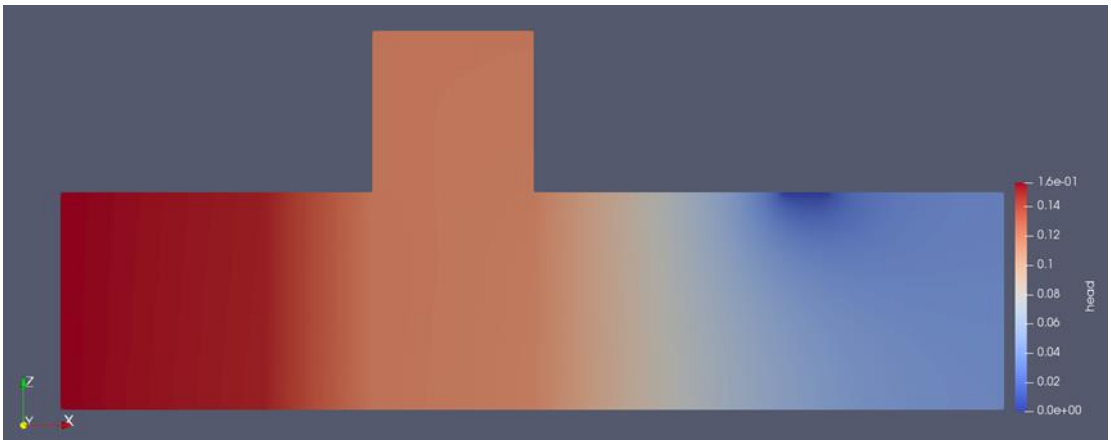

Figure 4.9 MS38 Heads at stage I when pipe has just reached barrier (comparable distribution for MS40)

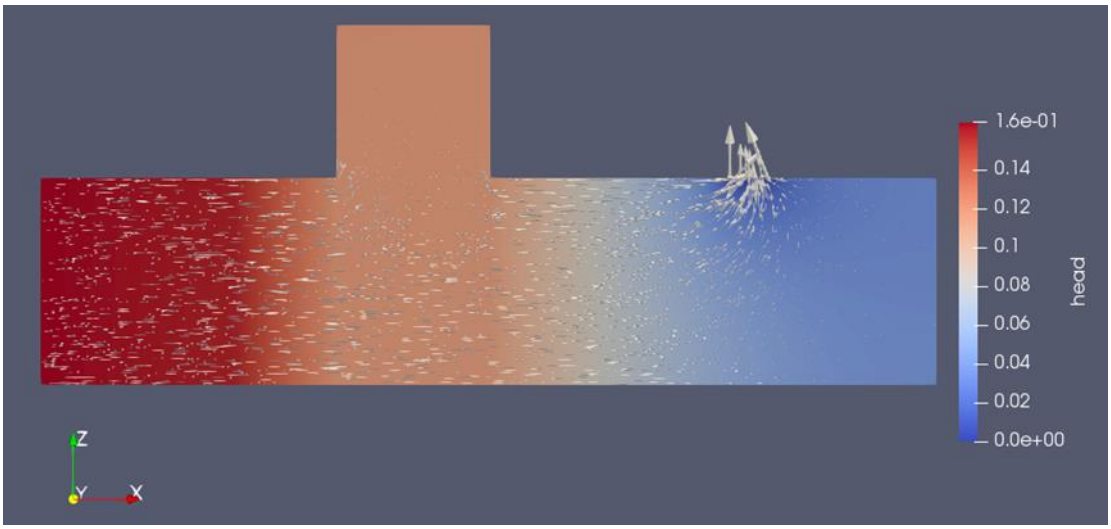

Figure 4.10 MS40 Head distribution and velocities at stage I (comparable distribution for MS38)

The figures show a horizontal flow pattern along the set-up with a concentration of flow at the outlet hole. There is almost no flow inside the protuberance, only in the transition zone of the lower and the upper barrier. Inside the protuberance there is no recognizable variation in head, making a calibration of the upper barrier material based on the head measurements meaningless for this stage. Therefore, the same hydraulic conductivity is assumed for both, the upper and the lower barrier material.

Table 4-4 Calibrated intrinsic permeability (fitted in with the measured heads and fluxes) for stage I

sand type	location	MS38 (input) K_{20} [m²]	MS38 (output) K_{20} [m²]	MS38 (input) k_{20} [m/s]	MS38 (output) k_{20} [m/s]
B25	upstream	1.82E-11	1.90E-11	1.76E-4	1.84E-4
B25	downstream	1.76E-11	1.90E-11	1.70E-4	1.84E-4
GZB3	upstream	4.60E-10	2.20E-10	4.42E-3	2.11E-3
GZB3	Upper barrier inside protuberance	4.82E-10	2.00E-10	4.63E-3	1.92E-3
GZB3	lower barrier below protuberance	4.71E-10	2.00E-10	4.52E-3	1.92E-3
sand type	**location**	**MS40 (input) K_{20} [m²]**	**MS40 (output) K_{20} [m²]**	**MS40 (input) k_{20} [m/s]**	**MS40 (output) k_{20} [m/s]**
B25	upstream	1.86E-11	2.80E-11	1.80E-4	2.71E-4
B25	downstream	1.88E-11	2.80E-11	1.82E-4	2.71E-4
GZB3	upstream	4.55E-10	4.50E-10	4.37E-3	4.32E-3
GZB3	Upper barrier inside protuberance	4.98E-10	(9.00E-10) *)	4.79E-3	(8.64E-3) *)
GZB3	lower barrier below protuberance	4.45E-10	9.00E-10	4.27E-3	8.64E-3

*) according to Figure 4.10 there is some flow in the lower zone of the protuberance in stage I. The calibration of the upper barrier inside the protuberance is not done by fitting with readings of the gauges along the protuberance, but by fitting with the readings of the other gauges along the top and the bottom of the container. Therefore, the same permeabilities used for both the upper and the lower barrier.

Figure 4.11 and Figure 4.12 show the measured and calculated heads for the positions of the gauges at the top and the bottom of the sand bed.

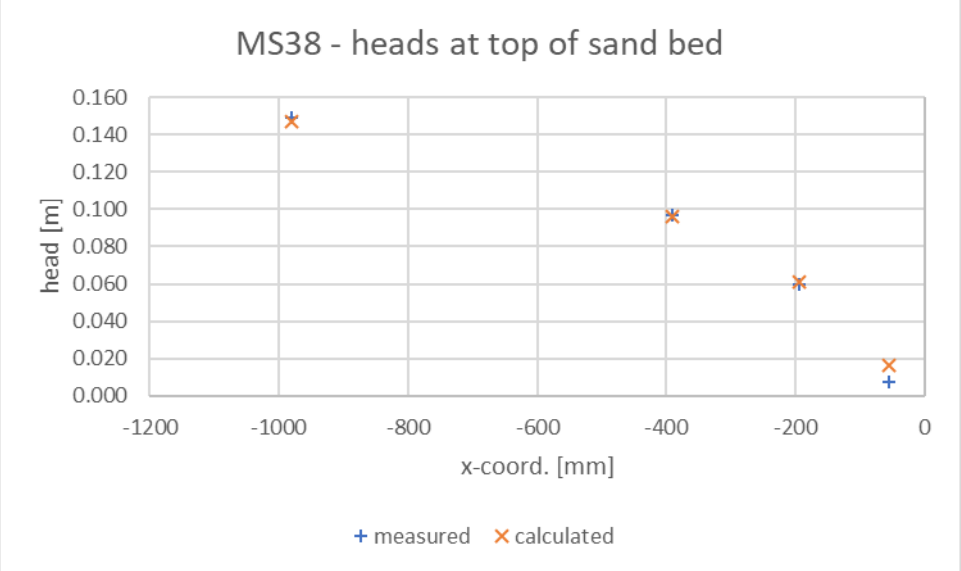

Figure 4.11 MS38: measured and calculated heads at top sand bed (stage I) on behalf of calibration intrinsic permeability

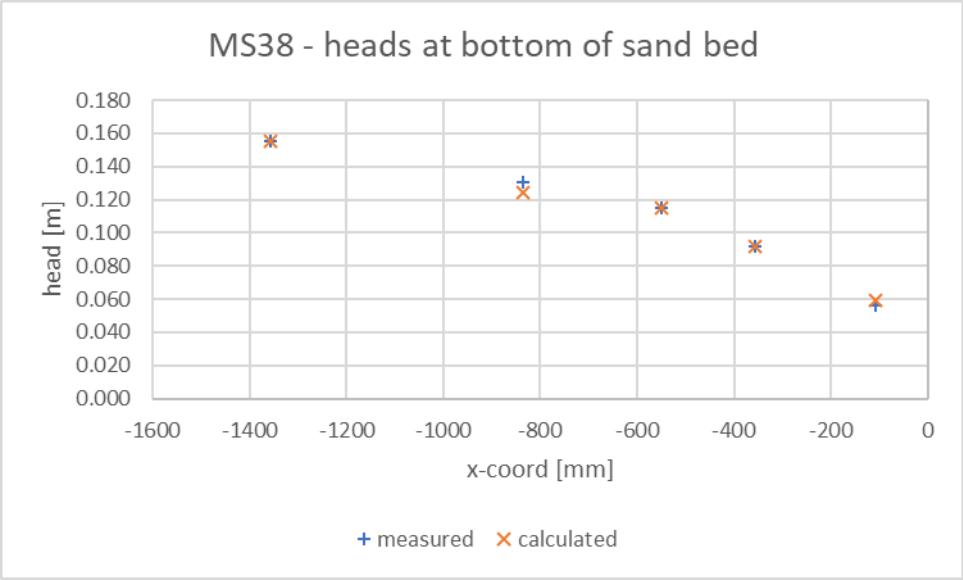

Figure 4.12 MS38: measured and calculated heads at bottom sand bed (stage I) on behalf of calibration intrinsic permeability

For both head profiles (MS38 top and bottom, Fig.4.11 and Fig 4.12) there is good agreement between measured and calculated data.

For test MS40 congruency is reached for the more important upstream locations (Figure 4.13 and Figure 4.14).

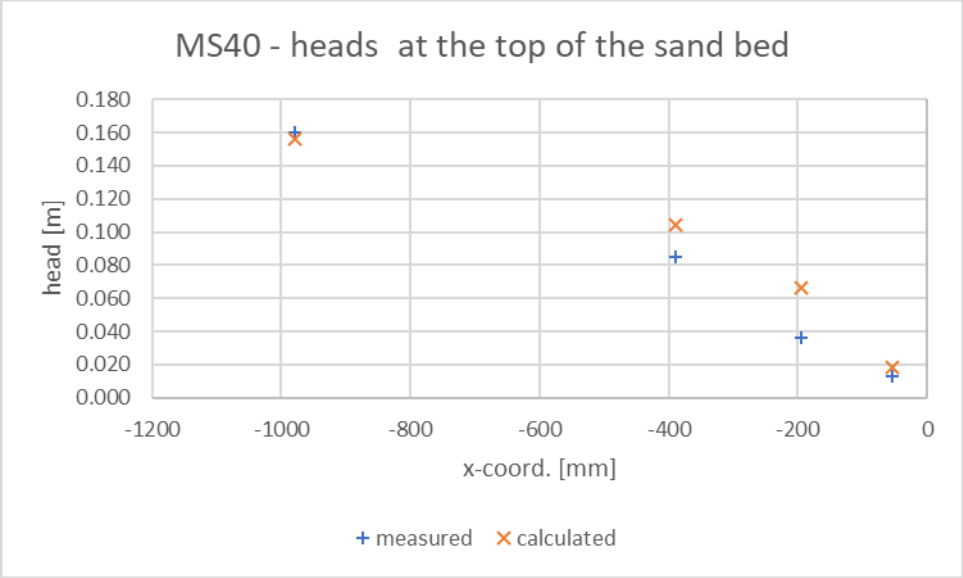

Figure 4.13 MS40: measured and calculated heads at top sand bed (stage I) on behalf of calibration intrinsic permeability

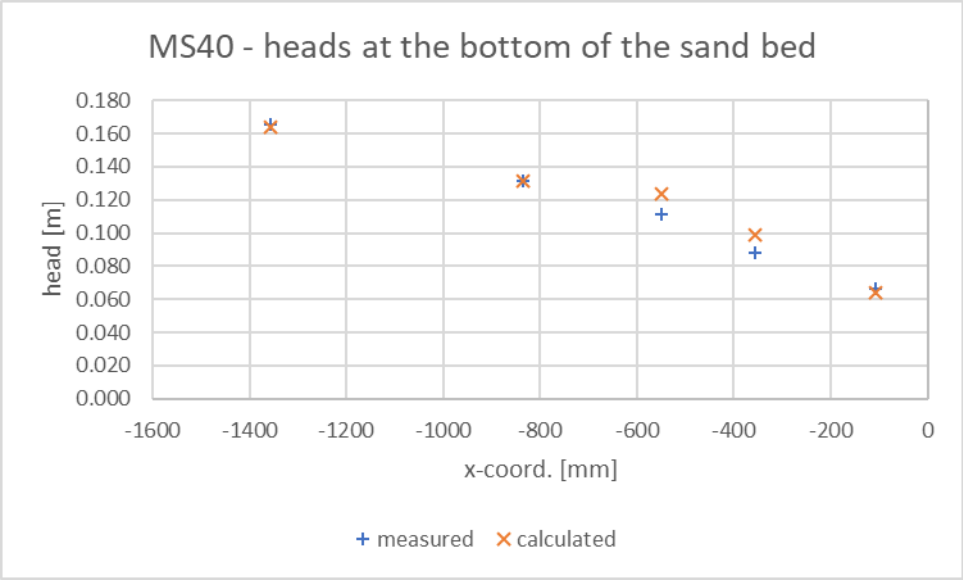

Figure 4.14 MS40: measured and calculated heads at bottom sand bed (stage I) on behalf of calibration intrinsic permeability

4.2.2 Head profiles close to failure

The calculated head profiles are compared to the measured heads at the critical stage just before applying the final head increment before failure. **Error! Reference source not found.** and Figure 4.18 show the head distribution for both tests. Figure 4.18 also shows the velocities. It appears that the head drop is clearly occurring in the upstream part of the set-up over the upstream background sand. Furthermore, it is shown that the main flow is in the direction of the outflow area along the slope of the barrier.

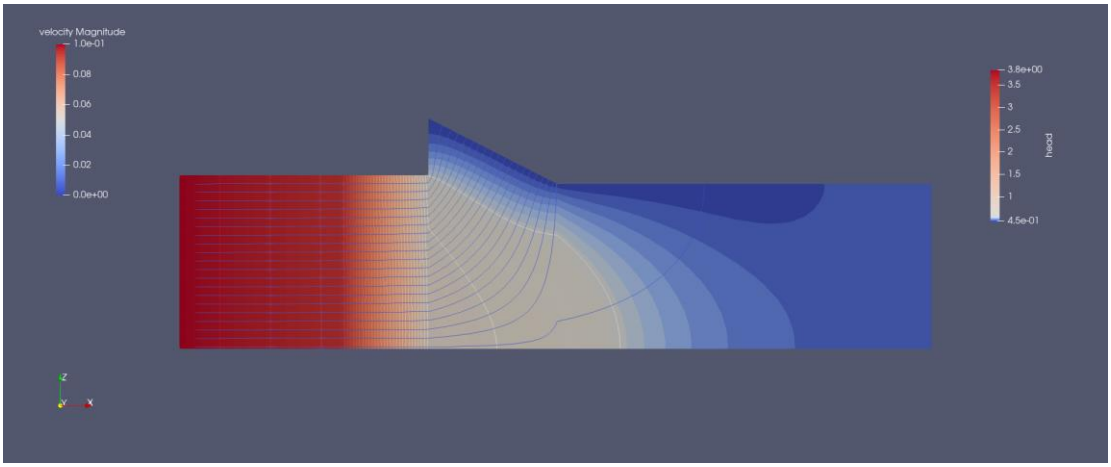

Figure 4.15 MS38. Head distribution, equipotential lines and flow paths at critical stage.

Almost all flow paths inside the barrier are leading to the slope surface and a distinct sequence of equipotential lines parallel to the slope surface with some divergence nearby the interface with the fine sand.

The velocity vectors in Figure 4.16, Figure 4.17 and Figure 4.19 show also a relatively uniform distribution along the slope with some peak values along the upper protuberance wall and at the toe of the slope adjoining the interface with the downstream background sand.

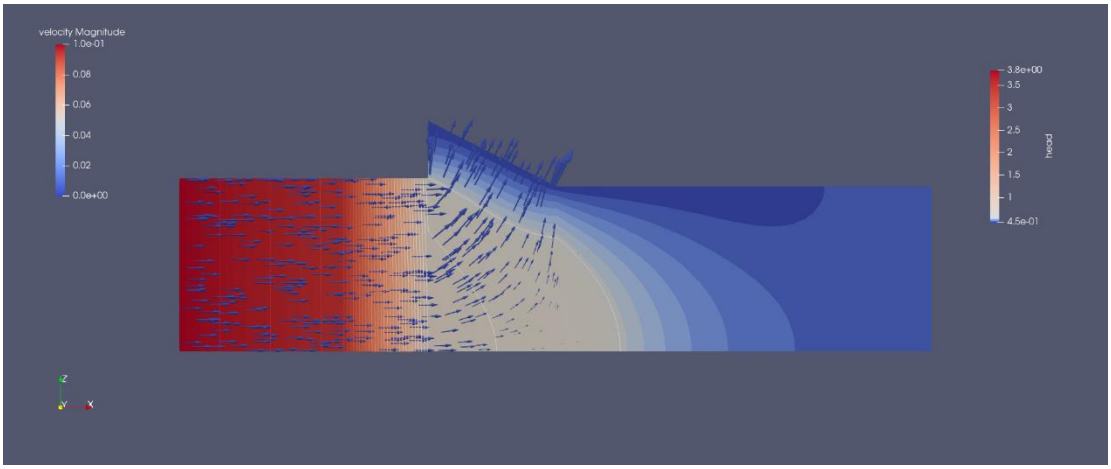

Figure 4.16 MS38. Head distribution and velocities at critical stage

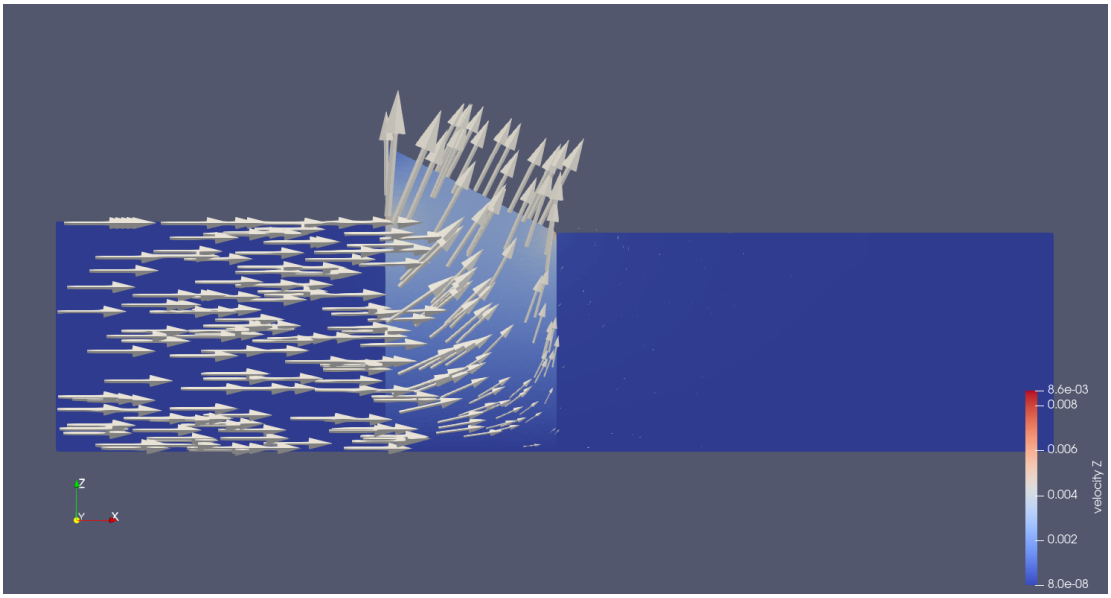

Figure 4.17 MS38. Velocity vectors.

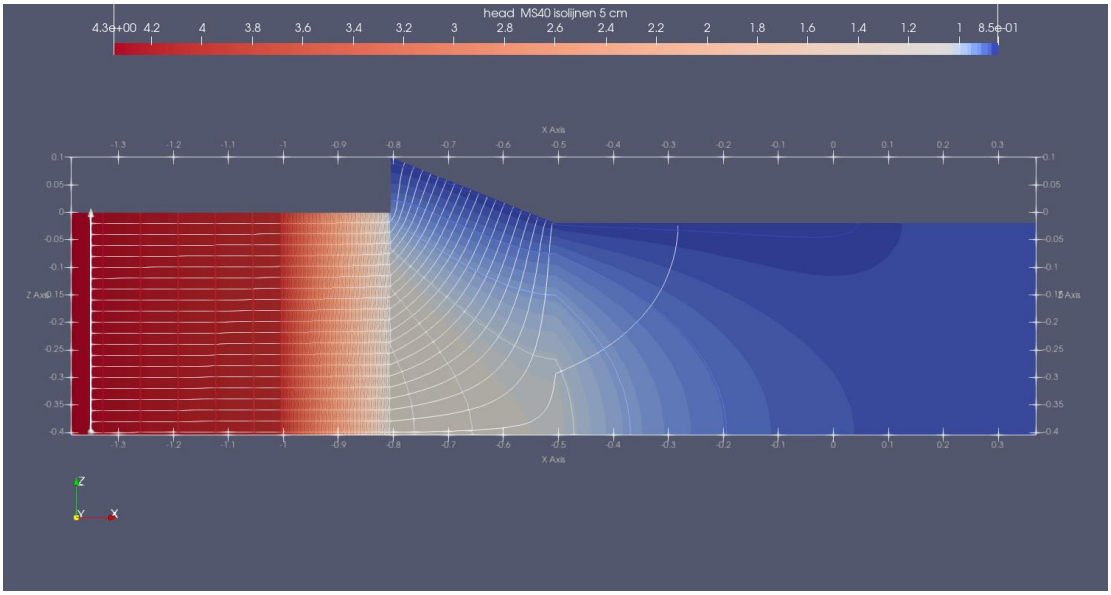

Figure 4.18 MS40. Head distribution at critical situation

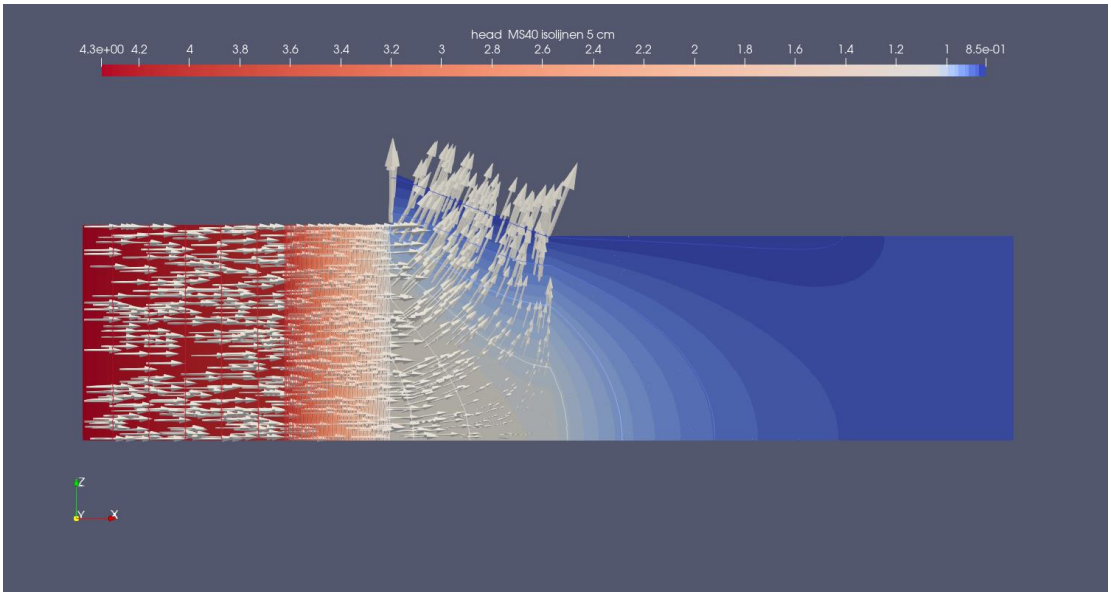

Figure 4.19 MS40. Velocity vectors.

As a result of the gentle slope and hence low height of the slope at the upstream side of the protuberance at the critical stage, in test MS40 most of the pressure gauges along the protuberance wall are located at the edge or outside the coarse sand slope and only give head measurements of the water inside the void of the protuberance. Therefore, only some reading points can be used for the calibration. This could argue in favour of modelling the test in an earlier stage at which more gauges are still inside the slope, in order to take more readings into account for achieving a supposable better fit. However, earlier attempts to get a better fit for the critical stage with a model without physically modelling the downstream pipe have had no success in reaching better calculated heads for the position of gauge p02.

Table 4-5 Calibrated intrinsic permeability and hydraulic conductivity (fitted in with the measured heads and fluxes) for critical stage

sand type	location	MS38 K_{20} [m²]	MS38 k_{20} [m/s]	MS40 K_{20} [m²]	MS40 k_{20} [m/s]
B25	upstream	1.78E-11	1.72E-04	1.99E-11	1.92E-04
B25	downstream	2.82E-11	2.73E-04	1.80E-11	1.74E-04
GZB3	upstream	2.97E-10	2.85E-03	4.07E-10	3.90E-03
GZB3	upper part of the barrier inside protuberance	3.71E-10	3.56E-03	4.73E-10	4.54E-03
GZB3	Lower part of the barrier below protuberance	3.71E-10	3.56E-03	4.21E-10	4.04E-03

Figure 4.20 and Figure 4.21 show the modelled and the measured heads for both tests at the critical stage. It turns out to be impossible to succed in matching the the calculated heads for the position of gauge p02 with its readings. For all other gauges it succeeded to match the readings with the calculated values.

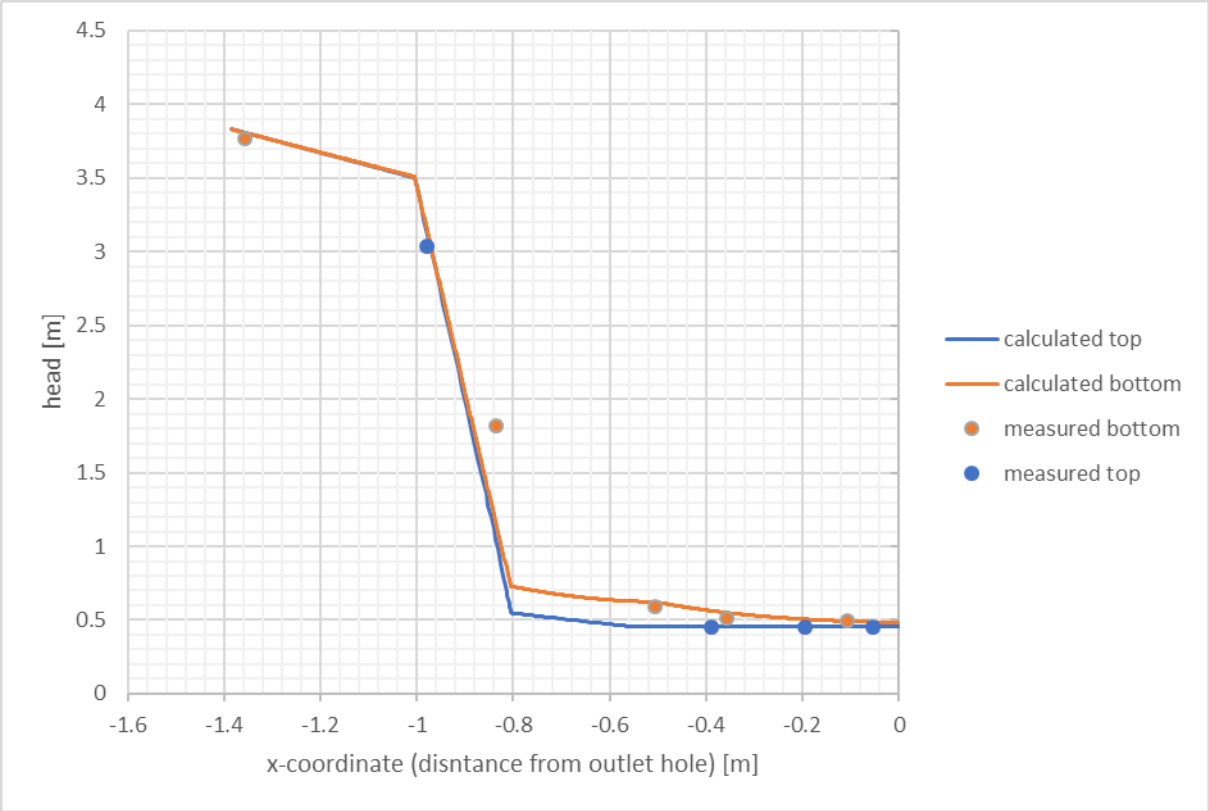

Figure 4.20 MS38. Modelled and measured heads at the top and the bottom of the sand bed at critical stage

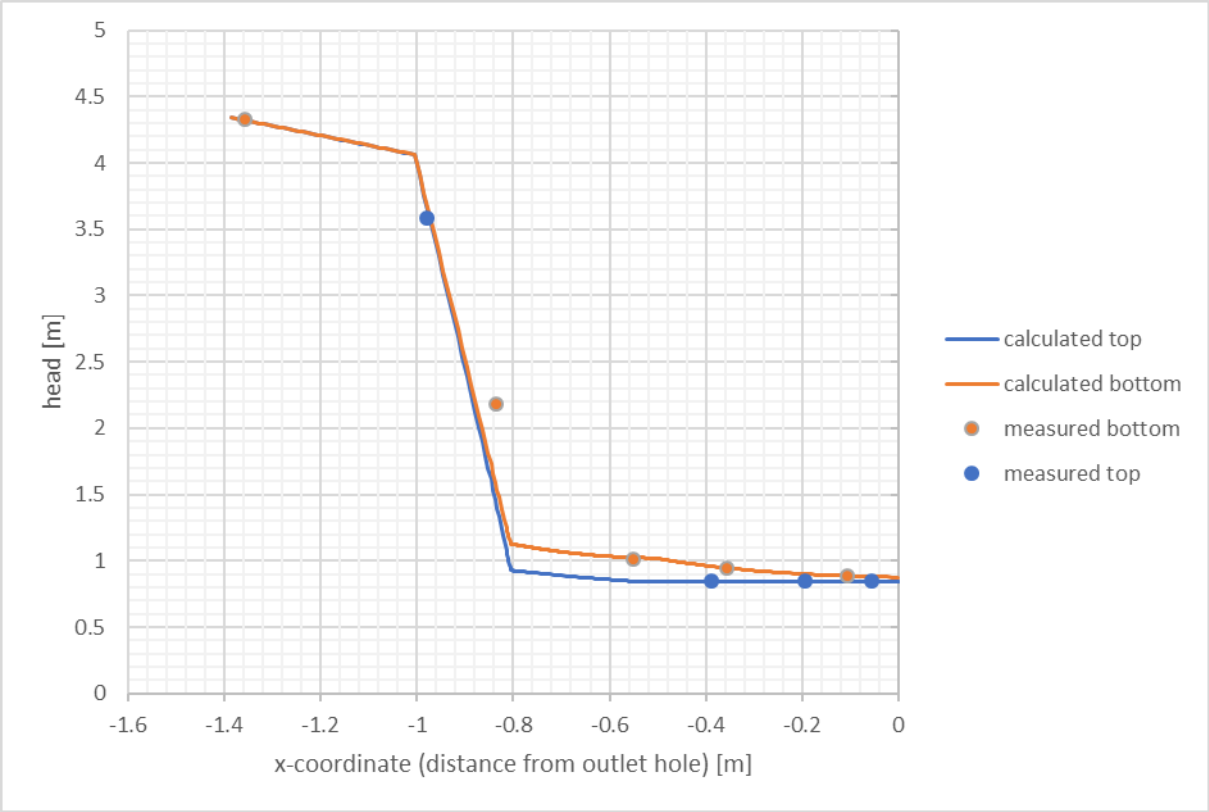

Figure 4.21 MS40. Modelled and measured heads at the top and the bottom of the sand bed at critical stage

The estimated upper and lower limit of the relative density are 1.1 and 0.9 respectively. Reckoning back the fitted hydraulic conductivity of the GZB3 inside the protuberance results in the following porosities and relative densities for the two tests:

MS38: $k = 3.56\ 10^{-3}$ m/s = $x_1\ n^3/(1-n)^2$ => n = 0.341

$RD = (n_{max} - n) / (n_{max} - n_{min}) = (0.448 - 0.341) / (0.448 - 0.363) = 1.25$

MS40: $k = 4.54\ 10^{-3}$ m/s = $x_1\ n^3/(1-n)^2$ => n = 0.363

$RD = (n_{max} - n) / (n_{max} - n_{min}) = (0.448 - 0.363) / (0.448 - 0.363) = 1.0$

The fit for the barrier hydraulic conductivity for MS38 results in an extreme high relative density, which is questionable, because the RD corresponding to the porosities according to the preparation was between 99% and 101%. Most of the head drop occurs across the fine upstream sand. The sensitivity of the permeability as a function of RD_{GZB3} is examined in section 4.2.5, where a good fit with the head measurements can be obtained for each of the variations. Thus, the fit is not very sensitive for variations in permeability or relative density of the barrier material.

For test MS40 the relative density derived from the fit is in better agreement with the RD values (95% in the protuberance and 107% in the lower part) according to the preparation.

The gradients at critical stage for this fit are shown in Appndix B.

4.2.3 Flow rate at critical stage

Figure 4.22 shows the line along the inlet over which the volume flux is determined to calculate flow rate at the inflow. The modelled flow rates according to the calibrated intrinsic permeabilities given in Table 4-5 are shown in Table 4-6.

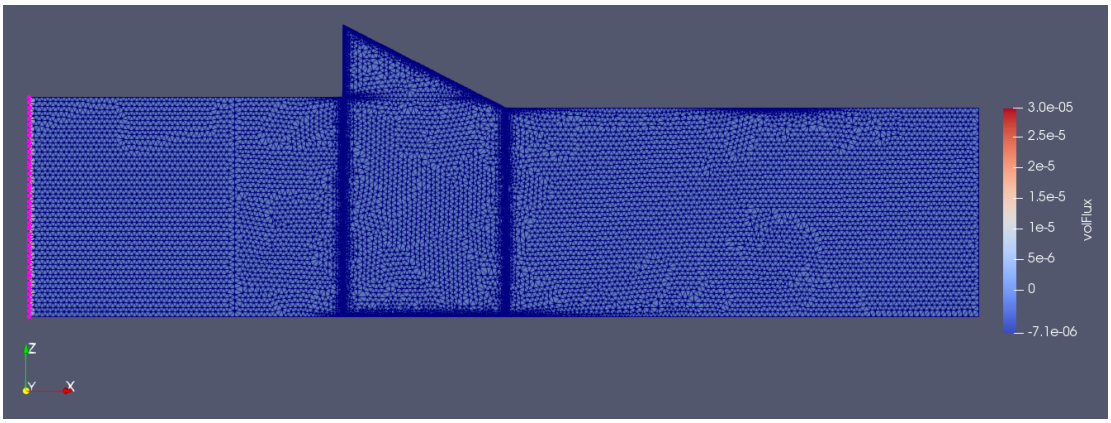

Figure 4.22 MS38. Line along the inlet used for calculation of volume flux

Table 4-6 Modelled and measured flow rates

Test	Modelled flow rate, l/min	Measured flow rate, l/min	Ratio modelled / measured flow rate
MS 38	52.8	52.8	1.00
MS 40	62.4	62.3	1.00

There is a good congruency in flows between the measured and calculated values for both tests as a result of the fits in respect to the measured discharge. Since the head loss in the barrier is limited in comparison to the head loss in the upstream sand, and the flow rate is mainly dependent on the hydraulic conductivities of the materials upstream of the barrier, it is difficult to precisely fit the

hydraulic conductivity of the barrier material based on the measurements, in particular because of the limited number of gauges inside the barrier which is stll allocatable for head readings at stage IV. Therefore, the permeability of the barrier material as determined in a standard permeability tests for different densities was used in the numerical calculations.

4.2.4 Sensitivity analysis concerning relative density of barrier material

4.2.4.1 Variation of the hydraulic conductivity

In this section the hydraulic conductivity of the barrier was varied for experiment MS38, to investigate the sensitivity of the fit with head measurements and flow rate for a broader range of the barrier hydraulic conductivity, in order to get an impression of the informational value of this calibration approach. This is only done for test MS38, because the results will be qualitatively the same in the matter of sensitivity.

It is assumed that the flux and the upstream readings are fitted well. For this sensitivity study the hydraulic conductivities for the background materials (B25 and upstream GZB3), geometry and mesh obtained in 4.2.2 have been maintained, while the hydraulic conductivity of the barrier material was varied. Table 4-7 provides the hydraulic conductivities of the background materials. Table 4-8 presents the hydraulic conductivities in the barrier material and the results of the calculations. The intrinsic hydraulic conductivities were chosen based on a variation in relative density of 50%, 70% and 100% and were calculated using the correlation described in Section 4.1.2.2 [Deltares, 2020b]. From the variations in permeability described in Appendix B it follows that it is not possible to fit the measurement readings of p02 well (see also Figure 4.25). Thus, further attempts to fit the readings for this gauge were omitted in the sensitivity analysis. However, it should be noticed that gauge p02 is not out of order, but that it is not possible to bring the readings in agreement with the calculations for this position (see also section 3.4.1.3 and Figure 4.25). Possibly something went wrong during its placement. This gauge is fixed by a tie-wrap inside the container at a certain distance from the bottom, so the actual position could somewhat deviate from the expected one.

The sensitivity analysis shows that the vertical gradient in the barrier at the upstream side of the protuberance is very sensitive to the hydraulic conductivity of the barrier (Table 4-8). The flow rate is not very sensitive to the variation (Table 4-8) as was expected, since the flow is determined by the upstream layers. If the permeability of these layers is constant, the flow is constant and according to Darcy's law the gradient is then inversely proportional with the permeability.

Table 4-7 Background sand hydraulic conductivities and intrinsic permeabilities

sand type	location	k [m/s]	K [m²]
B25	upstream	1.72E-04	1.78E-11
B25	downstream	2.73E-04	2.82E-11
GZB3	upstream	2.85E-03	2.97E-10

Table 4-8 Variations of RD and hydraulic conductivities of barrier material for sensitivity analyses

	RD [-]	k [m/s]	K [m2]	$H_{bottom\ slope}$ [m]	$H_{top\ slope}$ [m]	dh [m]	i_v [-]	flux [l/min]
MS38_RDGZB05	0.5	7.32E-03	7.62E-10	0.5007	4.52E-01	0.133	0.37	54.56
MS38_RDGZB07	0.7	6.09E-03	6.34E-10	0.5102	4.52E-01	0.133	0.44	54.20
MS38_RDGZB10	1.0	4.57E-03	4.76E-10	0.5285	4.52E-01	0.133	0.58	53.51

Figure 4.23 and Figure 4.25 illustrate the head distribution along the top and bottom of the sand box and the obtained fits for barrier relative densities of 0.5 and 1.0 for test MS38. An RD of 50% is

relatively improbable but gives an idea of the sensitivity. These figures illustrate that a good fit with the head measurements can be obtained for each of the variations (except for gauge P02). The fit is not very sensitive for variations in permeability of the barrier material. For a correct determination of the barrier hydraulic conductivity more measurement readings of other gauge positions would be necessary. Those reading are available, but this would mean to model the test for an earlier stage, but in that case also a wider range of hydraulic conductivity values would be expected.

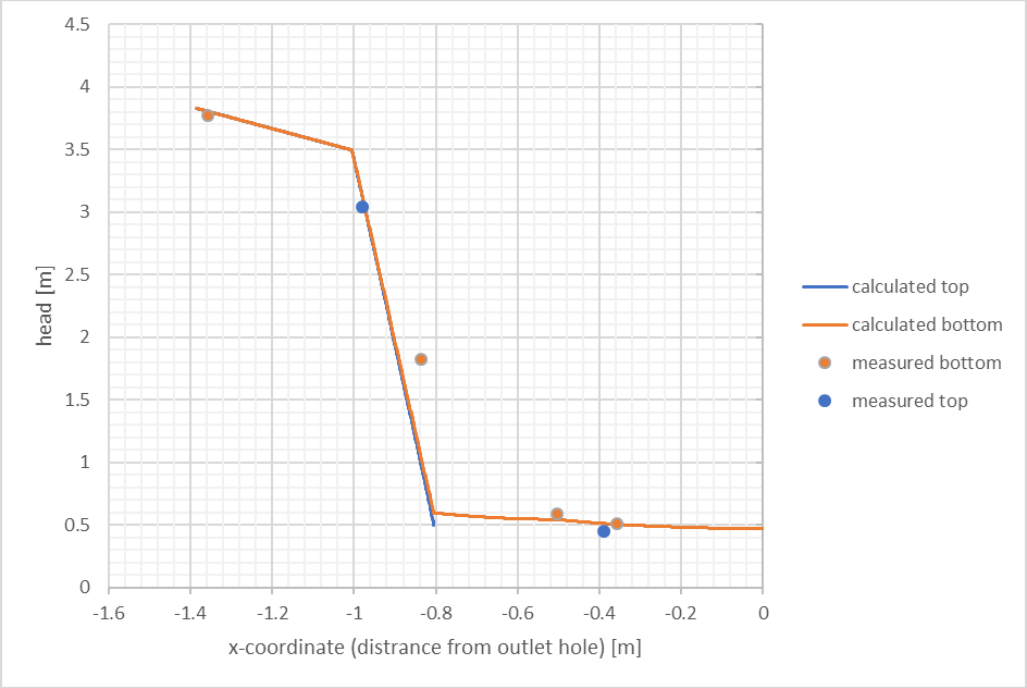

Figure 4.23 MS38. Fit of bottom and top hydraulic heads for barrier relative density of 50%

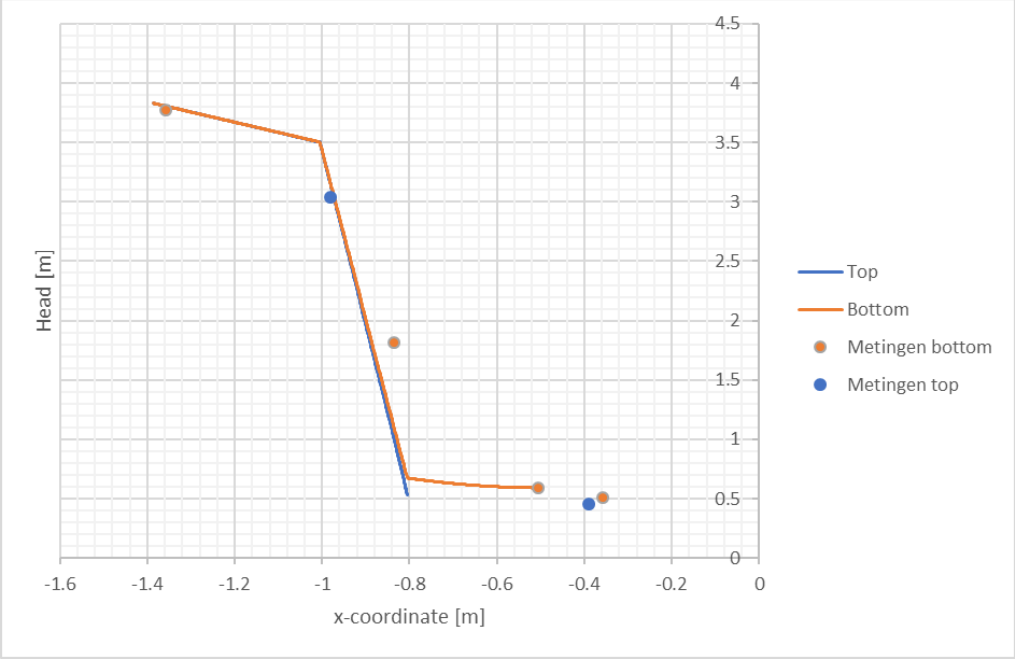

Figure 4.24 MS38. Fit of bottom and top hydraulic heads for barrier relative density of 100%.

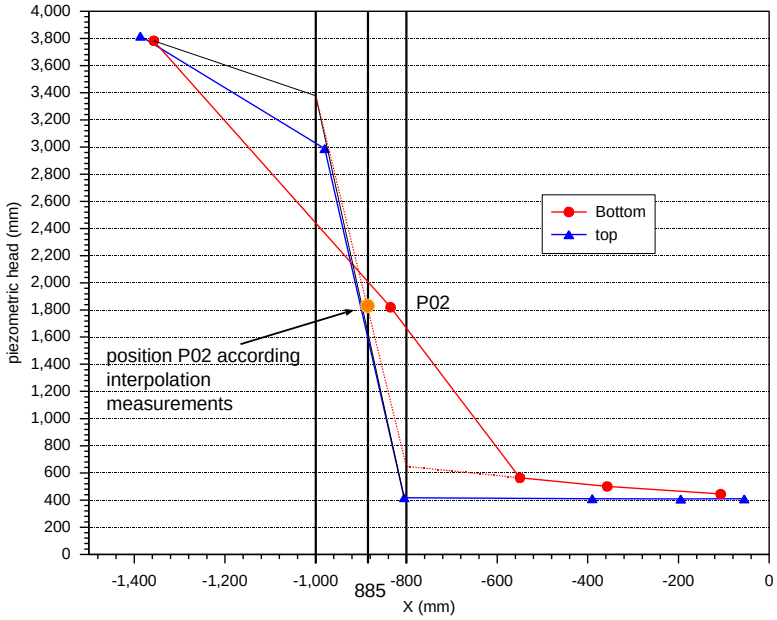

Figure 4.25 MS38. Fit of bottom and top hydraulic heads for barrier relative density of 100%. A linear interpolation between the measured values is done. Here it becomes apparent that a match with the readings of gauge p02 is utterly impossible. The thick red and blue line is simply a line through the measurement points. The thin line considers the permeability of the various layers and assumes a constant hydraulic gradient in each layer with a constant permeability. The vertical black lines at 800 and 1000 present the position of the fine sand upstream of the barrier and the line at 885 a possible position of P02 according to this interpolation.

4.2.4.2 Determination of exit gradients at critical stage

The sensitivity analysis in section 4.2.4.1 illustrates that the hydraulic conductivity of the barrier cannot be precisely determined using the flow rate and the head measurements during the experiments. The most accurate way to determine the exit gradients is to determine the hydraulic conductivity through the correlation with relative density. The relative density was determined quite accurately during the preparation of the experiments. It is estimated that the relative density can be determined with an accuracy of 10%. For both experiment MS38 and MS40 the barrier relative density was estimated to be around 1.0 (Deltares, 2020b). The exit gradients are therefore determined using relative densities of 0.9, 1.0 and 1.1.

Table 4-9 presents the hydraulic conductivities belonging to the relative densities of 0.9, 1.0 and 1.1, according to the correlation presented in (Deltares, 2020b). The other material properties are as described in section 4.2.4.1.

Table 4-9 estimated hydraulic conductivity and intrinsic permeability for the barrier (inside and below protuberance)

	RD [-]	porosity n [-]	K [m2]	k [m/s]
Lower limit	0.9	0.3715	5.24E-10	5.03E-03
Best guess	1	0.363	4.76E-10	4.57E-03
Upper limit	1.1	0.3545	4.32E-10	4.15E-03

Figure 4.27 and Figure 4.29 present the variation in exit gradient along the slope, based on the average gradient across the top 5 cm of the slope, and Figure 4.26 and Figure 4.28 present the variation in exit gradient along the top of the slope, based on the exit velocity along the slope. The gradients are higher for experiment MS40, which agrees with the larger flow rate and lower slope that were measured in experiment MS40.

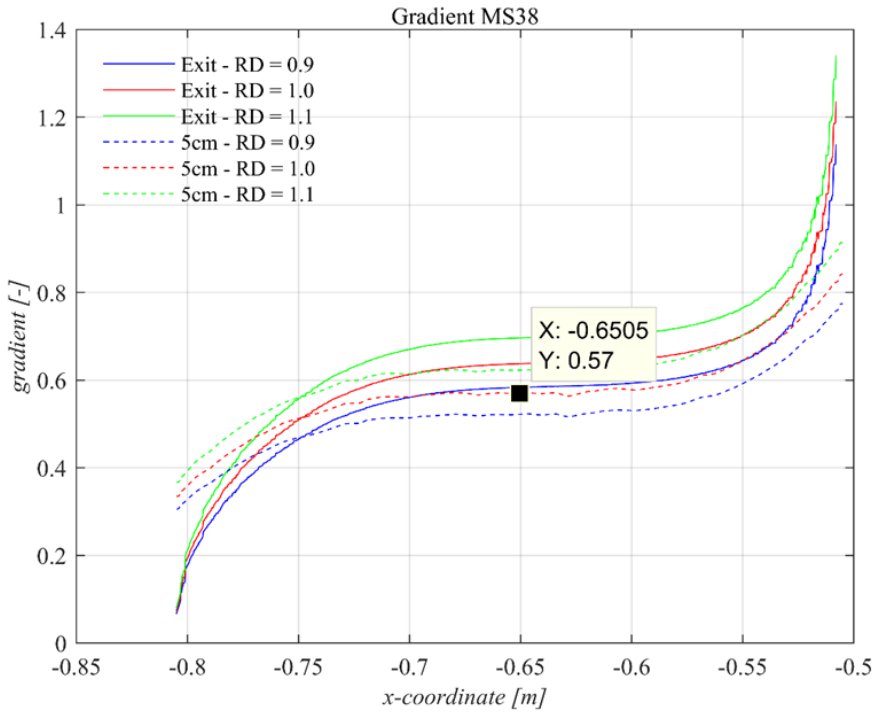

Figure 4.26 MS38. Outward gradients along the slope for different hydraulic conductivities. The denoted critical gradient is based on head difference over 5 cm (for RD = 100%).

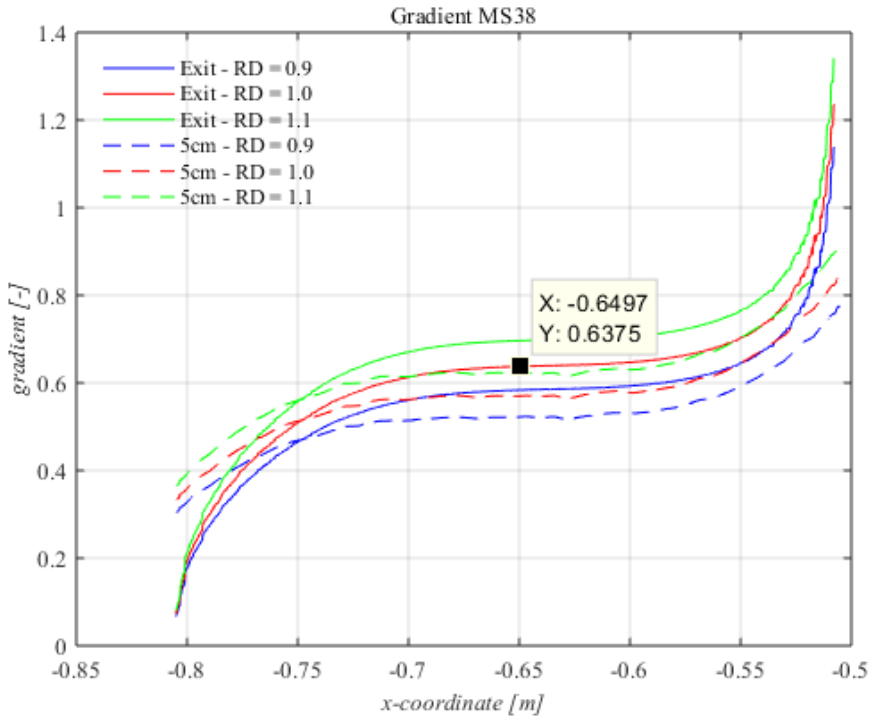

Figure 4.27 MS38. Outward gradients along the slope for different hydraulic conductivities. The denoted critical gradient is based on velocity/permeability at the outflow surface (for RD = 100%).

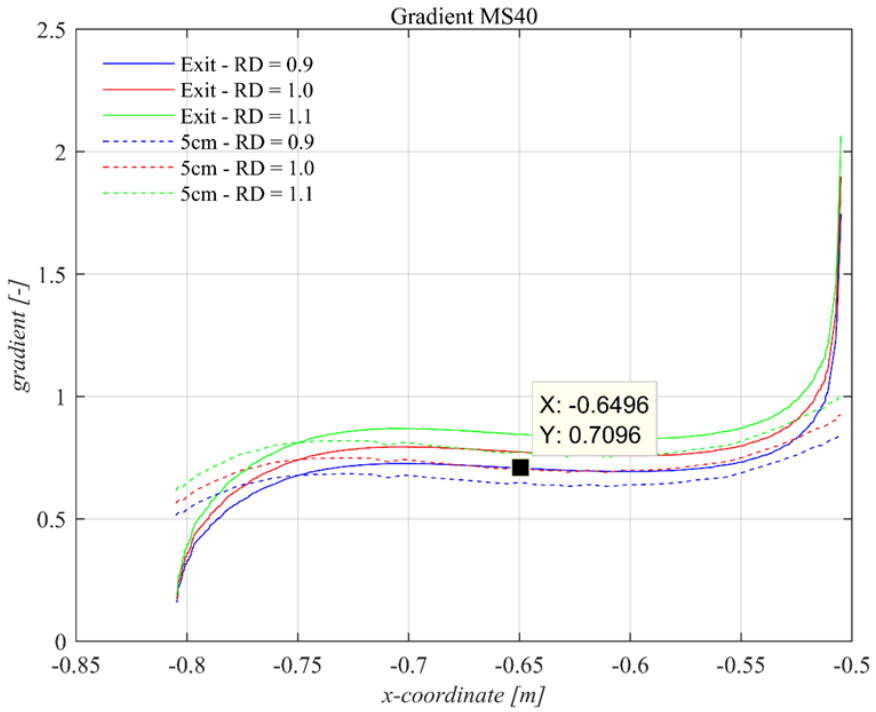

Figure 4.28 MS40. Outward gradients along the slope for different hydraulic conductivities. The denoted critical gradient is based on head difference over 5 cm (for RD = 100%).

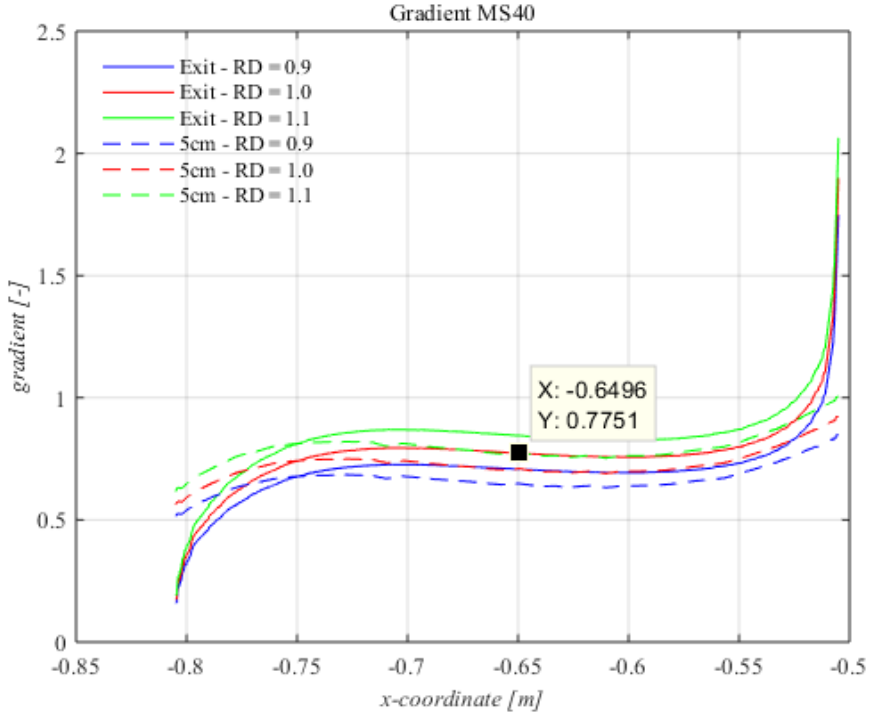

Figure 4.29 MS40. Outward gradients along the slope for different hydraulic conductivities. The denoted critical gradient is based on velocity/permeability at the outflow surface (for RD = 100%).

All curves with a solid line in these figures (for an RD of 0.9 – 1.1) are actually possible. The red lines show the best fit based on the measured relative densities in the test.

4.2.5 Discussion and Conclusions

The observations and the numerical calculations showed that overall the failure mechanism is corresponding with the mechanism expected in advance. The maximum head difference and the corresponding flow rate were well predicted (see Appendix A 4.5).

The numerical calculations presented in this chapter could not prove the general validity of the first hypothesis (see section 1.2), that the barrier is failing because of heave at the upstream side of the slope.

Before the CSB fluidizes, it is supposed that ground mechanical failure is occurring as a result of the low effective stresses. The failure model by fluidisation is still relevant because low effective stresses in the CSB are necessary for the occurrence of failure (see also test MS39).

The back-calculated gradients for the next-to-last load step are under the critical gradients for failure according to what the theoretical model is predicting: a gradient of 0.75 for a critical slope angle of 10° (calculated) and a gradient of 0.706 (mean of 0.775 and 0.638) for the measured slope angle of 22 - 27° for an RD_{GZB3} of 100%. The critical gradient in the CSB is therefore not higher than the average back-calculated gradient of the experiments: 0.70 perpendicular to the slope. Although not all the results can be explained precisely, the criterion regarding the outward gradient turns out to be sufficient enough to serve the purpose, which also turned out from the predictions. The stability of the CSB is sufficient according to the experiments.

The local critical gradient is depending on the slope angle. The outward gradient is for MS38 slightly lower than for MS40. The gradient in the middle of the barrier is lower than nearby the toe of the slope where failure seemed to start as a result of loss of effective stresses (not at all taking into account the asymptotic course of the gradient in the immediate vicinity of the toe).
Regarding the sensitivity of the perpendicular gradient for a relative density of the barrier material between 90% and 110% the outward gradient in the centre of the barrier, determined by using the outward velocity, is slightly lower as a result of the slightly lower hydraulic conductivity. It stands out that the outward gradient determined by using the head difference over a distance of 5 cm is slightly lower than those determined by using the outward velocity. In the former case the gradient seems te be very sensitive to the regarded distance. The value of the outward gradient based on the outward velocity seems to be more reasonable because the outward gradient directly beneath the slope surface is after all causative for the sand movement along the whole slope when starting the last load step.

The flow rate is mainly dependent on the hydraulic conductivities of the materials upstream of the barrier. The contrast in permeability determines the mamimum gradient in both tests. As to nearly equally high head differences across the set-up, the contrats should be the same in both tests, but the flow rate is considerably lower for MS38 (52.3 l/min vs. 62.3 l/min for MS40). However, the bulk hydraulic conductivity is lower for MS38 according to the fit, especially for the upstream part. The lower bulk permeability in MS38 could amongst others also be a result of clogging at the upstream interface between coarse sand and B25. Considerable clogging occurred in test MS39, but maybe there was already a slight impact in test MS38. Even though the pressure gauges do not seems to be influenced directly (there is a nearly linear fit between flow rate and head difference above a head difference of 1.5 m, see Figure 3.42), some indication of clogging was visible which could have influenced the test in its entirety. There is a slight filter cake of mould (a hint of orange at the interface in Figure 4.30). Test MS40 was conducted with a fully cleaned set-up.

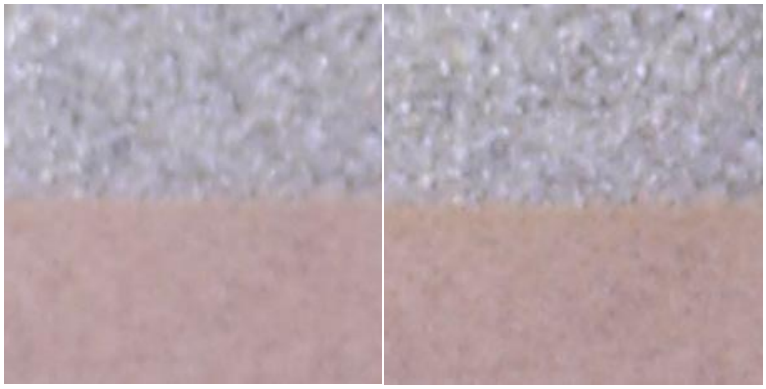

Figure 4.30 Upstream interface (GZB3/B25) at start of test (left-hand-side) and end of test (right-hand-side) for test MS38.

The influence of a possible less permeable layer cannot be very large, see Figure 4.31. In this figure the measured head at the top and bottom of the container at the moment of failure is shown for test MS40. The same graph is made for MS38 with the same x-axis, but the y-axis is enlarged in a way that the starting values left, and the end values right are in agreement. Doing this, it is possible to get an idea about the relative flow resistances in the set-up of the two tests. The steeper the slope the higher the relative resistance. The head for gauge P09 at -950 mm is relatively a bit higher for MS40 indicating that the relative flow resistance in the GZB sand upward of the CSB is a bit lower for MS40. However, for P02 at the bottom at -833 mm, it is the other way around.

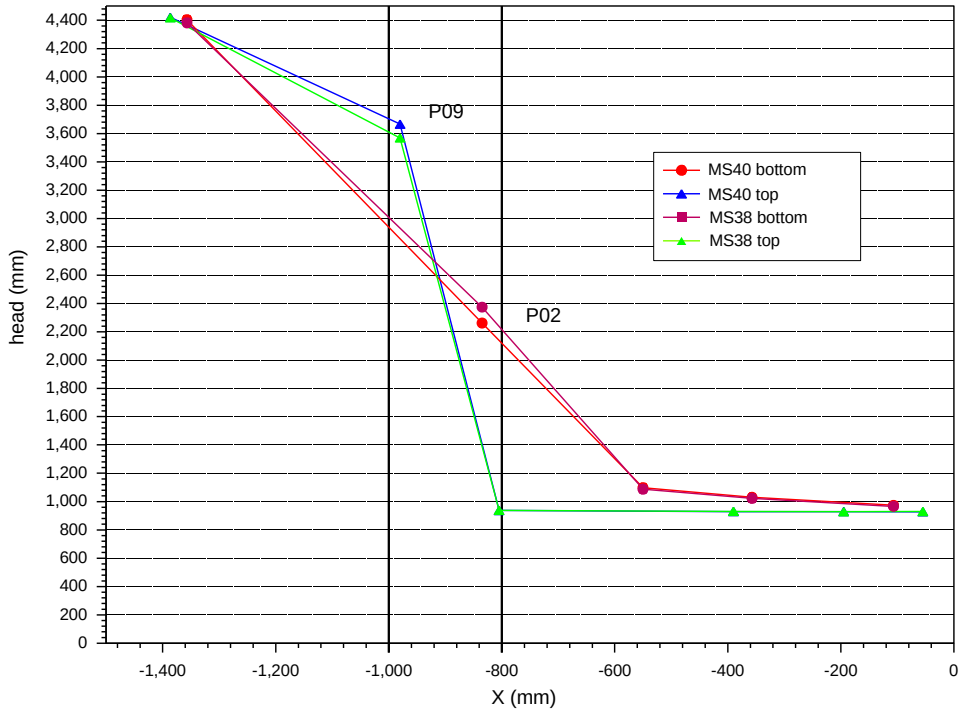

Figure 4.31 Measured head at the top and the bottom of the container at the moment of failure

It was not possible to fit the readings for pressure gauge p02 with the numerical outcome for the considered contrasts in hydraulic conductivity. For the numerical model of both tests the same setting concerning the position of the interfaces between GZB and B25 was used, the position of the barrier interfaces corresponding with the exact x-position of the inner surface of the protuberance. As a result of the preparation process the upstream side of the lower barrier (below the protuberance, inside the box) is circa 13 mm more downstream than the upper part of the barrier.

In the numerical model the position of this interface is the same as the inner surface of the protuberance. Instead the position of the upstream interface of the B25 was modelled 10 mm more upstream. This is marginal, but could influence the gauge at p02 slightly, but this does not explain the big differences between the measured and the calculated values for this gauge. To explain the measured head the pressure gauge or the boundary should have shifted around 35 mm, as explained with Figure 4.25.

5 How strong is a protruding CSB?

To evaluate the strength of a protruding CSB, it is compared with tests in the same set-up with a non-protruding CSB. However, a direct 1 to 1 comparison is not possible. The experiments described in this report, MS38 to MS40, were performed with a shorter upstream fine sand part, this was done because it was predicted that the maximum head difference that could be reached with the set-up, 5 m, was not sufficient to reach failure with the same upstream fine sand part as the in the previous non-protruding CSB tests. The upstream fine sand part was 3 times longer in the previous tests, since there is a nearly one-dimensional flow in that fine sand during the test, the test of this report can be compared with the previous tests, by multiplying the maximum head difference found with 3. The first test with a protruding barrier, MS37, had thinner sand layers (0.3 instead of 0.4 m and the sand had to move upwards after passing the CSB. The last aspect is difficult to take into account, but the thinner sand layer will lead to a lower discharge. This can be compensated for by multiplying the maximum head difference with ¾. The vertical movements of sand grains downstream of the CSB in test MS37 will lead to a bit increase in strength, but it is not possible to quantify this.

With these corrections the maximum head drop for the situation of the non-protruding barrier is presented in Figure 5.1. The figure presents the maximum head drop for MS37 with and without correction for the thinner sand layer. The figure shows that test MS38 and MS40 are quite comparable when it comes to maximum head drop. This head drop is determined from the measurements by taking into account the thinner upstream sand layer. The 10 m head drop could not have been reached with the set-up. The results for the non-protruding barrier show that the permeability contrast (permeability barrier divided by the permeability of the background sand) is important for the strength of the CSB.

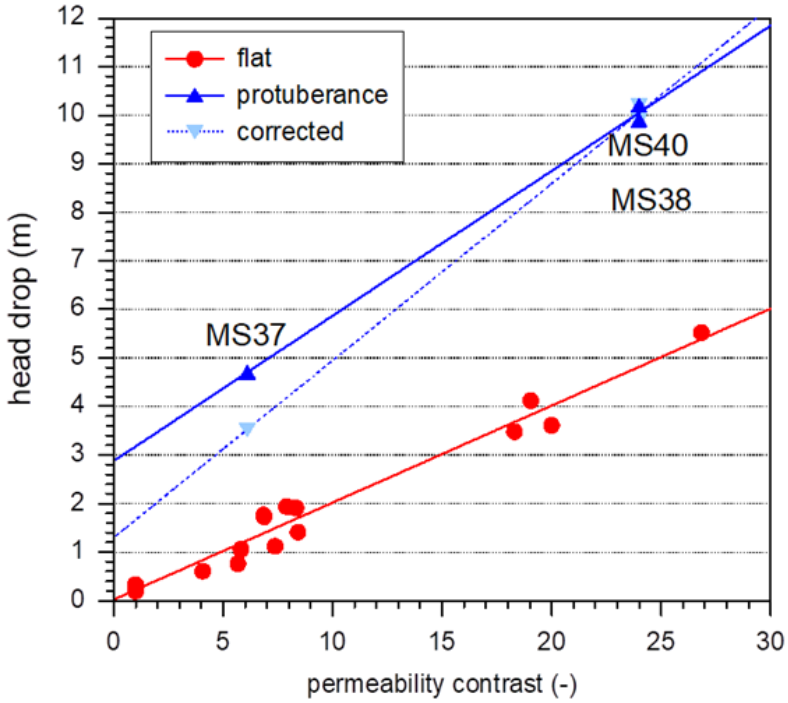

Figure 5.1 Results of experiments, maximum head drop over medium scale set-up as function of the permeability contrast.

The results of the non-protruding tests give also results for a permeability contrast of one. These are tests without CSB in homogeneous sand. These tests failed at a head drop of 0.2 or 0.3 m, while MS38 and MS40 would have failed at a head drop of around 10 m in the same set-up. For these tests the strength of sand with CSB is 30 to 50 times higher than for a situation without CSB. The protruding barrier is 2 times stronger than the non-protruding barrier.

6 Adapted conceptual model regarding the initial model

For the situation where the barrier penetrates the cover layer, the tentative conceptual model which was suggested in (Deltares 2020a) on the basis of test MS37 (where the protuberance was created by two silicon layers attached underneath the cover layer whereby the pipe first had to progress vertically downwards to get below the silicon layer) is slightly adapted by the results of the analysis of the two additional tests with protuberance where the pipe could grow horizontally to the barrier.

In (Deltares 2020a) a hypothesis of the process is formulated. In contrast to the test analysed in that report, where the pipe first had to progress vertically downwards a distance of 0.10 m to get below the silicone layer that simulates the cover layer into the barrier, the pipe in the tests described in the report on hand with an upward-facing protuberance immediately started to grow alongside the barrier when reaching it. Hence, the conceptional model had to be adapted. In the following passages the differences concerning the initial conceptual model based on MS37 are described.

6.1 Pipe formation downstream of the barrier

Pipe initiation and progression to the barrier (in a field situation) are similar to the situation where the barrier does not protrude into the cover layer.

In the first experiment (MS38), pipes initially progressed to the sides of the model rather than upstream to the barrier, which could be a consequence of the inevitable minor height differences in the bulkhead – B25 interface, which provides space for the B25 to loosen upon horizontal positioning of the test box, particularly in the corners. This provided a preferential flow path for the pipe at the side of the test box, which is not representative for practice. But in the second test (MS40) the pipe progressed immediately upstream to the centre line of the set-up (Figure 6.1).

In contrast, in test MS37 the vertical drop of 0.10 m at the edge of the silicone layer stopped pipe progression until the gradient was high enough to fluidize sand at the edge of the silicone layer and form a sand boil. Once this formed, the pipe could rapidly progress to the barrier below the silicone layer. However, this means that the head drop at which the pipe reached the barrier was higher than in a situation with a protuberance and the pipe downstream was also larger

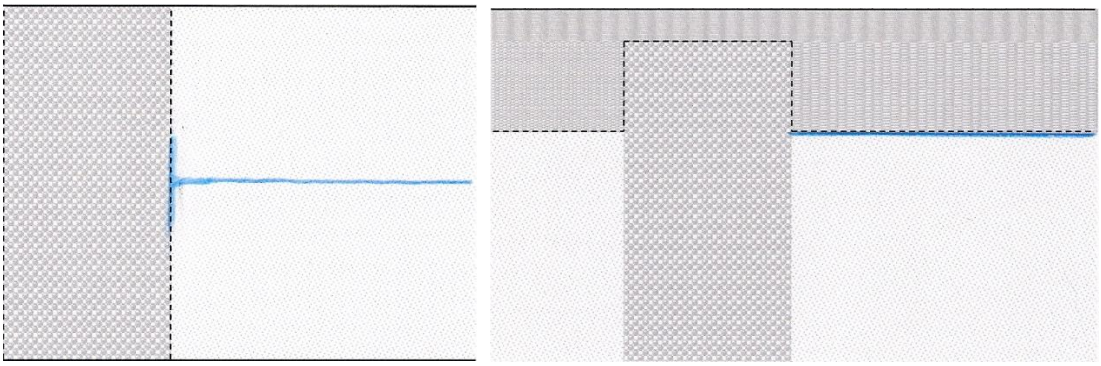

Figure 6.1 Pipe develops in upstream direction and is then growing further in lateral direction along the barrier

6.2 Damage of the barrier and pipe development along the barrier

When the pipe reaches the barrier in the centre of the model, flow inside the barrier converges to the pipe tip. There appears to be progression of the pipe parallel to the barrier prior to erosion of the

barrier. When the pipe along the CSB is deep enough, the support to the vertical side of the barrier is removed and grains from the barrier roll into the pipe. In the experiment, the barrier material at the downstream side of the protuberance subsided with the development of the lateral pipe along the barrier. At the downstream top of the barrier a flat ellipse formed along the wall and a slope formed in the upstream direction. The slope is also widening with the lateral pipe development. At the point where the pipe has reached the barrier, the flow rate in the test was sufficient to transport the eroded barrier grains through the pipe, as indicated by the observation of barrier material in the erosion pit in front of the barrier and near the outlet downstream. The pipe progresses further parallel to the barrier, creating a more 2D flow field and a wide slope in the barrier.
The erosion ellipse inside the top of the barrier widened parallel to the barrier interface due to lateral progression of the pipe downstream of the barrier simultaneously with erosion of the barrier in upstream direction until the lateral erosion was completed, see Figure 6.2 and Figure 6.3.

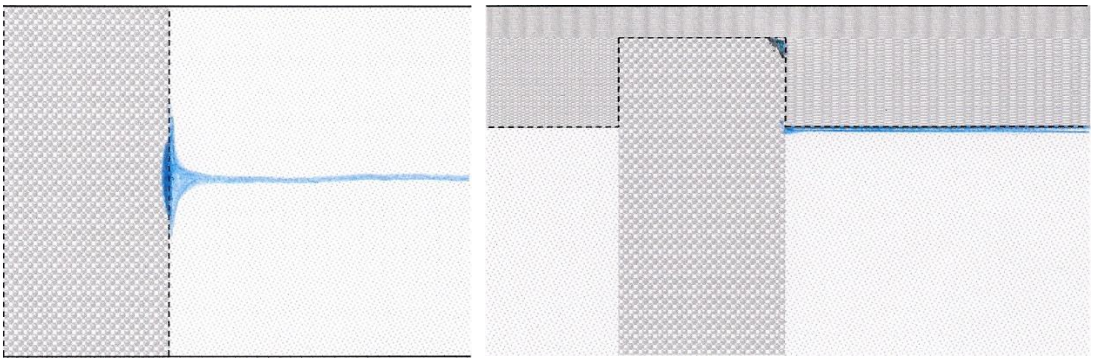

Figure 6.2 Start of lateral pipe development. As soon as the pipe in the downstream sand bed is deep enough coarse sand is spilling out of the protuberance.

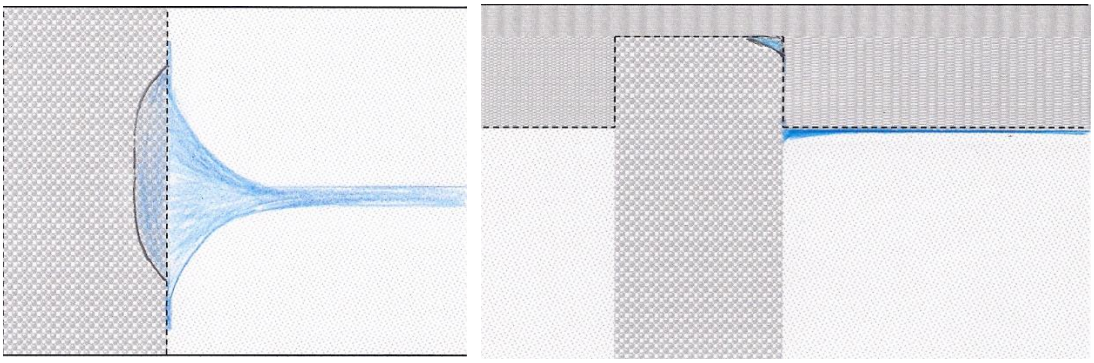

Figure 6.3 When the lateral pipe development is nearly finished, the erosion ellipse is still subsiding and widening.

In test MS37 however, there appears to have been very limited progression of the pipe parallel to the barrier prior to erosion of the barrier. This is indicated by the formation of a semi-circular erosion crater inside the barrier when the pipe reached the barrier, which suggests that a higher 3D-effect should be expected.

6.3 Erosion of the barrier

When the lateral pipe development has been completed, erosion increased, and the toe of the ellipse widened along the whole width with only slightly inclined sides (Figure 6.4).

The head drop was increased at that point at which the slope progressed upstream in the barrier. Two further head increments were kept constant for 2.25 and 3.5 hours respectively in test MS40. Constant head drop caused further progression of the slope upstream inside the barrier until the crest of the slope reached the upstream side of the protuberance. The slope forms a nearly symmetric ellipse (Figure 6.5).

During this time there was continued erosion in the barrier and continuous transport of coarse grains to the outlet cylinder and deposition behind the bulkhead at a constant hydraulic head difference. Erosion of the slope surface in the barrier seems not to be limited by erosion in the pipe downstream, because the main part of the downstream bed is paved by coarse sand.

In test MS38 seven load increments of 5 cm were applied without waiting until equilibrium until the slope reached the upstream side of the protuberance.

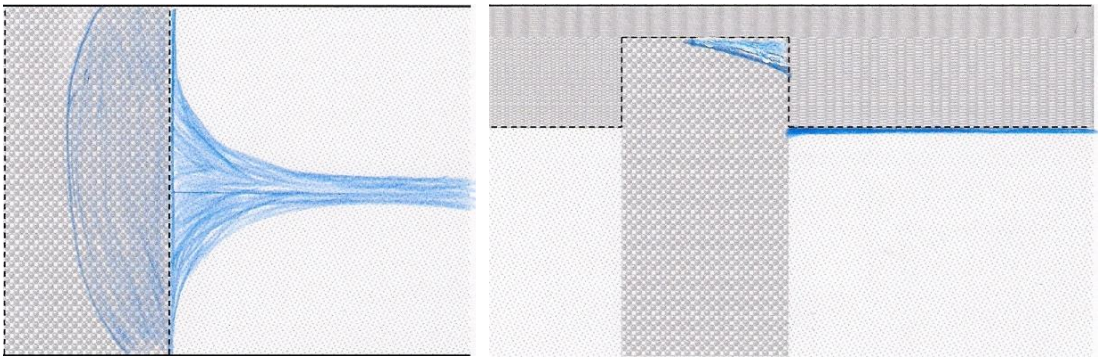

Figure 6.4 Ellipse is fully developed over the whole width of the set-up

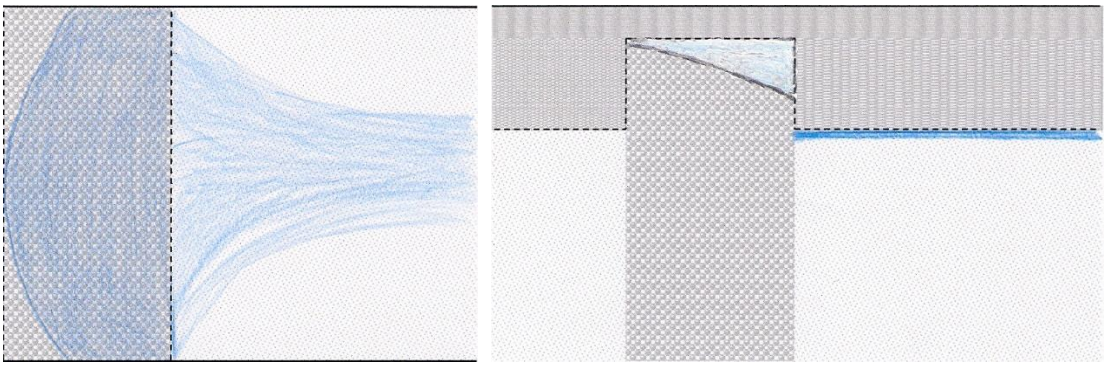

Figure 6.5 Nearly symmetric ellipse is growing to the upstream side and eroded coarse sand is paving the downstream sand bed.

From this it is inferred that there is not a stable situation anymore in the CSB when the erosion pipe reaches the CSB and the depth of the erosion pipe becomes larger than the grain size of the CSB material. The protuberance will empty, until there is a natural slope in the CSB, see also the right picture of Figure 1.1. This slope formation will go on also at a constant head difference over the set-up, until a new equilibrium is reached.

When this is reached (between Figure 6.4 and Figure 6.5), the CSB is stable against further erosion. Increasing the head will only lead to some flattening of the slope of the CSB in the protuberance because the increased gradient perpendicular to the slope will result in a flatter slope according to Equation 1 (Van Rhee / Bezuijen), although the slopes found are a bit steeper than according to this model.

After further increasing the head drop, the top of the slope began to lower and widen along the upstream side of the protuberance. During this period sand eroded along the whole surface of the slope and was transported over the sand bed to the outlet. The average angle of the slope seemed not to change much because the toe of the slope also lowered and widened with a comparable intensity and velocity. Finally, the toe of the slope subsided underneath the downstream bottom edge of the protuberance, making an open connection between the void inside the protuberance and the pipe of the downstream sand bed. From the moment that the open connection was reached, the opening began to widen slowly, and the intensity of sand erosion and transport decreased rapidly (Figure 6.6).

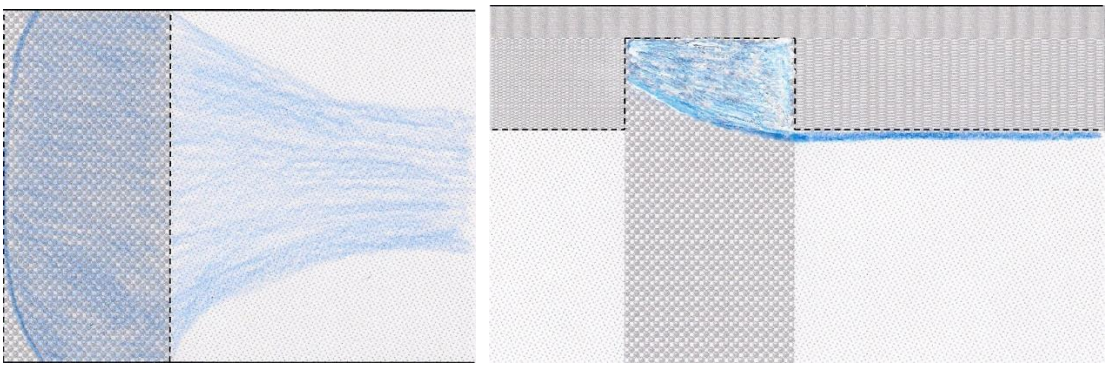

Figure 6.6 After the crest of the slope has reached the upstream protuberance wall the slope is further subsiding until the toe of the slope is below the downstream edge of the protuberance. After that the slope is getting less steep until the outward gradient along the slope is exceeding the critical value and the effective stress is getting lost.

The top of the slope was subsiding further with additional load increments of 10 cm which were twice as large as the increments applied until the connection was made. Only around 50-75% of the load steps led to material transport, so that the slope flattened out a bit. When the sand movement had stopped, a rather time-consuming (5-8 minutes) measurement of the slope surface by a laser – manually operated on a frame – had been carried out and a 5-minute interval had been completed. Thus, the load steps were increased thus mostly already after 15 to 30 minutes. Between the occurrence of connection and the application of the last load step the top of the slope subsided 10 cm and the slope flattened a bit (within 13 and 18 hours respectively and a head increase of around 3 m), which is remarkable.

Because of the relatively shallow protuberance, in MS37 the top of the slope kept in contact with the cover layer pipes formed from the edge of the slope horizontally to the upstream end of the barrier, because the critical gradient for primary erosion was exceeded at this point. The pipe progressed to the upstream interface of the barrier, but this did not yet lead to failure. As the head was further increased, erosion could be observed in the pipe, as well as erosion of the slope in the barrier.

6.4 Failure

After applying the last load increment of 10 cm, erosion occurred mainly along the toe of the slope and suddenly failure occurred. The lower part of the slope moved horizontally downstream while the crest of the slope moved downward. It appears that the heave process in the lower part of the slope, where the vertical sand volume is less heavy than at the upstream side of the slope and the gradients perpendicular to the slope are higher, is the critical process that determines the stability of the slope and hereby the stability of the barrier by reducing effective stress between the grains. The average outward gradient at the slope surface in the centre of the barrier is around 0.7

The lower part of the slope (down to the upper part of the aquifer) is fluidizing and sliding downstream. Because of the limited open space below the bottom edge of the protuberance, not all material of the sliding slope can move to the downstream sand bed, but accumulation occurred in front of the protuberance. The crest of the slope is lowering along the upstream side of the protuberance.
Subsequently, the upstream background sand was also fluidizing around the centre line of the set-up and moving downstream beneath the protuberance whereby a blowout occurred in the upstream part of the protuberance.

However, at the end of test MS37 failure appears to result from heave at the upstream end of the barrier.

In MS38 the slope formation in the CSB started at a head difference of 0.925 m over the set-up (p08 – p17) and failure of the construction occurred only at a head difference of 3.48 m. For MS40 this was 0.6 m and 3.56 m respectively. This shows the significant strength that is still available after some erosion of the CSB.

At failure, the horizontal gradient over the fine upstream background sand in test MS38 and MS40 is approximately 17. This fine sand is not stable on its own under such a high gradient. It would be stable if the gradient is a bit lower than 1. At this high gradient, it can only be stable if it is confined by the sand below and next to the moving sand and the CSB. This appears to be the case as long as there are effective stresses in the CSB. When these are reduced due to the vertical gradients in the CSB then the fine upstream sand is not stable anymore, as can be seen in Figure 3.34 and Figure 3.35. The horizontal gradient in these experiments is very high, in the field it will be less.

7 Conclusions and Recommendations

7.1 Conclusions

The aim of the tests with a protuberance was to validate the presumed failure mechanism which was devised based on MS37 (the test with a shallow protuberance) and to check if the critical gradient according to the conceptual model can be found in these tests. The primary conceptual model started with the hypothesis that the failure mechanism can be described by two models: slope instability (van Rhee & Bezuijen) and vertical heave (Terzaghi) at the upstream part of the protuberance. The hydraulic gradient at the surface of a sandy slope influences the stability of this slope.

Based on analysis of these two additional medium-scale experiments several conclusions can be drawn for the piping mechanism in the presence of a CSB when the barrier protrudes into the cover layer: In the whole, it appeared that the tests could be predicted well. In detail, there are some differences in the failure mechanism compared to the initial conceptual model. Both mechanisms are subsumed in one and the same model. The failure mechanism “loss of effective stress of the sand particles” is described by one equation, because the criterion of Van Rhee & Bezuijen for the continuum mode condition, for calculating the hydraulic gradient for the situation that is just stable, is identical with the Terzaghi criterion for fluidization for outward flow perpendicular to the slope when the slope angle β is becoming zero.

The observed and back-calculated process of internal erosion and slope development is still in accordance with the model of van Rhee & Bezuijen regarding flow rate and postdiction of the heads. However, the slope angles measured are a bit steeper than calculated with that model.

The criterion of Van Rhee & Bezuijen (1992) assumes a uniform gradient (uniform outward flow) along the slope surface as a result of the experimental set-up used for developing and underpinning this criterion which entails a linear course. In the experimental set-up of the CSB test a different non-uniform flow pattern is indicated by the numerical modelling. It turned out that the course of the gradient along the slope shows indeed a kind of plateau, but near the crown and the toe of the slope it shows an asymptotic curve progression which can be attributed to boundary effects due to the protuberance wall and the interface with the less permeable background sand. The average critical gradient in the centre of the barrier is 0.7 with a range of 0.04 (for an RD between 0.9 and 1.1). At the upstream edge of the barrier the outward gradient is a bit lower, which agrees with the flow pattern according to the postdiction of the tests. The peak value at the downstream edge of the barrier is negligible, because the high gradients near the toe of the slope are mainly due to the straight slope in the numerical model, whereas in the lab and field situation possible higher gradients at the toe of the slope will lead to flattening of the slope (as was observed during the experiments), with as a consequence lower gradients then predicted by the numerical model.

The criterion that is relevant in this case is the hydraulic gradient perpendicular to the surface of the slope nearby the toe of the slope and the equilibrium slope angle. Both tests failed at nearly the same head drop of around 3.4 m (after the deduction of head losses in the set-up) which is in accordance with the predicted critical head drop (Appendix A). The critical head drop at comparable tests without barrier was approximately 0.2 m.

Furthermore, the occurring slope angles do not correspond with the predicted angles according to the model of van Rhee & Bezuijen but are significantly steeper than the equilibrium slope angles that are predicted based on theory for outward directed seepage. According to this model the slope angle should get gentler due to an increasing gradient. This should finally result in gradients that

become higher at the upstream side of the barrier than on its downstream side, and lead to fluidization at the upstream side, but this mechanism is less probable because such a low slope angle of around 10° for the best guess of the gradient has not been reached in the tests. Failure occurred already at slope angles of around 22 – 27°.

A possible reason is that the angle op response is larger than assumed. The particle packing in the upper part of the barrier is probably less than in the centre of the barrier, but the difference between the calculated and the measured slope angle cannot be rationalized away. Figure 3.10 gives the impression that the slope is flatter near the toe than more upwards at the slope. It turned out that for steep slopes the gradient is increasing from crest to toe, resulting in a concave course of the slope near the toe. In the modelling an average slope angle is used, assuming linear course between the top of the slope and the toe. The observed slope angle is averaged over the whole slope and is therefore higher than the calculated one. Based on these considerations 22-27° seems to be a realistic range for the angle.

According to the tests the horizontal gradient in the upstream part of the set-up also seems to contribute to the mechanism. For gradients above 0.7 perpendicular to the slope of the barrier an extra phenomenon occurred in the medium-scale tests: loss of geotechnical stability as a result of loss of effective stress due to a high horizontal gradient upstream the barrier. However, this occurs in the set-up on hand, but is less likely in practice because the horizontal gradients in the upstream background sand will be less. For more detailed analyses of the geotechnical stability 3D PLAXIS calculations would be necessary with the horizontal gradients expected in the field as input.

The results and analyses of test MS37, MS38 and MS40, compared with the other tests without protuberance, indicate that a CSB which protrudes into the cover layer in the medium-scale tests will be able to retain a two times higher head drop than a barrier top level with the aquifer top. The reason for this increase in strength is that a larger outflow area is created by the slope of the protruding barrier and since the flow is limited by the upstream fine sand, this means that the gradient in the CSB is lower and thus that it is more stable.

It should be realized that maximum stability is only present when the slope in the protuberance is fully developed. This means that considerable sand transport and thus sand producing wells will exist before the maximum strength is present.

The gain in strength for a barrier protruding into the cover layer is highly dependent on the equilibrium slope, which was very steep in these tests. A lower friction angle of the CSB sand will lead to a shallower slope resulting in a somewhat lower gain in strength. The determining factor is the outflow area from the CSB into the downstream pipe. For a protruding barrier this can be much higher than for a horizontal barrier. The discharge is in both situations determined by the head difference over the fine background sand upstream. This means that the gradient perpendicular to the slope is inversely proportional to the outflow area, resulting in a much smaller gradient for the protruding barrier and thus a higher stability.

Due to this high stability, it was necessary in these tests to add an additional section of coarse sand upstream of the barrier, to create sufficient flow in order to reach failure of the set-up under given spatial and technical limits in the laboratory for creating a maximum head drop over the set-up. With this set-up a hydraulic gradient of around 17 could be reached in the background sand indicating that the CSB results in a very significant increase in strength. However, the very high horizontal gradients in the upstream background sand occurring during the tests were a result of the special configuration in this experimental set-up: the water-bearing bed of fine background sand was locked up between the Perspex cover plate and the bottom plate of the box, by what the upstream pressure has no way left to pass off, resulting in extremely high horizontal gradients. Under field conditions there is only one impermeable blanket layer, the very permeable aquifer itself extends much deeper (thickness of the aquifer) and wider (dike basis and foreland). There is a circularly approaching flow

of the relatively small CSB, where the gradient is concentrating and getting higher, but as a result of the circular flow arching is probably occurring inside the sand, which is generating more strength than in te experimental set-up. Thus, it is not possible that high water pressures will build up.

From previous tests and from the theory described in this report it is known that the permeability contrast between CSB and background sand is very important. A higher permeability contrast leads to a more stable barrier. However, movement of fine grains of the background sand into the barrier should be avoided. The allowable gradient in the field will be much less because in the field the sand layer is much thicker than the barrier, leading to a concentration of flow lines close to the barrier.

From test MS39 where mould-forming in the water reservoir lead to clogging at the interface CSB/B25 upstream of the barrier we can conclude that the reduction of the effective stress in the barrier as a result of the decreasing permeability of the upstream background sand is essential for failure of the barrier. The total head difference over the barrier and the upstream background sand were the same for this test compared to Test MS38 and MS40. However, the ground water flow was less and therefore also the reduction of the effective stress in the barrier was less and the effective stress in the background sand was high.

This shows also the importance of clogging in the field and its effect on the permeability of the background sand. Assuming a comparatively high inflow of clogging material or organic / biological particles into a piping sensitive sand layer with a CSB, we can assume that fine background sand will be clogged before the CSB will be reached. The permeability of the whole aquifer will decrease intensively. Therefore, it is worthwhile to perform in-situ permeability tests.

7.2 Recommendations

For practice the horizontal mechanism is unlikely to govern the strength, as it appears most likely that barriers will be constructed which protrude into the cover layer. If, as foreseen for the pilot location Gameren, the barrier thickness is in the order of 0.45 m, it is likely that the height is such that slopes that form in the barrier reach until the upstream end of the barrier and not to the cover layer on top of the barrier. Then, barrier strength is governed by the criteria of Terzaghi and of Van Rhee & Bezuijen (1992) as described in this report.

If wider barriers are constructed, the slopes that form could reach the top of the barrier, in that case the horizontal formation of pipes would be relevant and provide additional strength. For such application, a use of the horizontal strength criterion would be recommended, (see also Bezuijen et al., 2021).

For a wider application of the CSB, it is advised to investigate the further:

- The influence of the density of the background sand and the CSB on the strength of the barrier. For the barrier material it is possible to achieve the high demands on the relative density, but in practice the relative density of the background sand could be a problem regarding the sliding surface model.
- To check if high water pressures do really not occur upstream the barrier in a field situation like Gameren.
- Perform some more tests with a shallow barrier, since this will always be the situation in the field.
- Investigate the influence of the 3-D effect. This may be possible by using a small-scale model in the medium scale set-up.

Hereby, the number of gauges upstream of the barrier should be increased, in order to get a better insight in the gradients at the top and at the bottom of the set-up upstream of the barrier, especially when there are different areas of sand types (at least two gauges per layer zone at the top and at

the bottom of the box respectively), and to make head extrapolations possible. Furthermore, there should be more gauges installed for measuring absolute heads in the lower part of the upstream protuberance wall instead of differential gauges, or the drift of the differential gauges should be limited.

From the perspective of construction there are several practical points to consider. These are addressed in a separate report (Deltares 2021b).

8 References

Bezuijen et al. (2021)
Bezuijen A., Akrami, S., van Beek, V., Rosenbrand, E., 2021. On the Mechanism of Backward Erosion Piping in a CSB. ICSE-10 Washington, 17-20 October 2021, in press.

Deltares (2017a)
Koelewijn, A.R., van Beek, V.M., 2017. Feasibility study on the effectiveness of a coarse sand barrier as a piping measure. Report 1220240-004-GEO-0003.

Deltares (2017b)
Rosenbrand, E., van Beek, V.M., 2017. Factual Report small scale experiments coarse sand barrier Deltares Report 11200952-004-GEO-0003.

Deltares (2017c)
Rosenbrand, E., van Beek, V.M., 2017. Analysis report coarse sand barrier. Analysis of small-scale configuration (phase 2a). Deltares Report 11200952-006-GEO-0006.

Deltares (2018a)
Rosenbrand E., van Beek, V.M., 2018. Factual Report Medium Scale Experiments Coarse Sand Barrier Phase 2b. Deltares Report 11200952-007-GEO-0004

Deltares (2018b)
Rosenbrand E., van Beek, V.M., 2018. Analysis Report Coarse Sand Barrier Analysis of medium-scale configuration (phase 2b). Deltares Report 11200952-007-GEO-0013

Deltares (2019a)
Rosenbrand E., van Beek, V.M., 2019. Factual Report Delta Flume Experiments Coarse Sand Barrier Phase 2c. Deltares Report 11200952-010-GEO-0008

Deltares (2019b)
Rosenbrand E., van Beek, V.M., 2019. Analysis report coarse sand barrier Delta Flume tests (phase 2c). Deltares Report 11200952-012-GEO-0001

Deltares (2019c)
Rosenbrand E., van Beek, V.M., 2019. Factual Report Coarse Sand Barrier Medium Scale Experiments Stage II. Report 11200952-061-GEO-0001.

Deltares (2020a)
Rosenbrand E., van Beek, V.M., 2020. Analysis Report Coarse Sand Barrier. Medium-scale experiments stage II. Deltares Report 11200952-052-GEO-0004.

Deltares (2020b)
Terwindt, J., Förster, U., Koelewijn, A.R., Van Beek, V.M., 2020. Factual Report Medium-scale experiments with protruding coarse sand barrier. Deltares Report 11200952-064-GEO-0002.

Deltares (2020c)
Koelewijn, A.R., Van der Kolk, B.J., Noordam, A., 2020. Toepasbaarheid grofzandbarrière bij Gameren. Deltares report 11200952-058-GEO-0001.

Deltares (2021a)
Koelewijn, A.R., Van der Kolk, B.J., Noordam, A., Aboufirass, A., 2021. Ontwerp grofzandbarrière bij Gameren. Deltares report 11200952-068-GEO-0001.

Deltares (2021b)
Koelewijn, A.R., 2021. Foutenboom grofzandbarrière – toepassing op pilot Gameren, Aanzet tot ontwerp- en beoordelingsrichtlijn GZB. Deltares report 11200952-070-GEO-0002.

Kovacs (1981)
Kovacs, G., 1981. Seepage Hydraulics, Elsevier Scientific Publishing Company, Amsterdam, Oxford, New York.

Phillipe & Richard (2008)
Philippe, P. and Richard, T., 2008. Start and stop of an avalanche in a granular medium subjected to an inner water flow. Physical Review E. 77, 041306.

Van Rhee & Bezuijen (1992)
Van Rhee, C., Bezuijen, A., 1992. Influence of Seepage on Stability of Sandy Slope. Journal of Geotechnical Engineering. 118(8), pp 1236-1240.

Appendices

A Prediction models

This appendix contains the prediction models for the experiment.

The simulations are conducted:

a) to assess the likelihood of failure within the range of the heads that can be applied in the laboratory,
b) to investigate modifications to the sample configuration to increase the likelihood of failure
c) to investigate the effect of the pipe depth on the critical head and slope.
d) to predict the critical head and slope angle in the experiments for different contrasts.

An initial sensitivity analysis was done to investigate gradients that might be expected using permeabilities based on the first phase (small-scale tests) of the project. This analysis also addresses the effect of the depth of the toe of the slope. Subsequent analyses are performed using the newly derived correlation between permeability and porosity in (Deltares, 2020a) and are performed with a modified configuration that will increase the likelihood of failure in the laboratory. For these predictions, simulations with two different permeability contrasts have been performed: a realistic contrast in the experiments and one that is closer to the expected contrast in practice.

A.1 General Model input

A.1.1 Geometry

The geometry of a general model is shown in the figure below, the coordinates of the labelled points are shown in the corresponding table. The angle of the slope is varied as this is unknown in advance. Slope angles from 5° to 20° increasing in steps of 5° are modelled.
The depth of the toe of the slope is also unknown: for a 20° slope the effect of a toe at 0.03 m deep and of 0.01 m deep is investigated in the preliminary sensitivity analysis. The prediction models are conducted with a depth of 0.01 m.
As the preliminary sensitivity analysis shows that it is unlikely that failure will be achieved in a configuration with only background sand upstream of the barrier, analyses are done with 0.20 m of background sand directly upstream of the barrier, and barrier material upstream of this.

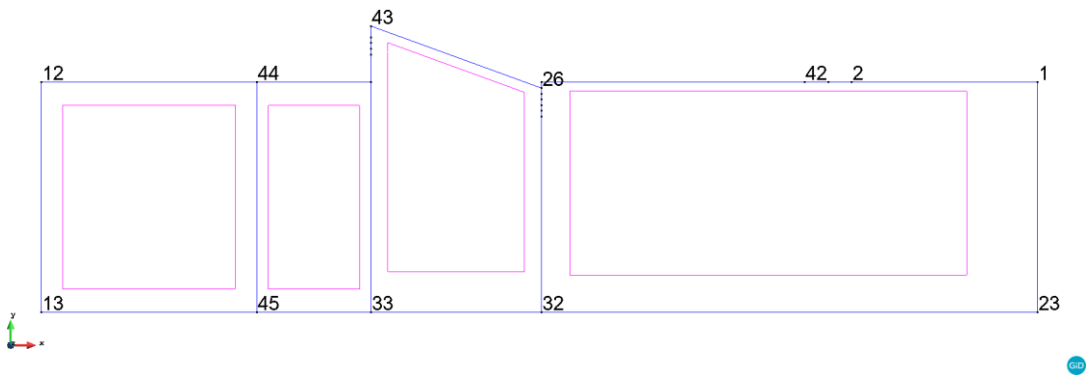

Figure A.1Geometry of the model, coordinates of labelled points are shown in the table below

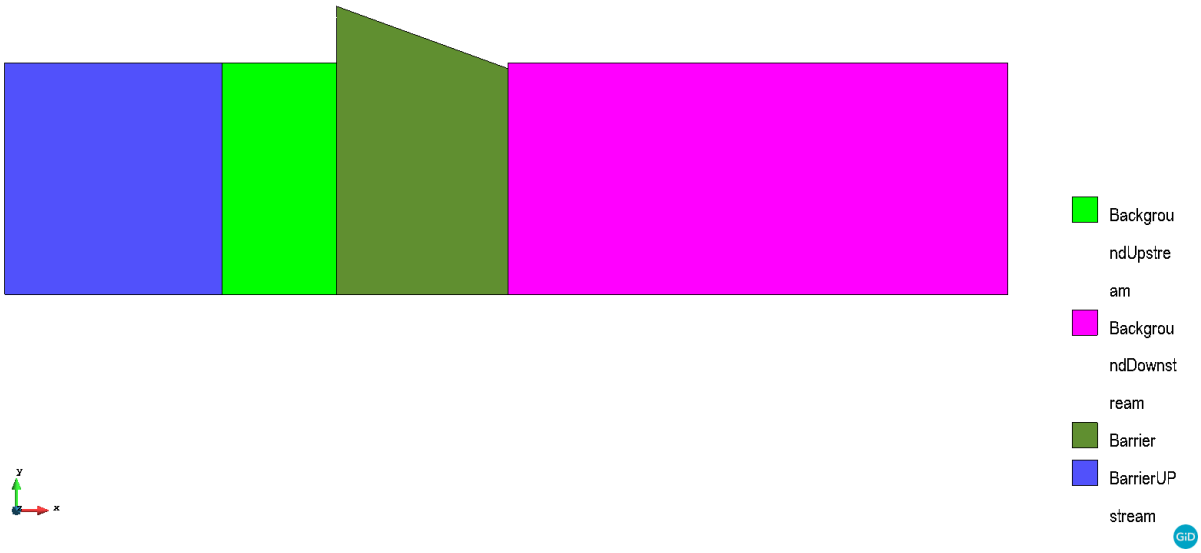

Figure A.2 Geometry of the model, materials

Table A.1Locations of labelled points in Figure A.1, model Pre_S020_T01_BG020.

point label	x coordinate (m)	y coordinate (m)
1	0.368	0
2	0.041	0
12	-1.385	0
13	-1.385	-0.404
23	0.368	-0.404
26	-0.505	-0.01
32	-0.505	-0.404
33	-0.805	-0.404
42	-0.041	0
43	-0.805	0.099
44	-1.005	0
45	-1.005	-0.404

A.1.2 Boundary conditions

The locations of boundary conditions are shown in Figure A.3. A constant head is applied at the inlet, equal to approximately the maximum water level that can be applied in this test configuration

(6 m). The outlet is formed by the slope in the barrier, the pipe in front of the barrier and the outlet hole. This is a constant head of 0 m. Other boundaries are closed.

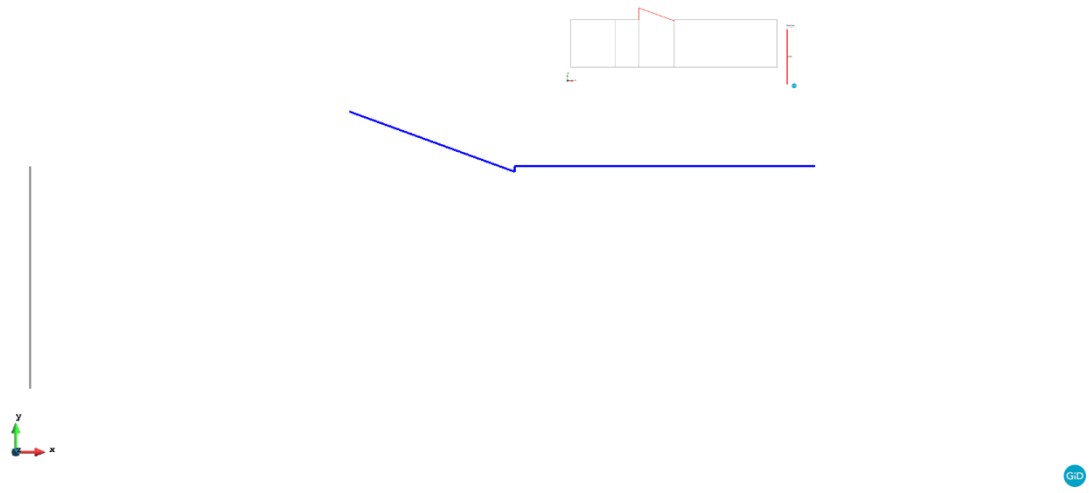

Figure A.3 Boundaries, grey upstream, blue downstream, model Pre_S020_T01_BG020 (the entire model is shown in the background to indicate where the boundaries are on the outline)

A.1.3 Mesh

The mesh is refined in the barrier as the gradients here are most important. Elements have a size of 0.001m on the lines indicated in Figure A.4. Gradually, the element size is increased to 0.01 m at the ends of the model. An unstructured mesh is used.

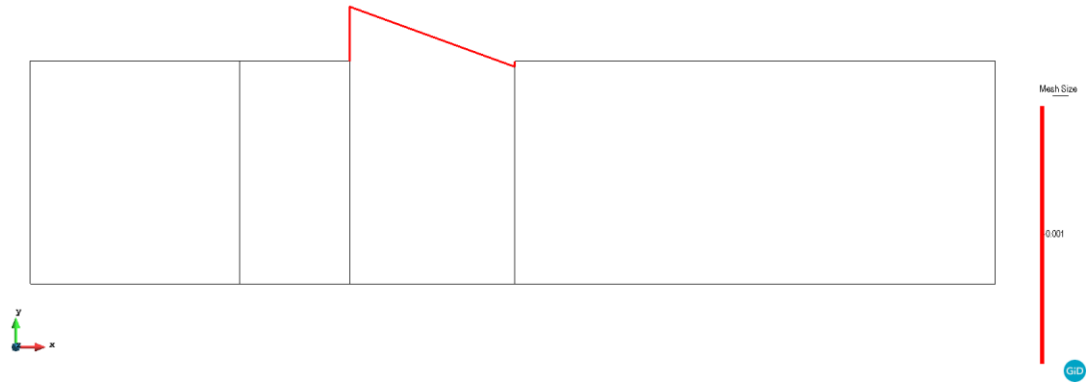

Figure A.4 Mesh refinement in barrier, model Pre_S020_T01_BG020

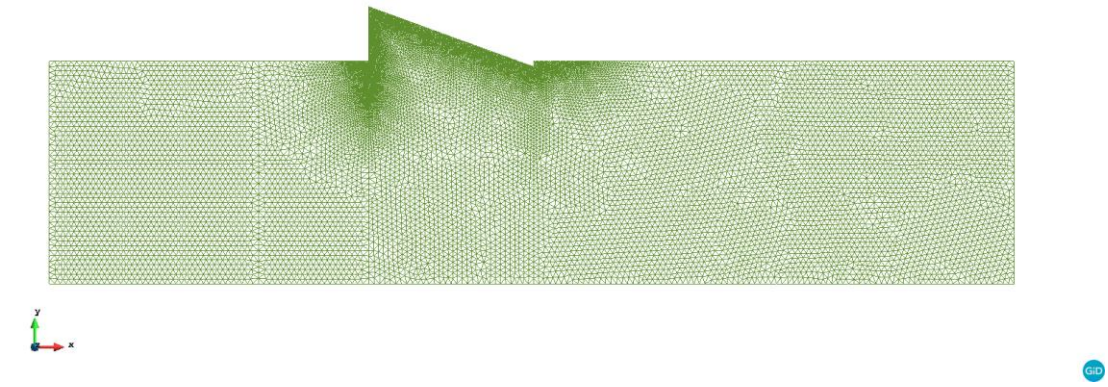

Figure A.5 Mesh, model Pre_S020_T01_BG020

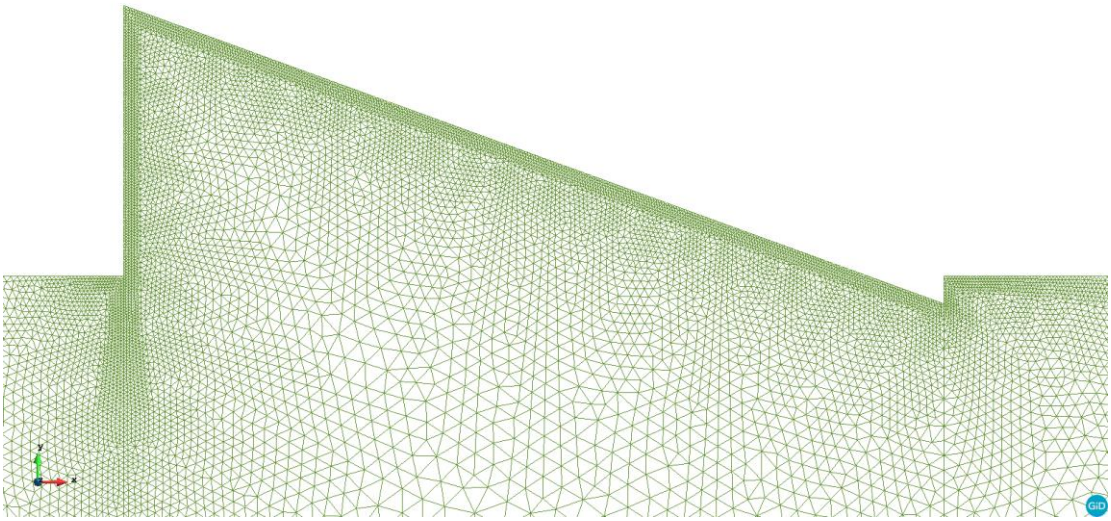

Figure A.6 Mesh close up, model Pre_S020_T01_BG020

A.1.4 Material properties

The used sand types are B25 and GZB3.

The water is incompressible and has a density of 998,6 kg/m^3 and a viscosity of 1E^{-3} Pa.s corresponding to laboratory temperatures of 18°C.

The hydraulic conductivity for the background sand is based on the correlations derived in earlier phases of the project.

A.1.4.1. Preliminary sensitivity analysis

An initial sensitivity analysis was done using correlations derived for small-scale tests in (Deltares 2017c). For GZB1 values from the old and new correlations could differ by a factor two (with higher

values in the 2017 results). Therefore, in the initial sensitivity analysis a variation was done to investigate the effect of contrast using the model with a slope of 20° and a toe depth of 0.03 and 0.01 m.

For this initial sensitivity analysis, the values used are shown in Table A.2.

*Table A.2 Initial sensitivity analysis hydraulic conductivities and RD: barrier is based on Deltares (2017c), background sand is based on Deltares (2020a). Name indicates the name which is appended to the model name for this hydraulic conductivity e.g. S_020_T_03_**Kgzb_m*** (Model name starting with *S_ indicates this model is for sensitivity analysis*).

Name	RD back-ground up-stream	RD back-ground down-stream	RD barrier	Hydraulic conductivity background upstream m/s	Hydraulic conductivity background downstream m/s	Hydraulic conductivity Barrier m/s	Contrast
…_Kgzb_m	1	1	1	1.70E-04	1.70E-04	6.30E-03	37
…_Kgzb_h	1	1	0.8	1.70E-04	1.70E-04	7.90E-03	46
…_Kgzb_l	1	1	0.9 but hydraulic conductivity × 2	1.70E-04	1.70E-04	4.26E-03	25

A.1.4.2. Predictions

For the prediction models, the permeability of the materials is not varied, the values used are based on the correlation for GZB 3 derived in Deltares (2020b).

Table A.3 Prediction models hydraulic conductivities and RD: barrier is based on Deltares (2020b), background sand is based on Deltares (2020a).

RD background upstream	RD background downstream	RD barrier and GZB3 upstream of background sand	Hydraulic conductivity background upstream m/s	Hydraulic conductivity background downstream m/s	Hydraulic conductivity Barrier m/s	Contrast
0.90	0.90	0.90	1.93E-04	1.93E-04	4.60E-03	24

A.2 General model analysis

The objective is to determine the critical head, based on the gradient which occurs at the upstream end of the slope, which can cause heave, and the outward directed gradient which affects the stability of the slope.

The heave gradient is evaluated from the surface of the slope, to the surface of the background sand (y = 0 m) at x location -0.795 m (i.e. 1 cm from the upstream edge of the barrier). In order to assess the situation where heave might occur at the upstream end of the slope, the computed vertical gradients are used to scale results to a situation where the vertical gradient = 1 (≈ critical heave gradient).

The outward directed gradient is evaluated over the centre portion of the slope between x = -0.60 m and x = 0.70 m. The gradient is computed between the surface of the slope and 5 cm into the slope as well as based on the velocities directed out of the slope.

The equilibrium angle for the slope is computed based on the slope equation of Kovacs (1981) (later also reported in van Rhee and Bezuijen, 1992 and Philippe and Richard, 2008). This equation can be rewritten as (Deltares 2020a):

$$\beta_{i,cr} = \alpha - \arcsin\left(\left[\frac{i}{\frac{(1-n)(\rho_s - \rho_w)}{\rho_w}}\right]\sin(\alpha)\right)$$

Equation 2

Symbols
- $\beta_{i,crit}$ = angle of the slope, [°]
- n = porosity, [-]
- ρ_w = density of water, [kg/m^3]
- ρ_w = density of grains, [kg/m^3]
- α = angle which characterises internal friction in the soil, [°]
- i = gradient perpendicular to the slope (outward direction is positive), [-]

A.3 Initial sensitivity analysis results

An overview of the models and the results from the initial sensitivity analysis is shown in Table A.4 and Table A.5. In these models, the entire area upstream of the barrier consists of background sand (i.e. no barrier material upstream of the background sand).

Table A.4 overview of models in initial sensitivity analysis (k is hydraulic conductivity)

Model name	slope angle	slope toe depth	k background upstream	k background downstream	k barrier	contrast
	°	m	m/s	m/s	m/s	
S_020_T_03_Kgzb_m	20	-0.03	1.70E-04	1.70E-04	6.30E-03	37
S_020_T_03_Kgzb_h	20	-0.03	1.70E-04	1.70E-04	7.90E-03	46
S_020_T_03_Kgzb_l	20	-0.03	1.70E-04	1.70E-04	4.26E-03	25
S_020_T_01_Kgzb_m	20	-0.01	1.70E-04	1.70E-04	6.30E-03	37
S_020_T_01_Kgzb_h	20	-0.01	1.70E-04	1.70E-04	7.90E-03	46
S_020_T_01_Kgzb_l	20	-0.01	1.70E-04	1.70E-04	4.26E-03	25

Table A.5 Results of models in initial sensitivity analysis (porosity is based on RD = 1 as used during permeability measurements in Deltares (2017c)

Model name	contrast	Gradient out of slope		heave distance	heave gradient	equilibrium slope angle		slope stable ?
		Average over 0.05 m below slope surface	Based on velocity at slope surface	(top of slope to y = 0 m) m	-	Based on average gradient out of slope	Based on velocity at slope surface	For angle of repose 35° and porosity .353
S_020_T_03_Kgzb_m	37	0.31	0.34	0.075	0.36	26	24	yes
S_020_T_03_Kgzb_h	46	0.25	0.27	0.075	0.29	27	27	yes
S_020_T_03_Kgzb_l	25	0.45	0.50	0.075	0.54	21	19	maybe
S_020_T_01_Kgzb_m	37	0.32	0.35	0.095	0.35	25	24	yes
S_020_T_01_Kgzb_h	46	0.26	0.28	0.095	0.28	27	26	yes
S_020_T_01_Kgzb_l	25	0.46	0.50	0.095	0.52	21	19	maybe

These results indicate that for the maximum head difference applied, a slope of 20° is more or less in equilibrium with the outward gradients for the lowest hydraulic conductivity of the barrier. Otherwise a steeper slope may form. In the final predictions, when the hydraulic conductivity of the barrier is better known, other gradients will be modelled.

The heave gradients are lower than values which would be expected to cause heave to occur. That indicates that in the current configuration, for the range of contrasts applied in these computations, it is unlikely that failure will be achieved. Possibly 3D effects might cause some additional concentration of flow, which would result in higher occurring gradients. Also, if the barrier material proved to have a lower hydraulic conductivity that would result in higher heave gradients that computed here. However, for the computation with the lowest hydraulic conductivity, the value was already half that of the value which would be expected for this material at *RD* 0.90 based on the 2017 correlation.

The effect of the toe of the slope on the outward gradients and on the heave gradients is relatively insignificant, despite it affecting the distance over which heave must occur. The reason for this lies in the head profile inside the barrier. The head profile below the top of the slope is parallel for the two models with Kgzb_l. This means that the heave gradient over a distance of 0.075 m will be similar to a gradient over 0.095 m.

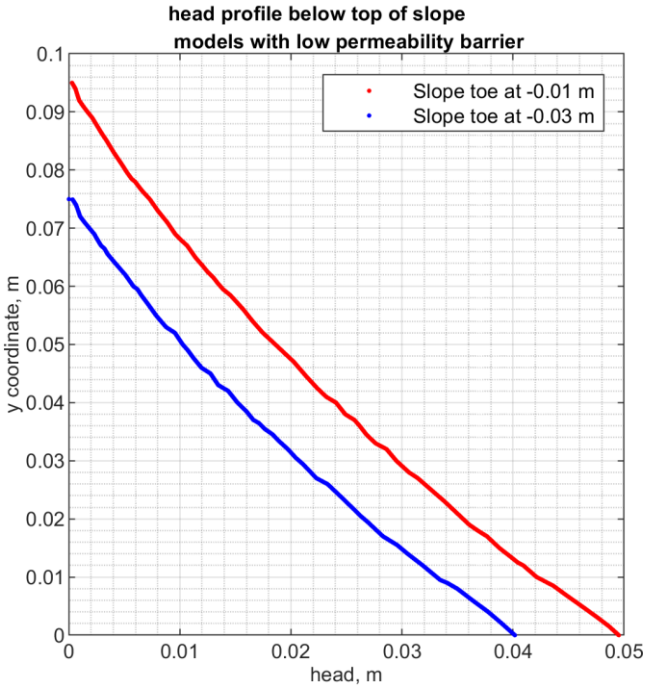

Figure A.7 Head at the tip of the slope for models S_020_T_03_Kgzb_l and S_020_T_01_Kgzb_l.

An example of the head profile and the gradients out of the slope is shown below for the model S_020_T_03_Kgzb_m (contrast 37).

Figure A.8 Head profile for model S_020_T_03_Kgzb_m head colours from 6 m (red) to 0 m (blue), head contours from 6 m to 0 m in steps of 0.10 m.

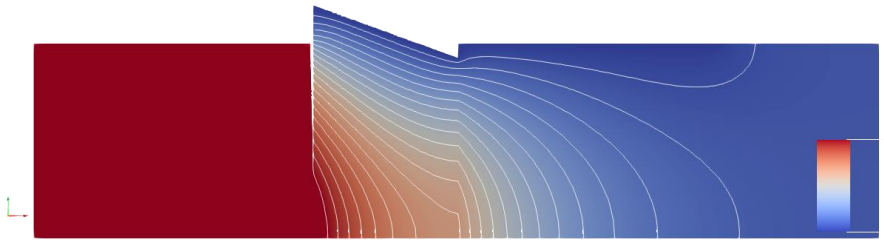

Figure A.9 Head profile for model S_020_T_03_Kgzb_m head colours from 0.10 m (red) to 0 m (blue), head contours from 0.10 m to 0 m in steps of 0.005 m.

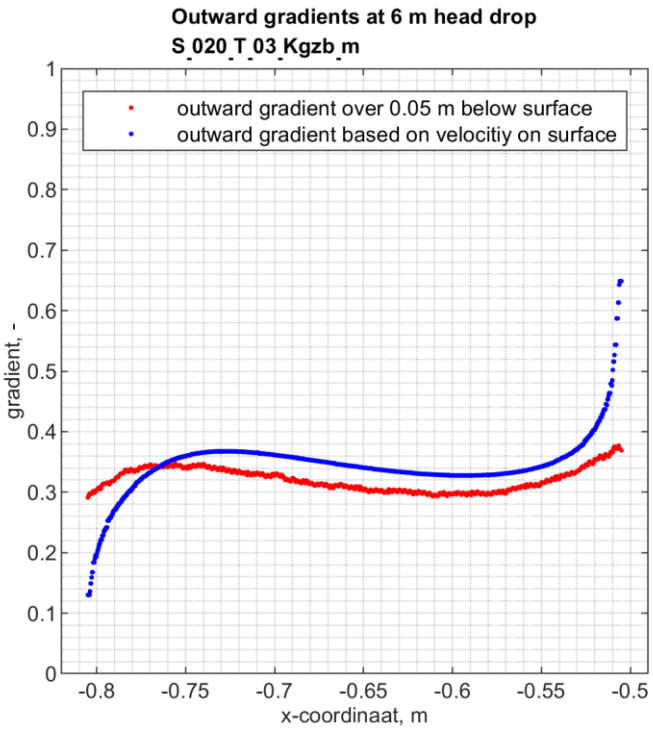

Figure A.10 Computed gradients out of slope for model S_020_T_03_Kgzb_m

A.3.1 Conclusions

With the expected contrasts it will not be possible to achieve failure in this configuration. For predictions, an area of 0.20 m upstream of the barrier will be modelled with B25 background sand, but the rest of the area up to the filter is filled with GZB3 in order to increase the gradients in the barrier. The new correlation for porosity-permeability for GZB3 is used.

A.4 Predictions Basis Contrast

Using the correlation between hydraulic conductivity and porosity derived for GZB3 in Deltares (2020b) results in a hydraulic conductivity contrast of 24. With this contrast, it is unlikely that gradients in the barrier would be sufficiently high to achieve failure. Therefore, all further models are done with a layer of GZB3 upstream of the background sand. This reduces the head loss in the sand upstream of the barrier and increases the gradients in the barrier.

An overview of the prediction models with the basis contrast is shown Table A.6. Results are shown in Table A.7 for a head drop of 6 m over the set-up. This is considered the maximum achievable head drop in this set-up.

Results are elaborated on in following subsections.

Table A.6 overview of basis prediction models (k is hydraulic conductivity)

Model name	slope angle	slope toe depth	k background upstream	k background downstream	k barrier	contrast
	°	m	m/s	m/s	m/s	
Pre_S005_T01_BG020	5	0.01	1.93E-04	1.93E-04	4.60E-03	24
Pre_S010_T01_BG020	10	0.01	1.93E-04	1.93E-04	4.60E-03	24
Pre_S015_T01_BG020	15	0.01	1.93E-04	1.93E-04	4.60E-03	24
Pre_S020_T01_BG020	20	0.01	1.93E-04	1.93E-04	4.60E-03	24

Table A.7 Results of models of basis predictions (equilibrium slope angles are for angle of repose 35° and porosity 0.3715 (RD = 0.9))

Model name	contrast	Gradient out of slope		Vertical distance at top of slope	Vertical gradient at top of slope	Equilibrium slope angle °		slope stable ?
		Average over 0.05 m below slope surface	Based on velocity at slope surface	(top of slope to y = 0 m) m	-	Based on average gradient out of slope	Based on velocity at slope surface	
Pre_S005_T01_BG020	24	1.23	1.27	0.015	2.61	-8	-10	no
Pre_S010_T01_BG020	24	1.27	1.33	0.041	1.96	-10	-13	no
Pre_S015_T01_BG020	24	1.281	1.360	0.068	1.628	-10	-14	no
Pre_S020_T01_BG020	24	1.26	1.36	0.095	1.41	-9	-14	no

The negative equilibrium slope angle indicates that even a horizontal slope would not be stable. It is noted that heave gradients above the critical heave gradient, as were calculated in these simulations, will not occur in the experiments. The results indicate that failure will likely occur below the maximum applied head of 6 m.

A.4.1 Situation without GZB3 upstream of background sand

Without GZB3 upstream of the background sand, gradients directed out of the slope and vertical gradients are relatively low. Gradients directed out of the slope are shown in Figure A.11. With 0.38 m of background sand replaced by GZB3 the outward directed gradients are 2.6 times higher than with only B25 background sand. With only background sand, a 20° slope (which was used in the model) would be stable and the vertical gradient is only 0.54. With GZB3 upstream, the 20° slope would not be stable, and the vertical gradient is sufficient for failure (Table A.7).

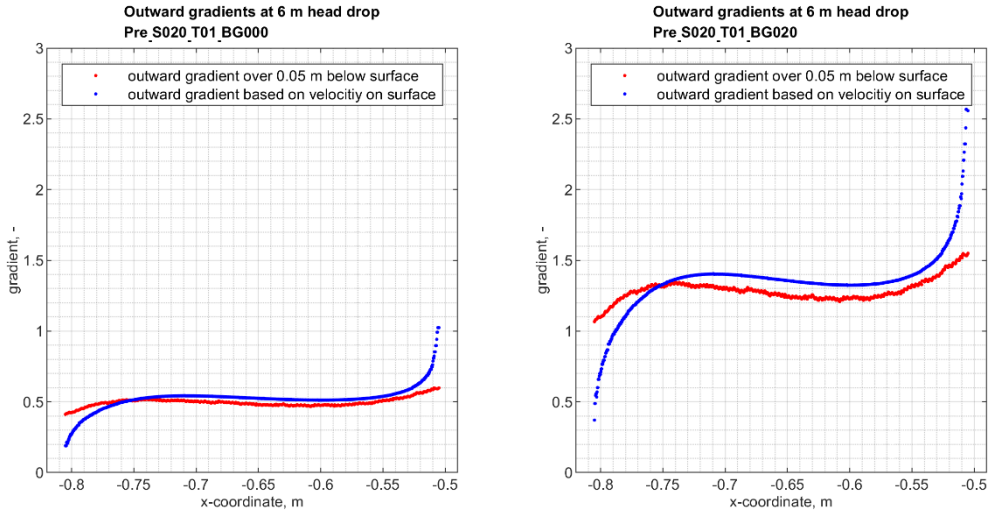

Figure A.11Left hand side, out of slope gradients for model without barrier material upstream of background sand. Right hand side, out of slope gradients for model with 0.38 m barrier material upstream of background sand.

A.4.2 Effect of slope angle on gradients out of slope

The gradient out of the slope shows a different curve depending on the slope angle. The gradients are shown for different slope angles in Figure A.12

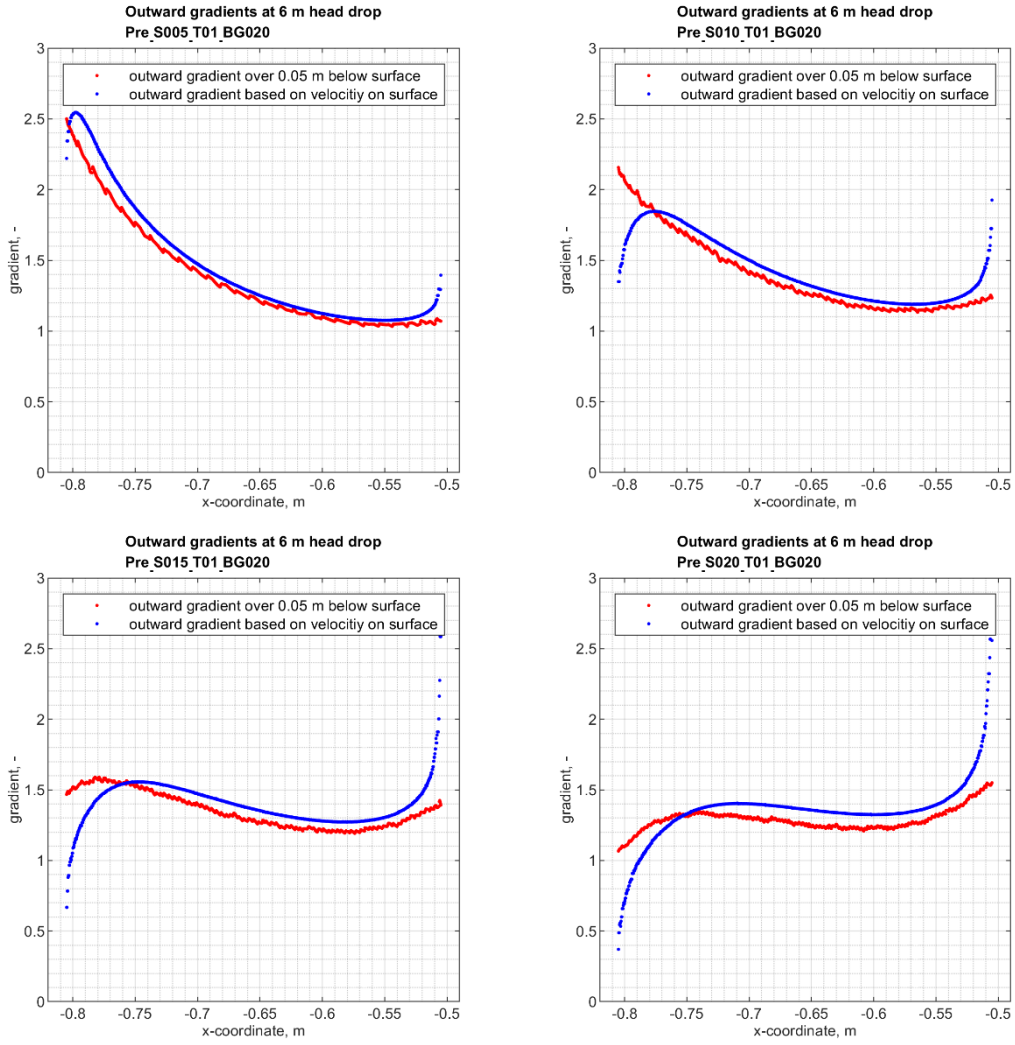

Figure A.12 Gradient out of the slope for models with different slope angles (top row left 5°, right 10°, bottom row left 15° right 20°).

A.4.3 Effect of slope angle on head distribution

The head distribution for the models with different slope angles is shown in Figure A.13.

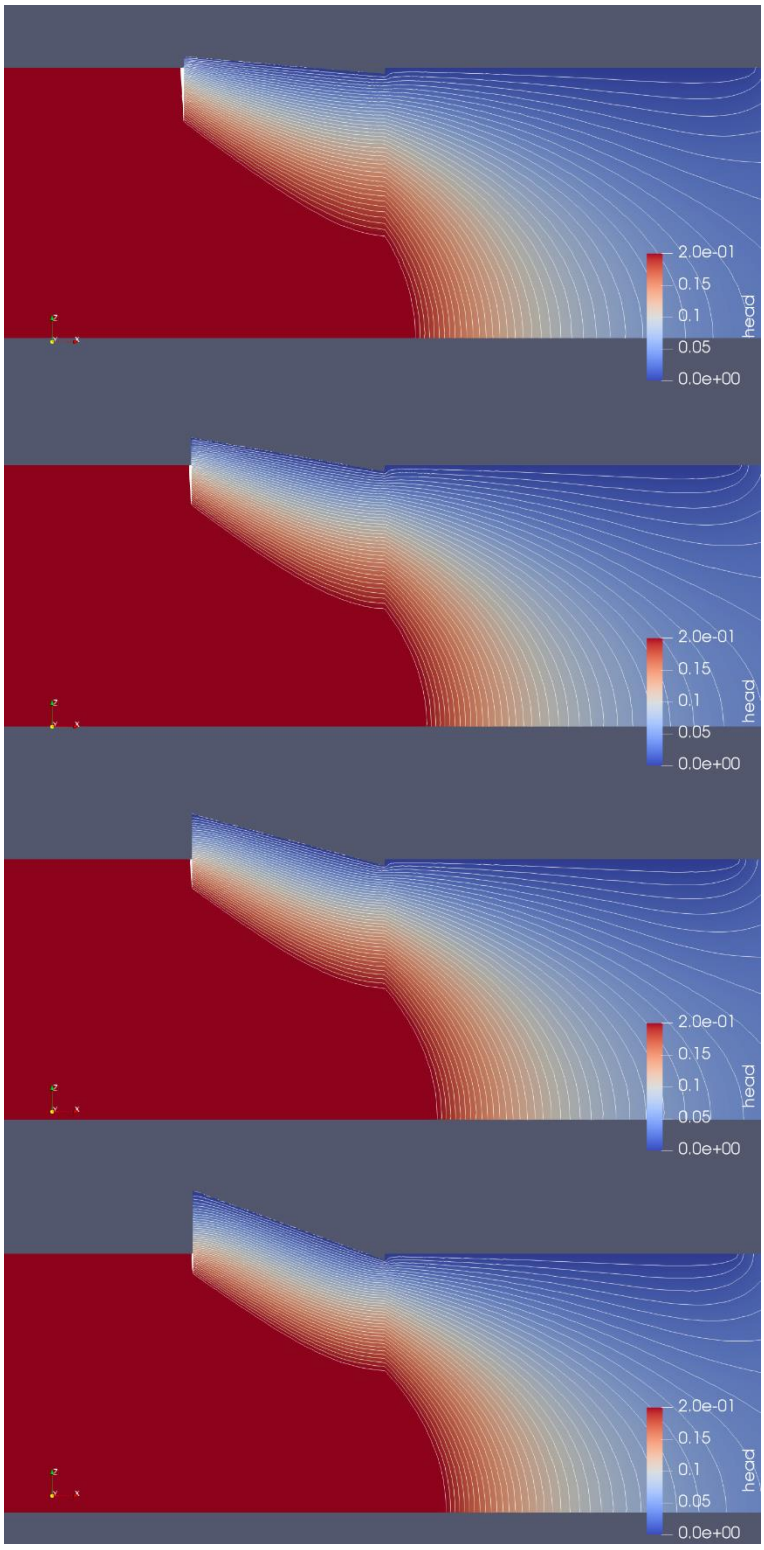

Figure A.13 Head profile for models with different slope angles (top to bottom: 5°, 10°, 15° and 20°).

A.4.4 Effect of slope angle on ratio vertical gradient/gradient out of slope

This head profile difference also results in a different ratio between the vertical gradient and the out of slope gradient for the two models. This ratio is shown as a function of slope angle in the figure below.

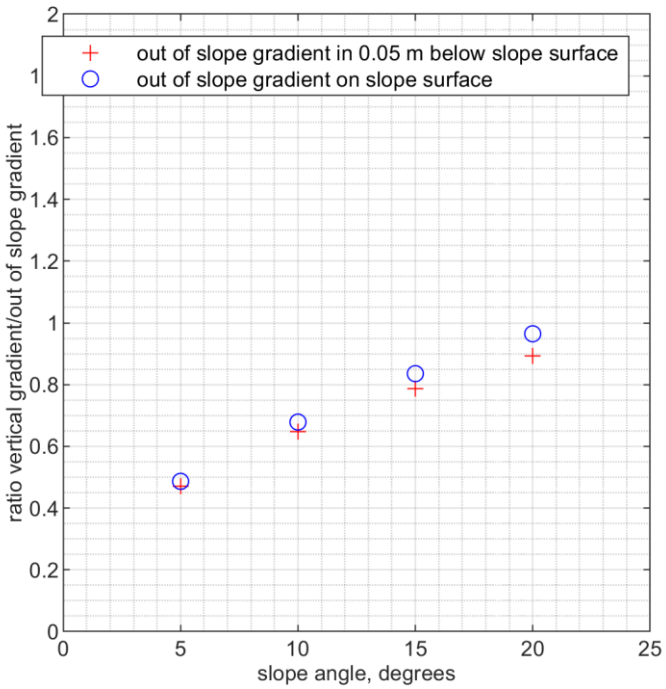

Figure A.14 Ratio of vertical gradient at the top of the slope to the out of slope gradient for models with different slope angles.

A.4.5 Situation where heave occurs

In order to assess the situation where heave might occur at the upstream end of the slope, the computed vertical gradients in Table A.7 are used to scale results to a situation where the vertical gradient $= 1$ ($\approx critical\ heave\ gradient$). This is shown in Table A.8.

With a slope of 15°, the head drop required to achieve heave is such that the out of slope angle is too high for a 15° slope. An 8-9° slope would be in equilibrium with this out of slope gradient. However, with a 10° slope, the head drop required to achieve heave would be in equilibrium with a 13-14° slope.

The hypothesis is that as the head is increased in the course of the experiment a slope will form with a slope that gradually becomes less steep until heave occurs. If the hydraulic conductivities are indeed as modelled here, and if there are no 3D effects, it is expected that the critical point (just prior to heave) occurs at a head drop in the order of 3.2 to 3.6 m, at which point the slope will be in the order of 10-12°.

Table A.8 Results for situations where the vertical gradient at the top of the slope = 1 (≈heave criterion)

Model name	contrast	Head drop for vertical gradient = 1	Gradient out of slope		Equilibrium slope angle °	
		m	Average over 0.05 m below slope surface	Based on velocity at slope surface	Based on gradient over 0.05 m below slope surface	Based on velocity at slope surface
Pre_S005_T01_BG020	24	2.3	0.470	0.485	20	20
Pre_S010_T01_BG020	24	3.1	0.645	0.678	14	13
Pre_S015_T01_BG020	24	3.7	0.787	0.835	9	8
Pre_S020_T01_BG020	24	4.3	0.890	0.963	6	3

A.4.6 Flow rate

The modelled flow rate is computed by multiplying the velocity at the inflow boundary by the dimensions of the inflow are (0.404× 0.881 m). The modelled flow rates are shown in Table A.9.

Table A.9 Modelled flow rates.

Model name	Slope angle, °	Flow rate at 6 m head drop, l/min	Head drop for vertical gradient 1, m	Flow rate at vertical gradient 1, l/min
Pre_S005_T01_BG020	5	109	2.3	42
Pre_S010_T01_BG020	10	109	3.1	55
Pre_S015_T01_BG020	15	108	3.7	67
Pre_S020_T01_BG020	20	108	4.3	77

A.5 Prediction lower contrast

Possibly the situation at the pilot location will have a lower contrast than was assumed in the current calculation due to a higher hydraulic conductivity of the background sand. Therefore, the analysis is also done for a situation where the hydraulic conductivity of the background sand is twice as high, so see whether the field situation deviates too much from the laboratory experiments, for a proper extrapolation

An overview of the prediction models with a lower contrast is shown Table A.6. Results are shown in Table A.7 for a head drop of 6 m over the set-up. This is considered the maximum achievable head drop in this set-up. As expected, the lower contrast causes less head loss in the background sand, such that for a head drop of 6 m, the critical heave gradient and the slope angle equilibrium are both heavily exceeded.

Results are compared to the results of the basis models in the following subsections.

Table A.10 overview of prediction models with lower contrast (k is hydraulic conductivity)

Model name	slope angle	slope toe depth	k background upstream	k background downstream	k barrier	contrast
	°	m	m/s	m/s	m/s	
Pre_S005_T01_BG020_K2	5	0.01	3.86E-04	3.86E-04	4.60E-03	12
Pre_S010_T01_BG020_K2	10	0.01	3.86E-04	3.86E-04	4.60E-03	12
Pre_S015_T01_BG020_K2	15	0.01	3.86E-04	3.86E-04	4.60E-03	12
Pre_S020_T01_BG020_K2	20	0.01	3.86E-04	3.86E-04	4.60E-03	12

Table A.11 Results of models with lower contrast (equilibrium slope angles are for angle of repose 35° and porosity .3715 (RD = 0.9))

Model name	contrast	Gradient out of slope		Vertical distance at top of slope	Vertical gradient at top of slope	Equilibrium slope angle °		slope stable ?
		Average over 0.05 m below slope surface	Based on velocity at slope surface	(top of slope to y = 0 m) m	-	Based on average gradient out of slope	Based on velocity at slope surface	
Pre_S005_T01_BG020_K2	24	2.13	2.20	0.015	4.78	NAN	NAN	no
Pre_S010_T01_BG020_K2	24	2.19	2.31	0.041	3.55	NAN	NAN	no
Pre_S015_T01_BG020_K2	24	2.22	2.36	0.068	2.92	NAN	NAN	no
Pre_S020_T01_BG020_K2	24	2.17	2.36	0.095	2.51	NAN	NAN	no

* the slope angle cannot be computed, due to the high out of slope gradients, even with a horizontal surface heave would occur.

A.5.1 Effect of contrast on gradients out of slope and vertical gradient

The gradients directed out of the slope are higher, as is the vertical gradient. With a lower contrast, a larger portion of the head drop is dissipated inside the barrier, resulting in these higher gradients.

Gradients are a factor 1.7 higher for the gradient out of the slope and 1.8 higher for the vertical gradient, independent of the slope angle.

Table A.12 Ratio of the modelled gradients for the models with a lower contrast / the basis model.

Model name	Ratio out of slope gradient with K2 to out of slope gradient basis models		Ratio vertical gradient with K2 to vertical gradient basis models
	Average over 0.05 m below slope surface	Based on velocity at slope surface	
Pre_S005_T01_BG020_K2	1.7	1.7	1.8
Pre_S010_T01_BG020_K2	1.7	1.7	1.8
Pre_S015_T01_BG020_K2	1.7	1.7	1.8
Pre_S020_T01_BG020_K2	1.7	1.7	1.8

The ratio between the vertical gradient and the out of slope gradient is therefore also approximately the same for the contrast of 12 as for the contrast of 24.

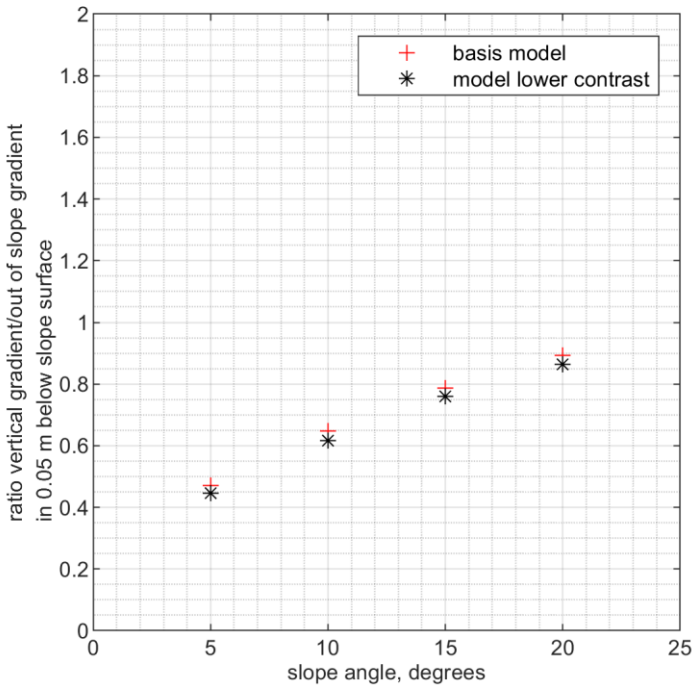

Figure A.15 Ratio of vertical gradient at the top of the slope to the out of slope gradient.

A.5.2 Situation where heave occurs

The situation where heave occurs is assumed to be for a vertical gradient of 1 as in Section A.4.5. Equilibrium slope angles are similar as for the basis models with a contrast of 24, suggesting that the critical point (just prior to heave) occurs at a head drop in the order of 1.8-2.0 m, at which point the slope will have a gradient in the order of 11-13° (if no 3D effects play a role).

Table A.13 Results for situations where the vertical gradient at the top of the slope = 1 (≈heave criterion)

Model name	contrast	Head drop for vertical gradient = 1	Gradient out of slope		Equilibrium slope angle °	
		m	Average over 0.05 m below slope surface	Based on velocity at slope surface	Based on gradient over 0.05 m below slope surface	Based on velocity at slope surface
Pre_S005_T01_BG020	24	2.3	0.470	0.485	20	20
Pre_S010_T01_BG020	24	3.1	0.645	0.678	14	13
Pre_S015_T01_BG020	24	3.7	0.787	0.835	9	8
Pre_S020_T01_BG020	24	4.3	0.890	0.963	6	3
Pre_S005_T01_BG020_K2	12	1.3	0.445	0.460	21	21
Pre_S010_T01_BG020_K2	12	1.7	0.619	0.651	15	14
Pre_S015_T01_BG020_K2	12	2.1	0.760	0.809	10	9
Pre_S020_T01_BG020_K2	12	2.4	0.864	0.937	7	4

A.5.3 Flow rate

The modelled flow rate is computed by multiplying the velocity at the inflow boundary by the dimensions of the inflow are (0.404× 0.881 m). The modelled flow rates are shown in Table A.9 for both the basis contrast and the lower contrast. The flow rates that result in a vertical gradient of 1 are very similar for the two models.

Table A.14 Modelled flow rates.

Model name	Slope angle, °	Flow rate at 6 m head drop, l/min	Head drop for vertical gradient 1, m	Flow rate at vertical gradient 1, l/min
Pre_S005_T01_BG020	5	109	2.3	42
Pre_S010_T01_BG020	10	109	3.1	55
Pre_S015_T01_BG020	15	108	3.7	67
Pre_S020_T01_BG020	20	108	4.3	77
Pre_S005_T01_BG020_K2	5	195	1.3	41
Pre_S010_T01_BG020_K2	10	194	1.7	55
Pre_S015_T01_BG020_K2	15	193	2.1	66
Pre_S020_T01_BG020_K2	20	192	2.4	76

A.5.4 Conclusions

These results indicate that although the critical head drop will be affected by contrast, the dimensions of the slope in the barrier will not. However, this is based on 2D models, possibly the contrast has more effect if the slope does not develop along the entire width of the model, or if the pipe downstream of the barrier does not progress along the width of the model. Although this can happen in reality and was probably even the case in the large-scale experiment, this is less likely in the medium-scale experiments which only have a limited width.

B Postdiction details

B.1 Variatiations of intrinsic permeabilities for fitting numerical results with measured values

Table B 1 Variation of intrinsic permeability for MS38

	x	y	critical head	A	B	C	D	E	F	G	H	I	J	K	B2	I2
	[mm]	[mm]	[m]	[m]	[m]	[m]	[m]	[m]	[m]	[m]	[m]	[m]	[m]	[m]	[m]	[m]
P01	-1357	-388	3.77	3.81	3.80	3.80	3.82	3.81	3.82	3.80	3.81	3.80	3.81	3.81	3.80	3.80
P02	-835	-388	1.82	1.15	1.30	1.21	1.21	1.28	1.13	1.25	1.18	1.15	1.20	1.28	1.31	1.15
P03	-550	-388	0.59	0.61	0.76	0.68	0.63	0.70	0.58	0.71	0.64	0.63	0.66	0.72	0.76	0.63
P04	-357	-388	0.51	0.54	0.62	0.58	0.55	0.59	0.53	0.59	0.56	0.55	0.57	0.60	0.62	0.55
P05	-107	-388	0.50	0.49	0.52	0.50	0.49	0.51	0.48	0.51	0.50	0.49	0.50	0.51	0.52	0.49
P09	-980	0	3.04	3.23	3.08	3.15	3.27	3.22	3.26	3.13	3.19	3.15	3.16	3.17	3.08	3.15
P15	*-390*	*0*	*0.45*	*0.45*	*0.45*	*0.45*	*0.45*	*0.45*	*0.45*	*0.45*	*0.45*	*0.45*	*0.45*	*0.45*	*0.45*	*0.45*
Flow [l/min]				56.5	51	59.4	32.6	44.2	47.5	42.4	38.8	35.6	35	34.2	52.8	52.8
sandtype	**location**			**A**	**B**	**C**	**D**	**E**	**F**	**G**	**H**	**I**	**J**	**K**	**B2**	**I2**
				K [m²]	**K [m²]**	**K [m²]**	**K [m²]**	**K [m²]**	**K [m²]**	**K [m²]**	**K [m²]**	**K [m²]**	**K [m²]**	**K [m²]**	**K [m²]**	**K [m²]**
B25	upstream			1.82E-11	1.9E-11	2.05E-11	1.05E-11	1.5E-11	1.5E-11	1.5E-11	1.3E-11	1.2E-11	1.2E-11	1.2E-11	1.97E-11	1.78E-11
B25	downstream			1.76E-11	1.9E-11	2.07E-11	1.9E-11	1.9E-11	1.9E-11	1.9E-11	1.9E-11	1.9E-11	1.9E-11	1.9E-11	1.97E-11	2.82E-11
GZB3	upstream			4.6E-10	2.2E-10	3.3E-10	3.3E-10	3.3E-10	4.6E-10	2.2E-10	2.5E-10	2E-10	2E-10	2E-10	2.28E-10	2.97E-10
GZB3	upper protrusion			4.82E-10	2E-10	3.3E-10	3.3E-10	3.3E-10	4.8E-10	2E-10	2.5E-10	2.5E-10	2E-10	1.5E-10	2.07E-10	3.71E-10
GZB3	lower protrusion			4.71E-10	2E-10	3.3E-10	2E-10	2E-10	4.7E-10	2E-10	2.5E-10	2.5E-10	2E-10	1.5E-10	2.07E-10	3.71E-10

Table B 2 Variation of intrinsic permeability for MS40

	x	y	critical head	A	C	D	E	F	G	F2
	[mm]	[mm]	[m]	[m]	[m]	[m]	[m]	[m]	[m]	[m]
P01	-1357	-388	4.33	4.32	4.32	4.32	4.33	4.32	4.32	4.32
P02	-835	-388	2.18	1.55	1.55	1.49	1.52	1.56	1.58	1.56
P03	-550	-388	1.02	1.01	1.01	0.99	0.99	1.02	1.04	1.02
P04	-357	-388	0.95	0.94	0.94	0.93	0.92	0.95	0.95	0.95
P05	-107	-388	0.89	0.88	0.88	0.88	0.88	0.89	0.89	0.89
P09	-980	0	3.59	3.72	3.70	3.70	3.73	3.68	3.66	3.68
P15	-390	0	0.85	0.85	0.85	0.85	0.85	0.85	0.85	0.85
Flow [l/min]			62.3	59.5	60.4	57.8	51.9	65.9	71.2	62.4
sandtype	**location**			**A**	**C**	**D**	**E**	**F**	**G**	**F2**
				K [m²]	**K [m²]**	**K [m²]**	**K [m²]**	**K [m²]**	**K [m²]**	**K [m²]**
B25	upstream			1.86E-11	1.9E-11	1.8E-11	1.6E-11	2.1E-11	2.3E-11	1.99E-11
B25	downstream			1.88E-11	1.9E-11	1.9E-11	1.9E-11	1.9E-11	1.9E-11	1.8E-11
GZB3	upstream			4.55E-10	4.3E-10	4.2E-10	4.3E-10	4.3E-10	4.3E-10	4.07E-10
GZB3	upper protrusion			4.98E-10	5E-10	5E-10	5E-10	5E-10	5E-10	4.73E-10
GZB3	lower protrusion			4.45E-10	4.45E-10	5E-10	4.45E-10	4.45E-10	4.45E-10	4.21E-10

B.2 Gradients at critical stage for numerical fits I2 (MS38) and F2 (MS40)

The gradient perpendicular to the slope surface and the vertical gradient on the upstream side of the barrier are considered most relevant for the erosion process. The gradient at the toe of the slope can be relevant for erosion of barrier material into the pipe downstream. The gradient perpendicular to the slope (in combination with the angle of repose) will be relevant for erosion along the slope. When the failure occurs, the vertical gradient in the lower part of the slope can be expected to play a role in fluidizing the barrier material causing slope failure.

B.2.1 Outward hydraulic gradients perpendicular to the slope

The gradient at the slope face can be calculated by computing the velocity along the surface line divided by the hydraulic conductivity or by computing the head difference between the point 5 cm away from the slope surface in the barrier (perpendicular to the slope) and the head at the point at the surface. Both methods are used, partly as a check on the calculated gradient and to be sure that the calculated gradient at the surface does not give very local results at the surface of the slope.

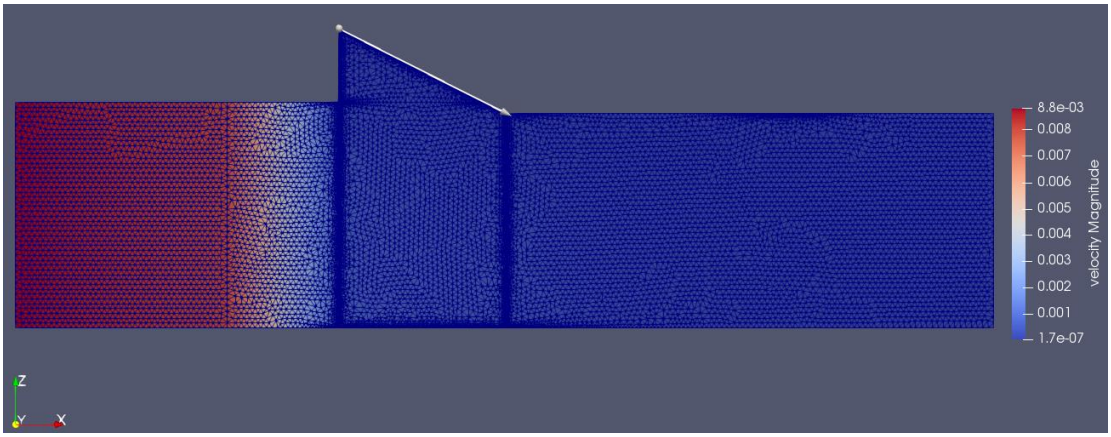

Figure B.1 MS38. Line for determining velocities perpendicular to surface line of the slope

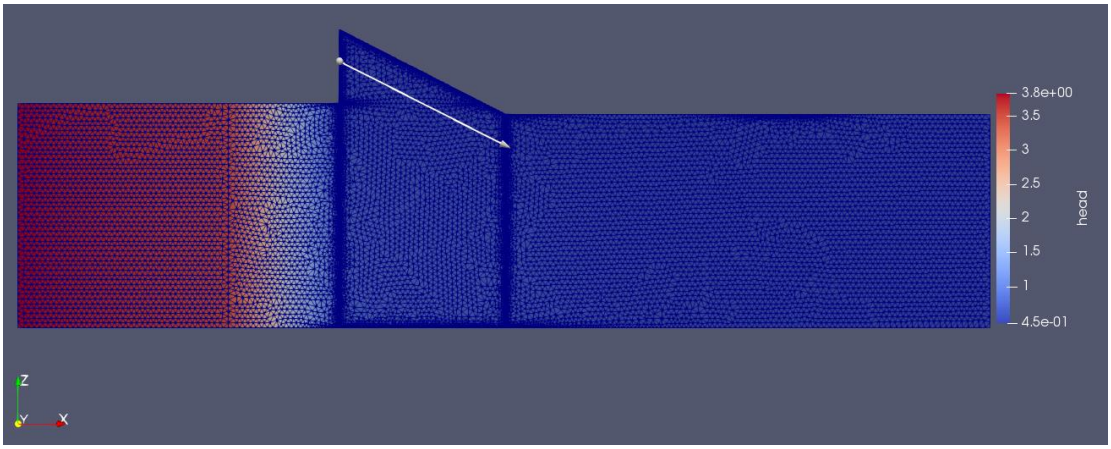

Figure B.2 MS38. Line for determining heads in the barrier in 5 cm distance perpendicular to the slope

The following figures show the computed gradients perpendicular to the slope along the slope in the barrier for both tetst for the fits I2 (MS38) and F2 (MS40), using both methods for determination of the gradient (see also Table 4-5)

Table B. 1 Calibrated intrinsic permeability and hydraulic conductivity (fitted in with the measured heads and fluxes) for critical stage

sand type	location	MS38 K_{20} [m²]	MS38 k_{20} [m/s]	MS40 K_{20} [m²]	MS40 k_{20} [m/s]
B25	upstream	1.78E-11	1.72E-04	1.99E-11	1.92E-04
B25	downstream	2.82E-11	2.73E-04	1.80E-11	1.74E-04
GZB3	upstream	2.97E-10	2.85E-03	4.07E-10	3.90E-03
GZB3	upper part of the barrier inside protuberance	3.71E-10	3.56E-03	4.73E-10	4.54E-03
GZB3	Lower part of the barrier below protuberance	3.71E-10	3.56E-03	4.21E-10	4.04E-03

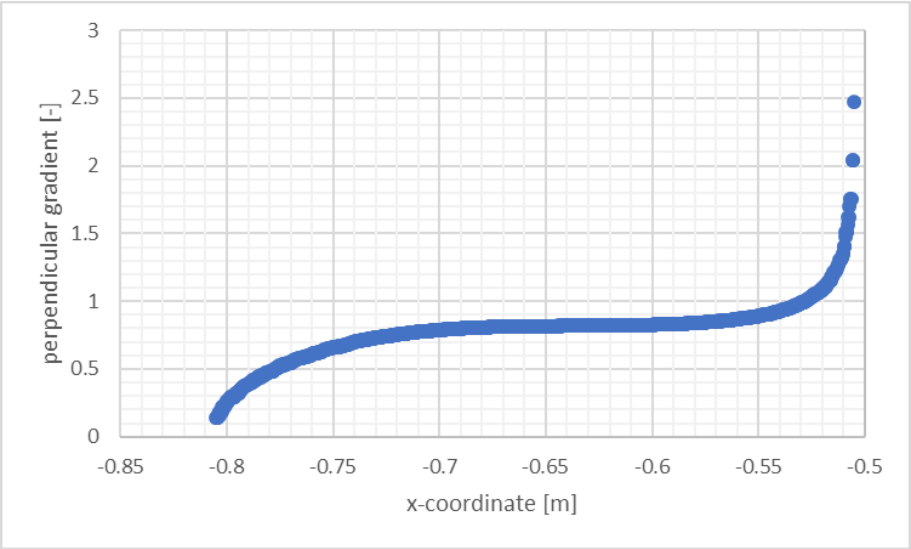

Figure B.3 MS38. Computed gradients perpendicular to the slope along the slope in the barrier (gradient as a function of velocity/k)

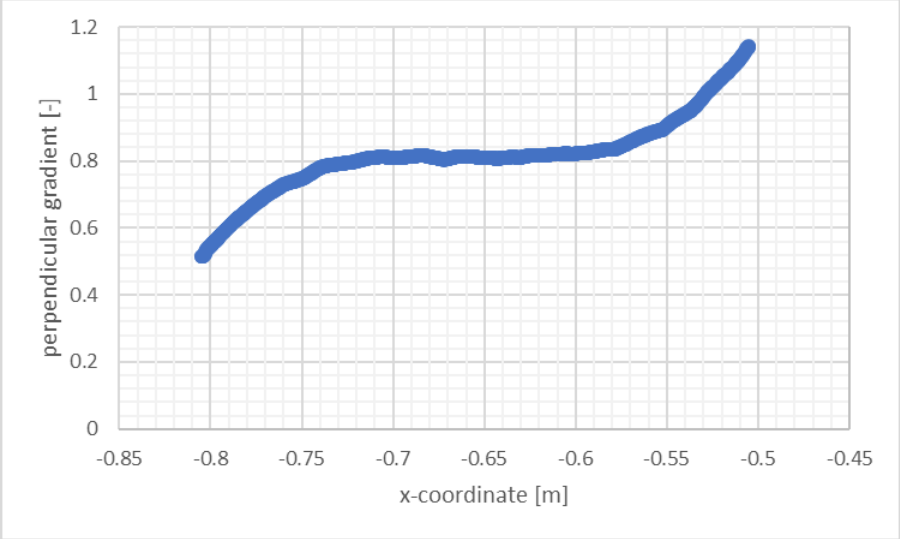

Figure B.4 MS38. Computed gradients perpendicular to the slope along the slope in the barrier (gradient over a distance of 5 cm parallel to surface line of the slope)

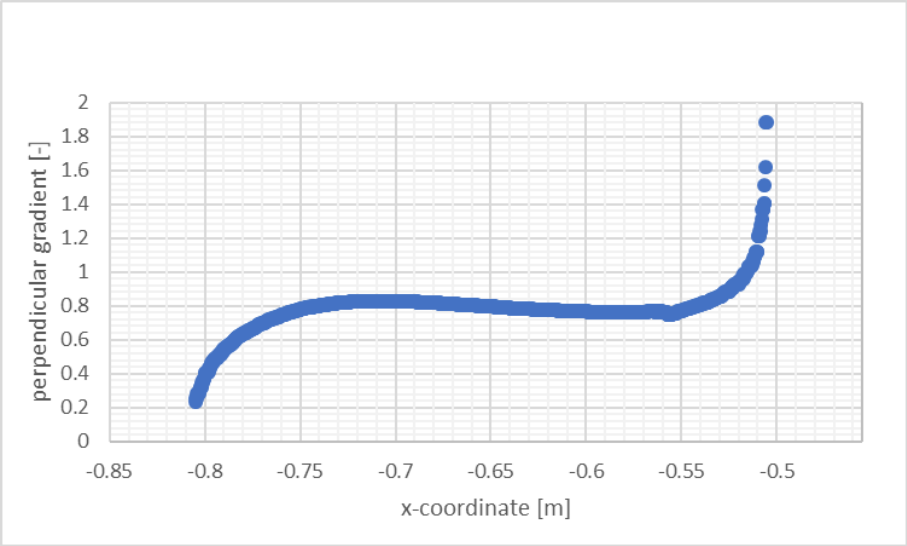

Figure B.5 MS40. Computed outward gradients perpendicular to the slope along the slope in the barrier (gradient as a function of velocity/k)

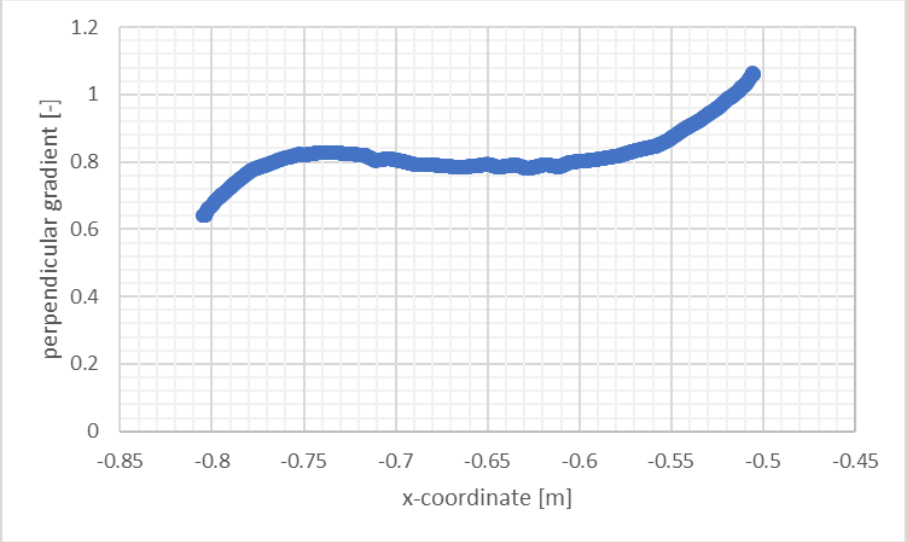

Figure B.6 MS40. Computed outward gradients perpendicular to the slope along the slope in the barrier (gradient over a distance of 5 cm parallel to surface line of the slope)

Abovementioned figures show for both tests at the used fit a comparable almost uniform outward gradient along a broad zone of the barrier slope, except for the peripheral area.

B.2.2 Vertical gradients

The vertical gradient at the upstream end of the slope between the top of the slope and the location at the level of the top of the sand bed is determined for three positions:

MS38: x = - 0.776 m iv = 0.711
x = - 0.794 m iv = 0.712
x = - 0.803 m iv = 0.714

MS40: x = - 0.775 m iv = 0.795
x = - 0.795 m iv = 0.809
x = - 0.804 m iv = 0.814

Further, the head along the remaining crest height at the upstream end of the slope from top to the bottom edge of the protuberance is given in Figure B.7 and Figure B.8.

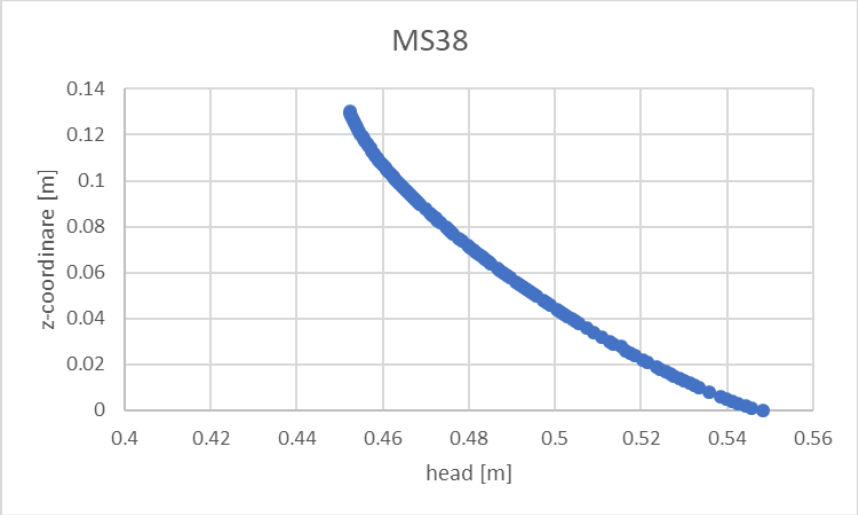

Figure B.7 MS38. Head profile below the top of the slope along protuberance wall

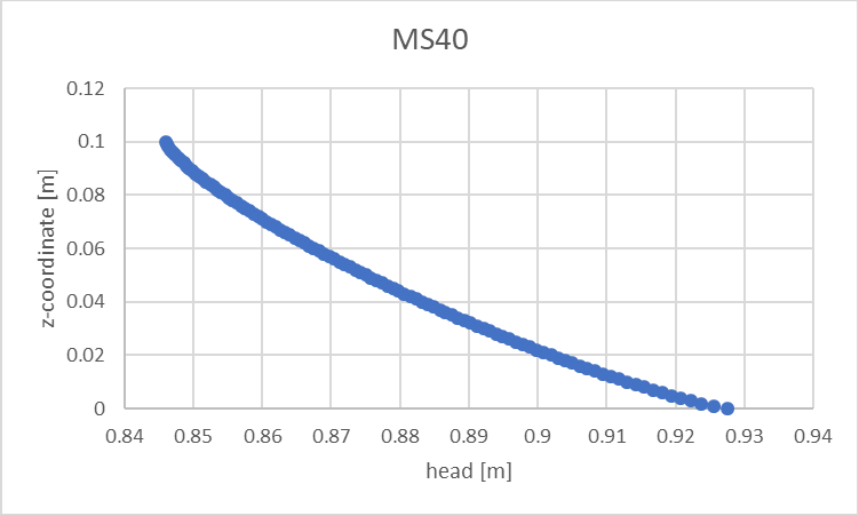

Figure B.8 MS40. Head profile below the top of the slope along protuberance wall

From the abovementioned figures and gradients, we can conclude that at the upstream side barrier the vertical gradient over the whole slope height is not sufficient to cause heave.

C Geotechnical stability against sliding of upstream fine sand

C.1 Introduction

When a structure with a CSB is loaded by a head drop, the water pressure will be transferred to the effective stress. When at the end of the tests described in this report there is a head drop of nearly 4 m, this is only possible when the pressure difference is transferred to the fine sand. The pressure drop in the CSB itself is limited and can be neglected in a first simplified model. The large loading on the fine sand means that this can only be stable when it is stabilized (locked) in the structure. presents a sketch of the fine sand and the CSB in the model tests. The downstream fine sand is closed in the experimental set-up and will not move and is therefore not drawn in the figure the right side of the figure can be seen as a fixed boundary. A possible slip failure line is indicated at the dotted line. Stabilizing forces for the fine sand above the dotted line are the friction between the sand above and below the dotted line and by the weight and friction of the CSB triangle. It should be realized that the CSB full weight of the CSB triangle cannot be used, since the upward directed gradient in the CSB will decrease the effective forces.

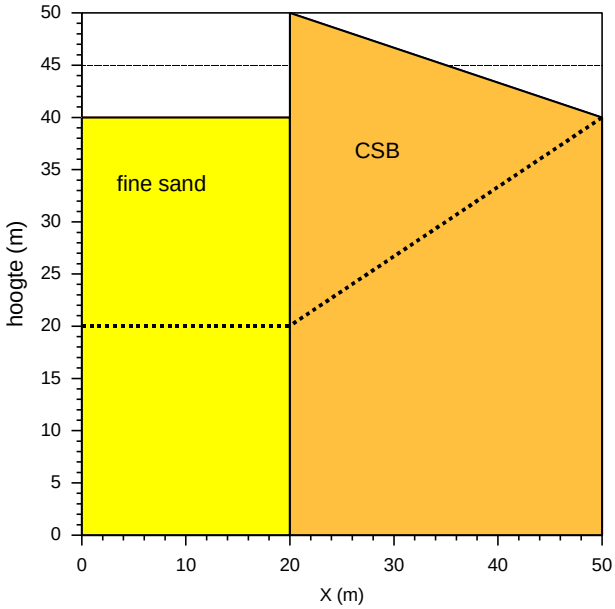

Figure C. 1 Sketch of fine sand and CSB in model tests.

The friction of the fine background sand along the failure line depends on the vertical stress at that location. The vertical stress will be low at the upstream part and will increase at the downstream side of the sand. Weight of the sand can be included, but will be of limited influence in these model tests, since the weight is the underwater weight of 0.2 m sand and the pressure difference is 4 m. In the following calculation the influence of the weight will therefore be neglected.

The aim of the calculation is to see what are the conditions that lead to a stable solution against geotechnical failure.

C.2 Calculation

The calculation starts with calculating the horizontal passive force that can be exerted by the CSB triangle to prevent moving the fine sand into the CSB. Without any gradients, the forces at the failure surface in the CSB are sketched in Figure C. 2.

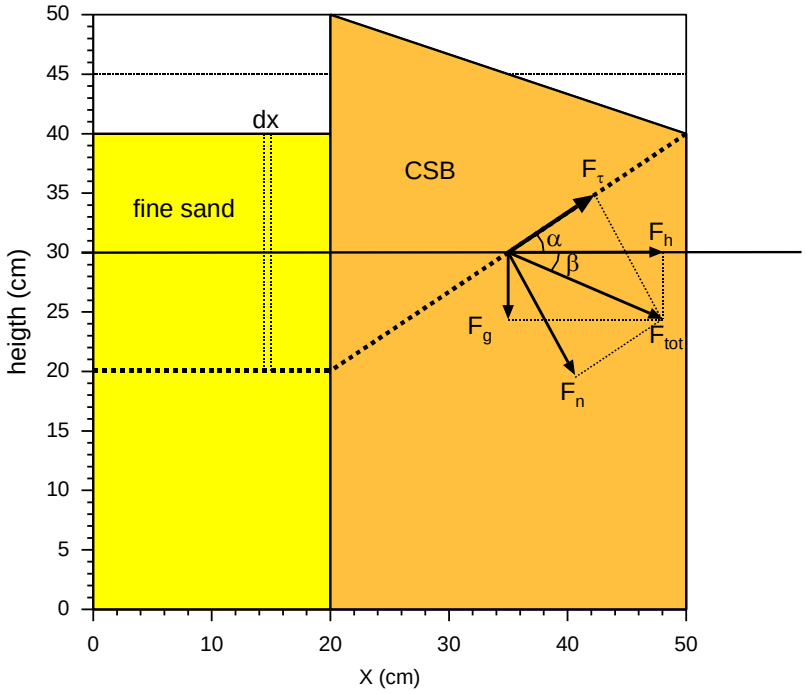

Figure C. 2 Forces on CSB triangle

From that it can be derived that the following relation applies:

$$F_h = F_g \tan(\phi + \alpha) \qquad \text{(Equation C. 1)}$$

Where:
F_h : the horizontal force (kN)
F_g : the weight of the triangle above the failure line (kN)
ϕ : the friction angle (degr)
α : angle of failure surface, see Figure C. 2 (degr)
β : angle between the total force on the failure slope and the horizontal, see Figure C. 2 (degr)

The effective force that is transmitted to the sand from the hydraulic gradient can be approximated the following way. Without between the walls, it can be written:

$$\rho g i = -\frac{d\sigma_h'}{dx} \qquad \text{(Equation C. 2)}$$

Where:
i : is the gradient (-)
g : the acceleration of gravity (m/s2)
ρ : the density of water (kg/m3)
σ'_h: the effective horizontal stress (kPa)
x : the length coordinate, see Figure C. 1

However, there is friction and the force on the fine sand is $\sigma'_h.h$ (kN/m) will be partly transmitted to the CSB triangle and partly it will be taken by the friction of the side walls and bottom of a plug of fine background sand that may be pushed out. Taking a segment *dx* the force equilibrium can be written as:

$$\frac{d\sigma'_h}{dx} + \frac{K_0 \tan\phi}{h}\sigma'_h = -\rho g i \qquad \text{(Equation C. 3)}$$

Where:
h : the height of the moving sand (m)
K_0 : the ratio between horizontal and vertical stress (-)

This equation is valid for a 2-D situation. In reality, there will be a 'plug' pushed out, which is a 3-D situation. This can be corrected for by taking a higher value of K_0. For example, if a plug is assumed with the same width and height, the K_0 value should be multiplied by 3 to get the right friction, assuming that the friction between the sand and the acrylic plate is only small. For $\sigma'_h = 0$ when x=o, this differential equation can be solved leading to:

$$\sigma'_h = \frac{\rho g h i}{K_0 \tan\phi}\left(1 - e^{-\frac{K_0 \tan\phi}{h}x}\right) \qquad \text{(Equation C. 4)}$$

For small values of *x* this leads to:

$$\sigma'_h = \rho g i x \qquad \text{(Equation C. 5)}$$

and for large values:

$$\sigma'_h = \frac{\rho g h i}{K_0 \tan\phi} \qquad \text{(Equation C. 6)}$$

For large values of *x*, the horizontal stress is therefore independent of x. In the medium scale set-up $\sigma'_h * h$ must be smaller than F_h, as defined in Equation (C.1).
For what conditions a soil plug would be stable is checked by some example calculations using the parameters of the Medium Scale set-up at loading (*i*=20), a friction angle of 35 degrees and a shear plane that is half way the upstream background sand, see Figure C. 2. The results are presented in Figure C. 3. The thick black horizontal line is the horizontal stress that can be resisted by the weight of the triangle. It is clear that the large gradient can only be resisted when the K_0 value is very high. The lowest value of K_0 is what is normally expected, the value of 1.28 is 3 times this value assuming that the three sides of a plug of 0.2 by 0.2 m contribute to the friction. However, a value of 10 is necessary to get a stable situation. Such a value is only possible when the sand is very dense and dilatancy occurs that increases the stress on the sides of the sand plug. In this calculation the influence of the gradient in the CSB is not taken into account, that would lead to an even higher value of K_0. A pessimistic assumption is on the other hand, that σ'_h is zero kPa for x=0 m. In reality there will be some horizontal stress and thus friction due to the densification of the sand.

If this calculation is correct, this means that the density of the upstream background sand is very important for the stability of the structure as tested in the model test. If the background sand is loose and will not dilate when loaded, geotechnical instability due to sliding of a sand plug of the background sand will occur much earlier than instability of the CSB due to the high gradients in the CSB.

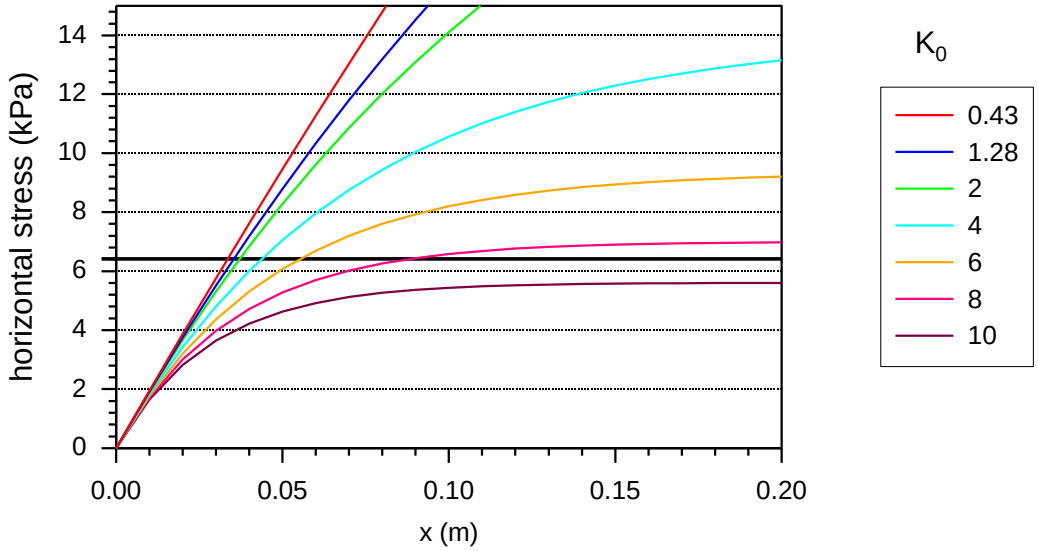

Figure C. 3 Results of calculations.

Deltares is an independent institute for applied research in the field of water and subsurface. Throughout the world, we work on smart solutions for people, environment and society.

Deltares

www.deltares.nl